Molecular and morphologic study of pancreatic cancer evolution

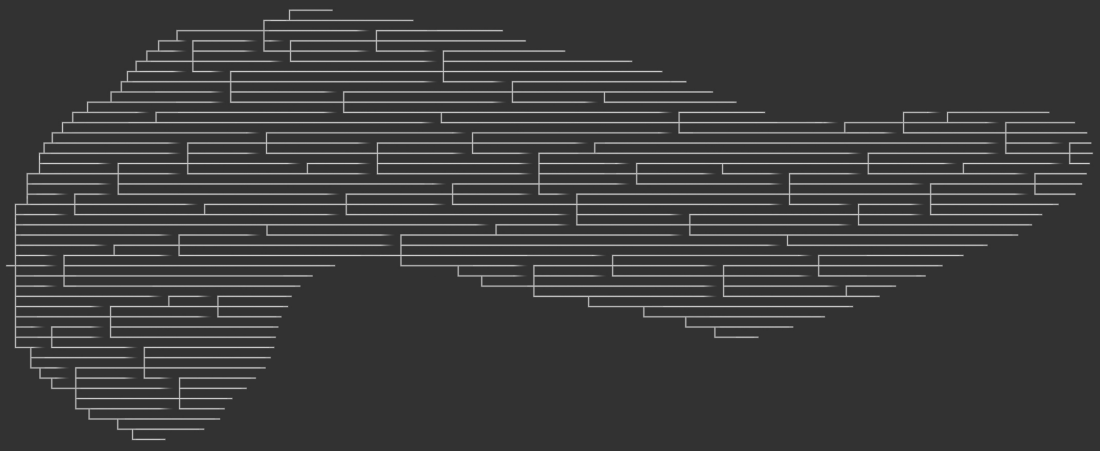

Michaël Noë

Molecular and morphologic study of pancreatic cancer evolution

PhD thesis, Utrecht University, the Netherlands

Printed by: Gildeprint Drukkerijen, Enschede

ISBN: 978-94-6402-155-4

The work described in this thesis was financially supported by the Dutch Digestive Foundation (MLDS CDG 14-02), the Nijbakker-Morra Foundation and the Living With Hope Foundation.

Molecular and morphologic study of pancreatic cancer evolution

Moleculaire en morfologische studie van alvleesklierkanker evolutie

(met een samenvatting in het Nederlands)

Proefschrift

ter verkrijging van de graad van doctor aan de Unversiteit Utrecht op gezag van de rector magnificus, prof. dr. H.R.B.M. Kummeling, ingevolge het besluit van het college voor promoties in het openbaar te verdedigen op woensdag 8 juli 2020 des middags te 6.00 uur

door

Michaël Patrick Marthe Noë

geboren op 21 april 1987 te Oudenaarde, België

Promotoren:	Prof. dr. G.J.A. Offerhaus Prof. dr. R. Hruban
Copromotoren:	Dr. L.A.A. Brosens Dr. L.D. Wood

Table of content

Chapter 1

General introduction

Pancreatic ductal adenocarcinoma (PDAC) is a tumor with a dismal prognosis, and this disease is predicted to soon be the leading cause of cancer death in the United States.[1] Unfortunately, little progress has been made in recent decades to improve the outcome for patients suffering from this disease.[2] The frequent detection of the tumor in a late and advanced stage is often cited as a reason for the bad prognosis, and earlier detection is considered a key goal for improving outcome Precursor lesions like pancreatic intraepithelial neoplasm (PanIN), intraductal papillary mucinous neoplasm (IPMN) and mucinous cystic neoplasm (MCN) are thought to be the non-invasive precursors of PDAC.[3] These lesions are abundant in the population, but only a few will give rise to a PDAC. Prophylactic treatment of the lesions can interrupt the further evolution to an invasive disease, but is also associated with procedure-associated morbidity and mortality. Because of the impact on prognosis when a precursor lesion becomes invasive, we hypothesized that this 'moment of invasion' is a clinically important event in the evolution of pancreatic cancers. The objective of this thesis project was to characterize genomic and structural changes associated with the conversion from benign precursor to invasive cancer. Relevant biomarkers of invasion could give more insight in the mechanism of invasion and could be used to stratify the risk in patients with clinically detectable, cystic precursors, like IPMNs and MCNs.

Although many researchers have previously studied invasion, it is still not clear what exactly gives a cell its invasive behaviour. Pathologically, invasion is defined as a breach of the basement membrane and the growth of the neoplastic cells beyond this membrane. Normal cells can show migration and invasion during certain physiological processes, like wound healing. However, normal cells stop these programs and the displaced cells can form epithelial inclusion cysts, like in the skin or the ovary. Cancer cells have lost these breaks and continue their invasion and migration, like wounds that do not heal.[4] In vitro invasion assays, like the transwell invasion assay or organoid models in collagen I matrix, do not recapitulate these basic principles, as normal cells in these assays show unopposed invasion that does not halt.[5] The assays often quantitatively measure invasion in order to differentiate 'normal' invasive behaviour versus 'pathologic' invasive behaviour. But the assays do not address what causes normal cells to halt invasion when cancer cells do not.

Therefore, to address this issue, we turned to other assays and techniques to study invasion in resection samples from patients with sporadic pancreatic cancer. We also study samples from patients with germline mutations in specific genes, which predispose these patients for pancreatic cancer. These cancer syndromes are very interesting to study the origin and the pathogenesis of cancer.

Next-generation DNA sequencing has made it possible to obtain a huge amount of data through massive parallel sequencing of millions of small reads (50-400 bases). This allows for the study of large regions cancer cell genomes, like the part of the genome that is eventually translated into proteins: the exonic regions of the genome or the exome. Whereas in the past, researchers would use one Sanger-sequencing experiment to study the sequence of a specific gene or gene-region, we can now investigate the sequence of all 20,000 genes of multiple patients and even of multiple samples from the same patient in one experiment.[6] This allows for the characterization not only of the driver genes of

cancer, but also the passenger mutations. Although passenger mutations are defined as not having an impact on the fitness of the neoplastic cell in its environment, studying them can inform us about the clonal evolution of a neoplasm or the relatedness of multiple neoplasms.[7] Using the principles of evolution, the clonal relationships of different samples can be inferred from the gradual accrual of driver-mutations and passenger-mutations. In the past, information about directionality of evolution often came from histopathologic assessments of the differentiation-grade of a sample from a neoplasm, which was not always without subjectivity. Passenger mutations are more abundant than driver mutations and can inform us about evolution at a higher resolution. Used as a molecular clock, we can estimate the timing between the origin of different clones, which allows us to relatively order clones with the same driver-mutations, but with different amounts of passenger-mutations.

For pathologists, the diagnosis of cancer is daily practice, and a combination of architectural and cytologic features serve as input for their trained eye to output a specific diagnosis. These features are extracted from tissue-slides: thin sections of the tissue of patients that can be transilluminated in order to get a two dimensional picture. Although 2D pictures have been proven to contain enough information for pathologists to make a diagnosis, we must acknowledge that we cannot appreciate all the features of what is inherently a space-occupying, three-dimensional disease.[8] Radiologists use three-dimensional scans in daily practice to study anatomy. The study of histopathology in three dimensions remains challenging. Serial tissue sectioning has been used, but this is labor-intensive and is associated with artefacts.[9,10] Modern tissue clearing techniques were developed to study the organization of neurons and their axons in the central nervous system of animal models.[11] The technique makes it possible to make the tissue translucent, which enables the excitation of fluorochromes on penetrated antibodies and the detection of the emitted light. We have optimized these techiques for use on human pancreatic samples, which have a dense extracellular matrix, which makes the penetration of antibodies more difficult. Our goal of studying cancer in three dimensions was to find out how cancers move through tissues and study their relationship with other structures like blood vessels and nerves.

Outline

In this thesis, we have utilized the described methods to investigate the evolution of pancreatic cancers and their precursors. In the first part, we focus on the precursors of pancreatic ductal adenocarcinoma. In chapter 2, we provide a summary of the literature on the pathology of pancreatic precursor lesions, with a focus on the pitfalls of diagnosing these lesions. Chapter 3 describes our evolutionary analysis of IPMNs and MCNs with an associated PDAC through whole-exome sequencing of multiple locations in these neoplasms, in order to identify molecular alterations that are specific to invasion. Chapter 4 evaluates the presence of driver-mutations in high-grade PanIN lesions without PDAC. In chapter 5, we compare the relatedness of IPMNs and PDACs through targeted sequencing of driver genes. Chapter 6 describes the lesions found in the GI-tract of patients with McCune-Albright syndrome and the presence of an activating *GNAS* mutation in these lesions. McCune-Albright syndrome patients are at risk for multiple abnormalities, among which IPMNs in the pancreas. In the second part of the thesis, we use tissue-clearing techniques to investigate pancreatic ductal adenocarcinomas. Chapter 7

evaluates the different tissue clearing principles and technologies. Chapter 8 describes the application of this technique on human pancreatic cancers with an antibody against CK-19. Chapter 9 expanded the study by the use of multiple antibodies against different proteins, to highlight specific structures in the tissue. Our tissue clearing techniques led to the observation of pancreatic cancer cells in the lumens of pancreatic veins. This observation is evaluated as an important factor in the dismal prognosis of pancreatic cancers in chapter 10. In the last part of this thesis, have studied molecular alterations in patients with pancreatic neuroendocrine tumor. In chapter 11, we compare the molecular features of small, pancreatic neuroendocrine tumors that metastasized to the liver and that did not metastasize. Chapter 12 is the molecular study of somatostatinomas, a pancreatic neuroendocrine tumor that is frequently observed in patients with neurofibromatosis type 1 (NF1). In chapter 13, we describe a patient with FAMMM-syndrome (germline CDKN2A-mutations), who is at high risk to develop a pancreatic ductal adenocarcinoma, in which a small neuroendocrine tumor was found in the pancreas.

REFERENCES

1. Rahib, L. et al. Projecting cancer incidence and deaths to 2030: the unexpected burden of thyroid, liver, and pancreas cancers in the United States. Cancer Res. 74, 2913–2921 (2014).
2. Siegel, R. L., Miller, K. D. & Jemal, A. Cancer statistics, 2019. CA Cancer J. Clin. 69, 7–34 (2019).
3. Noë, M. & Brosens, L. A. A. Pathology of Pancreatic Cancer Precursor Lesions. Surg. Pathol. Clin. 9, 561–580 (2016).
4. Dvorak, H. F. Tumors: wounds that do not heal. Similarities between tumor stroma generation and wound healing. N. Engl. J. Med. 315, 1650–1659 (1986).
5. Nguyen-Ngoc, K.-V. et al. ECM microenvironment regulates collective migration and local dissemination in normal and malignant mammary epithelium. Proc. Natl. Acad. Sci. U. S. A. 109, E2595–604 (2012).
6. Koboldt, D. C., Steinberg, K. M., Larson, D. E., Wilson, R. K. & Mardis, E. R. The next-generation sequencing revolution and its impact on genomics. Cell 155, 27–38 (2013).
7. Campbell, P. J. et al. Subclonal phylogenetic structures in cancer revealed by ultra-deep sequencing. Proc. Natl. Acad. Sci. U. S. A. 105, 13081–13086 (2008).
8. Tanaka, N. et al. Whole-tissue biopsy phenotyping of three-dimensional tumours reveals patterns of cancer heterogeneity. Nature Biomedical Engineering 1 (2017).
9. Ourselin, S., Roche, A., Subsol, G., Pennec, X. & Ayache, N. Reconstructing a 3D structure from serial histological sections. Image Vis. Comput. 19, 25–31 (2001).
10. Griffini, P., Smorenburg, S. M., Verbeek, F. J. & van Noorden, C. J. Three-dimensional reconstruction of colon carcinoma metastases in liver. J. Microsc. 187, 12–21 (1997).
11. Chung, K. et al. Structural and molecular interrogation of intact biological systems. Nature 497, 332–337 (2013).

Part 1

Molecular evolution of intraductal neoplasms

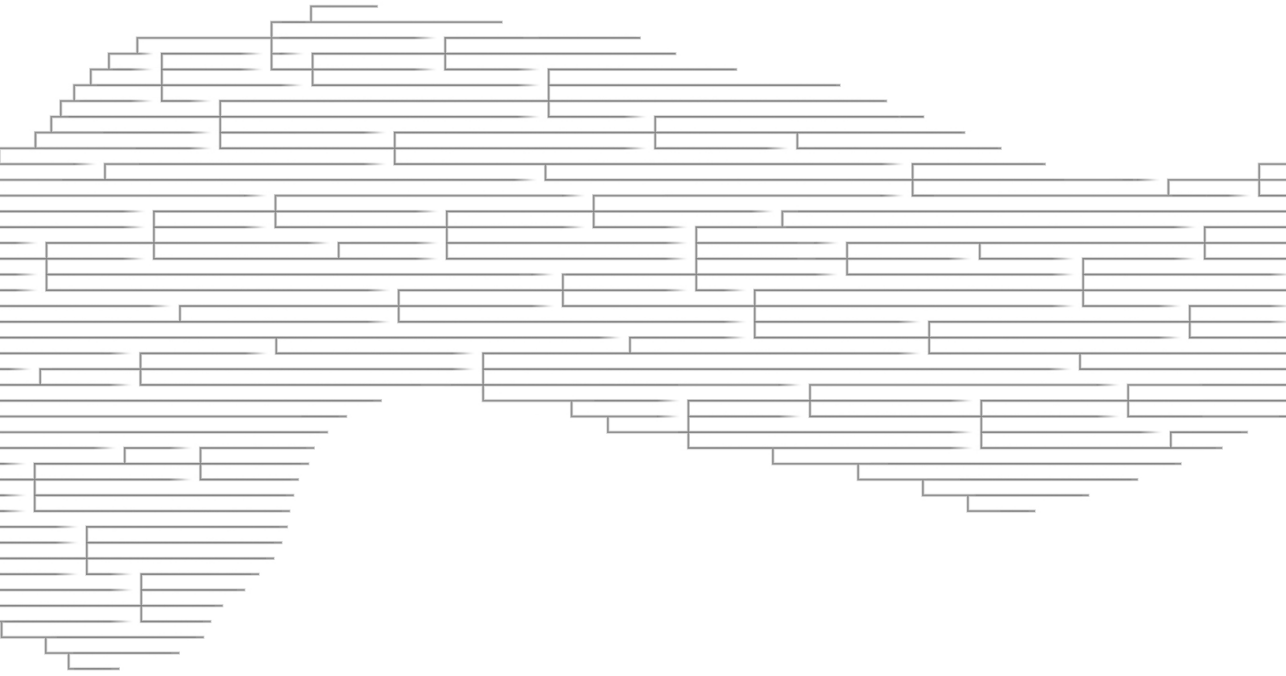

Chapter 2

Pathology of pancreatic cancer precursor lesions

Michaël Noë, Lodewijk A.A. Brosens

Surgical Pathology Clinics, December 2016

ABSTRACT

To better understand pancreatic ductal adenocarcinoma (PDAC) and improve its prognosis, it is essential to understand its origins. This article describes the pathology of the 3 well-established pancreatic cancer precursor lesions: pancreatic intraepithelial neoplasia, intraductal papillary mucinous neoplasm, and mucinous cystic neoplasm. Each of these precursor lesions has unique clinical findings, gross and microscopic features, and molecular aberrations. This article focuses on histopathologic diagnostic criteria and reporting guidelines. The genetics of these lesions are briefly discussed. Early detection and adequate treatment of pancreatic cancer precursor lesions has the potential to prevent pancreatic cancer and improve the prognosis of PDAC.

OVERVIEW

Noninvasive precursor lesions in the pancreas have been recognized for more than a century.[1] They have the ability to progress to pancreatic ductal adenocarcinoma (PDAC). However, it was not until 1999 that an international consensus meeting formed the basis for the current classification and definition of these precursor lesions.[2] Since then, multiple consensus meetings have been organized, updating the classification system with new insights.[3,4] Three precursor lesions are recognized: pancreatic intraepithelial neoplasia (PanIN), intraductal papillary mucinous neoplasm (IPMN), and mucinous cystic neoplasm (MCN). All of these meet the criteria for precursor lesion, as defined by a consensus conference, sponsored by the National Cancer Institute.[5] These precursors show a unique multistep morphologic and genetic progression to invasive carcinoma.

PANCREATIC INTRAEPITHELIAL NEOPLASIA

Clinical features

PanIN is the most common precursor lesion of PDAC. These lesions were first described a century ago by Hulst.[1] Both men and women are equally affected and the incidence tends to increase with age.[6–8] PanINs can be found in 82% of pancreata with invasive carcinoma, in 60% of pancreata with chronic pancreatitis, and in 16% of normal pancreata.[7] PanINs occur multifocally in patients with a family history of pancreatic adenocarcinoma.[9,10] Because of their small size (by definition <0.5 cm), these lesions cannot be seen on noninvasive abdominal imaging and they are not associated with clinical signs or symptoms. However, lobular atrophy and fibrosis can be clues for their presence. PanINs are typically found incidentally in resections or biopsy specimens.[6,11,12]

Pathologic features

PanINs are noninvasive, microscopic, epithelial neoplasms and by definition involve pancreatic ducts less than 0.5 cm in diameter.[2–4] PanINs are characterized by cuboid to columnar cells with varying amounts of apical cytoplasmic mucin and varying degrees of cytologic and architectural atypia. PanINs almost always show gastric foveolar differentiation.[4]

Hruban and colleagues[2] described the generally accepted PanIN scheme to classify these lesions in 2001. Three grades are discriminated in this scheme, based on the degree of epithelial atypia: PanIN-1, PanIN-2, and PanIN-3. PanIN-1 lesions are characterized by minimal nuclear atypia, inconspicuous nucleoli, and absent mitotic figures and can be further subdivided into flat (PanIN-1A) and micropapillary (PanIN-1B) types. Moderate nuclear atypia, pseudostratification, loss of polarity, hyperchromasia, and rare mitotic figures are features of PanIN-2. PanIN-3 lesions have marked atypia; contain (atypical) mitotic figures; show loss of polarity; and have a papillary, micropapillary, or occasional flat architecture (Figure 1). Cribriform structures, necrosis, and tufting of epithelial cells in the lumen may be present. PanIN-3 is almost exclusively found in association with invasive PDAC.[6,7] This feature is so striking that, in pancreata without a PDAC, a PanIN-3 lesion may serve as a surrogate marker for invasion

elsewhere.[7,13] Another pitfall is the extension of an infiltrating carcinoma in pancreatic ducts (ie, ductal cancerization) mimicking a PanIN-3 lesion. The close proximity of an invasive carcinoma to a ductal lesion, the abrupt transition from highly atypical epithelium to normal ductal epithelium, luminal obstruction, and ductal destruction are clues to consider ductal cancerization.[2,3,14]

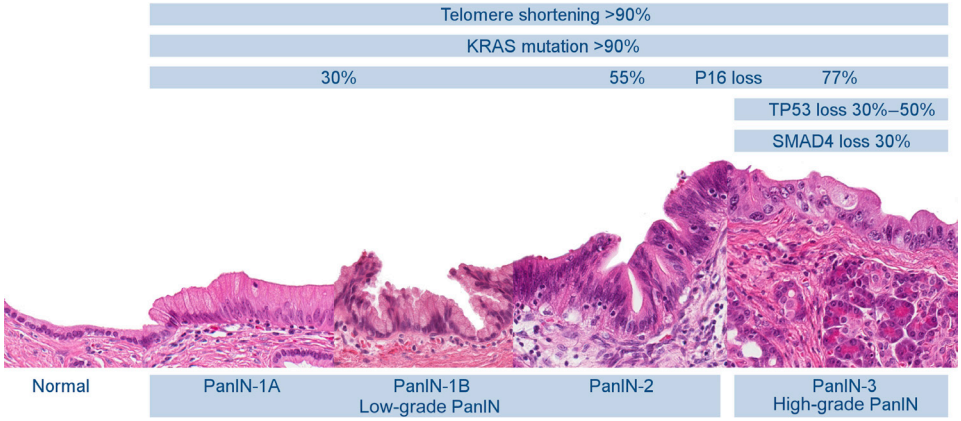

Figure 1. The progression of PanIN is associated with an increase in cellular atypia and accumulation of genetic mutations. PanIN-1 shows minimal nuclear atypia. PanIN-1A has a flat growth pattern, whereas PanIN-1B shows formation of micropapillae. PanIN-2 shows loss of cellular polarity. PanIN-1 and PanIN-2 are both grouped as low-grade PanIN. PanIN-3 or high-grade PanIN has the most severe nuclear and architectural atypia. The PanIN-3 lesion shown here is the variant with a flat architecture.

The clinical significance of PanIN-1 and PanIN-2 has been questioned by studies, because these lesions show little progression to PDAC.[7,15] Grading the lesions also showed poor interobserver agreement.[16] For these reasons, the latest consensus meeting advised the use of a 2-tiered grading system with low-grade PanIN (formerly PanIN-1A, PanIN-1B, and PanIN-2) and high-grade PanIN (formerly PanIN-3). Moreover, the presence of PanIN lesions of any grade at the surgical margin of pancreata resected for invasive PDAC does not influence patient prognosis and additional surgery is not required.[17]

PanINs show an increased expression of MUC 1 (Mucin 1) and MUC5AC (Mucin 5AC) in higher grades of dysplasia.[18–21] The opposite is seen for MUC6 (Mucin 6), showing reduced expression in higher grades of dysplasia.[19,22]

Molecular features

The early lesions with minimal cytologic atypia were not originally regarded as neoplastic, but instead were designated as hyperplasia or metaplasia.[23] After finding *KRAS* mutations, these lesions were considered neoplastic and the term pancreatic intraepithelial neoplasia was proposed.[2,13,24–27] It has been established that progression from low-grade PanIN to high-grade PanIN requires accumulation of genetic alterations, starting with an activating *KRAS* mutations and telomere shortening, followed by *CDKN2A* mutations and later *P53* and *SMAD4* mutations (Figure 1).[21,28–31]

Clinical features

The first description of intraductal mucinous neoplasms of the pancreas probably dates back to 1936.[32,33] Until 1994, these tumors were described under various names, each emphasizing a different morphologic feature of the tumor. In 1994, all these entities were grouped together under the term IPMN, as proposed by Morohoshi and colleagues.[34,35]

Initially, IPMN was considered a disease of older men, often with a history of cigarette smoking. However, a meta-analysis showed that there are geographic differences in the gender of patients with IPMN. The male/female ratios of main-duct type and branch-duct type IPMNs in Asia are 3 and 1.8, respectively. However, in the United States, these ratios are 1.1 and 0.76, and in Europe 1.5 and 0.66, respectively.[36] The mean age of patients at time of diagnosis is 60 to 66 years, irrespective of geographic location.[37–41] There is a lag time of 3 to 6 years before patients with noninvasive IPMN develop PDAC.[37–41] IPMNs are seen most frequently in patients with a family history of pancreatic cancer, Peutz-Jeghers syndrome, familial adenomatous polyposis, Lynch syndrome, Carney complex, and McCune-Albright syndrome.[10,42–48] Because IPMNs are detectable with medical imaging techniques, these lesions can serve as a target for a screening test for the early detection of pancreatic neoplasia.[10]

IPMNs are mucin-producing, epithelial neoplasms with an intraductal proliferation of dysplastic cells that usually form papillae. This process leads to cystic dilatation of the pancreatic ducts. Although most people diagnosed with IPMN are asymptomatic, some patients experience nonspecific symptoms, including vague abdominal pain, weight loss, nausea, jaundice, (recent-onset) diabetes, or steatorrhea.[49] Mild acute pancreatitis is more often seen if the IPMN involves the main duct. IPMN involving only small pancreatic ducts is most likely to be asymptomatic.[37,40,50–52] On endoscopy, a classic patulous papilla extruding mucus can be seen in 25% of patients with IPMN. It is also called a fish eye or fish mouth and is virtually diagnostic for the presence of an IPMN (Figure 2).[53,54]

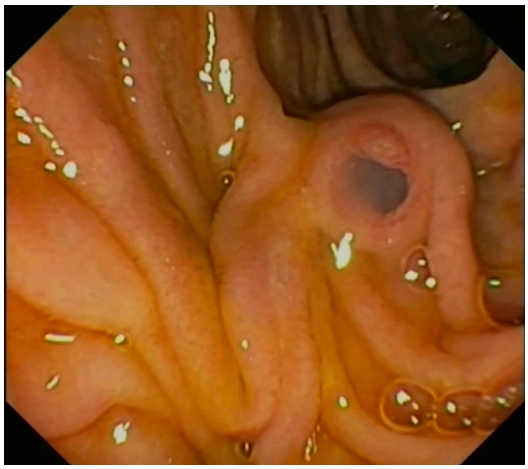

Figure 2. A classic patulous papilla extruding mucus also extruding mucus, also called fish eye or fish mouth, as seen on endoscopy in a patient with an IPMN.

IPMNs were thought to be rare pancreatic tumors, but the current widespread use of high-quality, cross-sectional abdominal imaging techniques has shown that pancreatic cysts and IPMNs are common. However, epidemiologic studies show great variety in the prevalence of pancreatic cysts because

of the use of different imaging techniques and different study populations.[55–64] If only cysts larger than 0.5 cm in patients imaged for other indications than pancreatic disorder and without a history of pancreatic disorder are considered, the prevalence is 10% to 21%.[56,57] A different study in a younger and partially healthy population scanned at a center for preventive medicine showed a much lower prevalence of 2.4%.[65] However, not all pancreatic cysts are IPMNs. About a third of resected asymptomatic pancreatic cysts seem to be IPMN.[52,66]

IPMNs are most frequently located in the proximal pancreas (the pancreatic head and the processus uncinatus). Based on the pancreatic ducts they involve on radiological and pathologic examination, IPMNs are classified as main-duct type IPMNs, branch-duct type IPMNs, or mixed type IPMNs, if the main duct and the branch ducts are both involved.[67] However, there is considerable discrepancy between the radiological and the histopathologic assessment of the involved ducts. Studies have shown that the main duct often shows some degree of involvement, even in IPMNs that were classic branch-duct type IPMNs by radiological imaging.[68] Fritz and colleagues[69] showed that 29% of the IPMNs that were considered as branch-duct type on preoperative imaging showed involvement of the main duct histologically. These branch-duct type IPMNs with minimal involvement of the main duct were very similar to pure branch-duct type IPMNs with regard to clinicopathologic features as well as clinical outcome.[68]

A compilation of 3568 resected IPMNs from 20 studies showed that invasive carcinoma was present in 43.6% of main-duct type IPMNs, in 45.3% of mixed type IPMNs, and in 16.6% of branch-duct type IPMNs.[70] The limited percentage of cancer in the resected pancreata shows the clinical problem of overtreatment of IPMNs and, in particular, of the branch-duct type IPMNs. Several guidelines have been proposed for clinical management of IPMNs but the quality of evidence supporting most recommendations is low (Table 1).[70–75]

Pathologic features

IPMNs have been defined in consensus meetings as “grossly visible, predominantly papillary or rarely flat, noninvasive mucin-producing epithelial neoplasm arising in the main pancreatic duct or branch ducts.”[3] By definition, IPMNs are at least 1.0 cm in diameter.[2–4]

As for PanIN, a consensus meeting recently recommended to grade the IPMNs with a 2-tiered grading system. The former IPMN with low-grade dysplasia and IPMN with intermediate-grade dysplasia become IPMN, low grade. The former IPMN with high-grade dysplasia becomes IPMN, high grade.[4]

Sendai Guidelines, 2006[71]	Updated Sendai Guidelines, 2012[70]	American Gastroenterological Association Guidelines, 2015[72]
Guideline for all cysts originating from the pancreatic duct system, suspected to be IPMN Criteria: • Pancreatic fluid cytology with high-grade dysplasia or carcinoma • Presence of a mural nodule • Symptoms • Main pancreatic duct diameter >0.6 cm • Branch duct diameter >3.0 cm	Guideline for all cysts originating from the pancreatic duct system, suspected to be IPMN High-risk stigmata: • Obstructive jaundice in a patient with a cystic lesion of the head of the pancreas • Enhancing solid component within cyst • Main pancreatic duct size ≥1.0 cm Worrisome features: • Pancreatitis • Main pancreatic duct size 0.5–0.9 cm • Cyst size ≥3.0 cm • Thickened enhanced cyst walls • Nonenhanced mural nodules • Abrupt change in the main pancreatic duct caliber with distal pancreatic atrophy • Lymphadenopathy	Guideline for asymptomatic cysts from branch ducts, suspected to be IPMN: High-risk features: • Cyst size ≥3.0 cm • Dilated main pancreatic duct • Presence of a solid component
If at least 1 criterion is present, consider resection	• If at least 1 high-risk stigma is present: consider resection • If no high-risk stigmata are present, but at least 1 worrisome feature is present, consider EUS with FNA In patients with positive cytology or concerning features on EUS (definite mural nodule, main duct features suspicious for involvement), consider resection	If at least 2 high-risk features are present: consider EUS with FNA In patients with positive cytology or concerning features on EUS (definite mural nodule, main duct features suspicious for involvement), consider resection

Abbreviations: EUS, endoscopic ultrasonography; FNA, fine-needle aspiration.

Table 1. A brief overview of the most important current guidelines for the management of IPMNs

IPMNs can be subtyped by their direction of differentiation as gastric, intestinal, pancreatobiliary, or oncocytic.[76]

- Gastric-type IPMN is characterized by cells that resemble the foveolar epithelium of the stomach with a single layer of cells with basally oriented nuclei and abundant mucinous cytoplasm. This epithelium can show a flat, papillary, or tubular/ductal growth pattern (Figure 3). This subtype is rarely associated with high-grade dysplasia compared with other subtypes.[77] However, when high-grade dysplasia is present, the architecture becomes complex and the cuboidal cells with enlarged nuclei become mucin depleted, features that are very similar to pancreatobiliary-type IPMN.[78] Some investigators consider these features as different grades of dysplasia, whereas others consider them as different subtypes of IPMN.[79,80] Gastric-type IPMNs typically involve the branch ducts.[81]

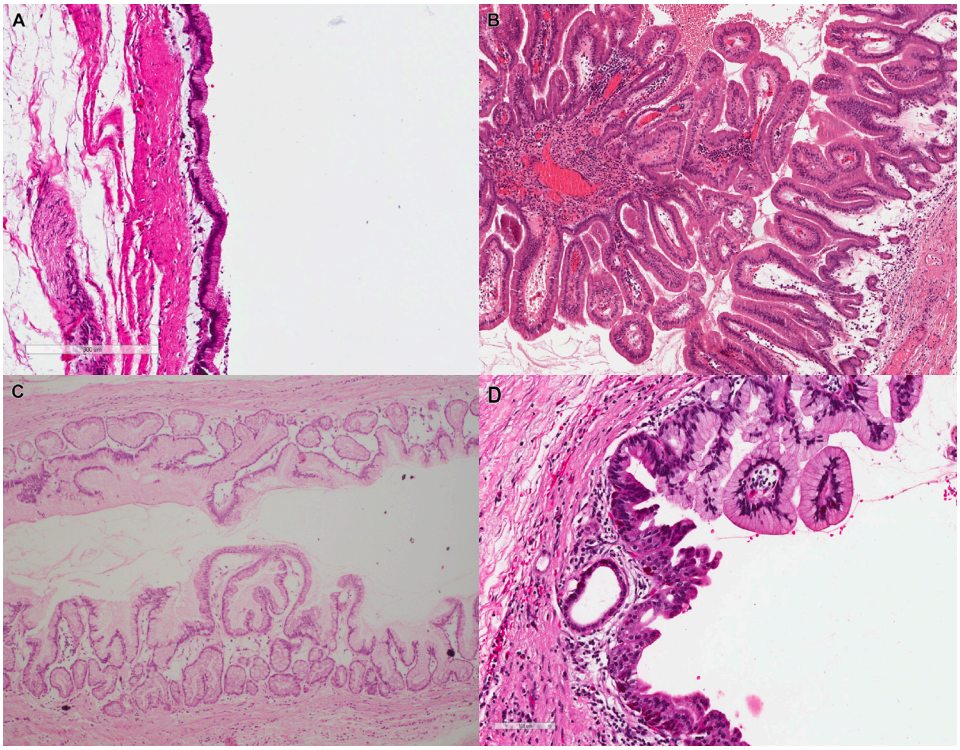

Figure 3. Gastric-type IPMN. (A) Gastric-type IPMN with a flat architecture and a single layer of gastric foveolar-type epithelium. (B) Gastric-type IPMN with a villous architecture. (C) Gastric-type IPMN with basal tubular/ductal growth. When tubular growth is extensive, these lesions have previously been designated as intraductal tubular adenoma, pyloric gland type, pyloric gland adenoma, or intraductal tubular adenoma (see Figure 8). (D) IPMN with low-grade and high-grade dysplasia. Some investigators consider this as different subtypes of IPMN (ie, gastric-type IPMN and pancreatobiliary-type IPMN, respectively) whereas others consider this as different grades of dysplasia of gastric-type IPMN.

- The pancreatobiliary-type IPMN is lined by cells with nuclei with marked variation in size and shape; these nuclei have irregular contours and prominent nucleoli and are most likely to progress to an invasive tubular carcinoma (Figure 4).[81]

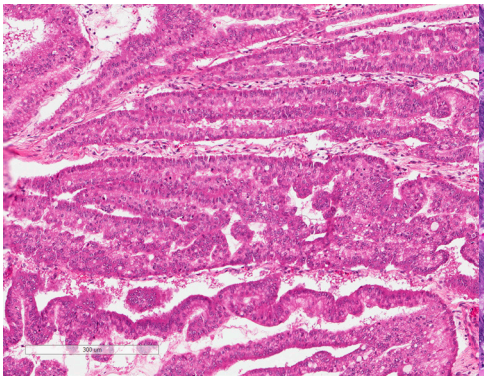

Figure 4. Pancreatobiliary-type IPMN lined by cells with marked atypia and prominent nucleoli.

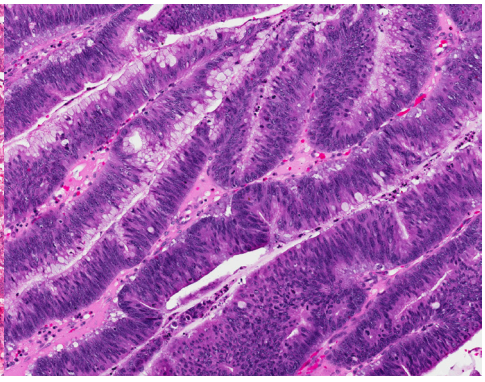

Figure 5. Intestinal-type IPMN with high-grade dysplasia composed of papillae lined by cells with elongated nuclei and some degree of pseudostratification reminiscent of a colonic villous adenoma. Note the scattered goblet cells.

- The intestinal-type IPMN is morphologically similar to a colonic villous adenoma. The nuclei of the cells are hyperchromatic, elongated, show some degree of pseudostratification, and contain variable amounts of intracellular mucin. The papillae are typically long and occasionally branching. This subtype most frequently involves the main duct (Figure 5).[81]
- Oncocytic-type IPMN is a rare entity, characterized by cells with abundant eosinophilic cytoplasm, caused by the accumulation of mitochondria. The nuclei of these oncocytic cells contain a single, prominent, eccentric nucleolus. The growth pattern of these oncocytic-type IPMNs is distinctive, consisting of arborizing papillae, lined by 1 to 5 layers of cuboidal cells. A specific feature is the punched-out spaces in the epithelium (Figure 6).

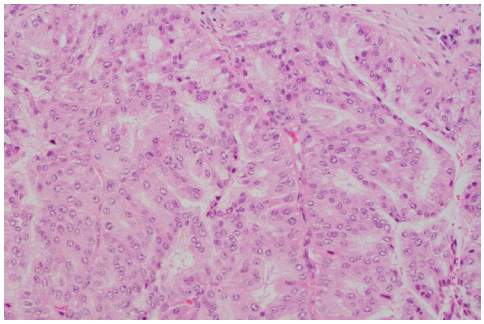

Figure 6. Oncocytic-type IPMN, composed of cells with abundant eosinophilic cytoplasm, reflecting the accumulation of mitochondria.

The 2010 World Health Organization classification of tumors of the digestive system provided an immunohistochemical aid for subtyping these IPMNs based on mucin stains. However, several studies have shown that some IPMNs are unclassifiable because of their uncharacteristic morphology and immunophenotype.[82–86] Mixed epithelial differentiation makes subtyping impossible in 25% of cases. For these reasons and because of the moderate interobserver agreement for morphologic subtyping of pancreatic IPMNs, subtyping of IPMNs has a poor reproducibility.[87] Studies have reported differences in prognosis between the various subtypes of IPMNs, despite the poor reproducibility, which suggests that associations between histologic type and prognosis may be even stronger than reported.[77,81,83,87–90] A recent meta-analysis reviewed 14 studies and showed that the pancreatobiliary-type IPMN is associated with the most aggressive behavior and gastric-type IPMN has the lowest risk of invasive carcinoma.[81]

Molecular features

Whole-exome sequencing of IPMNs revealed an average of 26 mutated genes per IPMN.[91] *KRAS* and *GNAS* are the most frequently mutated genes in 50% to 80% and 40% to 60% of IPMNs, respectively.[91,92] Moreover, *RNF43*, an E3 ubiquitin–protein ligase acting as a negative regulator of the Wnt-signaling pathway, is also frequently mutated in IPMN.[91] In addition, *P53* and *SMAD4* mutations can be found in high-grade dysplasia.

Evidence is accumulating for the existence of 2 distinct molecular progression pathways in IPMN[20,93]:

- Pancreatobiliary-type IPMN is highly associated with tubular carcinoma, which has a mutation profile resembling conventional pancreatic adenocarcinoma including *KRAS* mutations.[93–95] *GNAS* mutations are less common in this presumed pathway.
- Intestinal-type IPMNs and associated colloid carcinomas typically harbor *GNAS* mutations, which is another similarity between intestinal-type IPMN and colonic villous adenomas.[96]

These different pathways are also reflected in a different immunophenotype with colloid carcinomas being MUC1 negative (0%) and MUC2 positive (100%), whereas tubular carcinomas are typically MUC1 positive (63%) and MUC2 negative (1%).[20] Colloid carcinomas have a less aggressive behavior and a better prognosis than tubular carcinomas.[83,84] In gastric-type IPMNs, *KRAS* and *GNAS* mutations are identified equally. This finding suggests that gastric-type IPMNs are a heterogenic group of early lesions with a similar morphologic appearance, but, on a molecular level, are already committed to one of the 2 progression pathways.[93]

DIFFERENTIAL DIAGNOSIS: PANCREATIC INTRAEPITHELIAL NEOPLASIA VERSUS INTRADUCTAL PAPILLARY MUCINOUS NEOPLASM

By definition, PanINs are smaller than 0.5 cm and IPMNs are at least 1.0 cm, which means that there is an indeterminate range between PanIN and IPMN for intraductal neoplastic precursor lesions with a diameter of greater than or equal to 0.5 cm and less than 1.0 cm. These lesions can be either large PanINs or small IPMNs. Differentiation of the epithelium toward intestinal-type, pancreatobiliary-type, or oncocytic-type epithelium or a mutation specific for IPMN (such as *GNAS* mutation) are clues for an IPMN.[4,76] If these clues are present, these lesions can be called incipient IPMN. However, small, gastric-type lesions, without features of an IPMN, should be documented descriptively.[4]

Initially, PanINs were defined as lesions arising from the ductules or small ducts, whereas IPMNs involve the main pancreatic duct or its major branches.[2,97,98] However, several case reports suggested that some PanINs arise from larger ducts, including the main duct.[11,97,99] Some of these PanINs may cause obstruction and retrograde dilatation of the duct, causing it to expand beyond the 1.0 cm cutoff. To address these large and main duct PanINs, the 2004 consensus guidelines defined diagnostic criteria, apart from the size criteria, to distinguish PanINs from IPMNs[3]:

- Papillae in PanIN are not as tall and complex as those in IPMN
- Abundant luminal mucin production is a feature of IPMN
- MUC2 expression is a specific, but insensitive, marker of an IPMN and is generally not present in PanIN

INTRADUCTAL TUBULOPAPILLARY NEOPLASM

Clinical features

Intraductal tubulopapillary neoplasms (ITPNs) are rare intraductal neoplasms of the pancreas. They occur equally in men and women. Symptoms are nonspecific and include abdominal pain, diabetes, vomiting, and weight loss. About 50% of these neoplasms involve the head of the pancreas, 30% diffusely involve the pancreas,[100] 15% are localized in the tail of the pancreas,[101] and 40% of cases harbor an associated invasive carcinoma. With a 5-year survival of more than 30%, prognosis of an ITPN-associated invasive tumor is significantly better than the prognosis of conventional PDAC. Recurrence or metastasis to lymph nodes or to the liver is seen in about a third of cases. Even these

patients sometimes experience a protracted clinical course over more than 2 years, which is unusual for conventional PDAC.[100]

Pathologic features

ITPN is characterized by densely packed tubules that frequently lie back to back, forming large sheets. Tubulopapillary growth is sometimes seen. The cells are cuboidal with modest amounts of eosinophilic cytoplasm and do not contain apparent mucin. There is moderate nuclear atypia and increased mitotic activity (Figure 7). Extracellular mucin production is not prominent and cyst formation is less evident than in IPMN. Comedolike necrosis is sometimes present.[102]

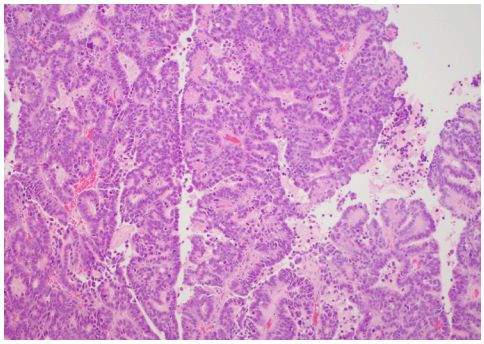

Figure 7. Intraductal tubulopapillary neoplasm with features of both tubular and papillary growth.

In contrast with IPMN, immunohistochemistry for MUC5AC is typically negative in ITPNs.[28,102] MUC1 and MUC6 are positive in 100% and 60% of cases, respectively.[102] Because of similar morphology and shared positivity for MUC6 with gastric and duodenal pyloric gland adenomas, ITPNs have previously been described as intraductal, tubular adenomas, pyloric gland type.[103,104]

Pitfalls in diagnostic pathology of ITPN:

- ITPN should be differentiated from gastric-type IPMN with extensive tubular growth (Figure 8). In the past, intraductal lesions with extensive tubular growth were distinguished from IPMN and designated as intraductal tubular adenoma, pyloric gland type or pyloric gland adenoma.103–111 Later, this entity was renamed intraductal tubular adenoma (ITA) and intraductal tubular carcinoma (ITC), depending on the degree of dysplasia. Further studies showed that ITAs were more related to gastric-type IPMNs and ITCs were a different entity, with a different immunoprofile and different molecular changes, now known as ITPN.[112]
- Occasionally, acinar cell carcinomas have a component of intraductal polypoid growth.[113] When this intraductal growth becomes predominant, acinar cell carcinoma can mimic other intraductal neoplasms, such as ITPNs (Figure 9). The architecture of both tumors can be very similar with sheets of back-to-back acinar structures. The presence of PAS+, diastase-resistant, apical, eosinophilic zymogen granules; intraluminal concretions; and prominent, central nucleoli are helpful features to distinguish acinar cell carcinomas from ITPNs (Figure 9).[114] Moreover, on immunohistochemistry, acinar cell carcinomas are positive for trypsin, chymotrypsin, and BCL10, and negative for CK19. ITPNs are negative for trypsin, chymotrypsin, and BCL10, but positive for CK19.[115]

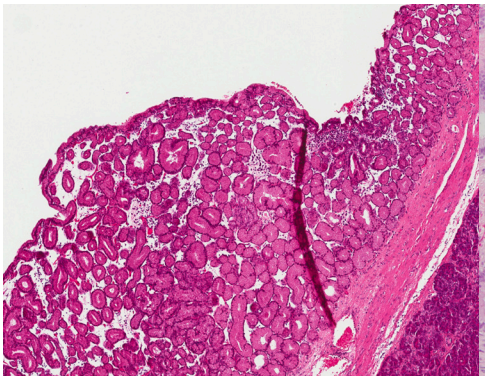

Figure 8. An intraductal, low-grade neoplasm, formerly known as an intraductal tubular adenoma (ITA), now better classified as a gastric-type IPMN with an extensive tubular/ductal growth pattern.

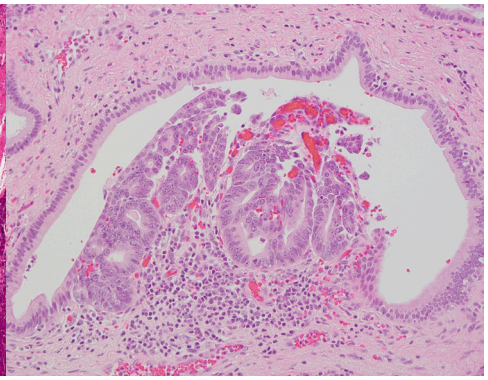

Figure 9. Intraductal growth of an acinar cell carcinoma showing acinar structures composed of cells with single, large, central nucleoli.

Molecular features

ITPNs also differ from IPMNs on a molecular level. *KRAS* and *GNAS* mutations, frequently found in IPMNs, are found in only 7% and 0% of ITPNs, respectively.[116–119] However, *PIK3CA* mutations are frequently seen in ITPNs (21%–27%).[116,120] As a component of the mammalian target of rapamycin (mTOR) pathway, *PIK3CA* is a potentially targetable mutation, because multiple drugs (like temsirolimus and everolimus) targeting the mTOR pathway have been tested and approved for clinical use.[121,122]

MUCINOUS CYSTIC NEOPLASMS

Clinical features

MCNs are almost exclusively seen in perimenopausal women. Only a few rare examples are documented in men.[123] This finding is in accordance with their counterparts in the hepatobiliary tree, mesentery, and retroperitoneum, and with the mixed epithelial and stromal tumor of the kidney, which are also more prevalent in women.[124–127] It has been hypothesized that pancreatic MCN develops from endodermal immature stroma, stimulated by female hormones.[128,129] MCNs are mainly located in the pancreatic body and tail and do not communicate with the pancreatic duct system.[130,131] The mean age of presentation of patients with a noninvasive MCN is 44 years. The mean age of presentation of patients with an MCN with associated adenocarcinoma is 55 years.[131]

Patients frequently present with nonspecific symptoms such as mild abdominal pain but some present with pancreatitis.[131]

Like IPMNs, MCNs frequently have high levels of carcinoembryonic antigen and mucinous epithelial cells in the cyst fluid.[132,133] An adenocarcinoma associated with MCN is found in 3% to 36% of resected MCNs. Overall, the mean percentage of adenocarcinoma found in 1096 resected MCNs from 9 studies was 16%,[128,130,131,134–139] which is less than is seen in main-duct type and mixed type IPMNs. Guidelines recommend resection of each MCN, irrespective of size.[70,71]

Pathologic features

MCNs are lined by columnar cells with abundant apical mucin. Dysplastic change of the epithelial lining is graded in a 2-tiered system, as recommended by the latest consensus meeting. The former MCN with low-grade dysplasia and MCN with intermediate-grade dysplasia are now both classified as MCN, low grade.[4] Two distinct features that distinguish this tumor from an IPMN are the presence of characteristic ovarian-type stroma and lack of communication with the pancreatic duct system[70,101] (Figure 10). When an MCN evolves into an invasive carcinoma, this is typically a tubular adenocarcinoma. MCNs rarely evolve into a colloid carcinoma, although an early study showed focal staining for CDX2 indicating intestinal differentiation in 51% of MCNs.[137,140] MCNs with malignant, sarcomatous stroma have been reported but are more likely spindle cell carcinomas rather than true mesenchymal neoplasms.[141–144]

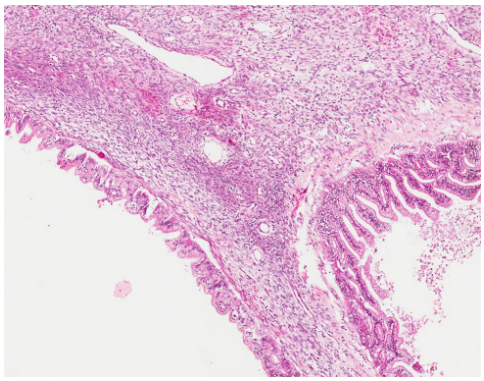

Figure 10. MCN with mucinous epithelium with low-grade dysplasia and characteristic ovarian-type stroma.

Ovarian-type stroma may be only focally present or not obvious because of fibrosis or hypocellularity.[128,136] Sometimes, nests of epithelioid cells are seen in the stroma, suggesting luteinization. Rarely, a corpus luteum can be seen in the stroma. The cells of the ovarian-type stroma frequently express progesterone and estrogen receptor, inhibin, caldesmon, alfa-SMA, and desmin.[124,135]

Molecular features

Whole-exome sequencing of the MCNs showed on average 16.0 ± 7.6 nonsynonymous somatic mutations and few loss of heterozygosity events compared with IPMNs,[91] which could explain the lower frequency of progression to an invasive carcinoma in MCNs, because there is a correlation between aneuploidy and a poor prognosis.[145] Only 1 region on chromosome 17q, containing the gene *RNF43*, was lost in more than 1 tumor. In 3 MCNs, intragenic mutations were found in the *RNF43* gene. Further analysis showed mutations in the 4 main pancreatic cancer genes *KRAS*, *CDKN2A*, *P53*, and *SMAD4*.[91]

SUMMARY

In the last 2 decades, a morphologic classification of precursor lesions to invasive adenocarcinoma of the pancreas has been established. Three precursor lesions are distinguished: PanIN, IPMN, and MCN. Each of these lesions has its own clinicopathologic manifestations. PanIN is the most prevalent precursor lesion, but is microscopic and not reliably detectable on imaging. IPMN is a macroscopic, cystic lesion, detectable on imaging and may therefore serve as a target for screening and prevention of pancreatic cancer. In addition, MCN is almost always found in the pancreatic body and tail of peri-

menopausal women. When detected in an early stage without associated adenocarcinoma, resection of IPMN and MCN is curative. However, because of the lack of biomarkers for high-risk lesions, selection of patients who benefit from resection is difficult. Further high-quality clinical and molecular studies are essential to improve clinical decision making in the management of these precursor lesions.[73–75]

REFERENCES

1. Hulst, S. P. L. Zur Kenntnis der Genese des Adenokarzinoms und Karzinoms des Pankreas. Virchows Arch. Pathol. Anat. Physiol. Klin. Med. 180, 288–316 (1905).
2. Hruban, R. H. et al. Pancreatic intraepithelial neoplasia: a new nomenclature and classification system for pancreatic duct lesions. Am. J. Surg. Pathol. 25, 579–586 (2001).
3. Hruban, R. H. et al. An illustrated consensus on the classification of pancreatic intraepithelial neoplasia and intraductal papillary mucinous neoplasms. Am. J. Surg. Pathol. 28, 977–987 (2004).
4. Basturk, O. et al. A Revised Classification System and Recommendations From the Baltimore Consensus Meeting for Neoplastic Precursor Lesions in the Pancreas. Am. J. Surg. Pathol. 39, 1730–1741 (2015).
5. Berman, J. J. et al. Precancer: a conceptual working definition -- results of a Consensus Conference. Cancer Detect. Prev. 30, 387–394 (2006).
6. Cubilla, A. L. & Fitzgerald, P. J. Morphological lesions associated with human primary invasive nonendocrine pancreas cancer. Cancer Res. 36, 2690–2698 (1976).
7. Andea, A., Sarkar, F. & Adsay, V. N. Clinicopathological correlates of pancreatic intraepithelial neoplasia: a comparative analysis of 82 cases with and 152 cases without pancreatic ductal adenocarcinoma. Mod. Pathol. 16, 996–1006 (2003).
8. Recavarren, C. et al. Histologic characteristics of pancreatic intraepithelial neoplasia associated with different pancreatic lesions. Hum. Pathol. 42, 18–24 (2011).
9. Brune, K. et al. Multifocal neoplastic precursor lesions associated with lobular atrophy of the pancreas in patients having a strong family history of pancreatic cancer. Am. J. Surg. Pathol. 30, 1067–1076 (2006).
10. Shi, C. et al. Increased Prevalence of Precursor Lesions in Familial Pancreatic Cancer Patients. Clin. Cancer Res. 15, 7737–7743 (2009).
11. Takaori, K. et al. Carcinoma in situ of the pancreas associated with localized fibrosis: a clue to early detection of neoplastic lesions arising from pancreatic ducts. Pancreas 17, 102–105 (1998).
12. Detlefsen, S., Sipos, B., Feyerabend, B. & Klöppel, G. Pancreatic fibrosis associated with age and ductal papillary hyperplasia. Virchows Arch. 447, 800–805 (2005).
13. Brat, D. J., Lillemoe, K. D., Yeo, C. J., Warfield, P. B. & Hruban, R. H. Progression of pancreatic intraductal neoplasias to infiltrating adenocarcinoma of the pancreas. Am. J. Surg. Pathol. 22, 163–169 (1998).
14. Ban, S., Shimizu, Y., Ogawa, F. & Shimizu, M. Re-evaluation of 'Cancerization of the Duct' by Pancreatic Cancers. (2007).
15. Konstantinidis, I. T. et al. Incidentally discovered pancreatic intraepithelial neoplasia: what is its clinical significance? Ann. Surg. Oncol. 20, 3643–3647 (2013).
16. Longnecker, D. S. et al. Histopathological diagnosis of pancreatic intraepithelial neoplasia and intraductal papillary-mucinous neoplasms: interobserver agreement. Pancreas 31, 344–349 (2005).
17. Matthaei, H. et al. Presence of pancreatic intraepithelial neoplasia in the pancreatic transection margin does not influence outcome in patients with R0 resected pancreatic cancer. Ann. Surg. Oncol. 18, 3493–3499 (2011).
18. Maitra, A. et al. Multicomponent analysis of the pancreatic adenocarcinoma progression model using a pancreatic intraepithelial neoplasia tissue microarray. Mod. Pathol. 16, 902–912 (2003).
19. Nagata, K. et al. Mucin expression profile in pancreatic cancer and the precursor lesions. J. Hepatobiliary. Pancreat. Surg. 14, 243–254 (2007).
20. Adsay, N. V. et al. The dichotomy in the preinvasive neoplasia to invasive carcinoma sequence in the pancreas: differential expression of MUC1 and MUC2 supports the existence of two separate pathways of carcinogenesis. Mod. Pathol. 15, 1087–1095 (2002).
21. Moriya, T. et al. Biological similarities and differences between pancreatic intraepithelial neoplasias and intraductal papillary mucinous neoplasms. Int. J. Gastrointest. Cancer 35, 111–119 (2005).
22. Basturk, O. et al. Preferential expression of MUC6 in oncocytic and pancreatobiliary types of intraductal papillary neoplasms highlights a pyloropancreatic pathway, distinct from the intestinal pathway, in pancreatic carcinogenesis. Am. J. Surg. Pathol. 34, 364–370 (2010).
23. Kozuka, S. et al. Relation of pancreatic duct hyperplasia to carcinoma. Cancer 43, 1418–1428 (1979).
24. Klimstra, D. S. & Longnecker, D. S. K-ras mutations in pancreatic ductal proliferative lesions. The American journal of pathology vol. 145 1547–1550 (1994).
25. Lemoine, N. R. et al. Ki-ras oncogene activation in preinvasive pancreatic cancer. Gastroenterology 102, 230–236 (1992).
26. Yanagisawa, A. et al. Frequent c-Ki-ras oncogene activation in mucous cell hyperplasias of pancreas suffering from chronic inflammation. Cancer Res. 53, 953–956 (1993).
27. DiGiuseppe, J. A. et al. Detection of K-ras mutations in mucinous pancreatic duct hyperplasia from

a patient with a family history of pancreatic carcinoma. Am. J. Pathol. 144, 889–895 (1994).
28. Lüttges, J. et al. Allelic loss is often the first hit in the biallelic inactivation of the p53 and DPC4 genes during pancreatic carcinogenesis. Am. J. Pathol. 158, 1677–1683 (2001).
29. van Heek, N. T. et al. Telomere shortening is nearly universal in pancreatic intraepithelial neoplasia. Am. J. Pathol. 161, 1541–1547 (2002).
30. Moskaluk, C. A., Hruban, R. H. & Kern, S. E. p16 and K-ras gene mutations in the intraductal precursors of human pancreatic adenocarcinoma. Cancer Res. 57, 2140–2143 (1997).
31. Brosens, L. A. A., Hackeng, W. M., Offerhaus, G. J., Hruban, R. H. & Wood, L. D. Pancreatic adenocarcinoma pathology: changing 'landscape'. J. Gastrointest. Oncol. 6, 358–374 (2015).
32. Werner, J., Fritz, S. & Büchler, M. W. Intraductal papillary mucinous neoplasms of the pancreas--a surgical disease. Nat. Rev. Gastroenterol. Hepatol. 9, 253–259 (2012).
33. Habán, G. Papillomatose und Carcinom des Gangsystems der Bauchspeicheldrüse. Virchows Arch. Pathol. Anat. Physiol. Klin. Med. 297, 207–220 (1936).
34. Sessa, F. et al. Intraductal papillary-mucinous tumours represent a distinct group of pancreatic neoplasms: an investigation of tumour cell differentiation and K-ras, p53 and c-erbB-2 abnormalities in 26 patients. Virchows Arch. 425, 357–367 (1994).
35. Morohoshi, T., Kanda, M., Asanuma, K. & Klöppel, G. Intraductal papillary neoplasms of the pancreas. A clinicopathologic study of six patients. Cancer 64, 1329–1335 (1989).
36. Ingkakul, T., Warshaw, A. L. & Fernández-Del Castillo, C. Epidemiology of intraductal papillary mucinous neoplasms of the pancreas: sex differences between 3 geographic regions. Pancreas 40, 779–780 (2011).
37. Salvia, R. et al. Main-duct intraductal papillary mucinous neoplasms of the pancreas: clinical predictors of malignancy and long-term survival following resection. Ann. Surg. 239, 678–85; discussion 685–7 (2004).
38. Chari, S. T. et al. Study of recurrence after surgical resection of intraductal papillary mucinous neoplasm of the pancreas. Gastroenterology 123, 1500–1507 (2002).
39. 39. Ingkakul, T. et al. Predictors of the presence of concomitant invasive ductal carcinoma in intraductal papillary mucinous neoplasm of the pancreas. Ann. Surg. 251, 70–75 (2010).
40. Sohn, T. A. et al. Intraductal papillary mucinous neoplasms of the pancreas: an updated experience. Ann. Surg. 239, 788–97; discussion 797–9 (2004).
41. Crippa, S. et al. Mucin-producing neoplasms of the pancreas: an analysis of distinguishing clinical and epidemiologic characteristics. Clin. Gastroenterol. Hepatol. 8, 213–219 (2010).
42. Maire, F. et al. Intraductal papillary and mucinous pancreatic tumour: a new extracolonic tumour in familial adenomatous polyposis. Gut 51, 446–449 (2002).
43. Gaujoux, S. et al. Pancreatic ductal and acinar cell neoplasms in Carney complex: a possible new association. J. Clin. Endocrinol. Metab. 96, E1888–95 (2011).
44. Gaujoux, S., Chanson, P., Bertherat, J., Sauvanet, A. & Ruszniewski, P. Hepato-pancreato-biliary lesions are present in both Carney complex and McCune Albright syndrome: comments on P. Salpea and C. Stratakis. Mol. Cell. Endocrinol. 382, 344–345 (2014).
45. Salpea, P. et al. Deletions of the PRKAR1A locus at 17q24.2-q24.3 in Carney complex: genotype-phenotype correlations and implications for genetic testing. J. Clin. Endocrinol. Metab. 99, E183–8 (2014).
46. Su, G. H. et al. Germline and somatic mutations of the STK11/LKB1 Peutz-Jeghers gene in pancreatic and biliary cancers. Am. J. Pathol. 154, 1835–1840 (1999).
47. Poley, J. W. et al. The yield of first-time endoscopic ultrasonography in screening individuals at a high risk of developing pancreatic cancer. Am. J. Gastroenterol. 104, 2175–2181 (2009).
48. Sparr, J. A., Bandipalliam, P., Redston, M. S. & Syngal, S. Intraductal papillary mucinous neoplasm of the pancreas with loss of mismatch repair in a patient with Lynch syndrome. Am. J. Surg. Pathol. 33, 309–312 (2009).
49. Ferrone, C. R. et al. Current trends in pancreatic cystic neoplasms. Arch. Surg. 144, 448–454 (2009).
50. Traverso, L. W., Peralta, E. A., Ryan, J. A., Jr & Kozarek, R. A. Intraductal neoplasms of the pancreas. Am. J. Surg. 175, 426–432 (1998).
51. Klöppel, G. Clinicopathologic view of intraductal papillary-mucinous tumor of the pancreas. Hepatogastroenterology 45, 1981–1985 (1998).
52. Fernández-del Castillo, C. et al. Incidental pancreatic cysts: clinicopathologic characteristics and comparison with symptomatic patients. Arch. Surg. 138, 427–3; discussion 433–4 (2003).
53. Tanaka, M., Kobayashi, K., Mizumoto, K. & Yamaguchi, K. Clinical aspects of intraductal papillary mucinous neoplasm of the pancreas. J. Gastroenterol. 40, 669–675 (2005).
54. Yamaguchi, K. & Tanaka, M. Mucin-hypersecreting tumor of the pancreas with mucin extrusion through an enlarged papilla. Am. J. Gastroenterol.

86, 835–839 (1991).
55. Zhang, X.-M., Mitchell, D. G., Dohke, M., Holland, G. A. & Parker, L. Pancreatic cysts: depiction on single-shot fast spin-echo MR images. Radiology 223, 547–553 (2002).
56. Matsubara, S. et al. Incidental pancreatic cysts found by magnetic resonance imaging and their relationship with pancreatic cancer. Pancreas 41, 1241–1246 (2012).
57. Moris, M. et al. Association Between Advances in High-Resolution Cross-Section Imaging Technologies and Increase in Prevalence of Pancreatic Cysts From 2005 to 2014. Clin. Gastroenterol. Hepatol. 14, 585–593.e3 (2016).
58. Lee, K. S., Sekhar, A., Rofsky, N. M. & Pedrosa, I. Prevalence of incidental pancreatic cysts in the adult population on MR imaging. Am. J. Gastroenterol. 105, 2079–2084 (2010).
59. Kimura, W., Nagai, H., Kuroda, A., Muto, T. & Esaki, Y. Analysis of small cystic lesions of the pancreas. Int. J. Pancreatol. 18, 197–206 (1995).
60. Spinelli, K. S. et al. Cystic pancreatic neoplasms: observe or operate. Ann. Surg. 239, 651–7; discussion 657–9 (2004).
61. Ikeda, M. et al. Morphologic changes in the pancreas detected by screening ultrasonography in a mass survey, with special reference to main duct dilatation, cyst formation, and calcification. Pancreas 9, 508–512 (1994).
62. Lee, S. H. et al. Outcomes of cystic lesions in the pancreas after extended follow-up. Dig. Dis. Sci. 52, 2653–2659 (2007).
63. Edirimanne, S. & Connor, S. J. Incidental pancreatic cystic lesions. World J. Surg. 32, 2028–2037 (2008).
64. Girometti, R. et al. Incidental pancreatic cysts on 3D turbo spin echo magnetic resonance cholangiopancreatography: prevalence and relation with clinical and imaging features. Abdom. Imaging 36, 196–205 (2011).
65. de Jong, K. et al. High prevalence of pancreatic cysts detected by screening magnetic resonance imaging examinations. Clin. Gastroenterol. Hepatol. 8, 806–811 (2010).
66. 66. Goh, B. K. P. et al. Cystic lesions of the pancreas: an appraisal of an aggressive resectional policy adopted at a single institution during 15 years. Am. J. Surg. 192, 148–154 (2006).
67. Nagai, K. et al. Intraductal papillary mucinous neoplasms of the pancreas: clinicopathologic characteristics and long-term follow-up after resection. World J. Surg. 32, 271–8; discussion 279–80 (2008).
68. Sahora, K. et al. Not all mixed-type intraductal papillary mucinous neoplasms behave like main-duct lesions: implications of minimal involvement of the main pancreatic duct. Surgery 156, 611–621 (2014).
69. Fritz, S. et al. Pancreatic main-duct involvement in branch-duct IPMNs: an underestimated risk. Ann. Surg. 260, 848–55; discussion 855–6 (2014).
70. Tanaka, M. et al. International consensus guidelines 2012 for the management of IPMN and MCN of the pancreas. Pancreatology 12, 183–197 (2012).
71. Tanaka, M. et al. International consensus guidelines for management of intraductal papillary mucinous neoplasms and mucinous cystic neoplasms of the pancreas. Pancreatology 6, 17–32 (2006).
72. Vege, S. S. et al. American gastroenterological association institute guideline on the diagnosis and management of asymptomatic neoplastic pancreatic cysts. Gastroenterology 148, 819–22; quize12–3 (2015).
73. Moayyedi, P., Weinberg, D. S., Schünemann, H. & Chak, A. Management of pancreatic cysts in an evidence-based world. Gastroenterology vol. 148 692–695 (2015).
74. Canto, M. I. & Hruban, R. H. Managing pancreatic cysts: less is more? Gastroenterology vol. 148 688–691 (2015).
75. Lennon, A. M., Ahuja, N. & Wolfgang, C. L. AGA Guidelines for the Management of Pancreatic Cysts. Gastroenterology vol. 149 825 (2015).
76. Furukawa, T. et al. Classification of types of intraductal papillary-mucinous neoplasm of the pancreas: a consensus study. Virchows Arch. 447, 794–799 (2005).
77. Furukawa, T. et al. Prognostic relevance of morphological types of intraductal papillary mucinous neoplasms of the pancreas. Gut 60, 509–516 (2011).
78. Adsay, N. V. et al. Pathologically and biologically distinct types of epithelium in intraductal papillary mucinous neoplasms: delineation of an 'intestinal' pathway of carcinogenesis in the pancreas. Am. J. Surg. Pathol. 28, 839–848 (2004).
79. Adsay, N. V., Conlon, K. C., Zee, S. Y., Brennan, M. F. & Klimstra, D. S. Intraductal papillary-mucinous neoplasms of the pancreas: an analysis of in situ and invasive carcinomas in 28 patients. Cancer 94, 62–77 (2002).
80. Ban, S. et al. Intraductal papillary mucinous neoplasm (IPMN) of the pancreas: its histopathologic difference between 2 major types. Am. J. Surg. Pathol. 30, 1561–1569 (2006).
81. Koh, Y. X. et al. Systematic review and meta-analysis of the spectrum and outcomes of different histologic subtypes of noninvasive and invasive intraductal papillary mucinous neoplasms. Surgery 157, 496–509 (2015).
82. Tsutsumi, K. et al. Expression of claudin-4 (CLDN4) mRNA in intraductal papillary mucinous

neoplasms of the pancreas. Mod. Pathol. 24, 533–541 (2011).
83. Nakata, K. et al. Invasive carcinoma derived from intestinal-type intraductal papillary mucinous neoplasm is associated with minimal invasion, colloid carcinoma, and less invasive behavior, leading to a better prognosis. Pancreas 40, 581–587 (2011).
84. Sadakari, Y. et al. Invasive carcinoma derived from the nonintestinal type intraductal papillary mucinous neoplasm of the pancreas has a poorer prognosis than that derived from the intestinal type. Surgery 147, 812–817 (2010).
85. Yonezawa, S., Higashi, M., Yamada, N., Yokoyama, S. & Goto, M. Significance of mucin expression in pancreatobiliary neoplasms. J. Hepatobiliary Pancreat. Sci. 17, 108–124 (2010).
86. Kobayashi, M., Fujinaga, Y. & Ota, H. Reappraisal of the Immunophenotype of Pancreatic Intraductal Papillary Mucinous Neoplasms (IPMNs)-Gastric Pyloric and Small Intestinal Immunophenotype Expression in Gastric and Intestinal Type IPMNs-. Acta Histochem. Cytochem. 47, 45–57 (2014).
87. Schaberg, K. B., DiMaio, M. A. & Longacre, T. A. Intraductal Papillary Mucinous Neoplasms Often Contain Epithelium From Multiple Subtypes and/or Are Unclassifiable. Am. J. Surg. Pathol. 40, 44–50 (2016).
88. Mino-Kenudson, M. et al. Prognosis of invasive intraductal papillary mucinous neoplasm depends on histological and precursor epithelial subtypes. Gut 60, 1712–1720 (2011).
89. Distler, M. et al. Pathohistological subtype predicts survival in patients with intraductal papillary mucinous neoplasm (IPMN) of the pancreas. Ann. Surg. 258, 324–330 (2013).
90. Kim, J. et al. Prognostic relevance of pathologic subtypes and minimal invasion in intraductal papillary mucinous neoplasms of the pancreas. Tumour Biol. 32, 535–542 (2011).
91. Wu, J. et al. Whole-exome sequencing of neoplastic cysts of the pancreas reveals recurrent mutations in components of ubiquitin-dependent pathways. Proc. Natl. Acad. Sci. U. S. A. 108, 21188–21193 (2011).
92. Wu, J. et al. Recurrent *GNAS* mutations define an unexpected pathway for pancreatic cyst development. Sci. Transl. Med. 3, 92ra66 (2011).
93. Tan, M. C. et al. *GNAS* and *KRAS* Mutations Define Separate Progression Pathways in Intraductal Papillary Mucinous Neoplasm-Associated Carcinoma. J. Am. Coll. Surg. 220, 845–854.e1 (2015).
94. Molin, M. D. et al. Clinicopathological correlates of activating *GNAS* mutations in intraductal papillary mucinous neoplasm (IPMN) of the pancreas. Ann. Surg. Oncol. 20, 3802–3808 (2013).
95. Hosoda, W. et al. *GNAS* mutation is a frequent event in pancreatic intraductal papillary mucinous neoplasms and associated adenocarcinomas. Virchows Arch. 466, 665–674 (2015).
96. Yamada, M. et al. Frequent activating *GNAS* mutations in villous adenoma of the colorectum. J. Pathol. 228, 113–118 (2012).
97. Takaori, K. Dilemma in classifications of possible precursors of pancreatic cancer involving the main pancreatic duct: PanIN or IPMN? J. Gastroenterol. 38, 311–313 (2003).
98. Takaori, K. Current understanding of precursors to pancreatic cancer. J. Hepatobiliary. Pancreat. Surg. 14, 217–223 (2007).
99. Kogire, M. et al. Atypical ductal hyperplasia of the pancreas associated with a stricture of the main pancreatic duct. Journal of gastroenterology vol. 38 295–297 (2003).
100. DS Klimstra, NV Adsay, D Dhall, M Shimizu, K Cymes, O Basturk, G Kloppel. Intraductal Tubular Carcinoma of the Pancreas: Clinicopathologic and Immunohistochemical Analysis of 18 Cases. Mod. Pathol. 20, 285 (2007).
101. Bosman, F. T., Carneiro, F., Hruban, R. H., Theise, N. D. & Others. WHO classification of tumours of the digestive system. (World Health Organization, 2010).
102. Yamaguchi, H. et al. Intraductal tubulopapillary neoplasms of the pancreas distinct from pancreatic intraepithelial neoplasia and intraductal papillary mucinous neoplasms. Am. J. Surg. Pathol. 33, 1164–1172 (2009).
103. Bakotic, B. W. et al. Pyloric gland adenoma of the main pancreatic duct. Am. J. Surg. Pathol. 23, 227–231 (1999).
104. Albores-Saavedra, J., Sheahan, K., O'Riain, C. & Shukla, D. Intraductal tubular adenoma, pyloric type, of the pancreas: additional observations on a new type of pancreatic neoplasm. Am. J. Surg. Pathol. 28, 233–238 (2004).
105. Kato, N., Akiyama, S. & Motoyama, T. Pyloric gland-type tubular adenoma superimposed on intraductal papillary mucinous tumor of the pancreas. Pyloric gland adenoma of the pancreas. Virchows Arch. 440, 205–208 (2002).
106. Chetty, R. & Serra, S. Intraductal tubular adenoma (pyloric gland-type) of the pancreas: a reappraisal and possible relationship with gastric-type intraductal papillary mucinous neoplasm. Histopathology 55, 270–276 (2009).
107. Nakayama, Y. et al. Intraductal tubular adenoma of the pancreas, pyloric gland type: a clinicopathologic and immunohistochemical study of 6 cases. Am. J. Surg. Pathol. 29, 607–616 (2005).
108. Fukatsu, H. et al. Intraductal tubular adenoma, pyloric gland-type, of the pancreas. Endoscopy 39 Suppl 1, E88–9 (2007).

109. Itatsu, K. et al. Intraductal tubular carcinoma in an adenoma of the main pancreatic duct of the pancreas head. J. Gastroenterol. 41, 702–705 (2006).
110. 110. Nagaike, K., Chijiiwa, K., Hiyoshi, M., Ohuchida, J. & Kataoka, H. Main-duct intraductal papillary mucinous adenoma of the pancreas with a large mural nodule. Int. J. Clin. Oncol. 12, 388–391 (2007).
111. Amaris, J. Intraductal mucinous papillary tumor and pyloric gland adenoma of the pancreas. Gastrointest. Endosc. 56, 441–444 (2002).
112. Chang, X., Jiang, Y., Li, J. & Chen, J. Intraductal tubular adenomas (pyloric gland-type) of the pancreas: clinicopathologic features are similar to gastric-type intraductal papillary mucinous neoplasms and different from intraductal tubulopapillary neoplasms. Diagn. Pathol. 9, 172 (2014).
113. Ban, D. et al. Pancreatic ducts as an important route of tumor extension for acinar cell carcinoma of the pancreas. Am. J. Surg. Pathol. 34, 1025–1036 (2010).
114. Basturk, O. et al. Intraductal and papillary variants of acinar cell carcinomas: a new addition to the challenging differential diagnosis of intraductal neoplasms. Am. J. Surg. Pathol. 31, 363–370 (2007).
115. Hosoda, W. et al. BCL10 as a useful marker for pancreatic acinar cell carcinoma, especially using endoscopic ultrasound cytology specimens. Pathol. Int. 63, 176–182 (2013).
116. Yamaguchi, H. et al. The discrete nature and distinguishing molecular features of pancreatic intraductal tubulopapillary neoplasms and intraductal papillary mucinous neoplasms of the gastric type, pyloric gland variant. J. Pathol. 231, 335–341 (2013).
117. Amato, E. et al. Targeted next-generation sequencing of cancer genes dissects the molecular profiles of intraductal papillary neoplasms of the pancreas. J. Pathol. 233, 217–227 (2014).
118. Xiao, H. D. et al. Molecular characteristics and biological behaviours of the oncocytic and pancreatobiliary subtypes of intraductal papillary mucinous neoplasms. J. Pathol. 224, 508–516 (2011).
119. Matsubara, A. et al. Frequent *GNAS* and *KRAS* mutations in pyloric gland adenoma of the stomach and duodenum. J. Pathol. 229, 579–587 (2013).
120. Yamaguchi, H. et al. Somatic mutations in PIK3CA and activation of AKT in intraductal tubulopapillary neoplasms of the pancreas. Am. J. Surg. Pathol. 35, 1812–1817 (2011).
121. Hudes, G. et al. Temsirolimus, interferon alfa, or both for advanced renal-cell carcinoma. N. Engl. J. Med. 356, 2271–2281 (2007).
122. Motzer, R. J. et al. Efficacy of everolimus in advanced renal cell carcinoma: a double-blind, randomised, placebo-controlled phase III trial. Lancet 372, 449–456 (2008).
123. Fallahzadeh, M. K., Zibari, G. B., Wellman, G., Abdehou, S. T. & Shokouh-Amiri, H. Mucinous cystic neoplasm of pancreas in a male patient: a case report and review of the literature. J. La. State Med. Soc. 166, 67–69 (2014).
124. Shiono, S. et al. Pancreatic, hepatic, splenic, and mesenteric mucinous cystic neoplasms (MCN) are lumped together as extra ovarian MCN. Pathol. Int. 56, 71–77 (2006).
125. Adsay, N. V., Eble, J. N., Srigley, J. R., Jones, E. C. & Grignon, D. J. Mixed epithelial and stromal tumor of the kidney. Am. J. Surg. Pathol. 24, 958–970 (2000).
126. Buritica, C. et al. Mixed epithelial and stromal tumour of the kidney with luteinised ovarian stroma. J. Clin. Pathol. 60, 98–100 (2007).
127. Matsubara, M. et al. Primary retroperitoneal mucinous cystadenoma of borderline malignancy: a case report and review of the literature. Int. J. Gynecol. Pathol. 24, 218–223 (2005).
128. Zamboni, G. et al. Mucinous cystic tumors of the pancreas: clinicopathological features, prognosis, and relationship to other mucinous cystic tumors. Am. J. Surg. Pathol. 23, 410–422 (1999).
129. Ridder, G. J., Maschek, H., Flemming, P., Nashan, B. & Klempnauer, J. Ovarian-like stroma in an invasive mucinous cystadenocarcinoma of the pancreas positive for inhibin. A hint concerning its possible histogenesis. Virchows Arch. 432, 451–454 (1998).
130. Yamao, K. et al. Clinicopathological features and prognosis of mucinous cystic neoplasm with ovarian-type stroma: a multi-institutional study of the Japan pancreas society. Pancreas 40, 67–71 (2011).
131. Crippa, S. et al. Mucinous cystic neoplasm of the pancreas is not an aggressive entity: lessons from 163 resected patients. Ann. Surg. 247, 571–579 (2008).
132. Park, W. G.-U. et al. Diagnostic performance of cyst fluid carcinoembryonic antigen and amylase in histologically confirmed pancreatic cysts. Pancreas 40, 42–45 (2011).
133. Cizginer, S. et al. Cyst fluid carcinoembryonic antigen is an accurate diagnostic marker of pancreatic mucinous cysts. Pancreas 40, 1024–1028 (2011).
134. Thompson, L. D., Becker, R. C., Przygodzki, R. M., Adair, C. F. & Heffess, C. S. Mucinous cystic neoplasm (mucinous cystadenocarcinoma of low-grade malignant potential) of the pancreas: a clinicopathologic study of 130 cases. Am. J. Surg. Pathol. 23, 1–16 (1999).
135. Izumo, A. et al. Mucinous cystic tumor of the pancreas: immunohistochemical assessment of 'ovar-

ian-type stroma. Oncol. Rep. 10, 515–525 (2003).
136. Reddy, R. P. et al. Pancreatic mucinous cystic neoplasm defined by ovarian stroma: demographics, clinical features, and prevalence of cancer. Clin. Gastroenterol. Hepatol. 2, 1026–1031 (2004).
137. Baker, M. L. et al. Invasive mucinous cystic neoplasms of the pancreas. Exp. Mol. Pathol. 93, 345–349 (2012).
138. Jang, K.-T. et al. Clinicopathologic characteristics of 29 invasive carcinomas arising in 178 pancreatic mucinous cystic neoplasms with ovarian-type stroma: implications for management and prognosis. Am. J. Surg. Pathol. 39, 179–187 (2015).
139. Kosmahl, M. et al. Cystic neoplasms of the pancreas and tumor-like lesions with cystic features: a review of 418 cases and a classification proposal. Virchows Arch. 445, 168–178 (2004).
140. Seidel, G. et al. Almost all infiltrating colloid carcinomas of the pancreas and periampullary region arise from in situ papillary neoplasms: a study of 39 cases. Am. J. Surg. Pathol. 26, 56–63 (2002).
141. Bakker, R. F. R., Stoot, J. H. M. B., Blok, P. & Merkus, J. W. S. Primary retroperitoneal mucinous cystadenoma with sarcoma-like mural nodule : a case report and review of the literature. Virchows Arch. 451, 853–857 (2007).
142. Hirano, H. et al. Undifferentiated carcinoma with osteoclast-like giant cells arising in a mucinous cystic neoplasm of the pancreas. Pathol. Int. 58, 383–389 (2008).
143. van den Berg, W. et al. Pancreatic mucinous cystic neoplasms with sarcomatous stroma: molecular evidence for monoclonal origin with subsequent divergence of the epithelial and sarcomatous components. Mod. Pathol. 13, 86–91 (2000).
144. Fukushima, N. & Zamboni, G. Mucinous cystic neoplasms of the pancreas: update on the surgical pathology and molecular genetics. Semin. Diagn. Pathol. 31, 467–474 (2014).
145. Southern, J. F., Warshaw, A. L. & Lewandrowski, K. B. DNA ploidy analysis of mucinous cystic tumors of the pancreas. Correlation of aneuploidy with malignancy and poor prognosis. Cancer 77, 58–62 (1996).

Chapter 3

Genomic characterization of malignant progression in neoplastic pancreatic cysts

Michaël Noë, Noushin Niknafs, Catherine G. Fischer, Wenzel M. Hackeng, Violeta Beleva Guthrie, Waki Hosoda, Marija Debeljak, Eniko Papp, Vilmos Adleff, James R. White, Claudio Luchini, Antonio Pea, Aldo Scarpa, Giovanni Butturini, Giuseppe Zamboni, Paola Castelli, Seung-Mo Hong, Shinichi Yachida, Nobuyoshi Hiraoka, Anthony J. Gill, Jaswinder S. Samra, G. Johan A. Offerhaus, Anne Hoorens, Joanne Verheij, Casper Jansen, N. Volkan Adsay, Wei Jiang, Jordan Winter, Jorge Albores-Saavedra, Benoit Terris, Elizabeth D. Thompson, Nicholas J. Roberts, Ralph H. Hruban, Rachel Karchin, Robert B. Scharpf, Lodewijk A. A. Brosens, Victor E. Velculescu, Laura D. Wood

Article under embargo, while under review at Nature Communications.

ABSTRACT

Intraductal papillary mucinous neoplasms (IPMNs) and mucinous cystic neoplasms (MCNs) are non-invasive neoplasms that are often observed in association with invasive pancreatic cancers, but their origins and evolutionary relationships are poorly understood. In this study, we analyzed 148 samples from IPMNs, MCNs, and small associated invasive carcinomas from 18 patients using whole exome or targeted sequencing. Novel alterations not previously appreciated in these lesions were identified in *ATM*, *GLI3*, and *SF3B1*, among others. Using evolutionary analyses, we established that both IPMNs and MCNs are direct precursors to pancreatic cancer. While mutations in most driver genes were shared between matched non-invasive and cancer samples, we identified mutations in *SMAD4* and *TGFBR2* that were restricted to invasive carcinoma and *RNF43* alterations that were largely in non-invasive lesions. Genomic analyses revealed genetic heterogeneity in non-invasive lesions even among driver genes and suggested an average window of over three years between the development of high-grade dysplasia and pancreatic cancer. Taken together, these data establish non-invasive IPMNs and MCNs as origins of invasive pancreatic cancer, identifying potential drivers of invasion, highlighting the complex clonal dynamics prior to malignant transformation, and providing opportunities for early detection and intervention.

INTRODUCTION

Pancreatic cancer is a deadly disease with a dismal prognosis that is predicted to soon be the second leading cause of cancer death in the United States.[1] However, like other epithelial malignancies, pancreatic cancer arises from non-invasive precancerous lesions that are curable if detected and treated early enough. Although the majority of pancreatic cancers are believed to originate in microscopic precancerous lesions (pancreatic intraepithelial neoplasia or PanIN), a significant minority arise in association with larger cystic neoplasms that can be detected using currently available imaging technologies.[2] These neoplasms, which include intraductal papillary mucinous neoplasms (IPMNs) and mucinous cystic neoplasms (MCNs), are frequently diagnosed incidentally on abdominal imaging, identifying a cohort of at-risk patients with an important opportunity for prevention of invasive pancreatic cancer.[2] However, prevention must be balanced with potential overtreatment of low-risk lesions, as pancreatic resection carries significant morbidity and even occasional mortality.[3] There is a critical need to understand the molecular alterations that are associated with the development of invasive cancer, as these represent potential biomarkers to identify cysts at high risk for progression to carcinoma and thus requiring clinical intervention.

Although genomic analyses have been performed on hundreds of invasive pancreatic cancers, relatively few non-invasive neoplasms have been analyzed comprehensively. Whole exome and targeted sequencing of small cohorts of IPMNs and MCNs have revealed driver genes characteristic of each type of cystic neoplasm,[4–6] while targeted analyses in larger cohorts have confirmed the prevalence of specific driver gene mutations that correlate with grade of dysplasia or histological subtype.[7] These studies have confirmed that hotspot mutations in the oncogenes *KRAS* and *GNAS* occur in low-grade lesions while mutations in other driver genes, including *CDKN2A*, *TP53*, *RNF43*, and *SMAD4*, occur with increasing prevalence in lesions with high-grade dysplasia or associated invasive carcinoma.[8] Targeted next generation sequencing has been used to analyze pancreatic driver genes in different regions of IPMNs, revealing a surprising degree of intratumoral genetic heterogeneity, even with respect to well-characterized driver gene mutations.[9–11] However, the above analyses were based on studies of either single regions from each neoplasm or a limited number of genes from multiple regions, and did not provide an analysis of the evolutionary relationship between different regions of pancreatic cysts and associated cancers. These limitations highlight the need for comprehensive genomic analysis of these cysts and associated invasive cancers to understand the molecular alterations that underlie the transition to invasive carcinoma.

In this study we performed whole exome sequencing of IPMNs and MCNs and their associated invasive carcinomas. Importantly, we focused our study on small invasive carcinomas (less than 2.5 cm) in order to more precisely analyze the genetic alterations that occur at malignant transformation in pancreatic tumorigenesis. In addition, in a subset of our samples, we performed deep targeted next generation sequencing on a larger set of additional tissue samples in order to assess mutated loci through entire neoplasms, including areas of low-grade dysplasia, high-grade dysplasia, and invasive

carcinoma. These analyses revealed important features of pancreatic tumorigenesis, including evolutionary relationships between different regions within cystic neoplasms as well as molecular alterations that may drive the transition from a non-invasive precursor lesion to invasive cancer.

RESULTS

Overall approach

In order to dissect the molecular relationships between non-invasive dysplastic lesions and invasive pancreatic cancers, we performed whole exome sequencing of 39 neoplastic tissue samples from 18 patients with small invasive carcinomas (<2.5cm) associated with neoplastic pancreatic cysts, including 16 patients with IPMNs and 2 patients with MCNs (Supplementary Table 1). Whole exome sequencing was performed on one sample from the non-invasive component with high-grade dysplasia and one sample from the invasive cancer in each case, and for three cases an additional non-invasive sample with low-grade dysplasia was also analyzed by whole exome sequencing. Matched normal samples were analyzed by whole exome sequencing in each case to exclude germline variants and to identify somatic mutations. Whole exome sequencing was performed with an average total coverage of 177x (distinct coverage of 145x), generating 1.3TB of sequencing data (Supplementary Table 2).

In addition to whole exome analyses, we performed targeted next generation sequencing of 109 microdissected tissue samples from 7 of the above cases (6 IPMNs and 1 MCN). For these targeted analyses, we performed laser capture microdissection to isolate neoplastic cells from every available tissue block of the non-invasive cyst and cancer specimens. Separate samples were microdissected based on grade of dysplasia, cell morphology, architecture, and spatial location. This resulted in 8 to 22 additional samples per case. The targeted panel analyses included all mutated loci identified in the whole exome sequencing of these seven cases, as well as the entire coding regions of 15 well-characterized pancreatic driver genes (Supplementary Table 3). The targeted sequencing had an average coverage of 508x (distinct coverage of 460x) (Supplementary Table 2).

We developed an integrated mutation calling pipeline to rigorously assess mutations in all sample types in our analyses in order to confidently identify even subclonal alterations in samples with low neoplastic purity (see Methods) (Figure 1). In addition, we utilized both on target and off target reads to examine focal copy number changes as well as loss of heterozygosity throughout the genome (Figure 2). From our whole exome sequencing analyses, we identified an average of 66 somatic mutations in samples from non-invasive components (range 26-111) and an average of 65 somatic mutations in invasive carcinoma samples (range 31-105) (Figure 1a, Supplementary Table 4). An average of 47 somatic mutations were shared between the non-invasive and invasive components, while 19 somatic mutations were unique to samples from non-invasive components and 20 somatic mutations were unique to samples from invasive cancer (Figure 1a).

Analysis of our combined whole exome and targeted sequencing data provided multiple insights into IPMN and MCN tumorigenesis. In every analyzed case, there were multiple shared mutations between the non-invasive and invasive components. These included both driver and passenger mutations, indicating that they shared a common phylogenetic ancestor (Figure 1a-1b). In addition, accumulation of unique mutations in both non-invasive and invasive components demonstrated independent evolution after the divergence of the subclone that gave rise to the invasive cancer (Figure 3, Supplementary Figures 1-18). Analysis of additional adjacent low-grade or high-grade samples from the same lesions revealed a subset of shared mutations, suggesting that these dysplastic lesions preceded the development of the invasive carcinoma (Figure 3, Supplementary Figures 1, 2, 3, 5 & 16). Evolutionary analyses showed a branched phylogeny in each case, with multiple clonally related but distinct dysplastic samples from each neoplasm (Figure 4). Overall, these data provide evolutionary evidence that IPMNs and MCNs were precursors to invasive pancreatic cancer, with low-grade regions usually preceding high-grade regions and ultimately resulting in invasive carcinoma.

Driver genes of IPMN/MCN tumorigenesis

Through whole exome and targeted sequencing analyses of 18 IPMNs/MCNs and associated invasive carcinomas, we confirmed the high prevalence of mutations in previously identified pancreatic driver genes, including mutations of *KRAS* (89% of cases), *GNAS* (28%), *CDKN2A* (44%), *TP53* (67%), *SMAD4* (50%), and *TGFBR2* (17%) (Figure 1b). Somatic mutations were also identified in *RNF43* (56%), which has been previously highlighted for its role as a driver in mucin-producing pancreatic cysts.[4] Somatic mutations were observed at low prevalence in key positions in the PI3K (*PIK3CA*, *TSC2*) and WNT (*APC*, *CTNNA2*, *CTNNB1*) signaling pathways as well as in *STK11* (Figure 1b, Supplementary Table 4). Alteration of these genes and pathways has been previously reported in a fraction of IPMNs.[4,7,12,13] The two MCNs analyzed were similar to the IPMNs in the cohort, with hotspot mutations in *KRAS*, homozygous deletion of *CDKN2A*, and inactivating mutations in *RNF43*, among others, but as expected these MCNs did not have *GNAS* alterations (Supplementary Figures 3 & 7).[6]

In addition to driver genes previously reported in IPMNs, our data provide an opportunity to discover novel drivers of IPMN tumorigenesis. We identified somatic mutations in the DNA damage response gene *ATM* in 17% of lesions, including one nonsense mutation (Figure 1b, Supplementary Table 4). In addition we identified alterations in Hedgehog pathway member *GLI3* in 5 of 18 cases (28%) (Figure 1b, Supplementary Table 4). We also identified somatic mutations in a previously described hotspot in *SF3B1*, which encodes a protein critical for RNA splicing (Figure 1b, Supplementary Table 4). Amplifications of the well-characterized driver genes *ERBB2* and *MYC* were each observed in a single case and have not been previously reported in IPMNs (Supplementary Table 5). Other altered genes with a previously unknown role in IPMN tumorigenesis include *MUC16* (4 cases), *PTPRT* (4 cases), and *CNTN5* (3 cases) (Figure 1b). Intriguingly, in one case, an *STK11* mutation was found in combination with biallelic *ATM* loss and cancer-specific, biallelic *KEAP1* loss – the combination of these three mutations has previously been reported in lung cancers (Supplementary Figure 3).[14]

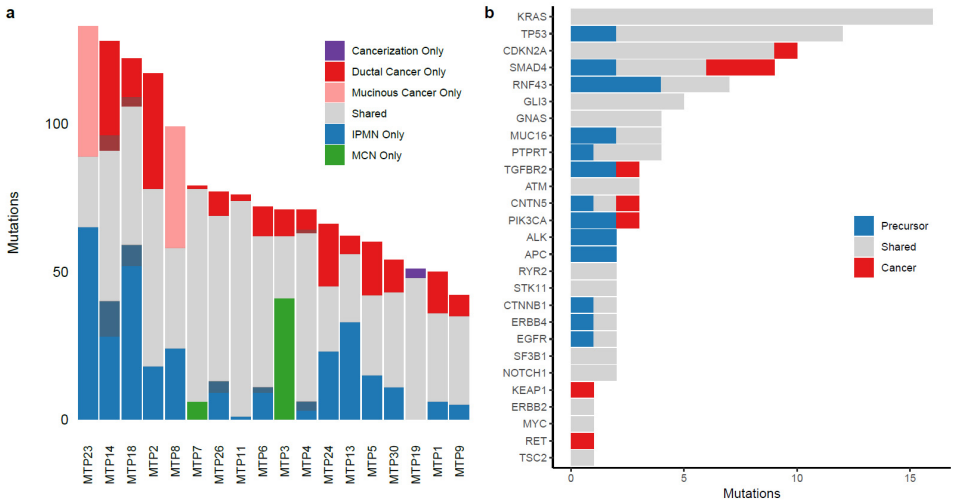

Figure 1. Somatic mutations identified in matched non-invasive and invasive cancer samples. a In each patient sample, multiple mutations were shared between the non-invasive and invasive cancer samples (gray). In addition, some mutations were limited to the non-invasive (blue/green), while others were limited to the cancer (red/pink). Darker colors indicate alterations that were likely restricted to one component but where sequencing coverage in the second component was limited. The proportions of shared and distinct mutations varied between different lesions. **b** Somatic mutations in the most frequently mutated genes are categorized as shared between non-invasive and cancer (gray), limited to non-invasive (blue), or limited to cancer (red). Mutations in some genes (such as *KRAS* were always shared), while other were enriched in samples from non-invasive (*RNF43*) or cancer (*SMAD4*).

Although *KRAS* mutations occur in the majority of IPMNs and are thought to initiate tumorigenesis in these lesions, two IPMNs lacked mutations in this gene. One case contained a hotspot mutation in codon 227 of *GNAS*, another potential initiator of IPMN tumorigenesis, as well as alterations in *TP53* and *RNF43* (Supplementary Figure 15). The other case lacked mutations in any of the frequently altered pancreatic driver genes but contained hotspot mutations in both *CTNNB1* (S45P) and *SF3B1* (H662Q) (Supplementary Figure 10). These cases highlight alternative pathways of initiation and progression in IPMNs lacking *KRAS* mutations.

Order of genetic alterations in IPMN/MCN tumorigenesis

Our multiregion sequencing approach of IPMNs/MCNs and associated invasive carcinomas provided insights into the order of specific genetic alterations in pancreatic tumorigenesis. In 17 of the 18 cases, at least one somatic mutation in the initiating driver genes *KRAS* and *GNAS* was shared between the non-invasive component and associated invasive cancer, with the remaining case lacking mutations in these genes. Somatic mutations in *TP53* and *CDKN2A* were also shared in the non-invasive component and associated invasive cancer in the majority of cases. In contrast, *SMAD4* had alterations confined to the invasive carcinoma in three cases and was shared between non-invasive and invasive samples in four cases (Figure 1b). Alteration of *TGFBR2*, which functions in the same signaling pathway as *SMAD4*, was also restricted to the cancer in one case (Figure 1b). The other genes with mutations restricted to the invasive cancer (*CDKN2A*, *CNTN5*, *PIK3CA*, *KEAP1*, and *RET*) only had this pattern in a single sample (Figure 1b).

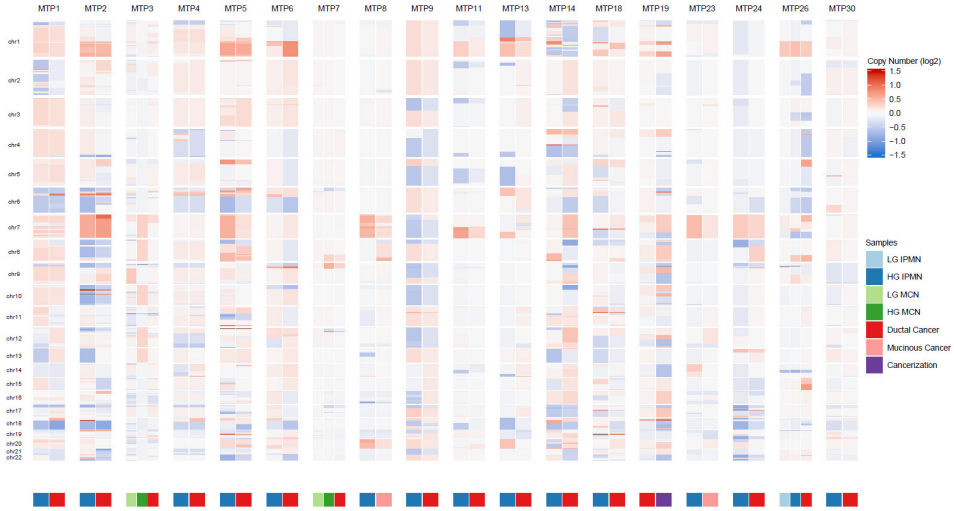

Figure 2. Copy number alterations identified in matched non-invasive and invasive cancer samples. Chromosomal gains (red) and losses (blue) are shown for each chromosome in each patient, with non-invasive samples on the left and cancer samples on the right.

Our study also identified driver mutations in subclones of non-invasive neoplasms that diverged from and were not present in invasive cancer. These included hotspots mutations in well-characterized oncogenes and inactivating mutations in tumor suppressor genes (e.g. *PIK3CA* p.E545K, *CTNNB1* p.S45F, *SMAD4* p.E33fs, and multiple inactivating *RNF43* mutations in patient MTP3) (Supplementary Figure 3). Mutations in *RNF43* were a particularly striking finding in these cases, as some non-invasive components contained several different *RNF43* mutations, each limited to a small number of sections and none involving the invasive cancer (Figure 3, Supplementary Figure 3). In addition to heterogeneity in RNF43 in early lesions, we also identified two cases with multiple mutations in *KRAS* in precursor lesions, of which only one was present in the invasive cancer. For example, in MTP19, KRAS p.G12V was present in the majority of IPMN samples, as well as all the invasive cancer samples, but there were an additional four other *KRAS* mutations (all occurring in hotspot positions) that were present in a small number of sections in low-grade IPMN samples (Figure 3). Intriguingly, these three low-grade IPMN regions shared no mutations with the invasive cancer, suggesting that they represented genetically independent clones.

Notably, while there were often many differences in the somatic point mutations identified in the matched non-invasive and invasive samples, the copy number profiles were quite similar between IPMN/MCNs and invasive cancers (Figure 2, Supplementary Table 6). While homozygous deletion of some genes occurred in the invasive cancer but not the non-invasive component, such as *CDKN2A* in MTP8 (Figure 3), analyses of chromosomal gains and losses through assessment of allelic imbalance revealed that an average of 91% of the genome was similar in copy number in matched non-invasive and invasive samples (Figure 2, Supplementary Table 6).

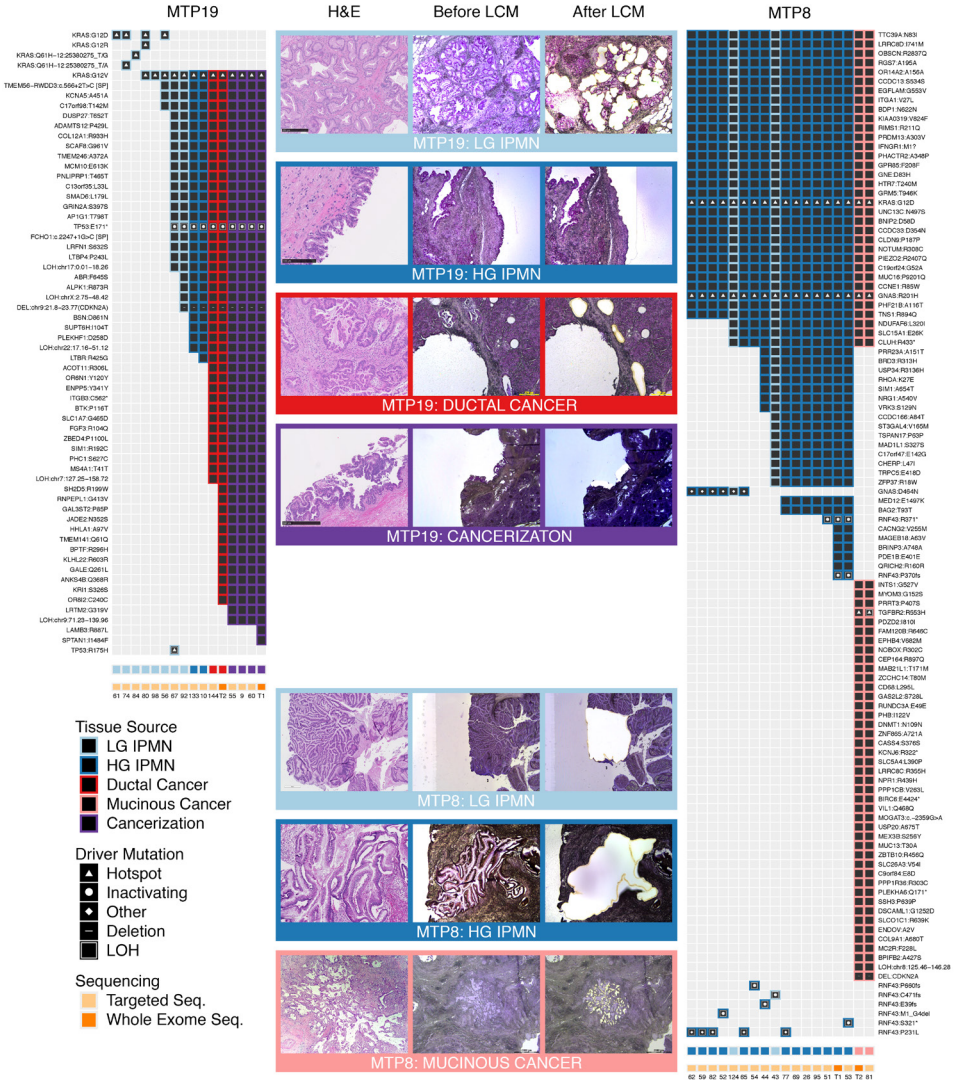

Figure 3. Somatic mutations identified in MTP19 and MTP8 in targeted and whole exome sequencing. We show mutations identified in each sample, including low-grade IPMN (light blue), high-grade IPMN (dark blue), ductal cancer (red), mucinous cancer (pink), and "cancerization" (purple). The type of sequencing analysis (targeted or whole exome) performed for each sample is indicated in a track on the bottom. Representative images of neoplastic tissue stained by hematoxylin and eosin, as well as isolated regions before and after laser capture microdissection are shown for MTP19 and MTP8.

Insights into pancreatic neoplasia revealed by sequencing analysis

The samples analyzed by targeted sequencing were characterized morphologically and meticulously isolated using laser capture microdissection. Even with this process, we identified samples in two cases that were characterized morphologically as IPMNs but through genomic and evolutionary analyses were determined to be identical to or descendants of the associated invasive cancers. For example, in MTP19, some of the samples originally identified morphologically as non-invasive IPMN (55, 9, 60, and T1) shared all the mutations present in the invasive cancer sample (T2) and contained additional

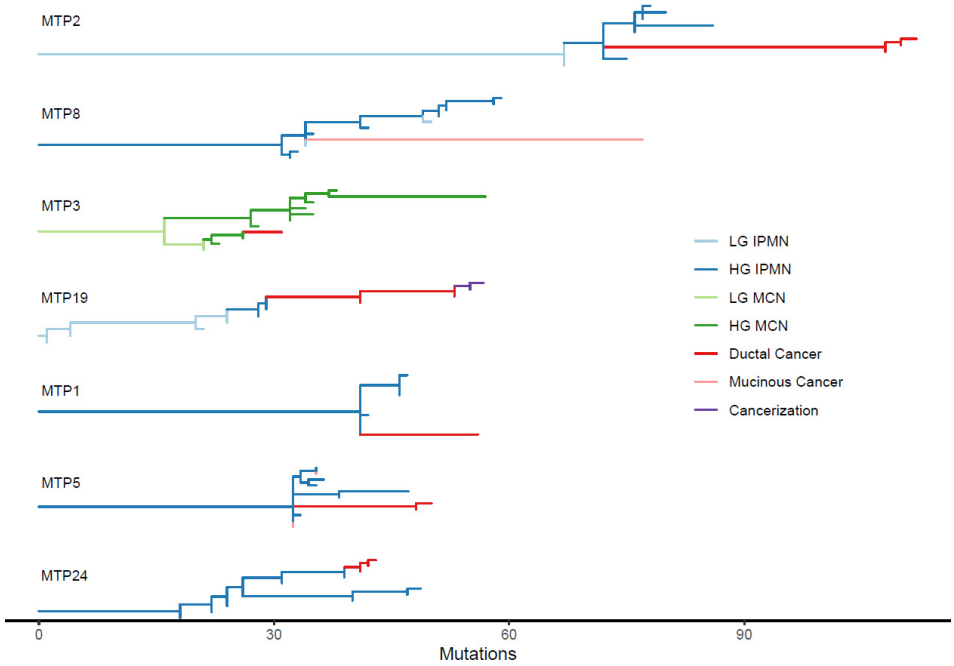

Figure 4. Evolutionary reconstruction of samples analyzed by whole exome and targeted sequencing. In all cases, non-invasive samples (blue/green) precede invasive samples (red/pink) in the evolutionary history. In MTP5, different invasive cancer samples are placed in different regions of the phylogeny, highlighting multiple independent invasion events in this lesion. In MTP19, a sample of "cancerization" (purple) has descended from invasive cancer samples.

mutations, suggesting that these samples descended from the cancer (Figures 3 & 4). Evolutionary analyses suggested that some of the morphologically identified IPMN samples in this case (as well as MTP1) actually represented intraductal spread of invasive carcinoma, also referred to as "cancerization" of the ducts. In these cases, after invading the stroma, the carcinoma invaded back into and colonized the cyst such that it was morphologically indistinguishable from IPMN with high-grade dysplasia.

In one case (MTP5), we also identified an interesting pattern of multifocal invasion of the carcinoma. In this case, we analyzed five different samples from invasive cancer – three samples were isolated from a mucinous carcinoma, and two samples were isolated from a ductal carcinoma. Based on evolutionary analyses of the patterns of shared and distinct mutations in the cancers and IPMNs, we conclude that there were multiple separate invasion events in this lesion, as represented by the mutations shared between the invasive cancers and non-invasive components as well as those that were unique to the specific invasive cancers (Figure 4, Supplementary Figure 5).

As our study represents the largest cohort of comprehensively sequenced IPMNs/MCNs, we also analyzed mutational signatures in our dataset. Intriguingly, our data contrast somewhat with the mutational signatures previously reported in pancreatic ductal adenocarcinoma (PDAC).[15,16] Like PDAC, the most prominent mutational signature is associated with age (Signatures 1A), which is identified in almost every case (Supplementary Figure 19). However, we also identified signatures associated with APO-

BEC enzymes (four cases), smoking (three cases), and mismatch repair deficiency (eleven cases). Although smoking is considered a risk factor for pancreatic cancer, until now the mutational signature associated with smoking has not been reported in pancreatic neoplasia.[17]

Evolutionary timeline of high-grade IPMN to PDAC

To estimate the time between the development of high-grade IPMN and PDAC, we evaluated Bayesian hierarchical models for the number of acquired mutations under a range of possible mutation rates. These models estimate the time interval between a founder cell of a PDAC and the ancestral precursor cell in the associated high-grade IPMN assuming that mutation rates and cell division times are constant throughout this period of development (see Methods). We performed this analysis on the paired WES data from 17 of our 18 cases (Supplementary Figure 20). We excluded MTP19 because our evolutionary analyses demonstrated intraductal spread of invasive carcinoma and as such, we lacked WES data from an IPMN sample in this case. In the 17 analyzed cases, the average median time to progression from IPMN to PDAC was 3.7 years, but the models showed a bimodal distribution. This median time was nearly 3 years for 13 patients, but nearly 7 years for 4 patients with more than 35 acquired mutations, highlighting potential variability in progression time between patients. For example, in patient MTP1, most models suggested an average of 2.8 years between the development of the IPMN and the PDAC (90% CI, 1.3–6.7 years). In contrast, for patient MTP2 with 36 additional mutations acquired in the PDAC, the transition appears to have been slower with an average estimate of 6.6 years (90% CI: 3.9–11.4 years) from the Bayesian models. Overall, these analyses suggest that for most patients there is a significant window of time between development of high-grade dysplasia and pancreatic cancer, providing an opportunity for surveillance and intervention.

DISCUSSION

This study represents the largest dataset of whole exome sequencing of IPMNs and MCNs to date. Importantly, our data established that both IPMNs and MCNs are direct precursors of invasive pancreatic cancer (Figure 4). This conclusion has been previously suggested by the morphological relationship between the non-invasive neoplasms and invasive cancer on traditional histologic sections, as well as shared driver gene mutations in targeted sequencing studies.[6,7,9,10] However, the presence of many shared driver and passenger mutations clearly demonstrated the common origin of IPMNs/MCNs and invasive pancreatic cancers in our study, and evolutionary analyses revealed that dysplastic lesions precede invasive cancers. Evolutionary analyses suggested that high-grade non-invasive lesions occur over 3 years before invasive carcinoma, providing a window of opportunity for early detection and intervention.

In this study, we identified somatic mutations in driver genes that had not been previously implicated in IPMNs/MCNs. For example, we identified alterations in the DNA damage response gene *ATM* in 17% of the analyzed cases. Germline mutations in *ATM* have been recently reported in patients that developed IPMNs, highlighting the potential importance of this gene in IPMN risk.[18] In addition, mucinous

(colloid) carcinomas are significantly more common than typical ductal carcinomas in patients with germline ATM mutations, further highlighting the link between mutations in this gene and IPMNs.[19] Somatic mutations in *GLI3*, which encodes a component of the Hedgehog signaling pathway, were identified in 28% of cases. Somatic mutations in *GLI3* were recently reported in a distinct morphological variant of pancreatic carcinoma (undifferentiated carcinoma with osteoclast-like giant cells) as well as at a low prevalence in sporadic PDAC, suggesting that the importance of *GLI3* mutations and its signaling pathway in pancreatic tumorigenesis may extend beyond IPMNs/MCNs.[20–22] The hotspot mutations in *SF3B1*, which encodes a protein critical for RNA splicing, are also novel drivers in the IPMN pathway. However, somatic mutations in this gene have been reported in a variety of other neoplasms, including hematologic malignancies and uveal melanoma.[23–25]

We highlight somatic alteration of the *SMAD4* pathway as a putative driver of progression to invasive cancer, as mutations in *SMAD4* or *TGFBR2* occurred only in invasive cancer samples in 4 of the 18 cases analyzed. *SMAD4* was the only gene with cancer-specific mutations in more than one case, highlighting the potentially unique role this gene plays in pancreatic carcinogenesis. This role has been previously suggested by next generation sequencing of high-grade PanINs showing an absence of *SMAD4* mutations in precancerous lesions, as well as cancer-specific *SMAD4* mutations reported in a paired PanIN/carcinoma analyses.[26,27] Loss of *SMAD4* expression limited to invasive carcinomas has been reported in MCN- and IPMN-associated invasive cancers, and targeted sequencing of a small number of IPMNs and matched cancers identified a single case with a *SMAD4* mutation occurring only in the cancer.[7,27,28] In our data, there were also four cases where mutations in *SMAD4* were shared between non-invasive and invasive cancer samples, and two where *SMAD4* mutations were limited to the non-invasive component. This suggests that the role of *SMAD4* mutations may not be universal and may depend on other factors, including cell intrinsic (such as somatic mutations in other driver genes) and cell extrinsic (such as stromal and immune microenvironment) mechanisms.

Although some of our cases had *SMAD4* mutations limited to the invasive cancer, most of the IPMN/MCN-associated cancers lacked driver gene alterations that were associated with invasive disease, suggesting that malignant progression is not universally driven by point mutations. Previous studies have specifically demonstrated the importance of copy number alterations and chromosomal rearrangements in pancreatic tumorigenesis. We did not identify large differences in the copy number profiles between non-invasive components and associated invasive cancers, suggesting that global genomic instability may be important as an early feature of tumorigenesis but is not likely to drive malignant transformation in many cases.

Our study also revealed prevalent genetic heterogeneity in driver gene mutations in early lesions, demonstrating more complex processes than previously suggested by traditional linear tumorigenesis models. Similar to our recently reported polyclonal origin of IPMNs,[11] we identified multiple independent clones initiated by distinct *KRAS* mutations in two cases in the current study. In addition, our study identified multiple distinct inactivating mutations in *RNF43* limited to unique tumor subclones, a pattern

previously observed by our group and not shared by other genes in our whole exome sequencing analyses.[11,29] In most cases, *RNF43* mutations were enriched in non-invasive components and absent from the associated invasive cancers. More generally, we observed multiple instances of clear driver mutations (including hotspot mutations in oncogenes as well as inactivating mutations in tumor suppressor genes) that were limited to the non-invasive components and not present in the associated invasive cancer. Thus, these mutations occur and clonally expand in the IPMN or MCN but are not present in the subclone that subsequently invades. These observations suggest unique selective processes at different time points in tumorigenesis, such that mutations selected in the precancerous lesion are not selected for (or are even selected against) in the invasive cancer.

In addition to these observations about clonal evolution in non-invasive lesions, our data also provide genetic evidence for multiple underappreciated processes in pancreatic neoplasia. First, we provide genetic evidence for intraductal spread of invasive carcinoma, also known as "cancerization."[30] In two of our cases (MTP1 and MTP19), the identified somatic mutations suggested that samples that were morphologically thought to be IPMN were actually of the same clone or clone descended from invasive cancer. These cases confirmed the morphological impression of the prevalence of this "cancerization" phenomenon, which likely has confounded many previous studies of precancerous pancreatic lesions.[30] In addition, we describe one case of IPMN with multiple independent invasion events (MTP5). This case contained invasive cancer with two different morphologies, one with typical ductal morphology and one with mucinous (colloid) morphology. Evolutionary analyses demonstrated that the ductal and mucinous carcinomas arose through independent invasion events and suggested that the multiple mucinous cancer samples comprised unique subclones that invaded independently from the IPMN. Although multifocal invasion has been described morphologically in IPMNs with multiple anatomically discrete invasive foci, in this case all the invasive carcinoma samples came from the same grossly defined "tumor", suggesting that multifocal invasion may be an underappreciated phenomenon in IPMNs.

The results of our study should also be considered in the context of studies of other precancerous lesions and associated invasive cancers. In particular, complementary studies that have employed whole exome sequencing to characterize microscopic pancreatic precancerous lesions (PanINs) and their co-occurring invasive carcinomas highlight the common evolutionary origin of PanINs and co-occurring PDACs.[26,31] Similar to our study, these studies reported a lack of consistent specific driver genes associated with invasive cancer, although cancer-specific *SMAD4* mutations were reported in two cases in one study.[26] Importantly, in our study the sequencing of additional precancerous samples (beyond the original paired samples analyzed by whole exome sequencing) provided a more detailed analysis of precancerous clonal evolution than previous studies.

As with all genomic analyses, our study does have some limitations. Compared to other genomic analyses of invasive pancreatic cancer, the sample size in our study is relatively small, with multi-region whole exome sequencing performed on 18 patients. Nevertheless, the whole exome and targeted analyses of 148 samples from these patients represents the largest genomic study of precancerous pan-

creatic lesions to date. In addition, our combined approach of whole exome and targeted sequencing may not have identified all mutations in all regions of these comprehensively analyzed IPMNs. Despite these limitations, the analyses provide a detailed view of the acquisition of mutations that characterize the invasive carcinoma, as well as genetic heterogeneity in well-characterized pancreatic driver genes. Finally, in this study, we focused entirely on genetic alterations, as the role of these mutations in driving tumorigenesis has been well documented. Our study provides evidence that the evolution to invasive cancer is likely to be driven by non-genetic mechanisms in some lesions, highlighting an important direction of future investigation.

In this study, we present a comprehensive evolutionary analysis of precancerous pancreatic cysts and associated invasive carcinomas. We demonstrate that IPMNs and MCNs are precursors of invasive pancreatic cancer, that novel alterations in *ATM*, *GLI3*, and *SF3B1* are present in these lesions, and that *SMAD4*/*TGFBR2* alterations are likely drivers of invasion in a subset of cases. Analyses of the evolutionary timeline between high grade precancerous lesions and pancreatic cancer suggest a window of more than 3 years for acquisition of these invasive characteristics. These data provide critical insights into pancreatic tumorigenesis and highlight an opportunity for surveillance of precancerous pancreatic cysts and early detection of pancreatic cancer.

REFERENCES

1. Rahib, L. et al. Projecting cancer incidence and deaths to 2030: the unexpected burden of thyroid, liver, and pancreas cancers in the United States. Cancer Res. 74, 2913–2921 (2014).
2. Basturk, O. et al. A Revised Classification System and Recommendations From the Baltimore Consensus Meeting for Neoplastic Precursor Lesions in the Pancreas. Am. J. Surg. Pathol. 39, 1730–1741 (2015).
3. Lermite, E. et al. Complications after pancreatic resection: diagnosis, prevention and management. Clin. Res. Hepatol. Gastroenterol. 37, 230–239 (2013).
4. Wu, J. et al. Whole-exome sequencing of neoplastic cysts of the pancreas reveals recurrent mutations in components of ubiquitin-dependent pathways. Proc. Natl. Acad. Sci. U. S. A. 108, 21188–21193 (2011).
5. Furukawa, T. et al. Whole-exome sequencing uncovers frequent *GNAS* mutations in intraductal papillary mucinous neoplasms of the pancreas. Sci. Rep. 1, 161 (2011).
6. Wu, J. et al. Recurrent *GNAS* mutations define an unexpected pathway for pancreatic cyst development. Sci. Transl. Med. 3, 92ra66 (2011).
7. Amato, E. et al. Targeted next-generation sequencing of cancer genes dissects the molecular profiles of intraductal papillary neoplasms of the pancreas. J. Pathol. 233, 217–227 (2014).
8. Fischer, C. G. & Wood, L. D. From somatic mutation to early detection: insights from molecular characterization of pancreatic cancer precursor lesions. J. Pathol. 246, 395–404 (2018).
9. Felsenstein, M. et al. IPMNs with co-occurring invasive cancers: neighbours but not always relatives. Gut 67, 1652–1662 (2018).
10. Omori, Y. et al. Pathways of Progression From Intraductal Papillary Mucinous Neoplasm to Pancreatic Ductal Adenocarcinoma Based on Molecular Features. Gastroenterology 156, 647–661.e2 (2019).
11. Fischer, C. G. et al. Intraductal Papillary Mucinous Neoplasms Arise From Multiple Independent Clones, Each With Distinct Mutations. Gastroenterology 157, 1123–1137.e22 (2019).
12. Schönleben, F. et al. PIK3CA mutations in intraductal papillary mucinous neoplasm/carcinoma of the pancreas. Clin. Cancer Res. 12, 3851–3855 (2006).
13. Sato, N. et al. STK11/LKB1 Peutz-Jeghers gene inactivation in intraductal papillary-mucinous neoplasms of the pancreas. Am. J. Pathol. 159, 2017–2022 (2001).
14. Skoulidis, F. et al. Co-occurring genomic alterations define major subsets of *KRAS*-mutant lung adenocarcinoma with distinct biology, immune profiles, and therapeutic vulnerabilities. Cancer Discov. 5, 860–877 (2015).
15. Alexandrov, L. B. et al. Signatures of mutational processes in human cancer. Nature 500, 415–421 (2013).
16. Cancer Genome Atlas Research Network. Electronic address: andrew_aguirre@dfci.harvard.edu & Cancer Genome Atlas Research Network. Integrated Genomic Characterization of Pancreatic Ductal Adenocarcinoma. Cancer Cell 32, 185–203. e13 (2017).
17. Alexandrov, L. B. et al. Mutational signatures associated with tobacco smoking in human cancer. Science 354, 618–622 (2016).
18. Skaro, M. et al. Prevalence of Germline Mutations Associated With Cancer Risk in Patients With Intraductal Papillary Mucinous Neoplasms. Gastroenterology 156, 1905–1913 (2019).
19. Hutchings, D. et al. Histomorphology of pancreatic cancer in patients with inherited ATM serine/threonine kinase pathogenic variants. Mod. Pathol. 32, 1806–1813 (2019).
20. Luchini, C. et al. Pancreatic undifferentiated carcinoma with osteoclast-like giant cells is genetically similar to, but clinically distinct from, conventional ductal adenocarcinoma. J. Pathol. 243, 148–154 (2017).
21. Biankin, A. V. et al. Pancreatic cancer genomes reveal aberrations in axon guidance pathway genes. Nature 491, 399–405 (2012).
22. Witkiewicz, A. K. et al. Whole-exome sequencing of pancreatic cancer defines genetic diversity and therapeutic targets. Nat. Commun. 6, 6744 (2015).
23. Martin, M. et al. Exome sequencing identifies recurrent somatic mutations in EIF1AX and SF3B1 in uveal melanoma with disomy 3. Nat. Genet. 45, 933–936 (2013).
24. Quesada, V. et al. Exome sequencing identifies recurrent mutations of the splicing factor SF3B1 gene in chronic lymphocytic leukemia. Nat. Genet. 44, 47–52 (2011).
25. Papaemmanuil, E. et al. Somatic SF3B1 mutation in myelodysplasia with ring sideroblasts. N. Engl. J. Med. 365, 1384–1395 (2011).
26. Murphy, S. J. et al. Genetic alterations associated with progression from pancreatic intraepithelial neoplasia to invasive pancreatic tumor. Gastroenterology 145, 1098–1109.e1 (2013).
27. Hosoda, W. et al. Genetic analyses of isolated high-grade pancreatic intraepithelial neoplasia (HG-PanIN) reveal paucity of alterations in TP53 and SMAD4. J. Pathol. 242, 16–23 (2017).

28. Iacobuzio-Donahue, C. A. et al. Dpc4 protein in mucinous cystic neoplasms of the pancreas: frequent loss of expression in invasive carcinomas suggests a role in genetic progression. Am. J. Surg. Pathol. 24, 1544–1548 (2000).
29. Kuboki, Y. et al. Single-cell sequencing defines genetic heterogeneity in pancreatic cancer precursor lesions. J. Pathol. 247, 347–356 (2019).
30. Hutchings, D. et al. Cancerization of the Pancreatic Ducts: Demonstration of a Common and Under-recognized Process Using Immunolabeling of Paired Duct Lesions and Invasive Pancreatic Ductal Adenocarcinoma for p53 and Smad4 Expression. Am. J. Surg. Pathol. 42, 1556–1561 (2018).
31. Makohon-Moore, A. P. et al. Precancerous neoplastic cells can move through the pancreatic ductal system. Nature 561, 201–205 (2018).

Chapter 4

Genetic analyses of isolated high-grade pancreatic intraepithelial neoplasia (HG-PanIN) reveal paucity of alterations in *TP53* and *SMAD4*

Waki Hosoda, Peter Chianchiano, James F. Griffin, Meredith E. Pittman, Lodewijk A.A. Brosens, Michaël Noë, Jun Yu, Koji Shindo, Masaya Suenaga, Neda Rezaee, Raluca Yonescu, Yi Ning, Jorge Albores-Saavedra, Naohiko Yoshizawa, Kenichi Harada, Akihiko Yoshizawa, Keiji Hanada, Shuji Yonehara, Michio Shimizu, Takeshi Uehara, Jaswinder S. Samra, Anthony J. Gill, Christopher L. Wolfgang, Michael G. Goggins, Ralph H. Hruban, Laura D. Wood

The Journal of Pathology, May 2017

ABSTRACT

High-grade pancreatic intraepithelial neoplasia (HG-PanIN) is the major precursor of pancreatic ductal adenocarcinoma (PDAC) and is an ideal target for early detection. To characterize pure HG-PanIN, we analysed 23 isolated HG-PanIN lesions occurring in the absence of PDAC. Whole-exome sequencing of five of these HG-PanIN lesions revealed a median of 33 somatic mutations per lesion, with a total of 318 mutated genes. Targeted next-generation sequencing of 17 HG-PanIN lesions identified *KRAS* mutations in 94% of the lesions. *CDKN2A* alterations occurred in six HG-PanIN lesions, and *RNF43* alterations in five. Mutations in *TP53*, *GNAS*, *ARID1A*, *PIK3CA*, and *TGFBR2* were limited to one or two HG-PanINs. No non-synonymous mutations in *SMAD4* were detected. Immunohistochemistry for p53 and SMAD4 proteins in 18 HG-PanINs confirmed the paucity of alterations in these genes, with aberrant p53 labelling noted only in three lesions, two of which were found to be wild type in sequencing analyses. Sixteen adjacent LG-PanIN lesions from ten patients were also sequenced using targeted sequencing. LG-PanIN harboured *KRAS* mutations in 94% of the lesions; mutations in *CDKN2A*, *TP53*, and *SMAD4* were not identified. These results suggest that inactivation of *TP53* and *SMAD4* are late genetic alterations, predominantly occurring in invasive PDAC.

INTRODUCTION

Pancreatic ductal adenocarcinoma (PDAC) is the third leading cause of cancer death in the United States, with a 5-year survival rate of only 7.7%.[1] Approaches to detect curable disease are crucial to improve outcomes, and high-grade precursors are the ideal target lesions of early detection.[2] Pancreatic intraepithelial neoplasia (PanIN), the common precursor to PDAC, is classified based on the grade of dysplasia of the neoplastic epithelium.[3] While low-grade PanINs (LG-PanINs) are common and low risk, high-grade PanINs (HG-PanINs) are regarded as lesions immediately preceding invasive PDAC and thus are a primary target for intervention.[4,5] Because these lesions cannot be detected by standard clinical and radiological approaches, molecular approaches, such as mutational analysis of pancreatic juice, will be critical for the detection of HG-PanIN.[6,7]

HG-PanIN lesions are rarely detected clinically, and knowledge about isolated HG-PanIN is limited. Most studies of HG-PanIN have been conducted using specimens that also harboured an invasive PDAC.[8–14] These studies are confounded by the fact that invasive carcinomas can grow back into and spread within the duct system ('cancerization of the ducts'), histologically mimicking HG-PanIN.[15] Thus, instead of HG-PanIN, many previous studies may have analysed intraductal invasive cancer, raising concerns about the reliability of these data.

To gain knowledge about HG-PanIN in the absence of invasive carcinoma (isolated HG-PanIN), we conducted a multicentre study investigating its clinicopathological and molecular characteristics. We found that while *KRAS* and *CDKN2A* were frequently targeted, *TP53* mutations were rare and *SMAD4* mutations were absent in isolated HG-PanIN.

MATERIALS AND METHODS

Our study cohort included 23 isolated HG-PanINs from 21 patients; samples were retrieved from the database of the Department of Pathology of The Johns Hopkins Hospital or collected from the participating institutions after the approval of the Institutional Review Board. Neoplastic cells were isolated from formalin-fixed, paraffin-embedded (FFPE) tissue sections by laser capture microdissection (supplementary material, Figure S1). DNA was extracted and analysed by targeted next-generation sequencing of pancreatic cancer driver genes using Ion AmpliSeq library preparation on an IonTorrent Personal Genome Machine (17 HG-PanINs and 16 LG-PanINs) or by whole-exome sequencing using Agilent SureSelect library preparation on an Illumina HiSeq (five HG-PanINs). In addition, immunohistochemistry for p53 and SMAD4 protein was performed on FFPE sections (18 HG-PanINs). Additional details are provided in the Supplementary materials and methods.

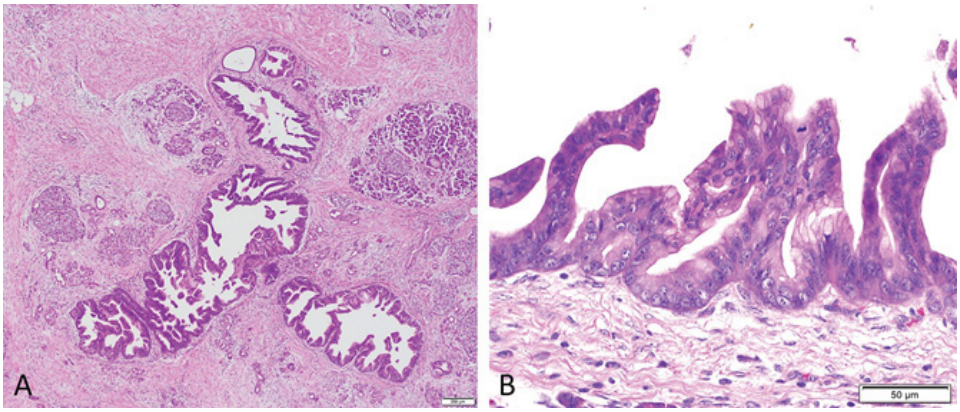

Figure 1. A representative isolated HG-PanIN. **a** The atypical proliferation spreads along the pancreatic duct. **b** Atypical cells showed cytological features of high-grade atypia, including irregular nuclear stratification, coarse chromatin, and prominent nucleoli.

RESULTS

Clinicopathological features of isolated HG-PanIN

Twenty-three HG-PanIN lesions were characterized from 21 patients (supplementary material, Table S1). The preoperative clinical findings included pancreatitis and irregular shape of the main pancreatic duct on imaging. Some of the HG-PanINs were identified incidentally in pancreata resected for other neoplasms, including neuroendocrine tumour/carcinoma and peri-ampullary cholangiocarcinoma. When HG-PanIN occurred with cholangiocarcinoma, we confirmed that both lesions harboured different mutations of *KRAS* using pyrosequencing and/or targeted sequencing.

Histologically, the extent of duct involvement by the HG-PanIN lesions varied (Figure 1 and supplementary material, Table S1). Of 23 lesions, 11 HG-PanIN lesions in nine patients showed extensive spread along the pancreatic duct and were clinically recognized due to pancreatitis or irregular shape of the main pancreatic duct on imaging. In contrast, ten HG-PanIN lesions in ten patients showed focal growth and were mostly discovered incidentally in pancreata resected for other lesions. Data were not available for two lesions. Importantly, all of the lesions, even those with extensive growth, met histological criteria for diagnosis of PanIN, not intraductal papillary mucinous neoplasm (IPMN), a distinct and larger precursor lesion.[15] LG-PanIN lesions were detected in all 21 patients.

Targeted sequencing of isolated HG-PanIN and associated LG-PanIN

Of 23 HG-PanIN lesions, sufficient lesional tissue for microdissection and sequencing was available in 20 lesions (Tables 1 and 2). Sufficient coverage for mutation analysis was obtained from 17 HG-PanIN lesions in 15 patients and 16 LG-PanIN lesions in ten patients (supplementary material, Tables S2, S3, and Figure S2).

KRAS was the most frequently mutated gene in HG-PanIN, with oncogenic hotspot mutations in 16 of 17 HG-PanIN lesions (94%). *RNF43* was altered in five HG-PanIN lesions from four patients, fol-

Patient ID	Lesion designation	Gene	Mutation position (hg19)		Mutation type	Consequence	Variant allele frequency*
			Nucleotide (genomic)	Amino acid (protein)			
PDS-2	B-12	*KRAS*	chr12:25398284C>T	p.G12D	Substitution	Missense	84% (2025; 2416)
	B-12	*RNF43*	chr17:56448310G>A	p.R113X	Substitution	Nonsense	14% (154; 1098)
	B-13†	*KRAS*	chr12:25398284C>T	p.G12D	Substitution	Missense	87% (635; 730)
PDS-3	B-14	*KRAS*	chr12:25398285C>G	p.G12R	Substitution	Missense	36% (953; 2641)
PDS-6	B-5	*KRAS*	chr12:25398285C>G	p.G12R	Substitution	Missense	39% (663; 1707)
PDS-7	B-6	*KRAS*	chr12:25398284C>T	p.G12D	Substitution	Missense	46% (1131; 2459)
	B-6	*CDKN2A*	chr9:21971108C>A	p.D84Y	Substitution	Missense	88% (213; 243)
	B-6	*RNF43*				LOH‡	
PDS-8	B-7	*KRAS*	chr12:25398284C>A	p.G12V	Substitution	Missense	39% (168; 429)
	B-7	*GNAS*	chr20:57484421G>A	p.R201H	Substitution	Missense	39% (152; 392)
	B-7	*RNF43*	chr17:56435161delC	p.G659Vfs	Deletion	Frameshift	52% (351; 669)
PDS-9	B-31	*GNAS*	chr20:57484421G>A	p.R201H	Substitution	Missense	37% (17; 46)
PDS-10	B-27	*KRAS*	chr12:25398284C>A	p.G12V	Substitution	Missense	47% (1483; 3135)
PDS-13	B-32	*KRAS*	chr12:25398284C>T	p.G12D	Substitution	Missense	35% (122; 347)
PDS-CC2	B-8	*KRAS*	chr12:25398284C>T	p.G12D	Substitution	Missense	40% (532; 1339)
	B-8	*ARID1A*	chr1:27100175_27100176insC	p.Q1327Afs	Insertion	Frameshift	28% (598; 2142)
PDS-16	HGPN-1	*KRAS*	chr12:25398284C>T	p.G12D	Substitution	Missense	42% (830; 1971)
PDS-18	HGPN-1	*KRAS*	chr12:25398284C>A	p.G12V	Substitution	Missense	86% (260; 304)
PDS-19	HGPN-1	*KRAS*	chr12:25398285C>G	p.G12R	Substitution	Missense	39% (296; 753)
	HGPN-1	*CDKN2A*	chr9:21971036C>A	p.D108Y	Substitution	Missense	71% (17; 24)
	HGPN-1	*TP53*	chr17:7574026C>A	p.G334V	Substitution	Missense	64% (2273; 3551)
PDS-20	HGPN-2	*KRAS*	chr12:25398284C>T	p.G12D	Substitution	Missense	45% (944; 2087)
	HGPN-2	*PIK3CA*	chr3:178952085A>G	p.H1047R	Substitution	Missense	43% (207; 481)
	HGPN-2	*RNF43*				LOH‡	
	HGPN-3†	*KRAS*	chr12:25398284C>T	p.G12D	Substitution	Missense	37% (668; 1783)
	HGPN-3†	*CDKN2A*	chr9:21971028C>T	p.W110X	Substitution	Nonsense	70% (85; 121)
	HGPN-3†	*TGFBR2*	chr3:30691885_30691895delTGGTGAGACTT	p.G155Lfs	Deletion	Frameshift	16% (8; 51)
	HGPN-3†	*RNF43*				LOH‡	
PDS-21	HGPN-2	*KRAS*	chr12:25398284C>T	p.G12D	Substitution	Missense	55% (769; 1395)
PDS-CC4	HGPN-1	*KRAS*	chr12:25398284C>A	p.G12V	Substitution	Missense	39% (252; 653)
	HGPN-1	*TP53*	chr17:7577548C>T	p.G245S	Substitution	Missense	48% (245; 514)

* Numbers in parentheses indicate the following: (variant reads; total reads).
† Two HG-PanIN lesions were separately microdissected and sequenced. In PDS-2, the degree of atypia differed between the two lesions; in PDS-20, the two lesions were spatially separate.
‡ Loss of heterozygosity (LOH) of RNF43 was manifested by marked reduction of one of the heterozygous SNP signals (at rs115553539 and rs9652855 in PDS-7, and at rs3744093 in PDS-20).

Table 1. Somatic mutations of isolated HG-PanINs identified by targeted sequencing

lowed by *CDKN2A* with mutations in three HG-PanINs. *GNAS* and *TP53* were each mutated in two HG-PanIN lesions, and *PIK3CA*, *TGFBR2*, and *ARID1A* in one HG-PanIN lesion each. Notably, no non-synonymous mutations in *SMAD4* were detected. LG-PanIN also frequently harboured *KRAS* mutations, which were identified in 15 of 16 lesions (94%). In three LG-PanIN lesions, two different *KRAS* mutations were detected, indicating that two different clones of LG-PanIN arose in pancreatic ducts in a small area (supplementary material, Figure S3). Other mutations in LG-PanIN included *RNF43* (n = 2) and *GNAS* (n = 2). No non-synonymous mutations of *CDKN2A*, *TP53*, or *SMAD4* were detected in LG-PanINs.

Case ID	Lesion designation	Gene	Mutation position (hg19)		Mutation type	Consequence	Variant allele frequency*
			Nucleotide (genomic)	Amino acid (protein)			
PDS-3	B-42	*KRAS*	chr12:25398284C>A	p.G12V	Substitution	Missense	30% (819; 2755)
PDS-6	B-43	*KRAS*	chr12:25398285C>G	p.G12R	Substitution	Missense	40% (333; 837)
PDS-7	B-36	*KRAS*	chr12:25398285C>A	p.G12C	Substitution	Missense	36% (1086; 2988)
	B-45	*KRAS*	chr12:25380275T>G	p.Q61H	Substitution	Missense	17% (43; 254)
	B-45	*KRAS*	chr12:25398284C>T	p.G12D	Substitution	Missense	16% (24; 153)
PDS-8	B-34	*KRAS*	chr12:25398284C>A	p.G12V	Substitution	Missense	47% (181; 386)
	B-34	*GNAS*	chr20:57484421G>A	p.R201H	Substitution	Missense	35% (11; 31)
	B-34	*RNF43*	chr17:56435161delC	p.G659Vfs	Deletion	Frameshift	54% (174; 323)
PDS-10	B-35	No mutations found					
	B-47	*KRAS*	chr12:25398285C>G	p.G12R	Substitution	Missense	40% (966; 2420)
	B-47	*RNF43*	chr17:56492825insA	p.E39X	Insertion	Nonsense	16% (17; 107)
PDS-13	B-37	*KRAS*	chr12:25398285C>G	p.G12R	Substitution	Missense	21% (452; 2187)
	B-38	*KRAS*	chr12:25398285C>G	p.G12R	Substitution	Missense	33% (1601; 4917)
	B-39	*KRAS*	chr12:25398285C>G	p.G12R	Substitution	Missense	30% (508; 1714)
PDS-CC2	B-40	*KRAS*	chr12:25398284C>T	p.G12D	Substitution	Missense	37% (988; 2685)
	B-41	*KRAS*	chr12:25398284C>A	p.G12V	Substitution	Missense	21% (764; 3671)
	B-41	*KRAS*	chr12:25398284C>T	p.G12D	Substitution	Missense	19% (713; 3671)
PDS-16	LGPN-1	*KRAS*	chr12:25398284C>A	p.G12V	Substitution	Missense	20% (925; 4656)
	LGPN-1	*KRAS*	chr12:25380276T>A	p.Q61L	Substitution	Missense	11% (272; 2426)
PDS-19	LGPN-1	*KRAS*	chr12:25398284C>A	p.G12V	Substitution	Missense	35% (460; 1318)
	LGPN-2	*KRAS*	chr12:25398284C>A	p.G12V	Substitution	Missense	26% (275; 1042)
PDS-21	LGPNc-1	*KRAS*	chr12:25380275T>G	p.Q61H	Substitution	Missense	37% (166; 446)
	LGPNc-1	*GNAS*	chr20:57484421G>A	p.R201H	Substitution	Missense	32% (18; 56)

* Numbers in parentheses indicate the following: (variant reads; total reads).

Table 2. Somatic mutations of isolated LG-PanINs identified by targeted sequencing

Copy number analysis of gene loci of *CDKN2A*, *TP53*, and *SMAD4* could be reliably performed in ten HG-PanINs and six LG-PanINs using the data from targeted next-generation sequencing. We identified loss of *CDKN2A* in three HG-PanINs from two patients. No copy number alterations in the assayed genes were identified in LG-PanINs.

HG-PanIN and adjacent LG-PanIN(s) were analysed by targeted sequencing in ten patients, including 16 pairs of HG-PanIN and LG-PanIN lesions. Interestingly, we found that 13 of 16 pairs of HG-PanIN and LG-PanIN fell into the group of molecularly independent, even though some were located on the same glass slide (Table 3 and supplementary material, Figure S3). There was only one pair of LG-PanIN and HG-PanIN that was 'likely related'.

Whole-exome sequencing of five isolated HG-PanINs

We performed whole-exome sequencing of five HG-PanIN lesions that were also analysed by targeted sequencing. The total number of somatic mutations in isolated HG-PanINs ranged from 30 to 175 (median 33) (supplementary material, Table S4). All somatic mutations identified in targeted sequencing were again detected (supplementary material, Table S5 and Figure S2). No mutations were identified in *TP53* or *SMAD4*.

Interestingly, one of the HG-PanIN lesions harboured 175 somatic mutations. This lesion harboured a somatic frameshift mutation, Q146Kfs of *MLH1*, likely resulting in the large number of somatic mutations in this lesion.[16,17]

Patient ID	HG-PanIN				LG-PanIN						Relationship between PanINs	
	Lesion (HG1)		Lesion (HG2)		Lesion (LG1)		Lesion (LG2)		Lesion (LG3)			
	Gene	Alteration	Gene	Alteration	Gene	Alteration	Gene	Alteration	Gene	Alteration	Histology	Mutation analysis
Between HG-PanIN lesions												
PDS-2	B-12		B-13								Contiguous (HG1 has more atypical features than HG2)	Likely related
	KRAS	p.G12D	*KRAS*	p.G12D								
	CDKN2A	Deletion	*CDKN2A*	Deletion								
	RNF43	p.R113X										
PDS-20	HGPN-2		HGPN-3								Separate	Indeterminate
	KRAS	p.G12D	*KRAS*	p.G12D								
	RNF43	LOH	*RNF43*	LOH								
	CDKN2A	Deletion	*CDKN2A**	p.W110X								
	PIK3CA	p.H1047R	*TGFBR2*	p.G155LfsX								
Between HG-PanIN and LG-PanIN(s)												
PDS-3	B-14				B-42						Separate (on the same glass slide)	Independent
	KRAS	p.G12R			*KRAS*	p.G12V						
PDS-6	B-5				B-43						Separate	Indeterminate
	KRAS	p.G12R			*KRAS*	p.G12R						
PDS-7	B-6				B-36		B-45				Separate (HG1 and LG1)	Independent (HG1 and LG1)
	KRAS	p.G12D			*KRAS*	p.G12C	*KRAS*	p.Q61H			Separate (HG1 and LG2)	Independent/indeterminate (HG1 and LG2)†
	CDKN2A	p.D84Y					*KRAS*	p.G12D				
	RNF43	LOH										
PDS-8	B-7				B-34						Separate (on the same glass slide)	Likely related
	KRAS	p.G12V			*KRAS*	p.G12V						
	GNAS	p.R201H			*GNAS*	p.R201H						
	RNF43	p.G659Vfs			*RNF43*	p.G659Vfs						
PDS-10	B-27				B-35		B-47				Separate (HG1 and LG1, on the same glass slide)	Independent (HG1 and LG1)
	KRAS	p.G12V			*KRAS*	Wild type	*KRAS*	p.G12R				
							RNF43	p.E39X			Separate (HG1 and LG2)	Independent (HG1 and LG2)
PDS-13	B-32				B-37		B-38		B-39		Separate (HG1 and LG1, on the same glass slide)	Independent (HG1 and LG1)
	KRAS	p.G12D			*KRAS*	p.G12R	*KRAS*	p.G12R	*KRAS*	p.G12R		
											Separate (HG1 and LG2, on the same glass slide)	Independent (HG1 and LG2)
											Separate (HG1 and LG3, on the same glass slide)	Independent (HG1 and LG3)
PDS-CC2	B-8				B-40		B-41				Contiguous (HG1 and LG1)	Indeterminate (HG1 and LG1)
	KRAS	p.G12D			*KRAS*	p.G12D	*KRAS*	p.G12D				
	ARID1A	p.Q1327Afs					*KRAS*	p.G12V			Separate (HG1 and LG2, on the same glass slide)	Independent/indeterminate (HG1 and LG2)†

* Copy number alteration of CDKN2A could not be assessed in HG2 (HGPN-3).

† Two types of *KRAS* mutations were observed in the same LG-PanIN lesion, indicating that two different clones were present. When the LG-PanIN lesion contained both discordant and identical *KRAS* mutations, both correlation categories of 'independent' and 'indeterminate' were designated.

Table 3. Relatedness of HG-PanIN and LG-PanIN

Patient ID	HG-PanIN				LG-PanIN						Relationship between PanINs	
	Lesion (HG1)		Lesion (HG2)		Lesion (LG1)		Lesion (LG2)		Lesion (LG3)			
	Gene	Alteration	Gene	Alteration	Gene	Alteration	Gene	Alteration	Gene	Alteration	Histology	Mutation analysis
PDS-16	HGPN-1				LGPN-1						Separate	Independent (HG1 and LG1)[†]
	KRAS	p.G12D			*KRAS*	p.G12V						
					KRAS	p.Q61L						
PDS-19	HGPN-1				LGPN-1		LGPN-2				Contiguous (HG1 and LG1)	Independent (HG1 and LG1)
	KRAS	p.G12R			*KRAS*	p.G12V	*KRAS*	p.G12V				
	CDKN2A	p.D108Y									Separate (HG1 and LG2)	Independent (HG1 and LG2)
	TP53	p.G334V										
PDS-21	HGPN-2				LGPNc-1						Contiguous	Independent
	KRAS	p.G12D			*KRAS*	p.Q61H						
					GNAS	p.R201H						

Copy number analysis of the whole-exome sequencing data revealed variations in 0 to 10 chromosomal loci (with a median of 5) (supplementary material, Table S6). Of these, deletion of the *CDKN2A* locus on chromosome 9 was detected in one HG-PanIN lesion. Other notable copy number variations included amplification of *MYC* in one lesion. The amplification of *MYC* was confirmed by fluorescence in situ hybridization (FISH) (supplementary material, Figure S3).

Immunolabelling for p53 and SMAD4

We performed immunolabelling for p53 and SMAD4 on HG-PanIN lesions (supplementary material, Figure S4). Aberrant expression of p53 was observed in 3 of 16 successfully labelled HG-PanINs, including two with diffuse nuclear labelling and one with lack of expression. Of note, only one of the three lesions with aberrant p53 expression had a somatic *TP53* mutation, while the other two were wild type. SMAD4 immunolabelling was retained in all 17 HG-PanIN lesions successfully stained.

DISCUSSION

HG-PanINs are a critical step in pancreatic tumourigenesis and potentially a key target of early detection approaches.[6,7] In order to understand this lesion, we used whole-exome and targeted DNA sequencing approaches to define the genetic alterations in HG-PanIN lesions. We overcame the confounding mimicker of HG-PanIN – cancerization of the ducts – by studying only HG-PanIN lesions from pancreata without invasive pancreatic cancer.

As expected from previous studies, we found that *KRAS* and *CDKN2A* are commonly targeted in PanIN lesions.[16–19] *KRAS* was mutated in 94% of the HG-PanIN lesions as well as 94% of the LG-PanIN lesions, consistent with the previous studies.[11,13] *CDKN2A* alterations (missense mutation and copy number loss) were also observed in HG-PanINs. In agreement with previous work, we did not find mutations or copy number loss of *CDKN2A* in LG-PanINs, suggesting that *CDKN2A* alteration may be a late event during PanIN tumourigenesis.[20,21]

Remarkably, in contrast to studies of HG-PanINs from pancreata with invasive carcinoma, we identified *TP53* mutations in only 2 of 17 HG-PanIN lesions (12%), and *SMAD4* mutations were completely absent.[9,10,12,14] Immunohistochemistry for p53 and SMAD4 also rarely showed aberrant expression of these tumour suppressor genes. What might explain this discrepancy in *TP53* and *SMAD4* alterations in HG-PanIN compared with previous studies? The studies that reported frequent *TP53* and *SMAD4* alterations all analysed HG-PanIN in the setting of invasive PDAC – as such, it is possible that many of the 'HG-PanINs' in these studies were actually intraductal spread of invasive cancer (which frequently contains these tumour suppressor gene alterations).[15] An alternative explanation for the discrepancy is that isolated HG-PanIN is biologically different from HG-PanIN associated with PDAC (which could be more advanced and perhaps more likely to have mutations in *TP53* and *SMAD4*).

Other noteworthy alterations in isolated PanINs in our study included mutations in *RNF43* and *GNAS*, which are frequent in IPMN. We cannot exclude the possibility that these HG-PanINs, if left in place, may have eventually grown into lesions large enough to meet size criteria for IPMNs.[22] Still, the presence of high-grade dysplasia argues that these are advanced lesions, not simply early pre-IPMNs.

In conclusion, we performed genetic analysis of isolated HG-PanIN lesions using next-generation sequencing. We confirmed *KRAS* and *CDKN2A* mutations in PanINs, but mutations of *TP53* and *SMAD4* were rarely found in isolated HG-PanIN. Our results suggest that inactivation of *TP53* and *SMAD4* is limited to, or predominantly occurs in, bona fide invasive carcinomas. These data will profoundly affect the interpretation of results from molecular screening approaches for pancreatic cancer.

REFERENCES

1. Siegel, R. L., Miller, K. D. & Jemal, A. Cancer statistics, 2016. CA Cancer J. Clin. 66, 7–30 (2016).
2. Lennon, A. M. et al. The early detection of pancreatic cancer: what will it take to diagnose and treat curable pancreatic neoplasia? Cancer Res. 74, 3381–3389 (2014).
3. Hruban, R. H. et al. Ductal adenocarcinoma of the pancreas. in WHO Classification of Tumours of the Digestive System (eds. Bosman, F. T., Carneiro, F., Hruban, R. H. & Theise, N. D.) 281–291 (International Agency for Research on Cancer, 2010).
4. Andea, A., Sarkar, F. & Adsay, V. N. Clinicopathological correlates of pancreatic intraepithelial neoplasia: a comparative analysis of 82 cases with and 152 cases without pancreatic ductal adenocarcinoma. Mod. Pathol. 16, 996–1006 (2003).
5. Ito, R. et al. Pancreatic intraepithelial neoplasms in the normal appearing pancreas: on their precise relationship with age. Hepatogastroenterology 55, 1103–1106 (2008).
6. Kanda, M. et al. Mutant TP53 in duodenal samples of pancreatic juice from patients with pancreatic cancer or high-grade dysplasia. Clin. Gastroenterol. Hepatol. 11, 719–30.e5 (2013).
7. Eshleman, J. R. et al. *KRAS* and guanine nucleotide-binding protein mutations in pancreatic juice collected from the duodenum of patients at high risk for neoplasia undergoing endoscopic ultrasound. Clin. Gastroenterol. Hepatol. 13, 963–9.e4 (2015).
8. Wilentz, R. E. et al. Inactivation of the p16 (INK4A) tumor-suppressor gene in pancreatic duct lesions: loss of intranuclear expression. Cancer Res. 58, 4740–4744 (1998).
9. Wilentz, R. E. et al. Loss of expression of Dpc4 in pancreatic intraepithelial neoplasia: evidence that DPC4 inactivation occurs late in neoplastic progression. Cancer Res. 60, 2002–2006 (2000).
10. Maitra, A. et al. Multicomponent analysis of the pancreatic adenocarcinoma progression model using a pancreatic intraepithelial neoplasia tissue microarray. Mod. Pathol. 16, 902–912 (2003).
11. Löhr, M., Klöppel, G., Maisonneuve, P., Lowenfels, A. B. & Lüttges, J. Frequency of K-ras mutations in pancreatic intraductal neoplasias associated with pancreatic ductal adenocarcinoma and chronic pancreatitis: a meta-analysis. Neoplasia 7, 17–23 (2005).
12. Furukawa, T. et al. Distinct progression pathways involving the dysfunction of DUSP6/MKP-3 in pancreatic intraepithelial neoplasia and intraductal papillary-mucinous neoplasms of the pancreas. Mod. Pathol. 18, 1034–1042 (2005).
13. Kanda, M. et al. Presence of somatic mutations in most early-stage pancreatic intraepithelial neoplasia. Gastroenterology 142, 730–733.e9 (2012).
14. Murphy, S. J. et al. Genetic alterations associated with progression from pancreatic intraepithelial neoplasia to invasive pancreatic tumor. Gastroenterology 145, 1098–1109.e1 (2013).
15. Basturk, O. et al. A Revised Classification System and Recommendations From the Baltimore Consensus Meeting for Neoplastic Precursor Lesions in the Pancreas. Am. J. Surg. Pathol. 39, 1730–1741 (2015).
16. Wang, L. et al. Whole-exome sequencing of human pancreatic cancers and characterization of genomic instability caused by MLH1 haploinsufficiency and complete deficiency. Genome Res. 22, 208–219 (2012).
17. Witkiewicz, A. K. et al. Whole-exome sequencing of pancreatic cancer defines genetic diversity and therapeutic targets. Nat. Commun. 6, 6744 (2015).
18. Jones, S. et al. Core signaling pathways in human pancreatic cancers revealed by global genomic analyses. Science 321, 1801–1806 (2008).
19. Waddell, N. et al. Whole genomes redefine the mutational landscape of pancreatic cancer. Nature 518, 495–501 (2015).
20. Rosty, C. et al. p16 Inactivation in pancreatic intraepithelial neoplasias (PanINs) arising in patients with chronic pancreatitis. Am. J. Surg. Pathol. 27, 1495–1501 (2003).
21. Fukushima, N. et al. Aberrant methylation of preproenkephalin and p16 genes in pancreatic intraepithelial neoplasia and pancreatic ductal adenocarcinoma. Am. J. Pathol. 160, 1573–1581 (2002).
22. Matthaei, H. et al. *GNAS* sequencing identifies IPMN-specific mutations in a subgroup of diminutive pancreatic cysts referred to as 'incipient IPMNs'. Am. J. Surg. Pathol. 38, 360–363 (2014).

4

Chapter 5

IPMNs with co-occurring invasive cancers: neighbours but not always relatives

Matthäus Felsenstein, Michaël Noë, David L. Masica, Waki Hosoda, Peter Chianchiano, Catherine G. Fischer, Gemma Lionheart, Lodewijk A.A. Brosens, Antonio Pea, Jun Yu, Georgios Gemenetzis, Vincent P. Groot, Martin A. Makary, Jin He, Matthew J. Weiss, John L. Cameron, Christopher L. Wolfgang, Ralph H. Hruban, Nicholas J. Roberts, Rachel Karchin, Michael G. Goggins, Laura D. Wood

Gut, September 2018

ABSTRACT

Objective: Intraductal papillary mucinous neoplasms (IPMNs) are precursor lesions that can give rise to invasive pancreatic carcinoma. Although approximately 8% of patients with resected pancreatic ductal adenocarcinoma have a co-occurring IPMN, the precise genetic relationship between these two lesions has not been systematically investigated.

Design: We analysed all available patients with co-occurring IPMN and invasive intrapancreatic carcinoma over a 10-year period at a single institution. For each patient, we separately isolated DNA from the carcinoma, adjacent IPMN and distant IPMN and performed targeted next generation sequencing of a panel of pancreatic cancer driver genes. We then used the identified mutations to infer the relatedness of the IPMN and co-occurring invasive carcinoma in each patient.

Results: We analysed co-occurring IPMN and invasive carcinoma from 61 patients with IPMN/ductal adenocarcinoma as well as 13 patients with IPMN/colloid carcinoma and 7 patients with IPMN/carcinoma of the ampullary region. Of the patients with co-occurring IPMN and ductal adenocarcinoma, 51% were likely related. Surprisingly, 18% of co-occurring IPMN and ductal adenocarcinomas were likely independent, suggesting that the carcinoma arose from an independent precursor. By contrast, all colloid carcinomas were likely related to their associated IPMNs. In addition, these analyses showed striking genetic heterogeneity in IPMNs, even with respect to well-characterised driver genes.

Conclusion: This study demonstrates a higher prevalence of likely independent co-occurring IPMN and ductal adenocarcinoma than previously appreciated. These findings have important implications for molecular risk stratification of patients with IPMN.

INTRODUCTION

Pancreatic ductal adenocarcinoma (PDAC) is one of the most aggressive human cancers.[1] PDAC arises from non-invasive precursor lesions which take several years to transform into invasive carcinoma, providing opportunity for early detection and surgical cure. Intraductal papillary mucinous neoplasms (IPMNs) are the most prevalent cystic precursor lesion in the pancreas.[2] Due to the potential for progression to invasive carcinoma, patients with IPMNs are routinely monitored, with surgical intervention recommended for clinical and radiological 'worrisome features' and 'high-risk stigmata'.[3] As more IPMNs are discovered incidentally on routine abdominal imaging, optimal surveillance for patients with these lesions is becoming a pressing clinical problem, highlighting the need to balance cancer prevention with overtreatment.[4,5]

Because of the ability to obtain cyst fluid by fine needle aspiration, pancreatic cysts (including IPMNs) are a promising application of molecular diagnostics.[6–8] In recent years, extensive next-generation sequencing analyses have comprehensively characterised the genomic landscape of PDAC, reaffirming the four driver genes altered in the vast majority of tumours (the oncogene *KRAS* and the tumour suppressor genes *TP53*, *CDKN2A* and *SMAD4*) as well as a much larger number of genes altered at low prevalence.[9–13] Additional studies have focused on genetic alterations in histologically distinct precursor lesions, elucidating the timing of specific mutations in pancreatic tumorigenesis.[14–16] Next-generation sequencing of cyst fluid DNA to identify key driver gene mutations can reliably distinguish IPMNs from other cystic lesions.[17,18] Perhaps more importantly, specific late-occurring driver gene mutations, such as *TP53* and *SMAD4*, may be able to distinguish low-grade from high-grade premalignant lesions, separating patients who benefit from surgical intervention.[6,7] This strategy may provide a promising tool for earlier detection of pancreatic carcinoma derived from IPMNs in the future. However, as it relies on mutations identified in the cyst fluid, this approach assumes that the invasive carcinoma arises from the co-occurring IPMN—it may not detect invasive carcinomas that arise from physically adjacent but genetically independent precursor lesions.

Multiple studies have described multifocal neoplasia in the pancreas, particularly in patients with IPMNs.[19–21] In pancreata with IPMNs, anatomically separate invasive carcinomas have been termed 'concomitant' carcinomas.[20,22,23] The traditional definition of IPMN with 'concomitant' carcinoma relies on the physical separation of the two lesions by an uninvolved segment of pancreatic parenchyma, assuming that the lack of physical proximity implies independent origin of both lesions.[22] However, it is possible that a genetically independent invasive carcinoma could arise in close proximity to an IPMN, making them indistinguishable from IPMN with associated invasive carcinoma by clinical and pathological features alone.

Genetic alterations can be used as molecular tools to assess the relatedness of IPMNs and co-occurring invasive cancers. For example, the identification of discordant *KRAS* and *GNAS* mutations in IPMNs and their concomitant invasive carcinomas has been reported and provides evidence for the

independent genetic origins of some neoplasms.[24,25] An accurate estimation of the proportion of genetically independent PDACs co-occurring with IPMNs is of significant clinical importance; cyst fluid analysis of the nearby IPMN in this situation would likely not identify mutations from the highest risk lesion, as the PDAC would not shed its high-risk mutant DNA molecules into the monitored cyst fluid unless the PDAC invaded the cyst wall.

In this study, we use targeted next-generation sequencing to analyse driver gene mutations in paired neoplastic samples from a cohort of IPMNs with co-occurring PDACs. Using the identified mutations, we determined relatedness and estimated the proportion of these lesions that are genetically independent.

METHODS

We identified all patients who underwent pancreatic resection with a diagnosis of co-occurring IPMN and invasive carcinoma over a 10-year period. We reviewed clinical and pathological data as well as H&E stained slides from each patient to confirm the diagnosis. Neoplastic cells from the invasive carcinoma, IPMN immediately adjacent to the invasive carcinoma (adj-IPMN) and IPMN without invasive carcinoma in the same tissue block (dist-IPMN) were separately isolated from formalin-fixed paraffin-embedded (FFPE) tissue sections by laser capture microdissection (LCM). In all but one case, the adj-IPMN and dist-IPMN samples came from the same grossly defined cyst. Thus, our cohort included only a single case of multifocal IPMN with two pathologically distinct IPMN lesions (IPP12). In addition, three met criteria for IPMN with concomitant carcinoma, with intervening uninvolved pancreas between the two lesions (IPP05, IPP11, IPP48). DNA was extracted from each sample, and DNA of sufficient quantity and quality was obtained from 76 invasive cancers and co-occurring IPMNs, including 56 ductal adenocarcinomas of the pancreas, 13 colloid carcinomas of the pancreas and 7 invasive cancers of the ampullary region (ampullary, distal bile duct and duodenal carcinomas). The cohort for this study initially excluded five patients with IPMN co-occurring with ductal adenocarcinoma that were analysed by whole exome sequencing in a separate study—these cases were selected based on their morphology suggestive of carcinoma arising from an IPMN, and the IPMN and ductal adenocarcinoma shared numerous somatic mutations in each case. These related cases are included in our final estimate of the prevalence of genetically unrelated IPMN/ductal adenocarcinoma in the ‘Discussion’ section and were used to confirm the accuracy of our relatedness assessment. All samples were analysed by targeted next generation sequencing of a custom panel of pancreatic driver genes using Ion AmpliSeq library preparation on an Ion Torrent Personal Genome Machine, and whole exome sequencing was performed on three selected cases by Personal Genome Diagnostics (Baltimore, Maryland, USA).[26] Mutations were identified using NextGENe software followed by visual inspection to minimise risk of artifactual calls.[27] The relatedness of the lesions from each patient was determined by a categorical algorithm as described in the ‘Results’ section. The validity of this approach was confirmed by an independent statistical model to evaluate the probability of relatedness based on the site-specific mutation distributions in our study cohort. In addition, immunohistochemistry (IHC) for p53 and SMAD4 protein

was performed on FFPE sections from selected cases.

RESULTS

IPMN lesions co-occurring in pancreata with invasive carcinoma

Within a period of 10 years (from 2006 to 2015), 159 patients diagnosed with invasive pancreatic or periampullary carcinoma and co-occurring IPMN underwent resection at The Johns Hopkins Hospital—112 of these patients had ductal adenocarcinoma, 35 had colloid carcinoma and 12 had a carcinoma of the ampullary region (ampullary, distal bile duct and duodenal carcinomas). In the same period, 1267 patients underwent resection for ductal adenocarcinoma without an associated IPMN; thus, approximately 8% of patients with ductal adenocarcinoma had a co-occurring IPMN. We obtained sufficient high-quality DNA for targeted next generation sequencing analysis from 76 co-occurring IPMN/invasive carcinoma. Of these, 56 were co-occurring IPMN/ductal adenocarcinomas of the pancreas as well as 13 co-occurring IPMN/colloid carcinomas of the pancreas and 7 co-occurring IPMN/carcinomas of the ampullary region. Clinical differences in stage and grade of the carcinoma are readily apparent between the different cohorts, as are differences in the co-occurring IPMNs (Table 1 and online Supplementary Table S1).[28] For example, while ductal adenocarcinomas and colloid carcinomas most often occurred in association with high-grade IPMNs, the IPMNs co-occurring with ampullary region carcinoma were typically low-grade, supporting the clinical assumption that ampullary and pancreatic neoplasms are usually independent. Moreover, colloid carcinomas of the pancreas co-occurred with IPMN of intestinal subtype whereas ductal adenocarcinomas were mostly associated with gastric and pancreatobiliary subtypes of IPMNs.

Although our cohort demonstrates that IPMNs and invasive carcinomas frequently occur in the same pancreata, it is not possible to determine relatedness from clinical and pathological features alone. To more accurately determine the genetic relationship between IPMNs and co-occurring invasive carcinomas, we performed targeted next generation sequencing analysis of a panel of pancreatic cancer driver genes for the entire cohort and whole exome sequencing for selected cases. From each case, we separately isolated neoplastic cells from the IPMN and invasive carcinoma using LCM (online Supplementary Figure S1). We collected IPMN adjacent to the carcinoma (adj-IPMN) and from a separate block not in direct contact with the invasive carcinoma (dist-IPMN) when available.

Molecular landscape of carcinomas and their co-occurring IPMNs

We performed targeted next generation sequencing of IPMN/PDAC driver genes using an IonTorrent Personal Genome Machine to an average coverage depth of >600× (online Supplementary Table S2). We compared mutations identified in the tumour samples to those in the matched normal tissue from each patient in order to exclude germline variants and report true somatic mutations (online Supplementary Figure S2). The majority of somatic mutations in the entire cohort (76 carcinoma samples and 95 IPMN samples) were missense mutations (88.1%), while nonsense mutations (5.3%), frameshift insertions/deletions (4.9%), in-frame insertions/deletions (0.9%) and splice site alterations (0.2%) made

Carcinoma	Total cases (adj.-IPMN/dist.-IPMN)	Gender	Age	Location carcinoma/adj.-IPMN	Location dist.-IPMN	Cancer			IPMN						
						T	N	Grade	Size (cm)	Grade	Type	Subtype			
Ductal adenocarcinoma	56 (53/42)	M 63.6% (35)	70.2	Head	36% (20)	T1	10.7% (6)	N0	30.4% (17)	1	3.6% (2)	2.9	LGD	19.6% (11)	BD	57.4% (27)	Gastric	61.8% (34)
		F 36.4% (21)	(+/–10.8)	Neck	28% (15)	T2	39.3% (22)	N1	69.6% (39)	2	62.5% (35)	(+/-2.5)	HGD	80.4% (45)	MD	29.8% (14)	Intestinal	7.2% (4)
				Body	20% (11)	T3	46.4% (26)			3	26.8% (15)				Mixed	12.8% (6)	Pancreatobiliary	23.6% (13)
				Tail	12% (6)	T4	3.6% (2)			4	3.6% (2)						Oncocytic	7.2% (4)
				Multifocal	–													
Colloid carcinoma	13 (11/9)	M 76.9% (10)	62.5	Head	50% (6)	T1	53.8% (7)	N0	92.3% (12)	1	61.5% (8)	4.9	LGD	0% (0)	BD	7.7% (1)	Gastric	0% (0)
		F 23.1% (3)	(+/– 11.9)	Neck	16.7% (2)	T2	23.1% (3)	N1	7.7% (1)	2	38.5% (5)	(+/-1.94)	HGD	100% (13)	MD	69.2% (9)	Intestinal	100% (13)
				Body	16.7% (2)	T3	23.1% (3)			3	0% (0)				Mixed	23.1% (3)	Pancreatobiliary	0% (0)
				Tail	16.7% (2)	T4	0% (0)			4	0% (0)						Oncocytic	0% (0)
				Multifocal	–													
Carcinoma of the ampullary region	7 (6/5)	M 42.8% (3)	74.1	Head	100% (7)	T1	0% (0)	N0	0% (0)	1	0% (0)	1.1	LGD	71.4% (5)	BD	71.4% (5)	Gastric	85.7% (6)
		F 57.2% (4)	(+/– 8.5)	Neck	0% (0)	T2	0% (0)	N1	100% (7)	2	57.1% (8)	(+/-0.19)	HGD	28.6% (2)	MD	14.3% (1)	Intestinal	0% (0)
				Body	0% (0)	T3	71.4% (5)			3	42.8% (6)				Mixed	14.3% (1)	Pancreatobiliary	14.3% (1)
				Tail	0% (0)	T4	28.8% (2)			4	0% (0)						Oncocytic	0% (0)
				Multifocal	0% (0)													
Significance*		ns	ns	ns	ns	<0.001	<0.001		<0.001			<0.001		0.009			<0.001	

* Tests were performed via ANOVA test for continuous variables or Fisher-Exact test for categorical variables.

ANOVA, analysis of variance; BD, branch duct; HGD, high grade dysplasia; IPMN, intraductal papillary mucinous neoplasm; LGD, low grade dysplasia; MD, main duct

Table 1. Clinical and pathological features of patients with IPMN and co-occurring carcinoma

up only a minor proportion of the identified somatic alterations (online Supplementary Table S3).

In our cohort of 56 ductal adenocarcinomas, *KRAS* was mutated in 91% and *TP53* in 57% of the invasive carcinomas (online Supplementary Figure S2). The two other major genetic drivers of ductal adenocarcinoma, *CDKN2A* and *SMAD4*, were altered by single nucleotide variants at lower prevalence, 11% and 30%, respectively. However, as these genes are also frequently altered by homozygous deletion, we performed copy number analysis on defined targeted loci which showed deletion of *CDKN2A* in 7% and *SMAD4* in 16% of ductal adenocarcinomas (online Supplementary Table S3). *GNAS* and *RNF43* mutations were frequently present in ductal adenocarcinomas, at 16% and 23%, respectively, highlighting that at least a subset of these PDACs likely arose from IPMNs.

GNAS mutations occurred in 85% (11 of 13) of colloid carcinomas, which are known to arise almost exclusively from intestinal-type IPMNs (online Supplementary Figure S2).[29,30] *TP53* mutations were detected in 46% of colloid carcinomas, but *KRAS* mutations were found in only 31% of cases. The vast majority (90%) of *GNAS* mutations in the entire carcinoma cohort (n=76) occurred at the hotspot codon 201, with a surprising enrichment of R201C mutations in colloid carcinomas (73% of *GNAS* mutations), in contrast to an enrichment of R201H mutations in ductal adenocarcinomas (75% of *GNAS* mutations) (online Supplementary Figure S3). Mutations in *CDKN2A* and *SMAD4* were rarely detected in colloid carcinomas.

Our cohort also included seven carcinomas of the ampullary region (ampullary, distal bile duct and duodenal carcinomas) with co-occurring IPMNs. In these cancers, *KRAS* was the most frequently altered driver with mutation in 71%, while *SMAD4* was the only other driver with mutation in more than one of these carcinomas (online Supplementary Figure S2).

IPMNs co-occurring with ductal adenocarcinomas, colloid carcinomas and ampullary region carcinomas were dissected

and separately analysed. IPMNs immediately adjacent to ductal adenocarcinomas (adj-IPMN; n=53) were characterised by prevalent mutations in IPMN-specific drivers such as *GNAS* (25%) and *RNF43* (36%), while they had fewer mutations in *CDKN2A* (7%), *TP53* (34%) and *SMAD4* (9%) compared with their neighbouring invasive carcinomas (online Supplementary Figure S2). IPMNs co-occurring with colloid carcinomas displayed a molecular signature characteristic of intestinal subtype IPMNs, showing a higher prevalence of alterations in *GNAS* (82%) and a lower prevalence of *KRAS* mutations (45%). At least one oncogenic hotspot mutation (in *KRAS* and/or *GNAS*) was identified in 92% of all IPMNs in our entire cohort of 76 patients (online Supplementary Table S3).

Validation of somatic mutations and their accuracy in classifying relatedness

In order to determine the relatedness of the IPMN and invasive carcinoma in each patient, we applied two independent analytic approaches. First, we developed a categorical algorithm based on shared mutations between the two lesions. 'Likely related' lesions shared more than two hotspot mutations or one mutation other than a hotspot mutation (see details in online supplementary methods), while 'likely independent' lesions had no shared mutations. In addition, as *GNAS* mutations are rare in ductal adenocarcinomas not derived from IPMNs, we considered IPMNs and invasive carcinomas with shared *GNAS* mutations as 'likely related'. Lesion pairs with only a shared hotspot *KRAS* mutation were designated as 'indeterminate'—the high prevalence of such hotspot mutations in IPMNs as well as ductal adenocarcinomas makes it an unreliable indicator of relatedness, as such a mutation could also occur independently by chance in unrelated lesions.

We confirmed the reliability of this classification in two ways. First, in order to determine the specificity of our 'likely related' categorization, we classified the relatedness of IPMNs and carcinomas from different patients in our cohort using the identified mutations (online Supplementary Figure S4). Of the 3136 total relatedness assessments of lesion pairs from different patients, only 60 (1.9%) were classified as 'likely related'. Of note, these 'likely related' classifications were almost exclusively driven by shared mutations in the *GNAS* hotspot in codon 201. However, this strategy for evaluating our algorithm likely overestimates 'false positives' in our classification of 'likely related' lesions. While common *GNAS* hotspot alterations are likely to be shared by IPMNs and IPMN-associated carcinomas from different patients, such mutations are unlikely to be shared by independent IPMNs and PDACs in the same patient, as such *GNAS* alterations are rare in PDACs arising outside of IPMNs.[10–12] Second, in order to determine the sensitivity of our 'likely related' classification, we performed our targeted next generation sequencing (NGS) assay on five pairs of co-occurring IPMN/PDAC with concrete evidence of relatedness based on numerous shared somatic mutations in whole exome sequencing performed for a separate study (online Supplementary Table S4). All five of these lesion pairs were classified as 'likely related' based on our categorical algorithm.

In order to further validate our relatedness assessment, we developed a quantitative statistical model to calculate the probability of the shared mutations in any two samples occurring by chance (online supplementary methods). These probabilities were plotted on heat maps, highlighting that the vast ma-

Patient ID	Diagnosis	Genetic alterations						Shared mutations		
		Carcinoma		adj-IPMN		dist-IPMN		Carcinoma / adj -IPMN	Carcinoma / dist -IPMN	adj-IPMN / dist -IPMN
IPP08	Ductal adenocarcinoma	KRAS: p.G12V	missense	KRAS: p.G12V	missense	KRAS: p.G12V	missense	KRAS: p.G12V	KRAS: p.G12V	KRAS: p.G12V
		RNF43: p.G67D	missense	RNF43: p.G67D	missense	GNAS: p.R201H	missense	RNF43: p.G67D		
		TGFBR2: p.P526L	missense	TGFBR2: p.P526L	missense			TGFBR2: p.P526L		
		ARID1A: p.Q2207X	missense					likely related*	indeterminate*	indeterminate*
								<0.00000001†	0.0403†	0.0407†
IPP14	Ductal adenocarcinoma	KRAS: p.G12D	missense	KRAS: p.G12D	missense	KRAS: p.G12D	missense	KRAS: p.G12D	KRAS: p.G12D	KRAS: p.G12D
		ARID1A: p.N1313S	missense	ARID1A: p.N1313S	missense	KRAS: p.Q61H	missense	ARID1A: p.N1313S	ARID1A: p.N1313S	ARID1A: p.N1313S
		RNF43: p.P686R	missense	RNF43: p.P686R	missense	ARID1A: p.N1313S	missense	RNF43: p.P686R	RNF43: p.P686R	RNF43: p.P686R
						RNF43: p.P686R	missense	likely related*	likely related*	likely related*
								<0.00000001†	<0.00000001†	<0.00000001†
IPP22	Ductal adenocarcinoma	KRAS: p.G12V	missense	KRAS: p.G12V	missense	GNAS: p.R201H	missense	KRAS: p.G12V	GNAS: p.R201H	GNAS: p.R201H
		GNAS: p.R201H	missense	GNAS: p.R201H	missense	TP53: p.V272L	missense	GNAS: p.R201H	TP53: p.V272L	TP53: p.V272L
		PIK3CA: p.H1047L	missense	PIK3CA: p.H1047L	missense	SMAD4: p.W398X	nonsense	PIK3CA: p.H1047L	SMAD4: p.W398X	SMAD4: p.W398X
		TP53: p.V272L	missense	TP53: p.V272L	missense			TP53: p.V272L		
		SMAD4: p.W398X	nonsense	SMAD4: p.W398X	nonsense			SMAD4: p.W398X		
								likely related*	likely related*	likely related*
								<0.00000001†	0.00607†	0.00679†
IPP26	Ductal adenocarcinoma	KRAS: p.G12V	missense	KRAS: p.G12D	missense	KRAS: p.G12D	missense	none	none	KRAS: p.G12D
		SMAD4: p.R372K	missense	GNAS: p.R201H	missense	GNAS: p.R201H	missense			GNAS: p.R201H
		ARID1A: p.M1300I	missense	TP53: p.R205Q				likely independent*	likely independent*	likely related*
								>0.9†	>0.9†	0.08
IPP43	Ductal adenocarcinoma	KRAS: p.G12D	missense	KRAS: p.G12V	missense	KRAS: p.G12V	missense	none	none	KRAS: p.G12V
		GNAS: p.R201C	missense	TP53: p.R196X	missense					
		PIK3CA: p.M1004V	missense	SMAD4: p.K70fs	frameshift					
								likely independent*	likely independent*	indeterminate*
								>0.9†	>0.9†	0.0407†
IPP54	Ductal adenocarcinoma	KRAS: p.G12V	missense	KRAS: p.G12A	missense	KRAS: p.G12D	missense	none	none	none
		TP53: p.V272L	missense			TP53: p.P390Lfs	frameshift			
								likely independent*	likely independent*	likely independent*
								0.9†	0.9†	0.9†
IPP38	Ductal adenocarcinoma	KRAS: p.G12V	missense	KRAS: p.G12R	missense	KRAS: p.G12V	missense	KRAS: p.G12V	KRAS: p.G12V	KRAS: p.G12V
		TP53: p.C275Y	missense	KRAS: p.G12V	missense					
		SMAD4: p.E235K	missense	ARID1A: p.D385H	missense					
								indeterminate*	indeterminate*	indeterminate*
								0.0403†	0.0403†	0.0407†

* Categorical assessment.
† Statistical assessment.
adj-/dist-IPMN, adjacent/distant IPMN; IPMN, intraductal papillary mucinous neoplasm; N/A, sample not available.

Table 2. Somatic mutations in representative cases of cancer and co-occurring IPMN

Patient ID	Diagnosis	Genetic alterations					Shared mutations		
		Carcinoma		adj-IPMN		dist-IPMN	Carcinoma / adj -IPMN	Carcinoma / dist -IPMN	adj-IPMN / dist -IPMN
IPC03	Colloid carcinoma	GNAS: p.R201C	missense	GNAS: p.R201C	missense	N/A	GNAS: p.R201C	N/A	N/A
		TP53: p.G245D	missense	TP53: p.G245D	missense		TP53: p.G245D		
							likely related*		
		PIK3CA: p.M1004I	missense						
IPC06	Colloid carcinoma	GNAS: p.R201C	missense	GNAS: p.R201C	missense	GNAS: p.R201C missense	GNAS: p.R201C	GNAS: p.R201C	GNAS: p.R201C
		TP53: p.H193R	missense	TP53: p.H193R	missense	TP53: p.H193R missense	TP53: p.H193R	TP53: p.H193R	TP53: p.H193R
						RNF43: p.C511F missense			
							likely related*	likely related*	likely related*
IPA03	Carcinoma of the ampullary region	TGFBR2: p.E270K	missense	KRAS: p.G12R	missense	GNAS: c.1018+1G>A Splice variant	none	none	none
				GNAS: p.R201C	missense				
							likely independent*	likely independent*	likely independent*
IPA07	Carcinoma of the ampullary region	KRAS: p.G12D	missense	KRAS: p.G12V	missense	KRAS: p.Q61H missense	none	none	none
				CDKN2A: p.G111fs	frameshift	GNAS: p.R201H missense			
							likely independent*	likely independent*	likely independent*

jority of lesion pairs with low probabilities were derived from the same patient (online Supplementary Figure S5). When comparing our categorical classification to these statistical measures, 'likely related' lesions had a mean probability of 0.0017 or <0.2% probability of sharing these mutation profiles by chance. In addition, 85% of cases classified as 'likely related' by our qualitative algorithm had a probability of <0.001, further demonstrating the robustness of our classification (online Supplementary Table S5). Also of note, as all of our 'likely independent' cases shared no somatic mutations, all had a probability of >0.9 in this approach, as approximately 9 million synthetic IPMN/PDAC pairs shared no somatic mutations (online supplementary methods). Cases classified as 'indeterminate' by our categorical algorithm cases had an average probability value of 0.049, highlighting a higher probability of developing shared mutation profiles by chance and supporting our reluctance to designate relatedness based on shared *KRAS* hotspot mutations alone.

Finally, in order to determine the frequency of sequencing errors that altered relatedness assessment in our targeted NGS assay, we conducted a validation experiment by resequencing 16 adj-IPMN/PDAC pairs with our assay at a much higher coverage (average coverage of 2,192X in the targeted region). We confirmed that >95% of the somatic mutations which conferred relatedness in these samples were present in the resequenced samples (see online Supplementary Table S6). In all cases, the relatedness classification was confirmed based on the results of this deep resequencing, underscoring the reliability of our original targeted NGS assay. Together, these results confirm that our method for evaluating genetic relatedness of these lesions was accurate.

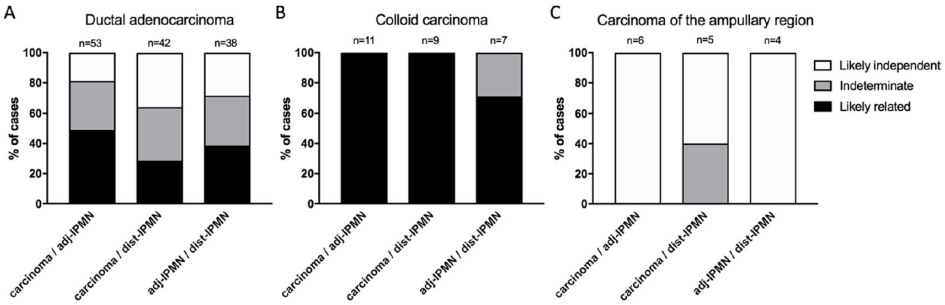

Figure 1. Relatedness of IPMNs and co-occurring carcinomas. Bars show the fraction of likely related (black), likely independent (white) and indeterminate (grey) neoplasms. For each patient the relatedness of three pairs of neoplasms was assayed: carcinoma and adj-IPMN (left), carcinoma and dist-IPMN (middle) and adj-IPMN and dist-IPMN (right). Molecular analysis of three different pancreatic cancer entities, ductal adenocarcinoma (A), colloid carcinoma (B) and carcinoma of the ampullary region (C), revealed a distinct prevalence of relatedness to co-occurring IPMN in each cancer type. adj-/dist-IPMN, adjacent/distant IPMN; IPMN, intraductal papillary mucinous neoplasm.

Relatedness of IPMNs to co-occurring carcinomas

Using our qualitative algorithm, 46% of the IPMN/ductal adenocarcinomas were 'likely related', further helping to establish IPMNs as precursor lesions to co-occurring ductal adenocarcinomas (Figure 1A and online Supplementary Table S7). Importantly, only a subset of these 'likely related' cancers (23%) harboured a *GNAS* mutation, highlighting the inadequacy of this IPMN-associated gene mutation as a single biomarker to identify IPMN-associated ductal adenocarcinomas. Surprisingly, despite the close anatomic proximity of the two lesions, a sizeable proportion (20%) of IPMNs and co-occurring ductal adenocarcinomas were 'likely independent', as they shared no driver gene mutations. The remaining IPMN/ductal adenocarcinoma pairs (34%) were classified as 'indeterminate', as their relatedness could not be confidently assigned by mutations in the driver genes in our targeted sequencing assay. Considering the five cases of known relatedness initially excluded from our cohort but later used for validation, we identified the following prevalences of relatedness in the entire cohort—'likely related': 51%, indeterminate: 31% and likely independent: 18%. Representative cases are presented in Table 2, overall proportions in Figure 1 and relatedness assessment for individual cases in online Supplementary Table S7.

Because they share only a *KRAS* hotspot, 'indeterminate' cases could be either related or independent. In order to more definitively determine the relatedness of these lesions, we performed whole exome sequencing on three cases classified as 'indeterminate' in our targeted NGS assay for which we had sufficient DNA (IPP17, IPP39, IPP41). Surprisingly, the whole exome sequencing data suggest that two of these three co-occurring IPMNs/PDACs are genetically independent, as they share no somatic mutations aside from the *KRAS* hotspot alteration (online Supplementary Table S8). In contrast, 21 somatic mutations were shared between the IPMN and PDAC in the other 'indeterminate' case, providing strong evidence that this PDAC arose from the co-occurring IPMN.

There was no correlation between IPMN/PDAC relatedness and clinicopathological features including cyst size, grade and histological subtype (online Supplementary Table S9). Many of the 'likely indepen-

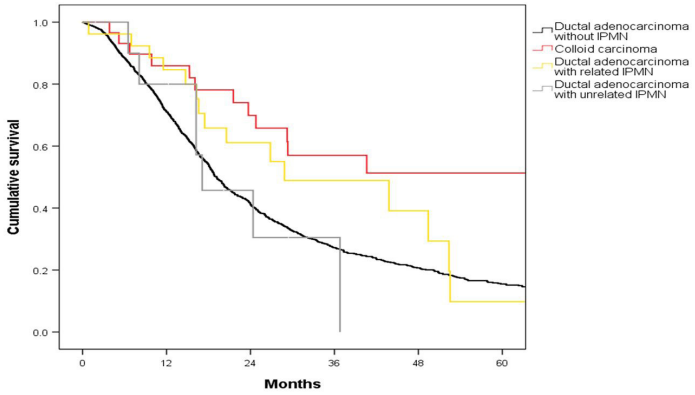

Pancreatic carcinoma cohorts at JHMI (2006-2015)	Cases	Survival (months)	CI*	Pairwise comparison (p-value)**
Ductal adenocarcinoma without IPMN	1266	19.2	18.0-20.3	0.001, 0.13, 0.28, 0.1, 0.005, 0.017
Colloid carcinoma	35	77.0	4.3-149.6	
Ductal adenocarcinoma with likely related IPMN***	26	28.8	21.2-36.5	
Ductal adenocarcinoma with likely independent IPMN***	10	16.2	14.2-18.3	

*Confidence interval [95%]
**Log-rank test
***based on targeted sequencing assay within this study

Figure 2. Survival analysis of patients with pancreatic cancer based on their molecular relationship with co-occurring IPMNs. Cumulative survival of ductal adenocarcinoma patients with and without co-occurring IPMNs after 5-year follow-up. Colloid carcinomas have significantly better survival than ductal adenocarcinoma without IPMN (P value 0.001; Log-rank test). Patients follow a divergent survival pattern when considering the relatedness of ductal adenocarcinomas with co-occurring IPMNs based on results of the targeted sequencing assay (P value: 0.017; Log-rank test). Ductal adenocarcinomas likely related to IPMNs show improved overall survival (28.8 months), while ductal adenocarcinomas likely independent of IPMNs have poorer survival similar to ductal adenocarcinoma without IPMN (16.2 months). IPMN, intraductal papillary mucinous neoplasm.

dent' cases were resected because preoperatively their IPMNs met criteria for resection; clinical and radiological features of the IPMN led to resection of 58% of 'likely independent' cases compared with 52% of 'likely related' cases. Thus, most of the IPMNs in the 'likely independent' cases were not merely incidental small cysts adjacent to large ductal adenocarcinomas. Crucially, mutations in driver genes that suggest a high risk for advanced disease (*TP53*, *SMAD4*) were not present in the co-occurring IPMN in 9 of 11 (82%) of 'likely independent' cases; thus, analysis of mutations in IPMN-derived DNA in cyst fluid would not have identified these patients as high-risk. Survival analysis revealed a significant trend towards improved survival in patients with 'likely related' IPMN/ductal adenocarcinomas cases compared with those with 'likely independent' lesions (P = 0.017; Log-rank test; Figure 2).

In contrast to the observation of unrelatedness of many of the adjacent IPMN/ductal adenocarcinoma cases, we found that all of the colloid carcinomas were 'likely related' to the co-occurring IPMN (Figure 1B). This result adds to the growing body of evidence that this histological subtype of pancreatic carcinoma develops essentially exclusively in the setting of an intestinal-type IPMN, making IPMN its obligate precursor.[29,30] The ampullary region carcinomas with co-occurring IPMNs serve as additional negative controls, as carcinoma of the ampullary region are not known to arise from IPMNs. As expected, all cases of carcinoma of the ampullary region and adj-IPMN were classified as 'likely independent' by our assay (Figure 1C).

Genetic heterogeneity in IPMNs

Heterogeneity with respect to driver gene mutations has been reported within grossly contiguous IPMNs.[8] In order to minimise the likelihood that such heterogeneity resulted in artifactual characterisation of lesions as 'likely independent', we analysed an additional section of IPMN from a separate tissue block. In all but one case (IPP12), the two IPMN samples were derived from the same grossly identified cyst. Genetic analysis of matched adj-IPMN and dist-IPMN from the same patient allowed us to describe such genetic heterogeneity within individual IPMNs in more depth.

Examining the relatedness of adj-IPMN and dist-IPMN to the co-occurring invasive carcinoma revealed distinct patterns. The majority of paired IPMN samples (69%) had the same relationship to the co-occurring ductal adenocarcinomas. Of the cases with discordant relationships, the majority (88%) of ductal adenocarcinomas were 'likely related' or 'indeterminate' to the adj-IPMN and 'likely independent' from the dist-IPMN. This suggests that anatomical distance is associated with genetic relatedness; IPMN lesions in close proximity to the invasive carcinoma were more likely to be related than IPMNs at a greater distance.

Comparing the alterations in the two distinct regions of the same IPMN, IPMN foci were 'likely related' to one another in 39% of the cases, whereas 28% were 'likely independent', highlighting the possibility of polyclonality in individual IPMNs. The relatedness of the remaining paired IPMN samples was 'indeterminate' in our assay. Intriguingly, the relatedness of the two IPMN samples varied in our different cancer groups. While 86% of the paired IPMN samples were 'likely related' in patients with colloid carcinoma, only 39% of such samples were 'likely related' in patients with ductal adenocarcinoma, and all of the paired IPMN samples were 'likely independent' in patients with carcinoma of the ampullary region.

Pancreatic ductal neoplasms (including both IPMNs and ductal adenocarcinomas) are typically initiated by oncogenic hotspot mutations. In 56 dissected IPMNs from patients with co-occurring ductal adenocarcinoma, 13 IPMNs (23%) harboured more than one mutation in the same oncogene, including 11 IPMNs with multiple *KRAS* mutations and 2 IPMNs with multiple *GNAS* mutations. Up to four different *KRAS* hotspot mutations in a single sample were detected (online Supplementary Figure S6). Intriguingly, this may still be an underestimation, as two additional IPMN samples submitted for whole exome sequencing revealed additional oncogenic hotspot mutations due to further sampling of the same blocks to collect additional DNA (online Supplementary Table S8). Only two ductal adenocarcinomas (4%) had multiple oncogene mutations, in both cases *KRAS*. Interestingly, the presence of multiple unique mutations in other driver genes in the same neoplasm was an uncommon event. However, even in 'likely related' cases, there were many mutations present in only a single sample, reflecting heterogeneity in driver mutations; only 64 of 104 identified somatic mutations were shared among related samples. Taken together, these data show that there is striking genetic heterogeneity within IPMNs, highlighting the challenges of capturing all the genetic alterations in a single tissue sample.

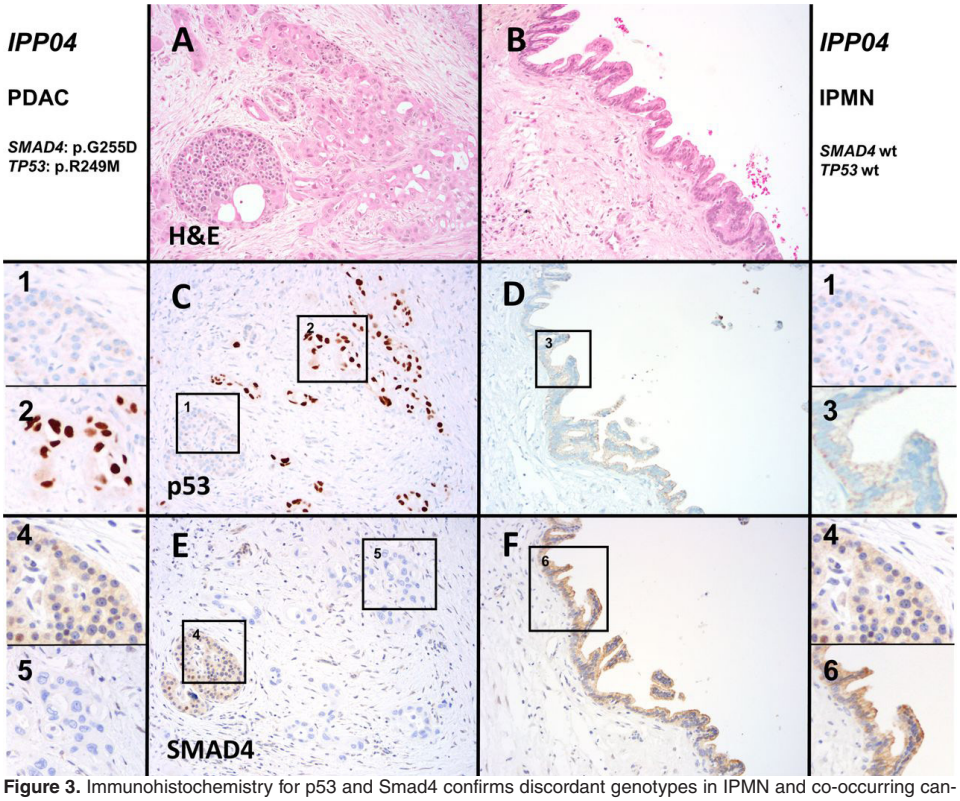

Figure 3. Immunohistochemistry for p53 and Smad4 confirms discordant genotypes in IPMN and co-occurring cancer. A representative H&E stained section shows case IPP04 (20× magnification), which harbours mutations in TP53 and SMAD4 in the ductal adenocarcinoma (**a**), while the adj-IPMN (**b**) is wild-type. In the ductal adenocarcinoma (**c**), strong-diffuse expression of p53 was found in contrast to normal expression in the adj-IPMN (**d**). Normal islets are shown in the inset as an internal control (1), while (2) shows a high-power view of cancer cells with aberrant p53 expression and (3) shows a high-power view of wild-type p53 expression pattern in the IPMN. Expression of Smad4 was lost in ductal adenocarcinoma (**e**), while expression was retained in adj-IPMN (**f**). Normal islets are shown in the inset as an internal control (1), while (2) shows a high-power view of cancer cells with loss of Smad4 expression and (3) shows a high-power view of retained Smad4 expression in the IPMN. adj-/dist-IPMN, adjacent/distant IPMN; IPMN, intraductal papillary mucinous neoplasm; PDAC, pancreatic ductal adenocarcinoma.

Spatial distribution of mutant and wild-type clones

Although we used LCM to obtain samples of IPMN and invasive carcinoma with high neoplastic cellularity, visualisation of mutant and wild-type clones in situ in tissue sections can confirm our targeted sequencing results, particularly in cases in which the IPMN and ductal adenocarcinomas have discordant mutations. Mutations in two of the tumour suppressor genes analysed, *TP53* and *SMAD4*, have well-documented effects on protein expression as assayed by IHC.[31,32] To more definitively assess the spatial distribution of mutant and wild-type clones, we performed IHC for SMAD4 and p53 protein expression in a subset of our IPMN/ductal adenocarcinoma cases analysed by next generation sequencing. For each protein, we analysed ductal adenocarcinoma and adj-IPMN from five patients who had discordant mutation status between the two lesions (online Supplementary Table S10).

In the p53 IHC assay, three of five cases with discordant *TP53* mutation status between IPMN and ductal adenocarcinoma showed the expected expression patterns in both components, with strong

and diffuse p53 expression limited to the invasive carcinoma (Figure 3). These three cases all had missense *TP53* mutations, while the remaining two had nonsense and frameshift mutations, which are not expected to cause the same aberrant p53 expression pattern.[32] In the SMAD4 IHC assay, three of five cases with discordant *SMAD4* mutation status in the IPMN and invasive ductal adenocarcinoma showed the expected expression pattern in both components, with loss of SMAD4 expression limited to the invasive ductal adenocarcinoma (Figure 3). Overall, these results confirm the discordant mutation status in the IPMN and ductal adenocarcinoma in the majority of cases (online Supplementary Table S10).

DISCUSSION

New diagnostic approaches are needed to more accurately identify patients with high-risk pancreatic lesions while they are still surgically curable.[4,33–35] Although imaging findings can stratify the risk of progression of pancreatic cysts, additional approaches are needed to further improve diagnostic sensitivity and specificity. Analysis of molecular alterations in biological samples (including cyst fluid and pancreatic juice) is a promising adjunct to existing clinical and radiological criteria, as alterations in specific genes (such as *TP53* and *SMAD4*) are closely associated with the development of high-risk neoplasia.[6,7,14] The identification of mutations in pancreatic cyst fluid is beginning to be applied as a clinical test to preoperatively diagnose and risk-stratify pancreatic cysts.[18,36,37] However, this approach assumes that the IPMN is the obligate precursor in cases where an invasive carcinoma develops. The high prevalence of multifocal neoplasia in the pancreas raises the possibility that a carcinoma co-occurring with an IPMN could arise from a genetically independent precursor, such as pancreatic intraepithelial neoplasia.[8,15,22]

The central objective of this study was to investigate the molecular relationship of co-occurring IPMNs and invasive carcinomas in an unbiased approach. Meticulous LCM to separately isolate DNA from two adjacent neoplasms, followed by next generation sequencing analysis of critical driver genes in pancreatic neoplasia, allowed us to estimate the relatedness in the majority of patients in our cohorts. More than one-sixth (18%) of the co-occurring IPMN/invasive ductal adenocarcinoma pairs appear to be genetically unrelated, meaning they shared no mutations in the assayed genes. Importantly, this is likely an underestimate of prevalence of unrelated lesions. Two of three cases that met clinical criteria for IPMN with 'concomitant' carcinoma (IPP05, IPP48) were classified as 'likely independent' in our assay, while the third (IP11) was classified as 'indeterminate', suggesting that at least a subset of the indeterminate cases also represent independent neoplasms. In addition, analysis of three different 'indeterminate' cases (IPP17, IPP39, IPP41) by whole exome sequencing revealed that two were genetically independent, as they did not share any other somatic mutations aside from the *KRAS* hotspot. This finding has clinical implications, as it suggests that in this subset of patients with IPMN, sampling and analysis of their IPMN cyst fluid would not be evaluating the precursor lesion destined to progress to invasive ductal adenocarcinoma. In the present invasive ductal adenocarcinoma cohort, more than 80% of unrelated IPMNs lacked mutations in high-risk genes (*TP53*, *SMAD4*) that are expected to be

detected in more than 50% of ductal adenocarcinomas. The implications for cyst fluid analysis should be more directly validated by comparing mutations identified in tissue samples and cyst fluid in future studies. Alternative samples for molecular analysis (such as secretin-stimulated pancreatic juice) may provide a more complete mutation profile of the entire pancreatic duct system and thus may be more able to overcome this issue.[6,7,25]

Through analysis of two different regions of each IPMN, our study also provides an assessment of genetic heterogeneity in these lesions. First, some IPMNs harboured two or more hotspot mutations in a single oncogene, suggesting presence of multiple clones within the dissected tissue. Intriguingly, the proportion of IPMNs with multiple hotspot mutations was notably more than that found in invasive ductal adenocarcinomas (23% vs 4%), perhaps suggesting a more diverse mixture of clones in lower grade lesions. In addition, many samples displayed discordant hotspot mutations in adj-IPMN and dist-IPMN, which were classified as 'likely independent' in one-third of patients. There were also notable differences in IPMN heterogeneity between cancer types. While a majority of the two IPMN samples co-occurring with colloid carcinoma were 'likely related', IPMNs that co-occurred with carcinoma of the ampullary region were mostly unrelated. This suggests that the IPMNs that give rise to colloid carcinomas are genetically more homogeneous, while those that co-occur with ampullary region carcinoma are more frequently heterogeneous (Table 1).

Overall, the results of our study support the hypothesis of field cancerisation, in which the entire pancreas of some patients is at increased risk for ductal neoplasia. We identify a sizeable proportion of patients in our cohort with two likely independent ductal neoplasms in a small area of the pancreas, highlighting the importance of multifocal neoplasia. In addition, many of the IPMNs analysed had multiple mutations in initiating driver genes, raising the possibility of polyclonality within one IPMN. However, our data do not provide any insight into the underlying mechanism of field cancerisation in the pancreas, though they do suggest that it is not mediated by somatic mutations in well-characterised driver genes. Of note, our study did not comprehensively address large chromosomal alterations as potential genetic drivers in pancreatic cancer precursor lesions. Although these alterations are less useful for determination of relatedness, recent studies suggest that they play an important role in driving pancreatic tumourigenesis, at least in a subset of patients.[38] Thus, they remain candidates for the alterations underlying field cancerisation in the pancreas, and future studies could incorporate such alterations into studies of precursor lesions to better address this hypothesis.

Some limitations of our study have to be considered. First, we were not able to confidently determine relatedness in a subset of our IPMN/ductal adenocarcinoma pairs; as demonstrated, more comprehensive sequencing such as whole exome sequencing can help to determine relatedness in these individuals. In addition, it is possible that 'likely independent' ductal adenocarcinomas arose out of a subclone of the co-occurring IPMNs that was not sampled or was too small to be detected by our approach. Low neoplastic cellularity and clonal heterogeneity may decrease the sensitivity of molecular analyses in these cases—we address this in several ways. First, we performed LCM of every IPMN

and PDAC to enrich neoplastic cellularity as much as possible. Second, we performed deep targeted sequencing (with an average coverage of >600×), improving our ability to detect rare subclones. Third, we sampled the IPMN immediately adjacent to the ductal adenocarcinoma (and thus most likely to be related) as well as a separate section to account for genetic heterogeneity. In addition, we performed validation of our mutation calls in a subset of samples at very high coverage (>2000×) to estimate the risk of misclassification of relatedness in the larger cohort—we confirmed >95% of the mutations conferring relatedness in the original samples. Finally, the early driver mutations should be present in high proportion in both components of related lesions, making this explanation far less likely than true genetic independence.

Collectively, our molecular analysis revealed an unexpected proportion of co-occurring IPMNs and invasive ductal adenocarcinomas that likely arose from genetically distinct precursor lesions in the pancreas. We also show that virtually all colloid carcinomas arise from their associated intestinal-type IPMNs and that ampullary region carcinomas (distal common bile duct, ampullary and duodenal carcinoma) do not arise from co-occurring IPMNs.

Molecular analysis of cyst fluid is a promising technique for risk stratification in patients with IPMN undergoing surveillance. However, we demonstrate that at least one-sixth of invasive ductal adenocarcinomas co-occurring with IPMNs are ‘likely independent’ and that more than 80% of those cases would not have identified high-risk alterations in analysis of IPMN-derived cyst fluid. This highlights a potential limitation of cyst fluid analysis and suggests a need for molecular approaches that more completely sample DNA from the entire pancreas.

REFERENCES

1. American Cancer Society. Cancer Facts & Figures. (2017).
2. Valsangkar, N. P. et al. 851 resected cystic tumors of the pancreas: a 33-year experience at the Massachusetts General Hospital. Surgery 152, S4–12 (2012).
3. Tanaka, M. et al. Revisions of international consensus Fukuoka guidelines for the management of IPMN of the pancreas. Pancreatology 17, 738–753 (2017).
4. Crippa, S. et al. Risk of misdiagnosis and overtreatment in patients with main pancreatic duct dilatation and suspected combined/main-duct intraductal papillary mucinous neoplasms. Surgery 159, 1041–1049 (2016).
5. Vege, S. S. et al. American gastroenterological association institute guideline on the diagnosis and management of asymptomatic neoplastic pancreatic cysts. Gastroenterology 148, 819–22; quize12–3 (2015).
6. Yu, J. et al. Digital next-generation sequencing identifies low-abundance mutations in pancreatic juice samples collected from the duodenum of patients with pancreatic cancer and intraductal papillary mucinous neoplasms. Gut 66, 1677–1687 (2017).
7. Kanda, M. et al. Mutant TP53 in duodenal samples of pancreatic juice from patients with pancreatic cancer or high-grade dysplasia. Clin. Gastroenterol. Hepatol. 11, 719–30.e5 (2013).
8. Wu, J. et al. Recurrent *GNAS* mutations define an unexpected pathway for pancreatic cyst development. Sci. Transl. Med. 3, 92ra66 (2011).
9. Cancer Genome Atlas Research Network. Electronic address: andrew_aguirre@dfci.harvard.edu & Cancer Genome Atlas Research Network. Integrated Genomic Characterization of Pancreatic Ductal Adenocarcinoma. Cancer Cell 32, 185–203. e13 (2017).
10. Bailey, P. et al. Genomic analyses identify molecular subtypes of pancreatic cancer. Nature 531, 47–52 (2016).
11. Witkiewicz, A. K. et al. Whole-exome sequencing of pancreatic cancer defines genetic diversity and therapeutic targets. Nat. Commun. 6, 6744 (2015).
12. Biankin, A. V. et al. Pancreatic cancer genomes reveal aberrations in axon guidance pathway genes. Nature 491, 399–405 (2012).
13. Jones, S. et al. Core signaling pathways in human pancreatic cancers revealed by global genomic analyses. Science 321, 1801–1806 (2008).
14. Hosoda, W. et al. Genetic analyses of isolated high-grade pancreatic intraepithelial neoplasia (HG-PanIN) reveal paucity of alterations in TP53 and SMAD4. J. Pathol. (2017) doi:10.1002/path.4884.
15. Amato, E. et al. Targeted next-generation sequencing of cancer genes dissects the molecular profiles of intraductal papillary neoplasms of the pancreas. J. Pathol. 233, 217–227 (2014).
16. Murphy, S. J. et al. Genetic alterations associated with progression from pancreatic intraepithelial neoplasia to invasive pancreatic tumor. Gastroenterology 145, 1098–1109.e1 (2013).
17. Wu, J. et al. Whole-exome sequencing of neoplastic cysts of the pancreas reveals recurrent mutations in components of ubiquitin-dependent pathways. Proc. Natl. Acad. Sci. U. S. A. 108, 21188–21193 (2011).
18. Springer, S. et al. A Combination of Molecular Markers and Clinical Features Improve the Classification of Pancreatic Cysts. Gastroenterology 149, 1501–1510 (2015).
19. Raman, S. P. et al. Histopathologic findings of multifocal pancreatic intraductal papillary mucinous neoplasms on CT. AJR Am. J. Roentgenol. 200, 563–569 (2013).
20. Pea, A. et al. Targeted DNA Sequencing Reveals Patterns of Local Progression in the Pancreatic Remnant Following Resection of Intraductal Papillary Mucinous Neoplasm (IPMN) of the Pancreas. Ann. Surg. (2016) doi:10.1097/SLA.0000000000001817.
21. Tamura, K. et al. Assessment of clonality of multisegmental main duct intraductal papillary mucinous neoplasms of the pancreas based on *GNAS* mutation analysis. Surgery 157, 277–284 (2015).
22. Yamaguchi, K. et al. Pancreatic ductal adenocarcinoma derived from IPMN and pancreatic ductal adenocarcinoma concomitant with IPMN. Pancreas 40, 571–580 (2011).
23. Ingkakul, T. et al. Predictors of the presence of concomitant invasive ductal carcinoma in intraductal papillary mucinous neoplasm of the pancreas. Ann. Surg. 251, 70–75 (2010).
24. Tamura, K. et al. Distinction of Invasive Carcinoma Derived From Intraductal Papillary Mucinous Neoplasms From Concomitant Ductal Adenocarcinoma of the Pancreas Using Molecular Biomarkers. Pancreas 45, 826–835 (2016).
25. Ideno, N. et al. Clinical significance of *GNAS* mutation in intraductal papillary mucinous neoplasm of the pancreas with concomitant pancreatic ductal adenocarcinoma. Pancreas 44, 311–320 (2015).
26. Jones, S. et al. Personalized genomic analyses for cancer mutation discovery and interpretation. Sci. Transl. Med. 7, 283ra53 (2015).
27. McCall, C. M. et al. False positives in multiplex PCR-based next-generation sequencing have

unique signatures. J. Mol. Diagn. 16, 541–549 (2014).
28. Basturk, O. et al. A Revised Classification System and Recommendations From the Baltimore Consensus Meeting for Neoplastic Precursor Lesions in the Pancreas. Am. J. Surg. Pathol. 39, 1730–1741 (2015).
29. Seidel, G. et al. Almost all infiltrating colloid carcinomas of the pancreas and periampullary region arise from in situ papillary neoplasms: a study of 39 cases. Am. J. Surg. Pathol. 26, 56–63 (2002).
30. Mino-Kenudson, M. et al. Prognosis of invasive intraductal papillary mucinous neoplasm depends on histological and precursor epithelial subtypes. Gut 60, 1712–1720 (2011).
31. Wilentz, R. E. et al. Immunohistochemical labeling for dpc4 mirrors genetic status in pancreatic adenocarcinomas : a new marker of DPC4 inactivation. Am. J. Pathol. 156, 37–43 (2000).
32. Yemelyanova, A. et al. Immunohistochemical staining patterns of p53 can serve as a surrogate marker for TP53 mutations in ovarian carcinoma: an immunohistochemical and nucleotide sequencing analysis. Mod. Pathol. 24, 1248–1253 (2011).
33. Schnelldorfer, T. et al. Long-term survival after pancreatoduodenectomy for pancreatic adenocarcinoma: is cure possible? Ann. Surg. 247, 456–462 (2008).
34. Fatima, J. et al. Pancreatoduodenectomy for ductal adenocarcinoma: implications of positive margin on survival. Arch. Surg. 145, 167–172 (2010).
35. Dal Molin, M. et al. Very Long-term Survival Following Resection for Pancreatic Cancer Is Not Explained by Commonly Mutated Genes: Results of Whole-Exome Sequencing Analysis. Clin. Cancer Res. 21, 1944–1950 (2015).
36. Nikiforova, M. N. et al. Integration of *KRAS* testing in the diagnosis of pancreatic cystic lesions: a clinical experience of 618 pancreatic cysts. Mod. Pathol. 26, 1478–1487 (2013).
37. Al-Haddad, M. et al. Performance characteristics of molecular (DNA) analysis for the diagnosis of mucinous pancreatic cysts. Gastrointest. Endosc. 79, 79–87 (2014).
38. Notta, F. et al. A renewed model of pancreatic cancer evolution based on genomic rearrangement patterns. Nature (2016) doi:10.1038/nature19823.

5

Chapter 6

Patients with McCune-Albright syndrome have a broad spectrum of abnormalities in the gastrointestinal tract and pancreas

Laura D. Wood, Michaël Noë, Wenzel Hackeng, Lodewijk A.A. Brosens, Feriyl Bhaijee, Marija Debeljak, Jun Yu, Masaya Suenaga, Aatur D. Singhi, Atif Zaheer, Alison Boyce, Cemre Robinson, James R. Eshleman, Michael G. Goggins, Ralph H. Hruban, Michael T. Collins, Anne Marie Lennon, Elizabeth A. Montgomery

Virchows Archiv, April 2017

ABSTRACT

McCune-Albright Syndrome (MAS) is a rare sporadic syndrome caused by post-zygotic mutations in the *GNAS* oncogene, leading to constitutional mosaicism for these alterations. Somatic activating *GNAS* mutations also commonly occur in several gastrointestinal and pancreatic neoplasms, but the spectrum of abnormalities in these organs in patients with MAS has yet to be systematically described. We report comprehensive characterization of the upper gastrointestinal tract in seven patients with MAS and identify several different types of polyps, including gastric heterotopia/metaplasia (7/7), gastric hyperplastic polyps (5/7), fundic gland polyps (2/7), and a hamartomatous polyp (1/7). In addition, one patient had an unusual adenomatous lesion at the gastroesophageal junction with high-grade dysplasia. In the pancreas, all patients had endoscopic ultrasound findings suggestive of intraductal papillary mucinous neoplasm (IPMN), but only two patients met the criteria for surgical intervention. Both of these patients had IPMNs at resection, one with low-grade dysplasia and one with high-grade dysplasia. *GNAS* mutations were identified in the majority of lesions analyzed, including both IPMNs and the adenomatous lesion from the gastroesophageal junction. These studies suggest that there is a broad spectrum of abnormalities in the gastrointestinal tract and pancreas in patients with MAS and that patients with MAS should be evaluated for gastrointestinal pathology, some of which may warrant clinical intervention due to advanced dysplasia.

INTRODUCTION

McCune-Albright syndrome (MAS) is defined by a clinical spectrum including skeletal, endocrine, and skin abnormalities - specifically, fibrous dysplasia of bone, hyperfunctioning endocrinopathies (such as precocious puberty), and café au lait macules.[1] This rare sporadic syndrome is caused by somatic (post-zygotic) activating mutations in *GNAS*, the gene coding for the G protein-alfa stimulatory subunit, leading to ligand-independent signaling, elevated cAMP levels, and activation of downstream signaling pathways.[2] The same *GNAS* mutations are also found as somatic alterations in a number of sporadic tumor types.

Somatic activating mutations at codon 201 (the same codon targeted in patients with MAS) have been reported in several gastrointestinal and pancreatic neoplasms, including intraductal papillary mucinous neoplasms (IPMNs) of the pancreas and pyloric gland adenomas (PGAs) of the stomach.[3,4] This genetic similarity raises the possibility that patients with MAS are also at increased risk for gastrointestinal and pancreatic neoplasms, which has been confirmed by reports of gastrointestinal and pancreatic abnormalities in patients with MAS. A small series of four patients with MAS revealed hamartomatous duodenal polyps, and pancreatic abnormalities were identified radiologically in approximately 20% of patients with MAS, with most believed to be IPMNs.[5,6]

In the current study, we report thorough upper endoscopic examination of seven patients with MAS, all selected for evaluation due to pancreatic cysts on magnetic resonance cholangiopancreatography (MRCP). Examination revealed a variety of polyps throughout the esophagus, stomach, and small intestine. In addition, all patients underwent endoscopic ultrasound (EUS) of their pancreas, revealing that all patients had EUS abnormalities suggestive of IPMN, and two of these patients underwent resection of IPMN due to worrisome radiologic features.

METHODS

Patients and samples

As part of a screening protocol at the National Institutes of Health, patients with MAS were screened for pancreatic lesions using magnetic resonance cholangiopancreatography (MRCP). All patients gave informed consent, and the protocol was approved by the Institutional Review Board of the National Institute of Dental and Craniofacial Research. The seven patients with pancreatic cysts on MRCP were referred to the Johns Hopkins Hospital for endoscopic evaluation. The clinical features of MAS in the patient cohort are described in Table 1. At upper endoscopy, biopsies were taken from the normal esophagus, stomach, and duodenum, as well as from any visible lesions. Endoscopic ultrasound (EUS) was performed, and cyst fluid was sampled for cysts >1.5 cm. Hematoxylin-and-eosin-stained sections of all biopsies were reviewed by two gastrointestinal pathologists (LDW and EAM) in order to reach a consensus diagnosis. Resection of gastrointestinal and pancreatic lesions was performed as clinically indicated, and all sections from resected specimens were reviewed.

Patient	Fibrous dysplasia	Café au lait macules	Precocious puberty	Hyperthyroidism	Hypophosphatemia	Neonatal Cushing's syndrome	*GNAS* mutation for initial diagnosis
1	yes	yes	no	yes	yes	no	R201C
2	yes	yes	yes	no	yes	no	not done
3	yes	yes	yes	no	no	no	not done
4	yes	yes	no	yes	no	no	not done
5	yes	yes	no	yes	no	yes	R201H
6	yes	yes	yes	yes	yes	yes	not done
7	yes	yes	no	no	no	no	R201C

Table 1. Clinical manifestations of McCune-Albright syndrome in patient cohort

Immunohistochemistry

A single section of each IPMN was analyzed for expression of MUC1, MUC2, MUC5, and CDX2 in order to determine the direction of differentiation. Immunostaining with MUC1, MUC2, and MUC5 antibodies was performed on an automated instrument (XT BenchMark, ROCHE-Ventana Medical Systems, Inc. Tucson, AZ). Sections were deparaffinized and hydrated and antigen retrieval with a high pH buffer (CC1 standard) was performed. Incubation with primary antibody was performed, followed by a biotin-labeled secondary antibody and chromogenic substrate as per manufacturer's instructions (I-View detection, 790-091. ROCHE-Ventana Medical Systems, Inc. Tucson, AZ). Immunostaining for CDX2 was developed on Bond-Leica automated instrument (Leica Microsystems, Bannockburn, IL). Following deparaffinization and heat-induced antigen retrieval, primary and secondary antibody incubation steps were performed. Immunoreactivity was visualized using DAB chromogen and a hematoxylin counterstain was applied to all tissue sections. Sections were incubated with the anti-MUC1 and anti-MUC5 antibodies (Vector Lab, Burlingame, CA) for 44 min at 1:100 dilution, with the anti-MUC2 antibody (NCL, LEICA, Bannockburn, IL) for 32 min at 1:50 dilution and with the anti-CDX2 antibody (Agilent Technologies, pre-diluted) for 15 min.

***GNAS* pyrosequencing**

On the basis of previously published findings, *GNAS* mutational analysis was restricted to the codon 201 hot spot contained within exon 8.[7] Mutations in codon 227 have been described in less than 5% of fibrous dysplasia cases.[8] For small lesions, 10 serial sections of formalin-fixed paraffin-embedded (FFPE) tissue were cut onto membrane slides. After deparaffinization in xylene, rehydration in decreasing concentrations of ethanol and staining with hematoxylin, lesional cells were captured by laser capture microdissection (LMD7000, Leica, Wetzlar, Germany). Tissue from larger lesions was cut onto coated glass slides, deparaffinized, rehydrated, and the lesional cells were scraped from these slides under a dissection microscope. When sufficient neighboring normal tissue was present, this was also selected for further analysis. DNA extraction was performed using the QIAamp DNA FFPE Tissue Kit (Qiagen, Valencia, CA, USA) according to the manufacturer's instructions. Mutations in codon 201 of *GNAS* were assessed by pyrosequencing according the manufacturer's instructions as previously described.[9] In brief, extracted DNA was amplified on the Veriti Thermal Cycler (Applied Biosystems, Foster City, CA, USA), with the following primers: forward primer, 5'-CCAGACCTTTGCTTTAGATTGG-3' and reverse primer, 5'-biotin-TCCACCTGGAACTTGGTCTC-3' and using the PCR SuperMix High Fidelity (Invitrogen, Carlsbad, CA, USA). PCR conditions were as follows: 95 °C × 15 min; 38 cycles

Patient	Age[a]	Location	Diagnosis	GNAS—lesional tissue	GNAS—normal tissue
1	20	Proximal esophagus	Gastric heterotopia/metaplasia	R201C	–
		Stomach body	Fundic gland polyp	WT	–
		Major papilla	Hamartomatous-type polyp	WT	WT
		Minor papilla	Gastric heterotopia/metaplasia	WT	–
2	22	Proximal stomach	Gastric hyperplastic polyps	WT	–
		Duodenal bulb	Gastric heterotopia/metaplasia	R201C	WT
		Duodenum	Gastric heterotopia/metaplasia	WT	WT
		Ampulla	Gastric heterotopia/metaplasia	WT	–
3	46	Gastroesophageal junction	Gastric hyperplastic polyp	R201H	–
		Duodenum	Gastric heterotopia/metaplasia	R201H	–
4	55	Proximal esophagus	Gastric heterotopia/metaplasia	WT	WT
		Proximal stomach	Multiple adenomatous lesions with high-grade dysplasia[b]	R201C	–
		Stomach	Fundic gland polyps	WT	–
		Stomach body	Foveolar hyperplasia	R201C	–
		Duodenum	Gastric heterotopia/metaplasia	WT	–
		Ampulla	Gastric heterotopia/metaplasia	R201C	–
		Pancreas	Intraductal papillary mucinous neoplasm with low-grade dysplasia	R201C	WT
5	27	Duodenum	Gastric heterotopia/metaplasia with adjacent neuroendocrine hyperplasia	R201H[c]	WT
		Pancreas	Intraductal papillary mucinous neoplasm with high-grade dysplasia	R201H	–
6	19	Proximal esophagus	Gastric heterotopia/metaplasia	R201C	–
		Proximal stomach	Gastric hyperplastic polyps	WT	–
		Proximal duodenum	Gastric heterotopia/metaplasia	R201C	–
		Duodenum	Gastric heterotopia/metaplasia	R201C	–
		Ampulla	Gastric heterotopia/metaplasia	R201C	WT
7	50	Proximal esophagus	Gastric heterotopia/metaplasia	R201C	–
		Gastroesophageal junction	Intestinal metaplasia	WT	–
		Distal esophagus	Gastric hyperplastic polyp	WT	–
		Duodenum	Gastric heterotopia/metaplasia	R201C	–
		Duodenum	Gastric heterotopia/metaplasia	R201C	R201C

[a] At first procedure at JHH
[b] See text for more complete description of these unusual lesions
[c] *GNAS* R201H mutation identified in gastric heterotopia but not in separately analyzed neuroendocrine hyperplasia

Table 2. Gastrointestinal and pancreatic lesions in patients with McCune-Albright syndrome

of 95 °C × 20 s, 53 °C × 30 s, 72 °C × 20 s; 72 °C × 5 min. Biotinylated PCR products were bound to streptavidin-coated sepharose beads (Streptavidin Sepharose High Performance, GE Health Care Bio-Sciences Corp, Piscataway, NJ, USA). After washing, the beads with PCR products were released in wells with the sequencing primer, 5'-TTTGTTTCAGGACCTGCTTCGC-3', and annealing buffer. Sequencing was done with the PyroMark Q24 (Qiagen), using the Pyromark Gold reagents (Qiagen).[10]

Next-generation sequencing

Digital next-generation sequencing on duodenal fluid samples was performed on the Ion Torrent PGM as previously described.[11] Targeted next-generation sequencing was performed on cyst fluid samples. Briefly, DNA was extracted from 200 µL of cyst fluid, and 4 ng of cyst fluid DNA was analyzed in duplicate. The target region was amplified using AmpliSeq reagents according to the manufacturer's instructions. The gene panel contained the hotspot regions of *KRAS*, *GNAS*, *BRAF*, and *PIK3CA* as well as the entire coding regions of *TP53*, *CDKN2A*, *SMAD4*, *RNF43*, *ARID1A*, *FBXW7*, *TGFBR2*, and *VHL*. Variants were identified by the NextGENe software (SoftGenetics) as previously described.[11]

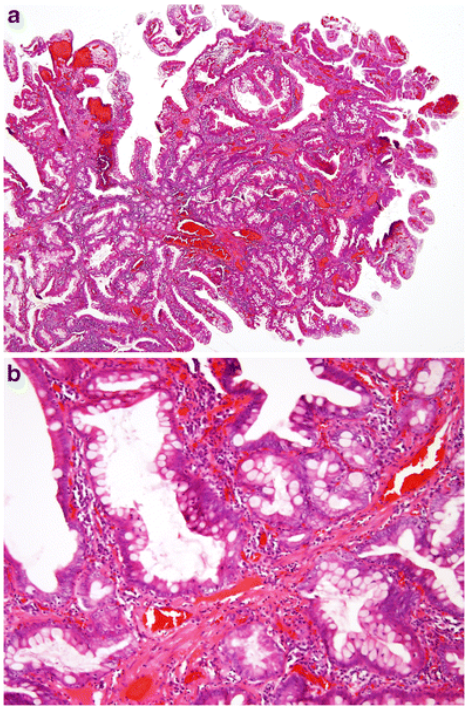

Figure 1. Hamartomatous polyp in patient **a** This ampullary polyp is characterized by nests of small intestinal mucosa partitioned by bands of smooth muscle. **b** The smooth muscle bands are not as prominent as those typically seen in Peutz Jeghers polyps

RESULTS

The MAS patients in our cohort were selected for endoscopic evaluation due to the presence of pancreatic abnormalities on magnetic resonance cholangiopancreatography (MRCP). All seven patients had multiple branch duct IPMNs (>5), and more than ten cysts were identified in five of the seven patients scattered throughout the head, body, and tail of the pancreas (average size of the largest cyst 22 mm, range 9–30 mm). In addition, five of the seven patients also had main duct IPMNs—one had diffuse involvement of the main duct, while the other four had segmental involvement (average size of the pancreatic duct with main duct IPMN 5.4 mm, range 5–9 mm). Pancreatic glandular atrophy was present in four of the five patients with main duct IPMNs. There were no mural nodules or pancreatic masses seen on contrast enhanced MRI and MRCP. Pancreatic EUS was performed at the time of upper endoscopy and also demonstrated multiple pancreatic cysts in each of the seven patients.

In the upper gastrointestinal tract of all seven patients, polyps were identified (Table 2). The most common lesion was heterotopic gastric mucosa (polypoid zones of non-neoplastic appearing oxyntic and/or foveolar-type mucin outside of the stomach), present in at least one location in the esophagus or small bowel in all seven patients. Of note, the absence of criteria to definitively distinguish gastric heterotopia from gastric metaplasia did not allow us to make this distinction in these samples, although the lack of mucosal injury in the adjacent tissues near the biopsied sites suggested heterotopia rather than metaplasia. In addition, gastric hyperplastic-type polyps were also common, occurring in 5/7 (71%) patients. They were unusual in that they were not associated with gastritis of either the environmental or autoimmune type. Fundic gland polyps were identified in two of the seven (29%) patients, while a single patient (14%) had a hamartomatous polyp of the ampulla of Vater presenting features similar but not identical to those of Peutz Jeghers polyps, with cords of smooth muscle partitioning off nests of mucosa with lamina propria (Figure 1). This lesion differed from a classic Peutz Jeghers polyp as it featured less smooth muscle and more inflammation than a typical Peutz Jeghers polyp. One patient (14%) had intestinal metaplasia at the gastroesophageal junction.

These small non-dysplastic lesions noted above encompassed the disease spectrum in five of the seven patients, who were only examined with endoscopic biopsies of the gastrointestinal tract. In addi-

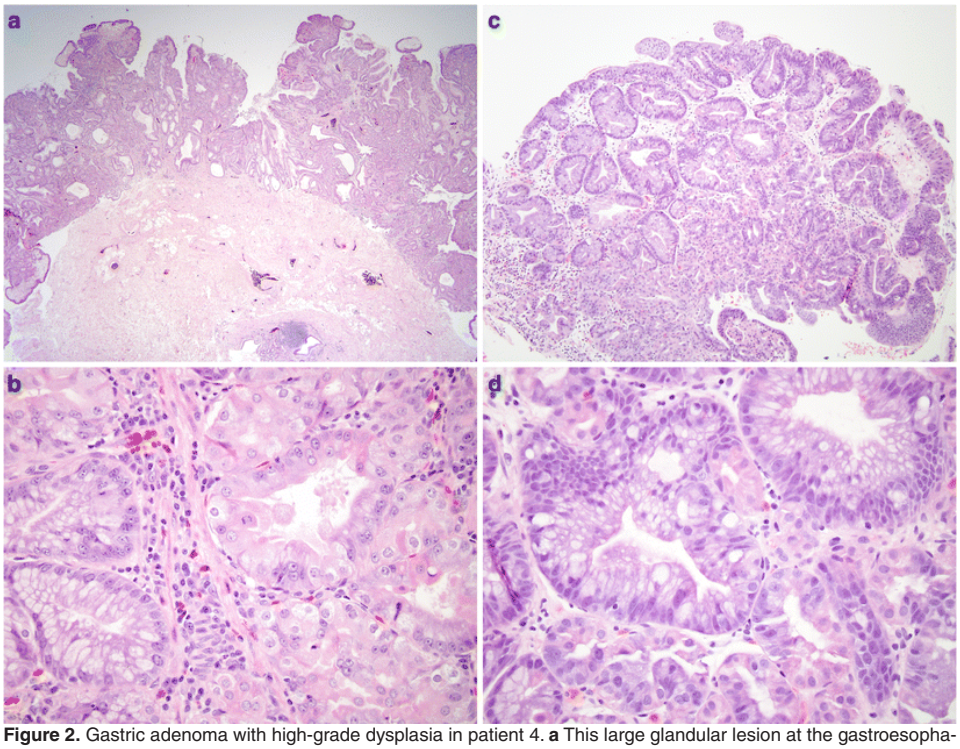

Figure 2. Gastric adenoma with high-grade dysplasia in patient 4. **a** This large glandular lesion at the gastroesophageal junction showed multiple directions of differentiation. **b** High-grade dysplasia was identified throughout the lesion, exhibiting irregularly fused glands, rounded nuclei with striking loss of nuclear polarity, and diffuse nuclear atypia. **c** Areas of pyloric and oxyntic differentiation were prominent. **d** Focal intestinal differentiation was also present.

tion, although all had abnormalities on pancreatic EUS suggestive of IPMN (confirming the radiologic impression on MRCP), none of these five had sufficiently concerning features on EUS to meet criteria for surgical intervention to address pancreatic neoplasia.

The remaining two patients (patients 4 and 5 in Table 1) had additional unusual lesions, and both underwent resection of pancreatic and gastrointestinal lesions. In addition to fundic gland polyps and gastric heterotopia, patient 4 had multiple dysplastic lesions in the proximal stomach and gastroesophageal junction (Figure 2). These lesions displayed a variety of directions of differentiation, including gastric foveolar, pyloric, oxyntic and intestinal, and at resection were found to have high-grade dysplasia but no invasive carcinoma. Resection of one radiologically worrisome IPMN in the pancreatic tail showed an IPMN with low-grade dysplasia (Figure 3). Immunohistochemistry revealed that the neoplastic IPMN cells strongly expressed MUC5, while expression of MUC1, MUC2, and CDX2 was weak and focal. Although the morphology and immunohistochemistry was most similar to a gastric-type IPMN, the MUC2 and CDX2 labeling raise the possibility of a mixed-type IPMN with some intestinal features.[12]

Patient 5 underwent a Whipple resection for an IPMN in the pancreatic head raising clinical concern. The resection specimen revealed a 2.3 cm IPMN with high-grade dysplasia (Figure 4). By immunohistochemistry, the neoplastic IPMN cells strongly expressed CDX2 and MUC2, while MUC5 was

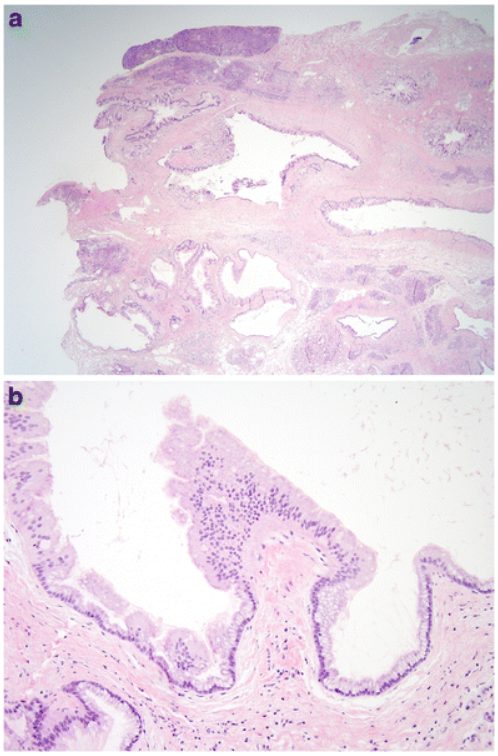

Figure 3. Intraductal papillary mucinous neoplasm in patient 4. **a** This cystic lesion was located in the pancreatic tail and clearly involves the pancreatic duct system. **b** The epithelium lining the cyst is mostly gastric-type with low-grade dysplasia

only weakly and focally expressed. Immunohistochemistry for MUC1 was negative in this lesion. Overall, the morphological and immunohistochemical findings were most consistent with an intestinal-type IPMN in this patient.[12] In addition, the duodenum showed multiple areas of nodular gastric heterotopia with associated neuroendocrine proliferation bordering on well-differentiated neuroendocrine tumors (Figure 5).

In a subset of lesions, selected for the availability of adjacent normal tissue, we performed pyrosequencing of the mutational hotspot in *GNAS* on formalin-fixed paraffin-embedded (FFPE) tissue from each lesion and adjacent normal tissue (Table 2). Both IPMNs had hotspot *GNAS* mutations, as did the unusual gastric adenomatous lesion in patient 4. In addition, *GNAS* mutations were also identified in 12 of 17 (71%) gastric heterotopic/metaplastic lesions. Intriguingly, in the duodenum of patient 5, a *GNAS* mutation was identified in the nodular gastric heterotopia, but the nearby neuroendocrine cell proliferation was wild-type. Of five gastric foveolar hyperplasia/gastric hyperplastic polyps, only two (40%) had *GNAS* mutations. Both fundic gland polyps were wild-type for *GNAS*, as was the ampullary hamartomatous-type polyp in patient 1. In all but one analyzed sample, the adjacent normal tissue was *GNAS* wild-type, even if the epithelium sampled was immediately adjacent to a lesion that had a *GNAS* mutation.

Pancreatic juice from patient 1 was collected from the duodenum following secretin stimulation and sequenced using digital next-generation sequencing (NGS) for pancreatic cancer driver genes. As described by Yu and colleagues, this technique necessitates 96 separate NGS reactions for each patient, greatly increasing the sensitivity and ability to discriminate true point mutations from false positives compared to traditional NGS.[11] However, copy number alterations are not accurately assessed due to the low prevalence of mutant alleles in these samples. In patient 1, digital NGS revealed the expected oncogenic hotspot mutation in *GNAS* (R201C) with a digital NGS score of 29, as well as a missense mutation in *RNF43* (R343H) with a digital NGS score of 10.[11] In addition, non-digital targeted NGS of the same driver genes was performed on aspirated cyst fluid from two patients. Analysis of cyst fluid from patient 4 revealed the predicted mutation in *GNAS* (R201C) with a mutant allele frequency of 40.3%, as well as hotspot mutations in *KRAS* (Q61H) with a mutant allele frequency of 4.3% and *PIK-*

3CA (Q546R) with a mutant allele frequency of 1.6%. Similarly, cyst fluid from patient 7 contained the predicted *GNAS* mutation (R201C) with a mutant allele frequency of 9.1%, as well as an inactivating mutation in *CDKN2A* (V115fs) with a mutant allele frequency of 2.6%. Of note, all of these NGS analyses were performed on either pancreatic juice collected from the duodenum or aspirated pancreatic cyst fluid—pyrosequencing of the *GNAS* hotspot as described above was the only molecular analysis performed on tissue samples.

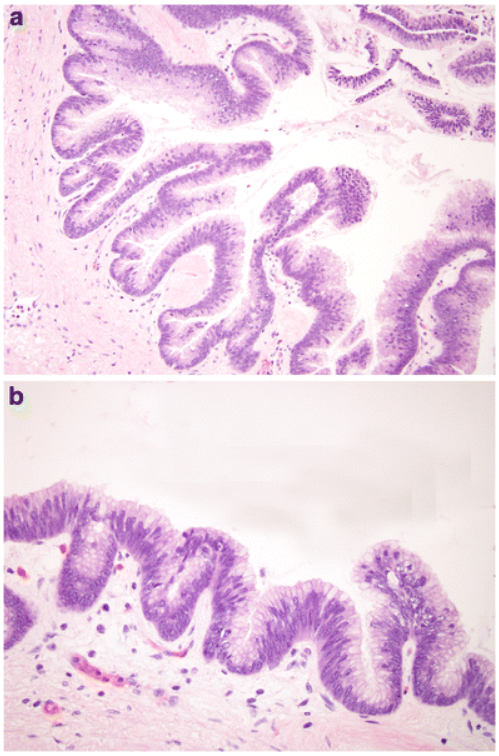

Figure 4. Intraductal papillary mucinous neoplasm in patient 5. **a** This cystic lesion was located in the pancreatic head and shows prominent papillae. **b** The epithelial lining shows intestinal differentiation and focal high-grade dysplasia, with elongated pencillate nuclei and areas with complete loss of nuclear polarity

DISCUSSION

The current study augments previous findings of gastrointestinal and pancreatic manifestations of MAS. In a study of four MAS patients, Zacharin and colleagues reported only hamartomatous polyps of the duodenum.[6] However, in that study, only relatively large polyps were examined histologically, while numerous small polyps of the stomach and small bowel were noted endoscopically but not biopsied. It is possible that these small unsampled polyps included the frequent gastric heterotopia/metaplasia noted in our cohort. Moreover, while the previous study reported significant histologic overlap with the hamartomatous polyps similar to those described in Peutz Jeghers syndrome, the smooth muscle proliferation in the hamartomatous polyp we examined was less striking than typically encountered in Peutz Jeghers syndrome. In addition, all patients in the previous study were in their teens or twenties, while our cohort had a broader age range, up to 55 years old, which allowed us to observe more advanced gastrointestinal manifestations of the syndrome. While our cohort is too small to make any statistically robust correlations between age and progression of the lesions, it is intriguing that the dysplastic gastric lesion manifested in the oldest patient, supporting the hypothesis that dysplasia takes decades to develop, even in patients with embryonic *GNAS* mutations. Overall, our study greatly broadens the spectrum of gastrointestinal findings in patients with MAS, adding frequent heterotopias as well as infrequent glandular dysplasia.

Gaujoux and colleagues previously reported imaging findings in hepatic and pancreatobiliary lesions in 19 MAS patients.[5] Four of these patients had pancreatic lesions, three of which were radiologically consistent with IPMNs. In addition, in a study of 272 unselected IPMN patients, Parvanescu and col-

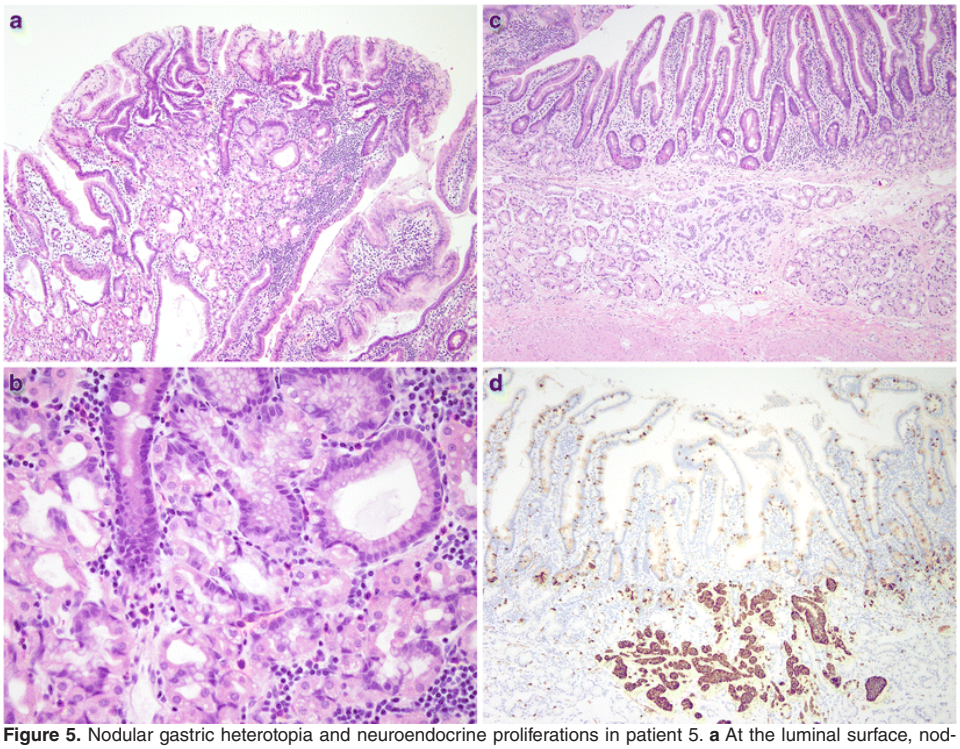

Figure 5. Nodular gastric heterotopia and neuroendocrine proliferations in patient 5. **a** At the luminal surface, nodular gastric heterotopia in the duodenum shows nodules of gastric-type epithelium. **b** No dysplasia is evident in the gastric-type epithelium. The presence of parietal cells suggests gastric heterotopia rather than gastric metaplasia. **c** Several areas of nodular gastric heterotopia had nearby underlying neuroendocrine cell proliferations. It is not clear whether these represent hyperplasia or neoplasia. **d** Synaptophysin stain confirms neuroendocrine differentiation of these cells. The largest neuroendocrine proliferation measures 10 mm

leagues report one patient with an intestinal-type IPMN associated with an invasive colloid carcinoma who had clinical features strongly suggestive of MAS.[13] In our cohort, all patients were selected for referral because they had pancreatic abnormalities at MRCP suggestive of IPMN. These findings were confirmed by EUS, and at resection two patients had a histologically proven IPMN. Although one patient had high-grade dysplasia (the patient was only 27 years old at diagnosis of pancreatic lesions), we did not find invasive carcinoma in either of the resected pancreata. By providing histologic confirmation of these IPMNs in patients with known MAS, our study confirms the association of IPMNs and MAS. However, it is not possible to determine the prevalence of IPMNs in unselected MAS patients from our study, as our cohort was biased by the criteria for referral to The Johns Hopkins Hospital for endoscopic evaluation—all patients in our study had pancreatic cysts on MRCP.

The spectrum of neoplasms reported here in MAS patients fits well with those known to have somatic *GNAS* mutations in sporadic lesions. For example, 60–80% of sporadic IPMNs have activating *GNAS* mutations.[3,14] Both of the IPMNs in this study had features of intestinal differentiation, and *GNAS* mutations have been reported to be more frequent in intestinal-type IPMNs.[3,9] In addition, activating *GNAS* mutations have also been reported in several gastrointestinal lesions, namely pyloric gland adenomas (PGAs), oxyntic gland adenomas (OGAs), gastric heterotopia, and gastric mucin cell metaplasia.[4,15,16]

The occurrence of *GNAS* mutations in sporadic cases of ectopic gastric mucosa fits well with our finding of this ectopic mucosa in all MAS patients analyzed. In addition, although we did not find any PGAs or OGAs, the dysplastic lesion in patient 4 exhibited oxyntic and pyloric differentiation so may be a variant of this process.

The previously reported gastric lesions that harbor *GNAS* mutations, both sporadic and syndromic, have a spectrum of overlapping morphology. Gastric tumors that have been described as oxyntic gland adenomas and pyloric gland adenomas have differentiation along the lines of chief and parietal cells (oxyntic gland adenomas) and antral/cardiac-type glands (pyloric gland adenoma), respectively. Additionally, some gastric polyps that arise in patients with familial adenomatous polyposis (FAP) can be classified as pyloric gland adenomas and also harbor *GNAS* mutations despite the history of FAP and its associated germline APC mutations.[17,18]

Pyloric gland adenomas consist of proliferations of closely packed tubules, each lined by a monolayer of round basally oriented nuclei with apically oriented eosinophilic ground glass cytoplasm.[19–21] They are most commonly detected in the stomach, where they are likely to arise in patients with autoimmune gastritis. Such patients have autoimmune loss of their parietal cells, and their gastric body mucosa is replaced by metaplastic glands with pyloric-type differentiation as well as by glands showing intestinal metaplasia, the perfect soil for the development of pyloric gland adenomas and other types of gastric neoplasms.[22] In contrast, the patients with MAS in our series did not have gastritis, yet they had adenomas with pyloric gland differentiation as well as hyperplastic polyps, both of which are often associated with gastritis.[20,23] Autoimmune gastritis has a female predominance and is found in about 2% of gastric biopsies in a tertiary care center.[24]

On the other hand, oxyntic gland adenomas (which have also been called chief cell adenomas) arise in normal oxyntic mucosa unaffected by gastritis and also harbor *GNAS* mutations. They consist of angulated glands that proliferate underneath the foveolar surface and show a variable mixture of cells that appear similar to chief cells punctuated by parietal cells. Their bland cytologic features raise the possibility that they are hamartomatous and indeed non-neoplastic, but their growth pattern is more in keeping with that of a neoplasm. In fact, colleagues in Japan regard lesions that we have termed oxyntic gland adenoma (chief cell adenoma) as low-grade adenocarcinomas based on their architectural features, despite the lack of reports of metastases and their indolent growth.[25] Other sporadic gastric-type proliferations that lack dysplasia found in the duodenum can similarly harbor *GNAS* mutations.[15]

It is of interest that the lesions detected in patient 4 showed several lines of differentiation, including *GNAS* mutation-associated gastric forms of differentiation as well as intestinal differentiation, the latter presumably a reflection of a more advanced lesion in keeping with the older age of patient 4. Indeed, superimposed intestinal differentiation in gastric pyloric gland adenomas can also be encountered in the setting of autoimmune gastritis, which features intestinal metaplasia. All of this suggests that *GNAS*

mutations are insufficient in themselves to drive aggressive neoplasms even if they might initiate indolent ones.

Our *GNAS* mutation analysis demonstrated that the IPMNs and adenomatous gastric lesion had mutations in the hotspot known to underlie the phenotype in MAS. In addition, the majority of samples of gastric heterotopia/metaplasia also had *GNAS* mutations. Considering the previous data reporting *GNAS* mutation in similar sporadic lesions, our results suggest that the early post-zygotic *GNAS* mutations play a role in the formation of these lesions. However, the lack of *GNAS* mutations in the fundic gland polyps, hamartomatous-type polyps, and other polyps calls into question the role of the mosaic *GNAS* mutations in the development of these lesions, which could be sporadic and thus unrelated to the MAS in these patients.

Although we performed targeted next-generation sequencing on samples from only a subset of the patients in our cohort, we identified mutations in several additional genes previously reported to be critical drivers of pancreatic tumorigenesis, including *KRAS* and *CKDN2A*.[3,26] Although more comprehensive sequencing will be necessary to fully describe the genomic landscape of pancreatic neoplasms in these patients, these preliminary findings suggest that they may be quite similar to sporadic IPMNs.

In summary, we report the pathologic spectrum of gastrointestinal and pancreatic lesions in patients with MAS. Overall, there is enrichment for lesions known to have *GNAS* mutations when they occur sporadically, including pancreatic IPMNs, gastric heterotopia, and gastric adenomas with pyloric gland and oxyntic differentiation. Although no patients in our series had invasive cancer, two had high-grade dysplasia, one in a gastric polyp and one in an IPMN. This raises the possibility of an increased risk for malignant transformation in MAS patients, particularly as they age. Although only a small series of patients is reported here since the condition is rare, these data suggest potential clinical utility in screening the gastrointestinal tract and pancreas in MAS patients in order to detect and remove high-risk lesions. Further longitudinal study in MAS cohorts will be necessary to better understand the natural history of gastrointestinal and pancreatic neoplasms in these patients.

REFERENCES

1. Boyce, A. M., Florenzano, P., de Castro, L. F. & Collins, M. T. Fibrous Dysplasia/McCune-Albright Syndrome. in GeneReviews® (eds. Adam, M. P. et al.) (University of Washington, Seattle, 2015).
2. Weinstein, L. S. et al. Activating mutations of the stimulatory G protein in the McCune-Albright syndrome. N. Engl. J. Med. 325, 1688–1695 (1991).
3. Wu, J. et al. Recurrent *GNAS* mutations define an unexpected pathway for pancreatic cyst development. Sci. Transl. Med. 3, 92ra66 (2011).
4. Matsubara, A. et al. Frequent *GNAS* and *KRAS* mutations in pyloric gland adenoma of the stomach and duodenum. J. Pathol. 229, 579–587 (2013).
5. Gaujoux, S. et al. Hepatobiliary and Pancreatic neoplasms in patients with McCune-Albright syndrome. J. Clin. Endocrinol. Metab. 99, E97–101 (2014).
6. Zacharin, M. et al. Gastrointestinal polyps in McCune Albright syndrome. J. Med. Genet. 48, 458–461 (2011).
7. Lumbroso, S., Paris, F., Sultan, C. & European Collaborative Study. Activating Gsalpha mutations: analysis of 113 patients with signs of McCune-Albright syndrome--a European Collaborative Study. J. Clin. Endocrinol. Metab. 89, 2107–2113 (2004).
8. Idowu, B. D. et al. A sensitive mutation-specific screening technique for *GNAS*1 mutations in cases of fibrous dysplasia: the first report of a codon 227 mutation in bone. Histopathology 50, 691–704 (2007).
9. Molin, M. D. et al. Clinicopathological correlates of activating *GNAS* mutations in intraductal papillary mucinous neoplasm (IPMN) of the pancreas. Ann. Surg. Oncol. 20, 3802–3808 (2013).
10. Chen, G. et al. A virtual pyrogram generator to resolve complex pyrosequencing results. J. Mol. Diagn. 14, 149–159 (2012).
11. Yu, J. et al. Digital next-generation sequencing identifies low-abundance mutations in pancreatic juice samples collected from the duodenum of patients with pancreatic cancer and intraductal papillary mucinous neoplasms. Gut 66, 1677–1687 (2017).
12. Adsay, N. V. et al. Pathologically and biologically distinct types of epithelium in intraductal papillary mucinous neoplasms: delineation of an 'intestinal' pathway of carcinogenesis in the pancreas. Am. J. Surg. Pathol. 28, 839–848 (2004).
13. Parvanescu, A. et al. Lessons from McCune-Albright syndrome-associated intraductal papillary mucinous neoplasms: : *GNAS*-activating mutations in pancreatic carcinogenesis. JAMA Surg. 149, 858–862 (2014).
14. Amato, E. et al. Targeted next-generation sequencing of cancer genes dissects the molecular profiles of intraductal papillary neoplasms of the pancreas. J. Pathol. 233, 217–227 (2014).
15. Matsubara, A. et al. Activating *GNAS* and *KRAS* mutations in gastric foveolar metaplasia, gastric heterotopia, and adenocarcinoma of the duodenum. Br. J. Cancer 112, 1398–1404 (2015).
16. Kushima, R. et al. Gastric adenocarcinoma of the fundic gland type shares common genetic and phenotypic features with pyloric gland adenoma. Pathol. Int. 63, 318–325 (2013).
17. Wood, L. D., Salaria, S. N., Cruise, M. W., Giardiello, F. M. & Montgomery, E. A. Upper GI tract lesions in familial adenomatous polyposis (FAP): enrichment of pyloric gland adenomas and other gastric and duodenal neoplasms. Am. J. Surg. Pathol. 38, 389–393 (2014).
18. Hashimoto, T. et al. Familial adenomatous polyposis-associated and sporadic pyloric gland adenomas of the upper gastrointestinal tract share common genetic features. Histopathology 67, 689–698 (2015).
19. Vieth, M., Kushima, R., Borchard, F. & Stolte, M. Pyloric gland adenoma: a clinico-pathological analysis of 90 cases. Virchows Arch. 442, 317–321 (2003).
20. Vieth, M. & Montgomery, E. A. Some observations on pyloric gland adenoma: an uncommon and long ignored entity! J. Clin. Pathol. 67, 883–890 (2014).
21. Chen, Z.-M., Scudiere, J. R., Abraham, S. C. & Montgomery, E. Pyloric gland adenoma: an entity distinct from gastric foveolar type adenoma. Am. J. Surg. Pathol. 33, 186–193 (2009).
22. Park, J. Y., Cornish, T. C., Lam-Himlin, D., Shi, C. & Montgomery, E. Gastric lesions in patients with autoimmune metaplastic atrophic gastritis (AMAG) in a tertiary care setting. Am. J. Surg. Pathol. 34, 1591–1598 (2010).
23. Abraham, S. C., Singh, V. K., Yardley, J. H. & Wu, T. T. Hyperplastic polyps of the stomach: associations with histologic patterns of gastritis and gastric atrophy. Am. J. Surg. Pathol. 25, 500–507 (2001).
24. Pittman, M. E., Voltaggio, L., Bhaijee, F., Robertson, S. A. & Montgomery, E. A. Autoimmune metaplastic atrophic gastritis. Am. J. Surg. Pathol. 39, 1611–1620 (2015).
25. Ueyama, H. et al. Gastric adenocarcinoma of fundic gland type (chief cell predominant type): proposal for a new entity of gastric adenocarcinoma. Am. J. Surg. Pathol. 34, 609–619 (2010).
26. Wu, J. et al. Whole-exome sequencing of neoplastic cysts of the pancreas reveals recurrent mutations in components of ubiquitin-dependent pathways. Proc. Natl. Acad. Sci. U. S. A. 108, 21188–21193 (2011).

Part 2

Three-dimensional histopathology through tissue clearing

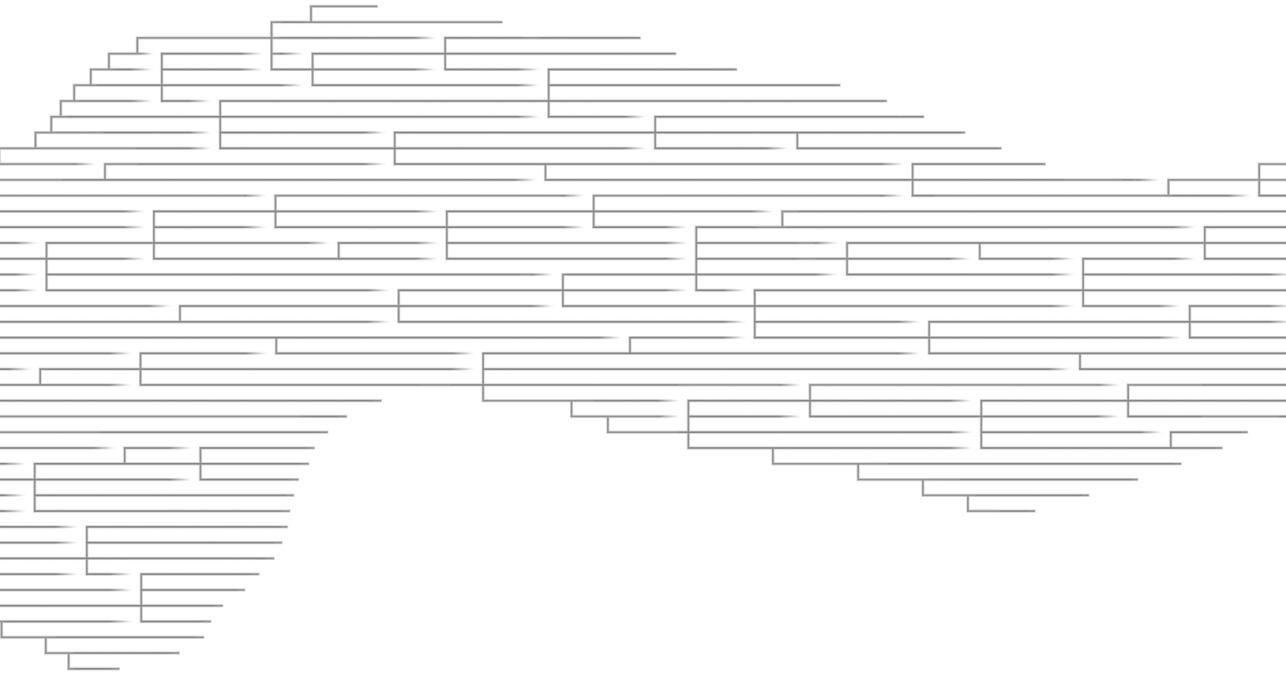

Chapter 7

A “clearer” view of pancreatic pathology: a review of tissue clearing and advanced microscopy techniques

Seung-Mo Hong, Michaël Noë, Carolyn Hruban, Elizabeth Thompson, D. Laura D. Wood, Ralph H. Hruban

Advances in Anatomic Pathology, January 2019

ABSTRACT

Although pathologic lesions in the pancreas are 3-dimensional (3D) complex structures, we currently use thin 2D hematoxylin and eosin stained slides to study and diagnose pancreatic pathology. Two technologies, tissue clearing and advanced microscopy, have recently converged, and when used together they open the remarkable world of 3D anatomy and pathology to pathologists. Advances in tissue clearing and antibody penetration now make even dense fibrotic tissues amenable to clearing, and light sheet and confocal microscopes allow labeled cells deep within these cleared tissues to be visualized. Clearing techniques can be categorized as solvent-based or aqueous-based techniques, but both clearing methods consist of 4 fundamental steps, including pretreatment of specimens, permeabilization and/or removal of lipid, immunolabeling with antibody penetration, and clearing by refractive index matching. Specialized microscopes, including the light sheet microscope, the 2-photon microscope, and the confocal microscope, can then be used to visualize and evaluate the 3D histology. Both endocrine and exocrine pancreas pathology can then be visualized. The application of labeling and clearing to surgically resected human pancreatic parenchyma can provide detailed visualization of the complexities of normal pancreatic anatomy. It also can be used to characterize the 3D architecture of disease processes ranging from precursor lesions, such as pancreatic intraepithelial neoplasia lesions and intraductal papillary mucinous neoplasms, to infiltrating pancreatic ductal adenocarcinomas. The evaluation of 3D histopathology, including pathology of the pancreatic lesions, will provide new insights into lesions that previously were seen, and thought of, only in 2 dimensions.

INTRODUCTION

The pathologic examination of biopsied or surgically resected tissue is central to advancing our understanding of disease mechanisms, establishing diagnoses, determining prognoses, and guiding decisions for treatments. Pathology examination can take place at the gross, microscopic, and molecular levels. For microscopic examination, most tissues are routinely formalin-fixed and paraffin-embedded. These tissue blocks are then thinly sectioned, stained with hematoxylin and eosin (H&E), and mounted on glass slides for examination using a standard light microscope. Although these thin H&E sections are immensely efficient and powerful tools for discovery and patient care, we have forgotten that they are extraordinarily thin, and therefore incomplete, representations of significantly larger pieces of tissue. As a result, lesions with complex and informative 3-dimensional (3D) anatomy are incompletely conceptualized as flat 2D architectures.

This 2D histology does not completely represent important characteristics of 3D lesions and can be misleading. For example, in the cancer biology field the budding of neoplastic cells at the leading edges of infiltrating adenocarcinomas had been interpreted in 2D to be the migration of single detached cancer cells, while, in fact, 3D reconstruction of consecutive sections of slides immunohistochemically labeled for cytokeratin revealed that in many instances these cells that appeared isolated in 2D were, in fact, 3D branch-like projections of collective cancer cells.[1] Perhaps more importantly, 3D relationships are lost in thin H&E sections. Cross sections of perineural invasion are easily appreciated in 2D sections in cancers, but in 2D one cannot define the point at which the cancer invaded the nerve. Histology viewed in 2D also leaves some questions unanswered. For example, immune cells are often appreciated in the neighborhood of neoplastic cells, but their distribution in 3D is unclear in 2D sections. Are they randomly scattered or is there a 3D architectural organization? As pathologists have viewed sections in 2 dimensions for so long, we have forgotten to think in 3 dimensions and to ask important architectural questions.

3D imaging has been adopted in other specialties, often with stunning results. 3D ultrasonography, 3D computed tomography, and 3D magnetic resonance imaging, have not only fundamentally changed clinical care, but they have also improved our understanding of diseases.[2–4] For example, 3D computed tomography of the pancreas can reveal the relationship of cancers of the head of the gland to major vessels such as the superior mesenteric artery and vein.[5,6] Similarly, 3D organoid cell culture systems of murine and human pancreata have recently been generated to recapitulate the characteristics of infiltrating pancreatic ductal adenocarcinomas better than flat 2D-cultured cell lines.[7] 3D visualization of 3D pancreatic lesions has great potential to expand our understanding of a broad variety of pathologies.

Recently, several groups have examined mouse and human pancreata in 3D using clearing and the results have been eye-opening.[8–12] For example, as discussed in greater detail later, our group applied clearing with immunolabeling for cytokeratin 19 to a series of surgically resected human pancreatic

cancers and showed that neoplastic glands of invasive cancer often track in the connective tissue parallel to muscular arteries.[12]

Clearing with 3D histopathologic evaluation of normal or pathologic lesions will provide new insights into the pathogenesis of diseases, and may provide an understanding of the 3D basis for diagnostic features appreciated in 2D.[13] In this review, we will discuss tissue clearing, and 3D microscopic examination with emphasis on the application of these technologies to the pancreas.

TISSUE CLEARING

Tissues are composed of a diverse mixture of cells, connective tissues, and fluids. Water is the most prominent fluid, and the structural components of cells are predominantly made of lipids and proteins. Each of these tissue components has a different refractive index (RI), and when light waves pass from a medium with one RI into a medium with a different RI, the light waves bounce (reflect) and bend (refract).[14] It is this irregular scattering, as well of absorption and reflection, of light as it passes through tissues that makes tissues opaque.

More specifically, RI is defined by ratio of the speed of light when light passes through a substance relative to the speed of light when it passes through a vacuum. For example, the RI of air is 1, that of water is 1.33, and that of the oil is 1.52.[15] As light passes from water rich tissues with a relatively low RI into lipid rich structures, such as cell membranes, with a higher RI, light will bend and scatter, creating optical nontransparency.[16]

Tissue clearing techniques work by creating tissues with a uniform RI which reduces the scattering light.[16] For example, the hydrogel embedding method creates tissues with uniform RIs in the range of 1.33 to 1.47, simple emersion methods create tissues with uniform RIs in the range of 1.42 to 1.52, and solvent-based methods create tissues with uniform RIs of 1.56 to 1.57.[17] The scattering of light is reduced in these tissues with uniform RIs, and when combined with the removal of pigments to reduce the absorption of light, the tissues become transparent.

Although this all sounds very new, tissue clearing has actually been around for almost a century. Tissue clearing was first introduced by the German anatomist Werner Spalteholz in 1911.[18] In order to study the coronary arteries, Spalteholz created transparent muscle tissue by sequentially soaking the tissues in alcohol, clover oil or xylene, and Canada balsam.[18] He finally established clearing solutions that included methyl salicylate, benzyl benzoate, and even wintergreen oil.[18] Over the ensuing decades, many different methods have been developed to clear tissues. The techniques can be divided into solvent-based clearing and aqueous-based clearing. Prototypes of solvent-based clearing techniques are benzyl alcohol, benzyl benzoate (BABB), an improved version of the clearing method used by Spalteholz, 3D imaging of solvent-cleared organs (3DISCO), immunolabeling-enabled 3DISCO and ultimate 3DISCO.[19–22] The aqueous-based clearing techniques can be subdivided in tech-

niques that use only simple immersion and techniques that use a hydrogel. The prototypes of the simple immersion technique are FocusClear, 2,2'-thiodiethanol, sucrose, ClearT, and see deep brain (SeeDB).[23–27] These techniques do not remove lipids, but replace the liquid in and around the tissue with a high RI, water-based solution. Although Scale and clear unobstructed brain imaging cocktail and computational analysis (CUBIC) are also aqueous-based clearing techniques, they also exploit the removal of lipids from the tissue and the use of urea to penetrate, partially denature and thus hydrate the hydrophobic regions of high RI proteins, to decrease the overall RI of the tissue.[28,29] Hydrogel-based clearing techniques immobilize the proteins in an acrylamide-based matrix and clear the tissue through the complete removal of all lipids from the tissue. Prototypes of this method are clear lipid-exchanged acrylamide-hybridized rigid imaging/immunostaining/in situ hybridization–compatible tissue hydrogel (CLARITY), passive clarity techniques and perfusion-assisted agent release in situ.[30,31] Each of these methods have their own strengths and weaknesses which have been well summarized elsewhere.[16,17,32,33] Although many different clearing methods have been developed, only a few of these methods have been applied to the pancreas, and even fewer to the dense fibrotic tissues that characterize human pancreatic cancer.[10–12,34–40]

Solvent-based clearing methods typically use methanol, with or without hexane, or tetrahydrofurane as extra dehydrant.[16,20] These reagents remove water and lipids from the tissues, resulting in homogenously dehydrated protein-rich dense samples with an average RI, higher (>1.5) than those of water and lipid.[16] More of the remaining lipids can be removed and the tissues further RI matched using a second step that includes BABB, dibenzyl ether, or methyl salicylate.[16–18] There are several short comings to these solvent-based clearing approaches: first, since water is essential for maintaining emissions from fluorescent protein chromophores, these solvent-based methods, which remove water, result in the rapid quenching of fluorescent signals.[16] Second, these solvent-based methods, again because they remove water, can cause significant tissue shrinkage.[30]

Aqueous-based methods have also been widely used to clear pancreatic parenchyma, especially normal tissues that are less fibrotic than are cancers.[10,11,35–40] These aqueous-based methods include SeeDB, CUBIC, and CLARITY, and they have the advantage of greater preservation of the fluorescent signals.[27–29] These methods use 1 of 3 approaches, (1) simple immersion of specimens into a water-based solution with a higher RI (1.42 to 1.56), similar to the RI of the lipids and proteins, (2) partial removal of lipids in combination with the hydration of the hydrophobic regions of proteins (hyperhydration) to lower the RI, or (3) hydrogel embedding in combination with the complete removal of lipids.16 Aqueous-based methods have some limitations including the requirement of electrophoresis devices, constant perfusion, or high temperatures,[41–44] which may prevent complete tissue clearing of dense fibrotic pancreatic parenchyma (desmoplastic reaction).

Although aqueous-based methods may be ideal to clear normal tissues, including normal pancreas tissue, these techniques may not be effective with abnormal tissues with dense fibrosis. Therefore, solvent-based methods may be preferred with dense fibrotic tissues. For example, as discussed in detail

below, we recently reported a modified iDISCO method to clear surgically resected human pancreas tissue and showed that this method could be used to visualize a number of pancreas lesions, including pancreatic intraepithelial neoplasias (PanINs) and intraductal papillary mucinous neoplasms (IPMNs), and even infiltrating pancreatic ductal adenocarcinomas.[12]

Irrespective of which specific approach is used, tissue clearing techniques, as noted above, can be thought of as having 4 basic steps: (a) pretreatment of specimens, (b) permeabilization and/or removal of lipid (delipidation), (c) immunolabeling (antibody penetration), and (d) clearing (RI matching) steps.[17] There are some exceptions, for example the hydrogel-based techniques, where the clearing step is performed before the immunolabeling step.

Pretreatment

Pretreatment steps are used for various reasons in the different protocols. In general, during this step, pigments are removed from the specimens as pigments may absorb light. Hydrogen peroxide (H2O2) is often used, because it reduces the internal pigments of the tissue and reduces autofluorescence of other proteins by oxidizing them.[21,45] Recently, N-butyldiethanolamine has also been shown to be a potent agent for decolorization.[46]

In the hydrogel-based methods, pretreatment is used to introduce acrylamide as a monomer into the tissue. This is carried out in combination with formaldehyde, to crosslink proteins, nucleic acids, and other small molecules to the monomer. Eventually, the monomer is polymerized at 37°C to form the hydrogel that keeps the bound molecules in place during delipidation.

Other agents can also be applied during pretreatment, depending on the tissue type. Bones can be demineralized with EDTA.[47]

Permeabilization and/or removal of lipid (delipidation)

A permeabilization step can help enhance the penetration of the clearing solution and the penetration of antibodies into tissue specimens. Lipid removal (delipidation) also contributes to tissue clearing, because lipids usually contribute to the inhomogeneity of RIs in biospecimens. However, lipid removal, when extreme, will also result in the removal of membrane proteins. Hydrogel-based methods use the hydrogel to keep the membrane proteins in place allowing for more extreme delipidation and tissue clearing.[30] Permeabilization and delipidation typically are accomplished using solvents (dichloromethane, methanol, tertiary butanol, tetrahydrofuran, dimethyl sulfoxide), sorbitol, urea, or detergents (sodium dodecyl sulfate, saponin, or triton X-100).[16]

Immunolabeling (Antibody Penetration)

Cell membranes are significantly more porous after lipids have been partially removed, facilitating the delivery of antibodies inside of the cells. Traditional immunolabeling of 5-μm sections depends on the simple diffusion of antibodies. However, antibody diffusion into the thick slabs of tissue used in clearing

is a slow process and can take several weeks.[30] Several methods have therefore been developed to improve antibody penetration in thick slabs of tissue.
Kim et al. devised a stochastic electrotransport system which enhances antibody penetration without affecting the low-electromobility molecules and which can be used together with CLARITY.[41] They further used a rotational electric field to selectively deliver antibodies throughout porous samples.[41]

Centrifugal forces applied with a bench-top centrifuge at a speed of 600 rcf have also been shown to improve the delivery of antibodies deep into tissue.[42] A similar effect can be achieved with the application of convectional flow forced by placing tissues and antibodies into the chamber of a syringe and then pumping the syringe under pressue.[42]

An alternative method, system-wide control of interaction time and kinetics of chemicals (SWITCH), has been introduced to improve antibody distribution.[43] In SWITCH the binding of antibodies is suppressed until antibodies reach even distribution throughout the tissue, then antibodies are "SWITCHED ON" to bind their target epitope using pH-dependent reactivity.[43]

Clearing (Refractive Index Matching)

As discussed earlier, in this step the RI of the specimens is homogenized using a variety of solutions, producing transparent specimens. The RI achieved with the hydrogel embedding method ranges from 1.33 to 1.47, while of the RIs achieved with simple emersion methods range from 1.42 to 1.52. The RIs with solvent-based methods range from 1.56 to 1.57.[17]

MICROSCOPY

Although conventional light microscope is good for the evaluation of thin 2D H&E slides, it is not suitable for evaluation of 3D architecture in thick slabs of cleared tissue. Therefore, light sheet microscopy, confocal microscopy, or 2-photon microscopy is used to evaluate the 3D histology of cleared samples. Familiarity with a few terms is needed before we discuss these different types of microscopes. The working distance of microscope is defined by the distance from the front edge of the microscope objective to the plane at which an area of the sample to be studied is in focus.[15] The numerical aperture of a microscope defines the ability of the objective to capture sample details and how much light enters the objective.[15] In general, long working distance (>5 mm) and high numerical aperture (>0.9) is recommended for evaluating the 3D histology of cleared tissues.[15,16]

Light Sheet Microscopy

Light sheet microscopy was developed to enhance the 3D visualization of large specimens.[48] Light sheet microscopy can be used to visualize volumetric specimens ranging in size all the way from <1 to up to 15 mm.[49] Light sheet microscopy works by optical sectioning with 2 thin counter-propagating sheets of LASER beams that are perpendicular to the focal plane of the objective.[50] The objective collects fluorescent light which is emitted only from this thin optical section.[49] 3D reconstruction of the

volumetric specimens can then be obtained by serial stacking of the images in the axial dimension.[50] Schematic illustration of how light sheet microscopy works to visualize 3D pancreatic tissues is depicted in Figure 1.

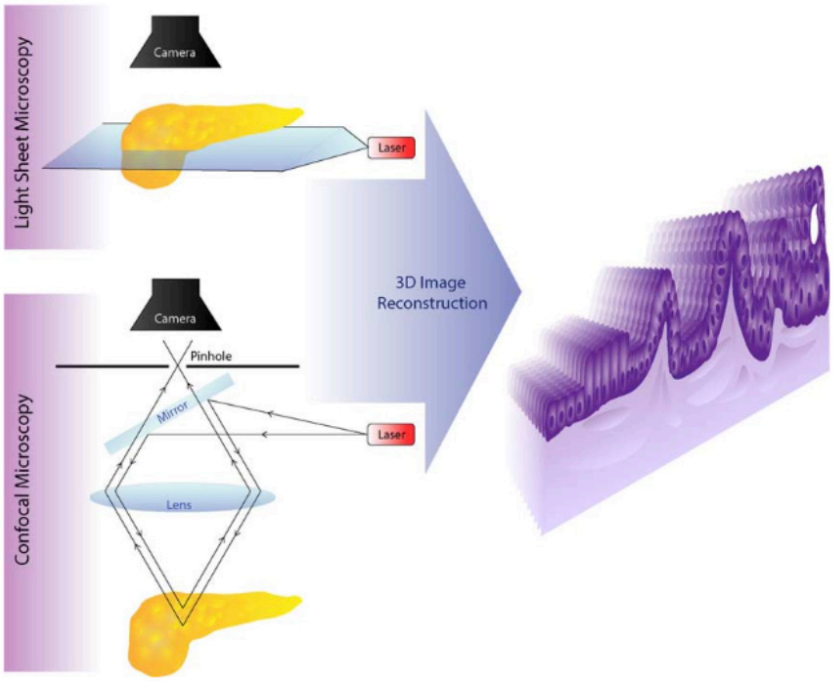

Figure 1. Schematic illustration of how light sheet and confocal LASER microscopy can be utilized to visualize 3D pancreatic tissues.Light sheet microscopy (top upper left) uses optical sectioning with 2 thin counter-propagating sheets of LASER beams that areperpendicular to the focal plane of the objective. The objective collects fluorescent light which is emitted only from this thin opticalsection. In confocal LASER microscopy (lower left), a LASER light illuminates only a highly delineated spot in the specimen. Only in-focusfluorescent light is allowed into the objective, and much of the out-of-focus fluorescent light is rejected. Serial stacking (right) of theobtained images from light sheet and confocal LASER microscopies enable 3D volumetric reconstruction of the images from pancreasspecimens.

Light sheet microscopes tend to cause less photobleaching effect and can produce 3D images that cover larger volumes at higher speeds than can confocal microscopes.[15] Another strength of light sheet microscopy is that it can be applied to large specimens as long working distances can be obtained when the objective is immersed into the specimen chamber medium.[49] However, lenses with longer working distances tend to have lower resolution.[15] As described below, confocal LASER microscopy can be used to obtain higher resolution images when needed.

Confocal (LASER Scanning) Microscopy

Confocal scanning microscopy has been used to characterize structural and cytologic details based on excitation of endogenous or exogenous fluorophores with or without the use of a LASER. Confocal LASER scanning microscopy works as a computer-assisted epifluorescent microscope, which rejects much of the out-of-focus fluorescent light. A LASER light is precisely focused to illuminate a highly delineated spot in the specimen. This reduces the fluorescent light emitted by tissues outside the

focal plane of the objective lens.[50] At each illuminated spot, fluorescent light emitted by the tissue is separated from the incident exciting LASER light using a dichroic mirror. In order to be detected the light also has to pass through a confocal pinhole, which rejects fluorescent light generated outside of the focal plane of the objective, and therefore most of the unwanted light scattered by the specimen is not seen.[50] Images are created by scanning diffraction limited spots in a raster pattern across the specimen with 2 mirrors mounted on coordinating galvanometer motors.[50] The light passing through the confocal pinhole is detected with a photomultiplier tube, and the signal is processed by a computer to create a digital image.[50] Schematic illustration of how confocal LASER microscopy works to visualize 3D pancreatic tissues is depicted in Figure 1.

Confocal microscopy can obtain near-real time images with histologic resolution.[51] Historically the imaging depth of confocal LASER scanning microscopy has been limited by the working distance of the objectives of the microscope, which typically do not exceed 4 mm.[52] However, microscope makers have recently developed customized objectives for use with specific clearing reagents. For example, Leica sells customized microscope specific for CLARITY, Olympus provides objectives for CLARITY, Scale, and SeeDB, and Zeiss makes objectives for several clearing reagents. The working distance for these specialized objectives is now to 5.6 to 8 mm,[15] theoretically allowing for the evaluation of 3D histology of tissues with up to 8 mm in thickness.

Two-photon (LASER Scanning) Microscopy

Two-photon LASER scanning microscopy uses long wavelength near-infrared LASERs, which can reduce light scattering and increase depth of penetration.[53] High-power pulsed LASERs are restricted to the focal plane resulting in excitation of 2 lower energy photons, which cause optical sectioning.[54] The lower energy 2 photons reduce phototoxicity and bleaching compared with confocal LASER scanning microscopy.[54] Imaging depth reach up to 1 mm.[54] Therefore, 2-photon microscopy can only be used for the evaluation of 3D histology of small sized tissues that are 1 to 2 mm in thickness.

SELECTED APPLICATIONS

Recently the successful clearing of pancreatic tissue has been reported by several groups.[10,12,34,35,37–39,45] Most of the previous studies have focused on clearing normal (nonfibrotic) pancreas and on imaging the endocrine components of the gland.[8,11,34,35,37–39] There have been only a few studies of the exocrine pancreas.[12] Previous studies that have applied clearing to the pancreas are summarized in Table 1.

Mouse Pancreas

Most of the previous studies that applied tissue clearing to the pancreas used the mouse pancreata, since the mouse pancreas is small and therefore more easily cleared and imaged.[34] Kim et al. characterized green fluorescent protein (GFP)-tagged beta-cell distribution in mouse pancreas after tissue clearing with sucrose.[34] Fu et al. reported islet microstructures and the vasculature of the mouse pancreas cleared with FocusClear.[35] The same group later reported streptozosin-treated injured islets had

Patient	Age[a]	Location	Diagnosis	GNAS—lesional tissue	GNAS—normal tissue
1	20	Proximal esophagus	Gastric heterotopia/metaplasia	R201C	–
		Stomach body	Fundic gland polyp	WT	–
		Major papilla	Hamartomatous-type polyp	WT	WT
		Minor papilla	Gastric heterotopia/metaplasia	WT	–
2	22	Proximal stomach	Gastric hyperplastic polyps	WT	–
		Duodenal bulb	Gastric heterotopia/metaplasia	R201C	WT
		Duodenum	Gastric heterotopia/metaplasia	WT	WT
		Ampulla	Gastric heterotopia/metaplasia	WT	–
3	46	Gastroesophageal junction	Gastric hyperplastic polyp	R201H	–
		Duodenum	Gastric heterotopia/metaplasia	R201H	–
4	55	Proximal esophagus	Gastric heterotopia/metaplasia	WT	WT
		Proximal stomach	Multiple adenomatous lesions with high-grade dysplasia[b]	R201C	–
		Stomach	Fundic gland polyps	WT	–
		Stomach body	Foveolar hyperplasia	R201C	–
		Duodenum	Gastric heterotopia/metaplasia	WT	–
		Ampulla	Gastric heterotopia/metaplasia	R201C	–
		Pancreas	Intraductal papillary mucinous neoplasm with low-grade dysplasia	R201C	WT
5	27	Duodenum	Gastric heterotopia/metaplasia with adjacent neuroendocrine hyperplasia	R201H[c]	WT
		Pancreas	Intraductal papillary mucinous neoplasm with high-grade dysplasia	R201H	–
6	19	Proximal esophagus	Gastric heterotopia/metaplasia	R201C	–
		Proximal stomach	Gastric hyperplastic polyps	WT	–
		Proximal duodenum	Gastric heterotopia/metaplasia	R201C	–
		Duodenum	Gastric heterotopia/metaplasia	R201C	–
		Ampulla	Gastric heterotopia/metaplasia	R201C	WT
7	50	Proximal esophagus	Gastric heterotopia/metaplasia	R201C	–
		Gastroesophageal junction	Intestinal metaplasia	WT	–
		Distal esophagus	Gastric hyperplastic polyp	WT	–
		Duodenum	Gastric heterotopia/metaplasia	R201C	–
		Duodenum	Gastric heterotopia/metaplasia	R201C	R201C

CLARITY indicates clear lipid-exchanged acrylamide-hybridized rigid imaging/immunostaining/in situ hybridization; CUBIC, clear unobstructed brain imaging cocktail and computational analysis; ECT, electrophoretic tissue clearing; GFAP, glial fibrillary acidic protein; GFP, green fluorescent protein; iDISCO, immunolabeling-enabled 3D imaging of solvent-cleared organs; KO, knock out; MIP, mouse insulin 1 promoter; NG2, neuron-glial antigen 2; seeDB, see deep brain; STZ, streptozotocin; TH, tyrosine hydroxylase; vAChT, vesicular acetylcholine transporter; WT, wild type

Table 1. Summary of celaring methods used to study mouse or human pancreas

Schwann cell and pericyte plasticity.[38] Tang et al. cleared mouse and human pancreata and identified a pancreatic neurovascular network and the coupling of ganglionic and islets via the network.[37,39]

Wong et al. applied a simplified CLARITY method that used acrylamide-free sodium dodecyl sulfate–based tissue delipidation to mouse pancreas tissue.[11] With this modified technique, they demonstrated differences in the distribution of beta-cells between wild type and mouse insulin 1 promoter GFP mice, the latter of which express enhanced green fluorescent protein (EGFP) under the control of the mouse insulin 1 promoter.[11]

Tainaka et al. cleared the whole body of a mouse, including the pancreas, using CUBIC-perfusion techniques, and demonstrated the superiority of CUBIC-perfusion over SeeDB methods in clearing techniques.[45] Lee et al. also cleared the whole body of a mouse, but they used the CLARITY technique.[40] They observed that the optimal electrical current conditions for the clearing of different mouse organs vary based on the consistency of the organs, and found that 250 mA was the best condition for clearing the mouse pancreas with the CLARITY technique.[40]

Human Pancreas

There have only been a handful of reports of clearing applied to the human pancreas.[8,12,37] These studies have provided novel insights into human diseases not appreciated in conventional 2D histology sections. Tang et al. cut surgically resected human pancreas to 350 µm thick sections using a vibratome, cleared the sections with RapiClear clearing solution, and observed the endocrine pancreas in these sections.[37] They were able to demonstrate subtle 3D relationships between the vasculature and the endocrine pancreas.[37] They observed alfa-cell distributions in the core and mantle layer of islets of Langerhans, and showed that as arterioles entered the core of the islets they break into capillaries. They also mapped the distribution of sympathetic nerve fibers along the islet microvasculature.[37] They found that condensed nerve fiber networks encircle the islets of Langerhans, and showed connections of nerve fibers from islets with microvasculature and ganglia.[37] In a separate study Fowler et al. sectioned pancreatic tissue at up to 5 mm of thickness, and cleared the sections by immersing them in fructose and thioglycerol.[8] Their observations were similar to those of Tang and colleagues. They demonstrated large islet vessels branching off into small capillaries.[8] Using 3D histologic evaluation, they were able to capture larger numbers of islets, which increased the statistical power of their observations.[8]

We applied a modified iDISCO method to clear thick slabs of grossly normal human pancreas parenchyma (up to 1.5-mm thick) and to slabs of human pancreatic ductal adenocarcinoma (0.6 mm in thickness) obtained from surgically resected specimens and the results were dramatic (Figure 2A).[12] Normal pancreatic tissue, intraductal precursor lesions of invasive cancer, including PanINs and IPMNs, and pancreatic ductal adenocarcinomas were all successfully cleared and visualized in 3D.[12] This allowed us to visualize features in 3D which were difficult to appreciate in previous thin 2D sections.

In normal pancreatic parenchyma, we observed the stunning 3D branching of the pancreatic duct system, as well as regularly distributed small periductal glands extending off of larger normal ducts.[12] We observed that some ductules, rather than separating as they branched as branches of a tree would, instead looped back to apparently rejoin the duct system (Supplemental Video 1, Supplemental Digital Content 1, http://links.lww.com/PAP/A23). Secondary changes of focal ductal obstruction were observed, including focal dilation of the lumina and acini in a lobule producing a ball of grapes appearance.[12] These cleared human pancreata could also be used to visualize, in 3D, the architecture of both PanINs and IPMNs (Supplemental Video 2, Supplemental Digital Content 2, http://links.lww.com/PAP/A24). The full size and shape of these lesions could be determined when the lesions were fully contained in the slab of tissue studied, and the intraluminal papillary projections were beautifully visualized.[12] When invasive cancers were cleared, the cancer cells were haphazardly arranged in 3D, forming, in some cases, sheets of mesenchymal appearing cells, and in others irregular-shaped tubular structures with numerous blunt-ended projections (Figure 2B). Invasive cancer growing into preexisting ducts (cancerization of ducts) was visualized in 3D.[12] In contrast to the nice uniform papillae of PanIN lesions, the invasive cancer cells in cancerization of ducts irregularly grew across the duct lumina, forming jagged bridges that spanned the lumina. The use of several different antibodies and fluorophores allows for the visualization of the expression of multiple proteins in 3D (Figures 2C, D).

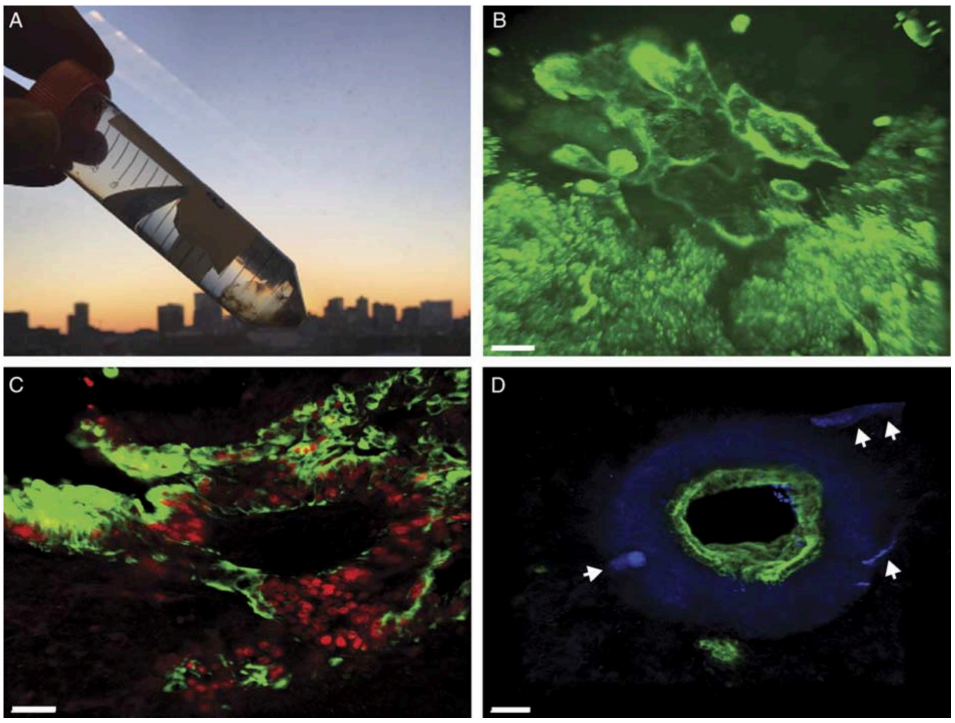

Figure 2. a Gross image of cleared human pancreas in a tube. **b** Imaging of pancreatic ductal adenocarcinoma demonstratedirregular-shaped branching cancer glands in the upper half, while normal pancreatic parenchyma is well-preserved on lower half (bar, 300 µm). **c** Dual p53 and cytokeratin 19 labeling of pancreatic ductal adenocarcinoma. Cytoplasmic cytokeratin 19 is labeled with greenand nuclear p53 is labeled with orange (bar, 30 µm). **d** Dual cytokeratin 19 (green) and desmin (blue) immunolabeling of a normalpancreatic duct. A subtle branching pattern of small vessels (arrowheads) is observed with dense blue staining at periphery of the duct(bar, 30 µm).

The 3D visualization of cleared human pancreatic cancer highlighted invasive carcinoma growing within blood vessels and a unique finding not fully appreciated in 2D sections. Long tubules of neoplastic cells were visualized growing in the surrounding connective tissue parallel to blood vessels. Although we labeled pancreatic tissues with cytokeratin 19, the blood vessels could also be detected by the distinct autofluorescent signal generated by their tortuous elastic lamina (not all autofluoresence is bad!). The finding of long tubes of invasive cancer growing parallel to blood vessels helps explain the 2D clinical finding that a gland next to a muscular vessel supports the diagnosis of cancer.[55] It also suggests a mechanism for this—there may be something structural in the perivascular connective tissue, perhaps a weak tissue plane, or small channels in the connective tissue, that leads to the preferential growth of neoplastic cells in this location.[12,56,57]

DISCUSSION

The confluence of advances in microscopy and tissue clearing has opened the door to the 3D visualization of human anatomy and diseases, and provides an extraordinary opportunity to advance our understanding of the true complexity of human diseases.[33,36,58] Several questions remain to be asked, and several opportunities are yet to be explored.

What is the maximal thickness of pancreatic parenchyma that can be visualized with current technologies? Using human exocrine pancreatic tissues, we evaluated up to 1.5-mm thick slabs of normal pancreas parenchyma and 0.6-mm thick slabs of pancreatic ductal adenocarcinoma sections.[12] Fowler et al. reported that they were able to evaluate up to 5-mm thick sections of normal pancreas parenchyma.[8] Considering the working distance for the specialized objectives used is currently as high as 8 mm, one could theoretically visualize sections as thick as 16 mm (flipping the piece over one can visualize 8 mm from each surface) with confocal LASER scanning microscopy.[15] With a light sheet microscope, one could go even deeper, but the cost would be that only lower power magnification would be available.[49] Future technical advances with development of advanced microscopic techniques may extend the limit of lesions that can be visualized in 3D.

Can antibody penetration be improved? Antibody penetration in thick pancreatic tissues, especially dense fibrotic desmoplastic stroma of pancreatic ductal adenocarcinomas, is a significant hurdle in the 3D study of these tissues. Several strategies can be applied to improve antibody penetration. Single-domain antibodies (Fab')2 or nucleic acid aptamers, which are smaller than standard antibodies, can penetrate thick pancreatic tissue may reduce time for labeling.[16] In addition, forces, such as centrifugal, pressure, or electrophoretic fields, can facilitate antibody penetrations.[40–42] We applied single-domain antibodies (Fab')2 and also used centrifugal forces to enhance antibody penetration and to reduce needed incubation times.[12] New technologies that improve antibody penetration will allow even more to be seen.

The application of multicolor immunolabeling to cleared pancreatic tissues provides unique opportunities to evaluate the 3D relationships of normal ducts, precursor lesions, invasive carcinoma, immune cells, islets of Langerhans, vessels, and nerve fibers (Supplemental Video 3, Supplemental Digital Content 3, http://links.lww.com/PAP/A25).[8,39] Fowler et al. demonstrated immunolabeling with 8 different primary antibodies using conjugated primary antibodies with a combination of fluorophores.[8] By using direct conjugation of fluorophores with probes may reduce the incubation time for secondary antibodies.[16] In addition, chances of nonspecific antibody bindings between multiple primary and secondary antibodies may be reduced. However, longer exposure times may be needed to visualize the weaker signals generated by conjugated primary antibodies. In contrast, Tang et al. showed immunolabeling with 5 different nonconjugated primary antibodies from 2 different species, including guinea pig and rabbit.[39] Although both groups used different methods, they wonderfully demonstrated multiple immunolabeling in endocrine pancreas. The potential here is clearly great.

New insights

The 3D visualization of cleared human pancreas will provide an extraordinary opportunity to understand the true complexity of human pancreatic lesions in many aspects. First, some genetic mutations are associated with changes in protein expression that can be visualized in 3D, potentially allowing for the 3D visualization of the patterns of driver gene mutation in precursor lesions and in invasive cancers. This 3D visualization may provide novel insight into pancreatic ductal adenocarcinoma tumorigenesis.

Recently developed 3D organoid systems of pancreatic ductal adenocarcinomas can be used as powerful research tools for drug screening and evaluation of new biomarkers for pancreatic ductal adenocarcinomas.[7,59] The parallels between 3D organoids and 3D cleared tissues, potentially will allow researchers to validate hypothesis generated studying organoids using cleared tissue and vice-versa.

Third, recent advances in therapies that modulate the immune system to treat patients with cancers of a number of organs, including lung, head and neck, and stomach, suggest great potential in defining the 3D relationships of immune and cancer cells.[60] 3D evaluation of microenvironment of pancreatic ductal adenocarcinomas, including special associations among cancer cells, stromal cells, and immune cells, may provide insights for immune-suppressive environments for pancreatic ductal adenocarcinomas and overcoming ways for immunotherapy-resistant mechanisms of cancers.

Fourth, vascular invasion is one of the most important mechanisms underlying distant metastases of pancreatic ductal adenocarcinomas.[61] Identifying mechanisms of vascular invasions with cleared pancreatic ductal adenocarcinoma tissues will be helpful for making therapeutic regimens for preventing vascular invasion of pancreatic ductal adenocarcinomas.

SUMMARY

Thanks to recent technological advances of tissue clearing and advanced microscopy, the remarkable world of 3D anatomy and pathology to pancreatic pathologists are newly opened to pathologists. The application of labeling and clearing to human pancreatic parenchyma can provide detailed visualization of normal pancreatic anatomy and it can be used to characterize the 3D architecture of various disease processes, including precursor lesions, such as PanINs and IPMNs, to infiltrating pancreatic ductal adenocarcinomas.

REFERENCES

1. Bronsert, P. et al. Cancer cell invasion and EMT marker expression: a three-dimensional study of the human cancer-host interface. J. Pathol. 234, 410–422 (2014).
2. Vannier, M. W. et al. Craniosynostosis: diagnostic value of three-dimensional CT reconstruction. Radiology 173, 669–673 (1989).
3. Yoffie, R. L., Vannier, M. W., Gutierrez, F. R., Knapp, R. H. & Canter, C. E. Three-dimensional magnetic resonance imaging of the heart. Radiol. Technol. 60, 305–309 (1989).
4. Levine, R. A., Weyman, A. E. & Handschumacher, M. D. Three-dimensional echocardiography: techniques and applications. Am. J. Cardiol. 69, 121H–130H; discussion 131H–134H (1992).
5. Wen, Z., Yao, F. & Wang, Y. 64-Slice spiral computed tomography and three-dimensional reconstruction in the diagnosis of cystic pancreatic tumors. Exp. Ther. Med. 11, 1506–1512 (2016).
6. Roth, H. R. et al. Spatial aggregation of holistically-nested convolutional neural networks for automated pancreas localization and segmentation. Med. Image Anal. 45, 94–107 (2018).
7. Boj, S. F. et al. Organoid models of human and mouse ductal pancreatic cancer. Cell 160, 324–338 (2015).
8. Fowler, J. L. et al. Three-Dimensional Analysis of the Human Pancreas. Endocrinology 159, 1393–1400 (2018).
9. Chien, H.-J. et al. 3-D imaging of islets in obesity: formation of the islet-duct complex and neurovascular remodeling in young hyperphagic mice. Int. J. Obes. 40, 685–697 (2016).
10. Butterworth, E. et al. High Resolution 3D Imaging of the Human Pancreas Neuro-insular Network. J. Vis. Exp. (2018) doi:10.3791/56859.
11. Wong, H. S. et al. Simple and Rapid Tissue Clearing Method for Three-Dimensional Histology of the Pancreas. Curr. Protoc. Cell Biol. 77, 19.20.1–19.20.10 (2017).
12. Noë, M. et al. Immunolabeling of Cleared Human Pancreata Provides Insights into Three-dimensional Pancreatic Anatomy and Pathology. Am. J. Pathol. (2018) doi:10.1016/j.ajpath.2018.04.002.
13. Roberts, N. et al. Toward routine use of 3D histopathology as a research tool. Am. J. Pathol. 180, 1835–1842 (2012).
14. Ariel, P. A beginner's guide to tissue clearing. Int. J. Biochem. Cell Biol. 84, 35–39 (2017).
15. Marx, V. Microscopy: seeing through tissue. Nat. Methods 11, 1209–1214 (2014).
16. Richardson, D. S. & Lichtman, J. W. Clarifying Tissue Clearing. Cell 162, 246–257 (2015).
17. Richardson, D. S. & Lichtman, J. W. SnapShot: Tissue Clearing. Cell 171, 496–496.e1 (2017).
18. Spalteholz, W. Über das Durchsichtigmachen von menschlichen und tierischen Präparaten, nebst Anhang: Über Knochenfärbung. (S. Hirzel, 1911).
19. Dodt, H.-U. et al. Ultramicroscopy: three-dimensional visualization of neuronal networks in the whole mouse brain. Nat. Methods 4, 331–336 (2007).
20. Ertürk, A. et al. Three-dimensional imaging of solvent-cleared organs using 3DISCO. Nat. Protoc. 7, 1983–1995 (2012).
21. Renier, N. et al. iDISCO: a simple, rapid method to immunolabel large tissue samples for volume imaging. Cell 159, 896–910 (2014).
22. Pan, C. et al. Shrinkage-mediated imaging of entire organs and organisms using uDISCO. Nat. Methods 13, 859–867 (2016).
23. Chiang, A.-S. et al. Insect NMDA receptors mediate juvenile hormone biosynthesis. Proc. Natl. Acad. Sci. U. S. A. 99, 37–42 (2002).
24. Staudt, T., Lang, M. C., Medda, R., Engelhardt, J. & Hell, S. W. 2,2'-thiodiethanol: a new water soluble mounting medium for high resolution optical microscopy. Microsc. Res. Tech. 70, 1–9 (2007).
25. Tsai, P. S. et al. Correlations of neuronal and microvascular densities in murine cortex revealed by direct counting and colocalization of nuclei and vessels. J. Neurosci. 29, 14553–14570 (2009).
26. Kuwajima, T. et al. ClearT: a detergent- and solvent-free clearing method for neuronal and non-neuronal tissue. Development 140, 1364–1368 (2013).
27. Ke, M.-T., Fujimoto, S. & Imai, T. SeeDB: a simple and morphology-preserving optical clearing agent for neuronal circuit reconstruction. Nat. Neurosci. 16, 1154–1161 (2013).
28. Hama, H. et al. Scale: a chemical approach for fluorescence imaging and reconstruction of transparent mouse brain. Nat. Neurosci. 14, 1481–1488 (2011).
29. Susaki, E. A. et al. Whole-brain imaging with single-cell resolution using chemical cocktails and computational analysis. Cell 157, 726–739 (2014).
30. Chung, K. et al. Structural and molecular interrogation of intact biological systems. Nature 497, 332–337 (2013).
31. Yang, B. et al. Single-cell phenotyping within transparent intact tissue through whole-body clearing. Cell 158, 945–958 (2014).
32. Azaripour, A. et al. A survey of clearing techniques for 3D imaging of tissues with special reference to connective tissue. Prog. Histochem. Cytochem. 51, 9–23 (2016).
33. Seo, J., Choe, M. & Kim, S.-Y. Clearing and Labeling Techniques for Large-Scale Biological Tissues. Mol. Cells 39, 439–446 (2016).

34. Kim, A., Kilimnik, G. & Hara, M. In situ quantification of pancreatic beta-cell mass in mice. J. Vis. Exp. (2010) doi:10.3791/1970.
35. Fu, Y.-Y. et al. Three-dimensional optical method for integrated visualization of mouse islet microstructure and vascular network with subcellular-level resolution. J. Biomed. Opt. 15, 046018 (2010).
36. Tanaka, N. et al. Mapping of the three-dimensional lymphatic microvasculature in bladder tumours using light-sheet microscopy. Br. J. Cancer 118, 995–999 (2018).
37. Tang, S.-C. et al. Human pancreatic neuro-insular network in health and fatty infiltration. Diabetologia 61, 168–181 (2018).
38. Tang, S.-C., Chiu, Y.-C., Hsu, C.-T., Peng, S.-J. & Fu, Y.-Y. Plasticity of Schwann cells and pericytes in response to islet injury in mice. Diabetologia 56, 2424–2434 (2013).
39. Tang, S.-C. et al. Pancreatic neuro-insular network in young mice revealed by 3D panoramic histology. Diabetologia 61, 158–167 (2018).
40. Lee, H., Park, J.-H., Seo, I., Park, S.-H. & Kim, S. Improved application of the electrophoretic tissue clearing technology, CLARITY, to intact solid organs including brain, pancreas, liver, kidney, lung, and intestine. BMC Dev. Biol. 14, 48 (2014).
41. Kim, S.-Y. et al. Stochastic electrotransport selectively enhances the transport of highly electromobile molecules. Proc. Natl. Acad. Sci. U. S. A. 112, E6274–83 (2015).
42. Lee, E. et al. ACT-PRESTO: Rapid and consistent tissue clearing and labeling method for 3-dimensional (3D) imaging. Sci. Rep. 6, 18631 (2016).
43. Murray, E. et al. Simple, Scalable Proteomic Imaging for High-Dimensional Profiling of Intact Systems. Cell 163, 1500–1514 (2015).
44. Treweek, J. B. et al. Whole-body tissue stabilization and selective extractions via tissue-hydrogel hybrids for high-resolution intact circuit mapping and phenotyping. Nat. Protoc. 10, 1860–1896 (2015).
45. Tainaka, K. et al. Whole-Body Imaging with Single-Cell Resolution by Tissue Decolorization. Cell 159, 911–924 (2014).
46. Kubota, S. I. et al. Whole-Body Profiling of Cancer Metastasis with Single-Cell Resolution. Cell Rep. 20, 236–250 (2017).
47. Greenbaum, A. et al. Bone CLARITY: Clearing, imaging, and computational analysis of osteoprogenitors within intact bone marrow. Sci. Transl. Med. 9, (2017).
48. Helmchen, F. & Denk, W. Deep tissue two-photon microscopy. Nat. Methods 2, 932–940 (2005).
49. Becker, K., Jährling, N., Saghafi, S. & Dodt, H.-U. Ultramicroscopy: light-sheet-based microscopy for imaging centimeter-sized objects with micrometer resolution. Cold Spring Harb. Protoc. 2013, 704–713 (2013).
50. Fritzky, L. & Lagunoff, D. Advanced methods in fluorescence microscopy. Anal. Cell. Pathol. 36, 5–17 (2013).
51. Ragazzi, M., Longo, C. & Piana, S. Ex Vivo (Fluorescence) Confocal Microscopy in Surgical Pathology: State of the Art. Adv. Anat. Pathol. 23, 159–169 (2016).
52. Yushchenko, D. A. & Schultz, C. Tissue clearing for optical anatomy. Angew. Chem. Int. Ed Engl. 52, 10949–10951 (2013).
53. Tanaka, K. et al. In vivo optical imaging of cancer metastasis using multiphoton microscopy: a short review. Am. J. Transl. Res. 6, 179–187 (2014).
54. Bousso, P. & Moreau, H. D. Functional immunoimaging: the revolution continues. Nat. Rev. Immunol. 12, 858–864 (2012).
55. Sharma, S. & Green, K. B. The pancreatic duct and its arteriovenous relationship: an underutilized aid in the diagnosis and distinction of pancreatic adenocarcinoma from pancreatic intraepithelial neoplasia. A study of 126 pancreatectomy specimens. Am. J. Surg. Pathol. 28, 613–620 (2004).
56. Friedl, P. & Alexander, S. Cancer invasion and the microenvironment: plasticity and reciprocity. Cell 147, 992–1009 (2011).
57. Benias, P. C. et al. Structure and Distribution of an Unrecognized Interstitium in Human Tissues. Sci. Rep. 8, 4947 (2018).
58. Qiu, H. et al. Comparison of conventional and 3-dimensional computed tomography against histopathologic examination in determining pancreatic adenocarcinoma tumor size: implications for radiation therapy planning. Radiother. Oncol. 104, 167–172 (2012).
59. Huang, L. et al. Ductal pancreatic cancer modeling and drug screening using human pluripotent stem cell- and patient-derived tumor organoids. Nat. Med. 21, 1364–1371 (2015).
60. Johnson, B. A., 3rd, Yarchoan, M., Lee, V., Laheru, D. A. & Jaffee, E. M. Strategies for Increasing Pancreatic Tumor Immunogenicity. Clin. Cancer Res. 23, 1656–1669 (2017).
61. Hong, S.-M. et al. Vascular invasion in infiltrating ductal adenocarcinoma of the pancreas can mimic pancreatic intraepithelial neoplasia: a histopathologic study of 209 cases. Am. J. Surg. Pathol. 36, 235–241 (2012).

7

Chapter 8

Immunolabeling of cleared human pancreata provides insights into three-dimensional pancreatic anatomy and pathology

Michaël Noë, Neda Rezaee, Kaushal Asrani, Michael Skaro, Vincent P. Groot, Pei-Hsun Wu, Matthew T. Olson, Seung-Mo Hong, Sung Joo Kim, Matthew J. Weiss, Christopher L. Wolfgang, Martin A. Makary, Jin He, John L. Cameron, Denis Wirtz, Nicholas J. Roberts, G. Johan A. Offerhaus, Lodewijk A.A. Brosens, Laura D. Wood, Ralph H. Hruban

The American Journal of Pathology, July 2018

ABSTRACT

Visualizing pathologies in three dimensions can provide unique insights into the biology of human diseases. A rapid and easy-to-implement dibenzyl ether–based technique was used to clear thick sections of surgically resected human pancreatic parenchyma. Protocols were applicable to both fresh and formalin-fixed, paraffin-embedded tissue. The penetration of antibodies into dense pancreatic parenchyma was optimized using both gradually increasing antibody concentrations and centrifugal flow. Immunolabeling with antibodies against cytokeratin 19 was visualized using both light sheet and confocal laser scanning microscopy. The technique was applied successfully to 26 sections of pancreas, providing three-dimensional (3D) images of normal pancreatic tissue, pancreatic intraepithelial neoplasia, intraductal papillary mucinous neoplasms, and infiltrating pancreatic ductal adenocarcinomas. 3D visualization highlighted processes that are hard to conceptualize in two dimensions, such as invasive carcinoma growing into what appeared to be pre-existing pancreatic ducts and within venules, and the tracking of long cords of neoplastic cells parallel to blood vessels. Expanding this technique to formalin-fixed, paraffin-embedded tissue opens pathology archives to 3D visualization of unique biosamples and rare diseases. The application of immunolabeling and clearing to human pancreatic parenchyma provides detailed visualization of normal pancreatic anatomy, and can be used to characterize the 3D architecture of diseases including pancreatic intraepithelial neoplasia, intraductal papillary mucinous neoplasm, and pancreatic ductal adenocarcinomas.

INTRODUCTION

Since the days of Virchow, pathologists have been studying diseases in two dimensions.[1] For centuries, standard hematoxylin and eosin (H&E)-stained slides have framed our field of vision and therefore have narrowed the conceptual framework through which diseases are viewed. Although radiologists and experimental pathologists have broken through this framework with technologies such as three-dimensional (3D) computed tomography and organoid models, most morphologic studies of in situ human pathology still are viewed and conceptualized in two dimensions.[2,3]

Visualizing pathologies in three dimensions provides insight into the biology of human diseases. Lesions can be measured accurately, the spatial relationships of various tissue and cell components can be defined, and morphologic changes can be put in the appropriate multidimensional context.[2,4] The addition of immunolabeling for protein and in situ hybridization for RNA would allow one to visualize protein and gene expression in 3D space, creating a true multidimensional landscape.

We present a simple clearing and labeling method to visualize intact thick sections of normal and diseased human pancreatic parenchyma in three dimensions.[5–7] Organic solvents were selected to clear stroma-rich human tissues.[8,9] Proteins are preserved, allowing for immunofluorescent labeling of protein expression with an optimized protocol for penetration of antibodies in dense pancreatic tissue. In this study, cytokeratin 19 (CK19) was labeled to visualize the pancreatic ductal system, and the autofluorescent features of collagen and elastin were exploited to visualize blood vessels.

This methodology has a number of potential applications. The volume of small lesions, such as pancreatic intraepithelial neoplasia (PanIN) lesions, may be determined, the 3D relationships of cells (neoplastic, inflammatory, and so forth) to important structures (vessels, nerves, ducts, and so forth) may be defined, and changes in protein expression may be defined as cells interact, such as when neoplastic cells invade into tissues. When DNA and RNA studies are added in the future, the methodology may be used to define the drivers of 3D morphology.[10,11]

MATERIALS AND METHODS

This study was approved by our Institutional Review Board. Briefly, intact slabs (up to 2.0 × 2.0 × 0.5 cm) of excess normal or diseased surgically resected human pancreatic parenchyma were harvested. These included 17 slabs of grossly normal pancreatic parenchyma, 7 slabs of infiltrating pancreatic ductal adenocarcinoma with adjacent pancreatic parenchyma, and 2 slabs with a grossly dilated pancreatic duct, grossly suspicious for intraductal papillary mucinous neoplasm. Four of the 17 slabs of normal pancreatic parenchyma were first formalin-fixed and paraffin-embedded.

Fresh samples

Fresh tissues were fixed as quickly as possible after surgical resection in 80% methanol/20% dimethyl

sulfoxide (DMSO) to dehydrate the tissues and precipitate proteins to stop autolysis of the tissue by pancreatic enzymes. Fixation was performed overnight at room temperature. The following day, the tissues were rehydrated and fixed in neutral-buffered 10% formalin or 4% paraformaldehyde for 24 hours at room temperature. Next, the tissues were dehydrated with 70% methanol, 95% methanol, and 3 × 100% methanol, followed by chilling the tissue for an hour at 4°C in 100% methanol. Tissues then were incubated overnight in 66% dichloromethane/33% methanol at room temperature. Samples then were washed twice in 100% methanol and then 5% hydrogen peroxide was added to the 100% methanol for overnight incubation to oxidize endogenous pigments and autofluorescent proteins, resulting in increased tissue clearing and decreased tissue autofluorescence. Tissues were rehydrated in 1× phosphate-buffered saline (PBS) and then washed twice for an hour each in PBS/0.2% Triton X-100 (Millipore Sigma, St. Louis, MO). Next, the tissues were incubated for 4 days in a permeabilization solution of PBS/20% DMSO/0.2% Triton X-100/0.3 mol/L glycine at 37°C. Glycine was added to prevent background labeling.

Formalin-fixed, paraffin-embedded samples

After harvesting, four of the tissues were formalin-fixed and paraffin-embedded. The tissues were released from the block by dissolving the paraffin in xylene at 37°C. The tissues then were washed 3 times in 100% methanol and chilled for an hour at 4°C, followed by incubation overnight in 66% dichloromethane/33% methanol at room temperature. Samples were washed twice in 100% methanol. Five percent hydrogen peroxide was then added to the 100% methanol for overnight incubation. Tissues were rehydrated in PBS and washed twice for an hour each in PBS/0.2% Triton X-100, and then incubated for 2 days in PBS/20% DMSO/0.2% Triton X-100/0.3 mol/L glycine at 37°C. Glycine was added to prevent background labeling.[9]

Immunolabeling

Antigen blocking was performed by incubating the tissues in PBS/0.2% Triton X-100/10% DMSO/6% donkey serum for 2 days at 37°C. Samples then were washed twice in PBS/0.2% Tween-20 with 10 µg/mL heparin for 1 hour each at 37°C. Heparin was added to prevent background labeling.9 The extracellular matrix is a significant physical barrier for the penetration of antibodies.[12–14] Two approaches were used to increase the penetration of the primary antibody, rabbit anti-human CK19. First, the antibody concentration was increased gradually over 4 days from a starting dilution of 1/800 to a final dilution of 1/200. Specifically, primary antibody (rabbit anti-human CK19; Abcam, Cambridge, UK) incubation was performed in PBS/5% DMSO/3% donkey serum/0.2% Tween-20 with 10 µg/mL heparin at a dilution of 1/800 on the first day. For the next 3 days, the antibody concentration was increased every day by 1/800 (1/800, 2/800, 3/800, and so forth) until a final dilution of 1/200. As a second approach, centrifugal flow (600 × g) was also used to promote antibody penetration.[14] During these 4 days of antibody incubation, the tissues were centrifuged consecutively for 12 hours at 600 × g and shaken for 12 hours at 37°C. After the primary antibody was applied to the tissues, they were washed 5 times with PBS/0.2% Tween-20 with 10 µg/mL heparin for 1 hour each at room temperature. A pepsin-digested secondary antibody fragment with a smaller molecular weight than an intact IgG antibody was used

to increase tissue penetration of the secondary antibody. The secondary antibody fragment (Alexa Fluor 488 AffiniPure F(ab')2 fragment, donkey anti-rabbit IgG; Jackson ImmunoResearch, West Grove, PA) was incubated for 4 days and protected from light. During this time, the tissues were alternatively centrifuged for 12 hours at 600 × g and shaken for 12 hours at 37°C. The tissues were then washed 5 times with PBS/0.2% Tween-20 with 10 µg/mL heparin for 1 hour each at room temperature and protected from light.

Tissue Clearing

The tissues were dehydrated with 70% methanol, 95% methanol, and 3 × 100% methanol, followed by a 3-hour incubation in 66% dichloromethane/33% methanol at room temperature while shaking. Right before clearing in dibenzyl ether (DBE) for at least 48 hours, the tissues were incubated in 100% dichloromethane for 15 minutes.

Imaging

Immunolabeled tissues were visualized in three dimensions using either the Ultramicroscope II (Light Sheet Microscope; LaVision BioTec, Bielefeld, Germany) or the LSM800 (confocal laser scanning microscope; Carl Zeiss, Jena, Germany). The Ultramicroscope II is equipped with a Neo sCMOS camera (Andor Technology, Belfast, UK) and a 4× objective lens that was immersed in DBE in the imaging chamber. Alexa 488 signals of ductal cells were visualized with a bandpass filter set with an excitation range of 480/40 nm and an emission range of 525/50 nm. Although autofluorescence of the tissues was reduced as described in Fresh Samples and Formalin-Fixed, Paraffin-Embedded Samples, the elastic lamina and collagen of blood vessels still had detectable autofluorescence. This autofluorescence, combined with the unique morphology of elastic lamina, was used to identify vessels without the use of additional labeling. Autofluorescence was observed in an additional filter set of the LaVision Ultramicroscope II (excitation, 405/40 nm; emission, 460/50 nm). For the LSM800 microscope, the tissue was submerged in DBE in a petri dish to match the refractive index and to obtain a flat surface at the interface between materials of different refractive indices. We used both the 5× and 10× objectives. The 488-nm argon laser was used to excite the Alexa 488 fluorochrome, and the range of visualized emitted light was set at 510 to 615 nm. Autofluorescence was observed best in the LSM800 microscope when the 405-nm laser was used and the range of visualized emitted light was set between 410 and 470 nm. However, the autofluorescence signal also was observed while visualizing the Alexa 488 fluorochrome with both the Ultramicroscope II and the LSM800. 3D reconstructions were made with Imaris Software version 8.4 (Bitplane, Zurich, Switzerland).

Validation

Four of the cases were embedded in paraffin after labeling, clearing, and visualization. DBE was removed by washing it away with methanol (5 times for >1 hour), followed by rehydration with PBS. Tissues then were formalin-fixed and paraffin-embedded, and sectioned for routine H&E staining. The pathologies observed in the cleared tissues were compared with those in the H&E-stained slides.

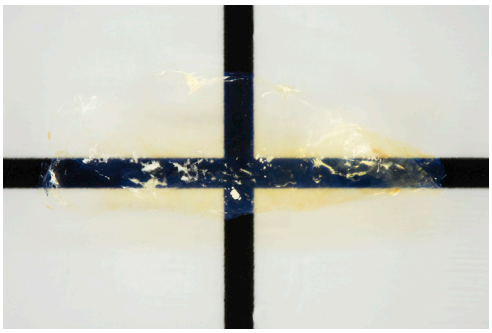

Figure 1. Gross image of cleared human pancreatic parenchyma. In this 5-mm–thick cleared section of pancreatic tissue, the refractive index matching reduces light scattering and produces cleared tissue that enables fluorescent microscopy of deeper structures. Original magnification, ×2.5.

All 26 thick sections of human pancreatic parenchyma were cleared successfully (Figure 1). Normal parenchyma, fatty parenchyma, and even densely fibrotic parenchyma were cleared. All sections were labeled with an antibody targeting CK19. CK19 was selected as the first marker to examine in three dimensions because it allows visualization of the normal epithelial components of the pancreas, pancreatic cancer precursor lesions, and invasive pancreatic cancer, providing broad insights into normal and neoplastic processes in the human pancreas. Although the penetration of antibody into the dense fibrotic tissue of human pancreatic cancer was increased by applying centrifugal flow, the penetration obtained with fibrotic cancerous tissues was not as great as that observed with normal pancreatic parenchyma. CK19 labeling could be visualized from 0.7 to 1.5 mm into the normal tissue sections and 0.3 to 0.6 mm into the pancreatic ductal adenocarcinoma sections. Because depth-based limitations were not encountered when visualizing autofluorescent signals in the tissue, it can be concluded that the depth of visualization was limited by antibody penetration, not by efficacy of clearing or visualization capabilities of the light sheet microscope.

Normal Parenchyma

The 3D branching of ducts was visualized easily, and small periductal glands extending off of larger ducts into the stroma could be appreciated (Figure 2A and Supplemental Videos S1, S2, and S3). As has been described in rat pancreatic parenchyma, some of the ductules in the normal pancreas formed loops instead of linear branches (Figure 2A and Supplemental Video S2). Localized dilation of the ductules in a lobule was seen in one case, probably secondary to downstream obstruction (Supplemental Video S3).

Precursor Lesions

Immunolabeling highlighted microscopic PanIN and intraductal papillary mucinous neoplasm lesions. The neoplastic papillary projections of the PanIN and intraductal papillary mucinous neoplasm lesions into the lumina of ducts was readily appreciated (Figure 2B and Supplemental Video S4). A PanIN in one case measured 2.8 mm × 0.5 mm × 0.5 mm.

Invasive Carcinoma

Invasive ductal adenocarcinomas were also well visualized (Figure 2C). The appearance of the neoplastic cells varied greatly, from sheets of individual cells embedded in the stroma (Supplemental Video S5), to large hollow globular clusters of cells with numerous blunt projections, to haphazardly

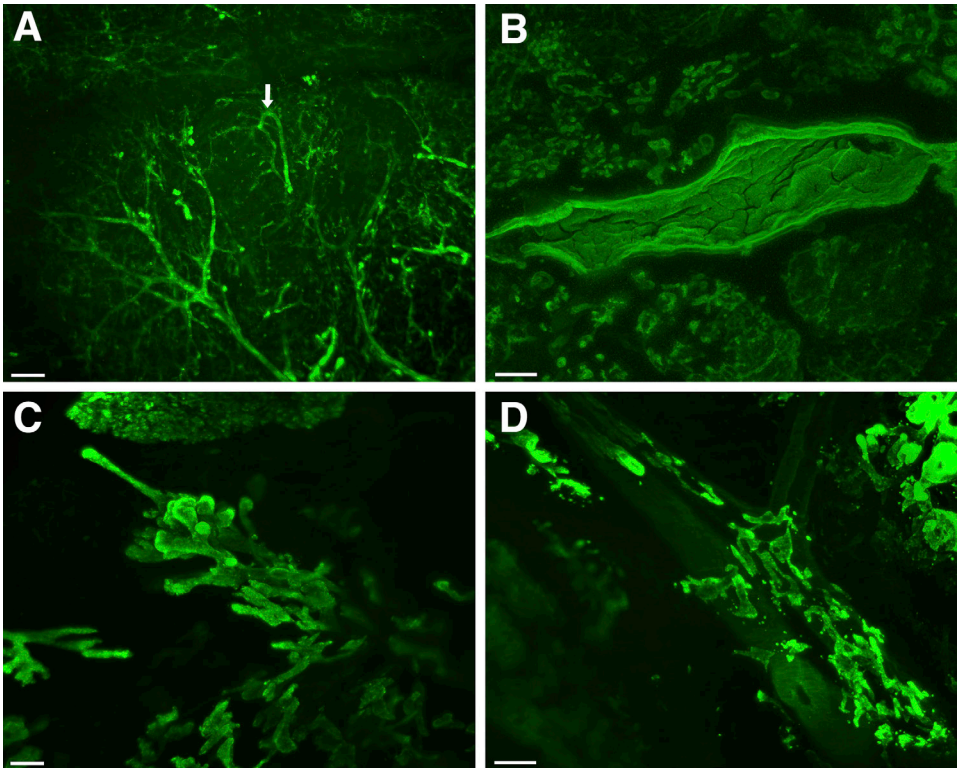

Figure 2. Three-dimensional imaging of normal and neoplastic human pancreatic parenchyma. Sections of grossly normal and neoplastic human pancreas were immunolabeled with antibodies for cytokeratin 19 and then cleared. **a** In the normal pancreas, the branching morphology at the edge of a lobule can be seen, including one of the ducts with looping (arrow). **b** PanIN precursor lesions are identified in sections of grossly normal human pancreas—these lesions have intraluminal papillary projections of columnar epithelial cells. **c** Imaging of grossly identified pancreatic ductal adenocarcinoma shows multiple patterns of invasion, including growth as invasive long and thin ductal structures. **d** Analysis of pancreatic ductal adenocarcinoma shows a unique pattern of perivascular spread of malignant cells. The blood vessel passing from the upper left to the lower right is identifiable by its autofluorescence. In this tumor, invasive carcinoma grows in the perivascular space, parallel to the vessel. Scale bars: 200 μm (a, c, and d); 150 μm (b).

arranged discrete long thin tubes (Figure 2C and Supplemental Video S6). Visualization in 3D allowed for the identification of cancerization of a duct (Supplemental Video S7), with bridging of neoplastic cells across the duct lumen. A remarkable finding was of invasive carcinoma growing in the connective tissue parallel to blood vessels (Figure 2D and Supplemental Video S8), as well as invasive carcinoma growing within blood vessels (Supplemental Videos S9 and S10). The blood vessels could be identified based on the autofluorescence and distinct morphology of the arterial elastic lamina. Specific CK19 labeling and nonspecific autofluorescence of the arterial elastic lamina could be distinguished reliably by careful visualization of the tissue and use of different excitation wavelengths and filters. The arterial elastic lamina produced a distinct narrow bright wavy line that was unique in fluorescent intensity, pattern, and thickness, distinguishing it from specific CK19 labeling of neoplastic epithelial cells. Moreover, the autofluorescence of the arterial elastic lamina remained in wavelengths and filters outside of the 488-nm Alexa Fluor filter that highlighted specific CK19 labeling.

Validation

With the exception of slight retraction of some epithelial cells into the lumina of ducts, tissue morphology was remarkably well preserved in the H&E sections taken after the tissue clearing. These H&E sections validated the interpretation of the 3D findings in all four cases (Supplemental Figure S1).

DISCUSSION

The 3D visualization of cleared human solid organs provides an extraordinary opportunity to understand the true complexity of human diseases.[2,4–7] The application of labeling and clearing to human pancreatic parenchyma provides detailed visualization of normal pancreatic anatomy, and can be used to characterize the 3D architecture of disease processes ranging from PanIN to invasive carcinoma. Importantly, with the addition of multicolor immunolabeling, the 3D relationships of normal ducts, precursor lesions, invasive carcinoma, immune cells, islets of Langerhans, vessels, and nerves should be visualizable.[10,15]

Clearing methodologies have been described for 100 years.[7] The more recent addition of immunolabeling using fluorescent antibodies has opened the door to 3D microscopy. These techniques were first applied to small pieces of tissue from experimental models, but technological improvements in large-scale microscopy have opened up this technology to the study of a broad array of human diseases.[4] The basic principle underlying clearing is that light scattering, which occurs when photons transition through tissues with different refractive indices, can be reduced by matching refractive indices within tissue.[8,16] Lipid-containing membranes have a high refractive index, whereas water-based cytosol and interstitial fluid have a low refractive index. Dehydration and replacement of the cytosol and the interstitial fluid with a material with a high refractive index (such as DBE), followed by submersion of tissue in DBE during imaging, reduces light scattering, the main cause of tissue opaqueness. In contrast, other clearing techniques [eg, Clear Lipid-exchanged Acrylamide-hybridized Rigid Imaging/Immunostaining/in situ-hybridization-compatible Tissue hYdrogel (CLARITY)] exploit the removal of membranes to match the refractive indices.[11] Unlike 3D reconstruction of histology from serially sectioned tissues, clearing avoids artifacts introduced when tissue is physically sectioned.

Poor antibody penetration can limit the application of clearing to dense tissues.[14] This problem was addressed by gradually increasing the concentration of antibody and with centrifugal flow.[14] A novel feature of our protocol is the combination of these strategies to increase antibody penetration with DBE-based tissue clearing to effectively visualize fibrotic human pancreatic tissue in three dimensions. In so doing, we were able to visualize processes such as cancerization of the ducts and cancer growing within a long segment of a vein. In addition, although it is known that the two-dimensional histologic finding of a gland next to a muscular vessel is suggestive of invasive cancer, here we show using 3D visualization that such proximity is not a random event.[17,18] Cords of neoplastic cells often run parallel to muscular blood vessels. Thus, this novel finding, observed in three dimensions, explains a long-known diagnostic aid in surgical pathology. For years, the presence of a gland next to a muscularized blood

vessel in the pancreas has been recognized as a two-dimensional histologic feature of malignancy in the pancreas.[18] Until our study, it was not clear whether this co-localization was simply owing to the haphazard growth of the neoplastic glands of pancreatic cancer or a more directed process. Our results show preferential invasion of malignant glands in the interstitium parallel to blood vessels. The mechanism for this preferential invasion remains to be elucidated—possibilities range from cancer growing within longitudinal perivascular interstitial tracks as well as chemical attractants.[19,20]

We anticipate that this approach will provide new understandings of a wide range of processes, from the 3D anatomy of immune responses to neoplastic cells, to the events that take place at the leading edges of cancers as the neoplastic cells interact with normal parenchyma. In addition, this technique can also be applied to animal models of human disease (such as genetically engineered mouse models or xenograft models) to interrogate 3D anatomy at specific time points in disease progression.[21–23] Importantly, just as the two-dimensional microscopic visualization of human diseases helped generate new hypotheses hundreds of years ago, so too is our hope that the 3D visualization of diseases of the pancreas will generate new hypotheses and new biological insights.

REFERENCES

1. Weller, C. V. Rudolf Virchow--Pathologist. Sci. Mon. 13, 33–39 (1921).
2. Qiu, H. et al. Comparison of conventional and 3-dimensional computed tomography against histopathologic examination in determining pancreatic adenocarcinoma tumor size: implications for radiation therapy planning. Radiother. Oncol. 104, 167–172 (2012).
3. Boj, S. F. et al. Model organoids provide new research opportunities for ductal pancreatic cancer. Mol Cell Oncol 3, e1014757 (2016).
4. Tanaka, N. et al. Whole-tissue biopsy phenotyping of three-dimensional tumours reveals patterns of cancer heterogeneity. Nature Biomedical Engineering 1 (2017).
5. Richardson, D. S. & Lichtman, J. W. Clarifying Tissue Clearing. Cell 162, 246–257 (2015).
6. Richardson, D. S. & Lichtman, J. W. SnapShot: Tissue Clearing. Cell 171, 496–496.e1 (2017).
7. Seo, J., Choe, M. & Kim, S.-Y. Clearing and Labeling Techniques for Large-Scale Biological Tissues. Mol. Cells 39, 439–446 (2016).
8. Azaripour, A. et al. A survey of clearing techniques for 3D imaging of tissues with special reference to connective tissue. Prog. Histochem. Cytochem. 51, 9–23 (2016).
9. Renier, N. et al. iDISCO: a simple, rapid method to immunolabel large tissue samples for volume imaging. Cell 159, 896–910 (2014).
10. Lin, P.-Y., Peng, S.-J., Shen, C.-N., Pasricha, P. J. & Tang, S.-C. PanIN-associated pericyte, glial, and islet remodeling in mice revealed by 3D pancreatic duct lesion histology. Am. J. Physiol. Gastrointest. Liver Physiol. 311, G412–22 (2016).
11. Lee, H., Park, J.-H., Seo, I., Park, S.-H. & Kim, S. Improved application of the electrophoretic tissue clearing technology, CLARITY, to intact solid organs including brain, pancreas, liver, kidney, lung, and intestine. BMC Dev. Biol. 14, 48 (2014).
12. Flessner, M. F., Choi, J., Credit, K., Deverkadra, R. & Henderson, K. Resistance of tumor interstitial pressure to the penetration of intraperitoneally delivered antibodies into metastatic ovarian tumors. Clin. Cancer Res. 11, 3117–3125 (2005).
13. Calve, S., Ready, A., Huppenbauer, C., Main, R. & Neu, C. P. Optical clearing in dense connective tissues to visualize cellular connectivity in situ. PLoS One 10, e0116662 (2015).
14. Lee, E. et al. ACT-PRESTO: Rapid and consistent tissue clearing and labeling method for 3-dimensional (3D) imaging. Sci. Rep. 6, 18631 (2016).
15. Tang, S.-C. et al. Pancreatic neuro-insular network in young mice revealed by 3D panoramic histology. Diabetologia 61, 158–167 (2018).
16. Becker, K., Jährling, N., Kramer, E. R., Schnorrer, F. & Dodt, H.-U. Ultramicroscopy: 3D reconstruction of large microscopical specimens. J. Biophotonics 1, 36–42 (2008).
17. Hruban, R. H. & Klimstra, D. S. Adenocarcinoma of the pancreas. Semin. Diagn. Pathol. 31, 443–451 (2014).
18. Sharma, S. & Green, K. B. The pancreatic duct and its arteriovenous relationship: an underutilized aid in the diagnosis and distinction of pancreatic adenocarcinoma from pancreatic intraepithelial neoplasia. A study of 126 pancreatectomy specimens. Am. J. Surg. Pathol. 28, 613–620 (2004).
19. Friedl, P. & Alexander, S. Cancer invasion and the microenvironment: plasticity and reciprocity. Cell 147, 992–1009 (2011).
20. Benias, P. C. et al. Structure and Distribution of an Unrecognized Interstitium in Human Tissues. Sci. Rep. 8, 4947 (2018).
21. Fu, X., Guadagni, F. & Hoffman, R. M. A metastatic nude-mouse model of human pancreatic cancer constructed orthotopically with histologically intact patient specimens. Proc. Natl. Acad. Sci. U. S. A. 89, 5645–5649 (1992).
22. Hingorani, S. R. et al. Trp53R172H and KrasG12D cooperate to promote chromosomal instability and widely metastatic pancreatic ductal adenocarcinoma in mice. Cancer Cell 7, 469–483 (2005).
23. Hiroshima, Y. et al. Selective efficacy of zoledronic acid on metastasis in a patient-derived orthotopic xenograph (PDOX) nude-mouse model of human pancreatic cancer. J. Surg. Oncol. 111, 311–315 (2015).

8

Chapter 9

Three-dimensional visualization of cleared human pancreas cancer reveals that sustained epithelial-to-mesenchymal transition is not required for venous invasion

Seung-Mo Hong, DongJun Jung, Ashley Kiemen, Matthias M. Gaida, Tadashi Yoshizawa, Alicia M. Braxton, Michaël Noë, Gemma Lionheart, Kiyoko Oshima, Elizabeth D. Thompson, Richard Burkhart, Pei-Hsun Wu, Denis Wirtz, Ralph H. Hruban, Laura D. Wood

Modern Pathology, November 2019

ABSTRACT

Venous invasion is three times more common in pancreatic cancer than it is in other major cancers of the gastrointestinal tract, and venous invasion may explain why pancreatic cancer is so deadly. To characterize the patterns of venous invasion in pancreatic cancer, 52 thick slabs (up to 5 mm) of tissue were harvested from 52 surgically resected human ductal adenocarcinomas, cleared with a modified iDISCO method, and labeled with fluorescent-conjugated antibodies to cytokeratin 19, desmin, CD31, p53 and/or e-cadherin. Labeled three-dimensional (3D) pancreas cancer tissues were visualized with confocal laser scanning or light sheet microscopy. Multiple foci of venous and even arterial invasion were visualized. Venous invasion was detected more often in 3D (88%, 30/34 cases) than in conventional 2D slide evaluation (75%, 25/34 cases, $P < 0.001$). 3D visualization revealed pancreatic cancer cells crossing the walls of veins at multiple points, often at points where preexisting capillary structures bridge the blood vessels. The neoplastic cells often retained a ductal morphology (cohesive cells forming tubes) as they progressed from a stromal to intravenous location. Although immunolabeling with antibodies to e-cadherin revealed focal loss of expression at the leading edges of the cancers, the neoplastic cells within veins expressed e-cadherin and formed well-oriented glands. We conclude that venous invasion is almost universal in pancreatic cancer, suggesting that even surgically resectable PDAC has access to the venous spaces and thus the ability to disseminate widely. Furthermore, we observe that sustained epithelial mesenchymal transition is not required for venous invasion in pancreatic cancer.

INTRODUCTION

Pancreatic ductal adenocarcinoma (PDAC) is one of the leading causes of cancer death in the United States. It is estimated that about 56,770 Americans will be diagnosed and 45,750 patients will die of PDAC in 2019.[1] Most patients with pancreatic cancer are diagnosed with advanced disease, usually liver metastases, and only 10% of patients have localized disease.[1] Even patients with low-stage disease who undergo surgery only have a 34% 5 year-survival rate.[1] Although the aggressiveness of PDAC is clearly due to several factors, it has been hypothesized that the high prevalence venous invasion in PDAC explains the rapid development of liver metastases and therefore the aggressiveness of disease in most patients with PDAC.[2]

The reported prevalence (65%) of venous invasion is higher in PDAC than in cancers of other abdominal organs.[3,4] Because veins in the pancreas drain directly into the liver, venous invasion in PDAC may explain the almost universal development of liver metastases in patients with this disease.[2–6] Venous invasion in PDACs is not only very common, but it also has a distinctive morphology. The neoplastic cells within the veins replace the endothelial cells and grow as well-oriented lumen-forming cells along the inner wall of the vessels, creating a unique pancreatic intraepithelial neoplasia-like histology.[3] Our understanding of the process of venous invasion of PDAC beyond this is limited in part due to emphasis on thin two-dimensional (2D) hematoxylin and eosin (H&E) tissue sections.[7] Therefore, the goal of the present study is to characterize venous invasion in human PDAC in 3D.

Technical advances in tissue clearing, antibody penetration, and advanced microscopes now enable the 3D visualization of dense fibrotic tissues, including human PDACs.[7,8] We previously reported the 3D analysis of human PDAC using clearing and a single marker (cytokeratin 19).[8] We reported that infiltrating cancer cells preferentially grow in the connective tissue parallel to blood vessels, and we also observed neoplastic cells growing within blood vessels.[8] In order to more precisely define the process of venous invasion in PDAC, we now apply multiple markers (antibodies to cytokeratin 19, desmin, p53, CD31, and e-cadherin) to a larger well-characterized series of cleared surgically resected PDACs. We confirm that venous invasion occurs in the vast majority of PDACs and observe that sustained epithelial–mesenchymal transition (EMT) is not required for venous invasion.

MATERIALS AND METHODS

Patients and tissue preparation

After approval from the institutional review boards, a total of 52 pancreas tissue slabs (up to $20 \times 10 \times 5\,mm^3$) were examined. These included 34 fresh cancer tissues harvested from 34 patients who underwent pancreatic resection at the Johns Hopkins Medical Institutions for PDAC, and 18 pancreas tissue slabs from formalin-fixed paraffin embedded (FFPE) PDAC samples from 18 patients who underwent surgical resection at the University Hospital Heidelberg, Heidelberg, Germany. These latter cancers were selected because they were known to have venous invasion by 2D H&E microscopy.

Fresh samples

All fresh pancreatic tissues were processed as previously described.[8] In brief, tissues were fixed overnight at room temperature in 80% methanol/20% dimethyl sulfoxide (DMSO) to dehydrate the tissues and precipitate proteins to prevent autolysis by pancreatic enzymes, and then the tissues were rehydrated and fixed in 4% paraformaldehyde at room temperature for 1 day. They were then dehydrated with serially concentrated methanol (1×50% methanol, 1×80% methanol, 1×90% methanol, and 3×100% methanol), chilled at 4 °C for 1 h in 100% methanol, and incubated overnight in 66% dichloromethane/33% methanol at room temperature. To oxidize endogenous pigments and autofluorescent proteins, tissues were washed twice in 100% methanol and then 5% H2O2 was added for overnight incubation. Tissues were rehydrated in 1x phosphate-buffered saline (PBS) and then washed twice for 1 h each in PBS/0.2%Triton X-100 (Millipore Sigma, St. Louis, MO). Next, the tissues were incubated for 2 days in a permeabilization solution of PBS/20% DMSO/0.2% Triton X-100/0.3 mol/L glycine at 37 °C. Blocking reagent of 6% donkey serum, 10% DMSO in PTx.2 was incubated for 2 days.

Formalin-fixed, paraffin-embedded samples

Eighteen FFPE tissues were released from the paraffin block by dissolving the paraffin in xylene at 37 °C. The tissues then were washed three times in 100% methanol and chilled at 4 °C for 1 h, followed by overnight incubation in 66% dichloromethane/33% methanol at room temperature. The tissues were then washed twice in 100% methanol, and 5% H2O2 was added to the 100% methanol for overnight incubation. Tissues were rehydrated in PBS and washed twice for an hour each in PBS/0.2% Triton X-100, and then incubated in PBS/20% DMSO/0.2% Triton X-100/0.3 mol/L glycine at 37 °C for 2 days. Glycine was added to prevent background labeling.

Multiplex immunolabeling

Nonspecific antigens were blocked by incubating the tissues in PBS/0.2% Triton X-100/10% DMSO/6% donkey serum at 37 °C for 2 days. Samples then were washed twice in PBS/0.2% Tween-20 with 10 mg/mL heparin each at 37 °C for 1 h. Heparin was added to prevent background immunolabeling. Multiple primary antibodies, including cytokeratin 19 (EP1580Y, rabbit monoclonal; final dilution, 1:200; Abcam, Cambridge, UK), desmin (goat polyclonal; final concentration, 1:100, LifeSpan Biosciences, Seattle WA), CD31 (JC/70A, mouse monoclonal; final concentration, 1:100, Thermo Fisher Scientific, Waltham, MA), p53 (DO-7, mouse monoclonal; final concentration, 1:100, Thermo Fisher Scientific), and e-cadherin (M168, mouse monoclonal; final concentration, 1:150; Abcam) were used. These antibodies were applied in varying combinations, with a maximum of four antibodies used on any one tissue. Tissue from all 34 freshly harvested PDAC cases were labeled with at least both cytokeratin 19 and desmin. In addition, 24 of the 34 freshly harvested PDAC cases were also labeled with antibodies to p53, 24 PDAC cases with antibodies to CD31 and 8 with antibodies to e-cadherin. Diffuse nuclear p53 labeling was noted in 14 of the 24 cases (58%), which aided in the identification of invasive carcinoma. Similarly, all 18 FFPE PDAC cases were labeled with at least both cytokeratin 19 and desmin. In addition, 7 of these 18 PDACs were also labeled with antibodies to CD31 and 8 with antibodies to e-cadherin.

Because dense desmoplastic stroma in PDACs is a significant physical barrier for the penetration of antibodies, four approaches were used to increase antibody penetration: First, the antibody concentration was gradually increased for 4 consecutive days. Second, during these 4 days of antibody incubation, the tissues were centrifuged consecutively for 12 h at 600 × g and shaken at 37 °C for 12 h. After the primary antibody was applied to the tissues, they were washed five times with PBS/0.2% Tween-20 with 10 mg/mL heparin for 1 h each at room temperature. Third, pepsin-digested secondary antibody fragments with smaller molecular weights than intact IgG antibodies were used to increase tissue penetration of the secondary antibodies. The fragmented secondary antibodies, including Alexa Fluor 488-conjugated AffiniPure F(ab')2 fragment donkey anti-rabbit IgG (Jackson ImmunoResearch,West Grove, PA), DyLight 405-conjugated AffiniPure F(ab')2 fragment donkey anti-goat IgG (Jackson ImmunoResearch), and Cyanine 3-conjugated AffiniPure F(ab')2 fragment, donkey anti-mouse IgG (Jackson ImmunoResearch), were incubated for 4 days and protected from light. During this time, the tissues were alternatively centrifuged for 12 h at 600 × g and shaken for 12 h both at 37 °C. Fourth, after centrifugation and shaking, the tissues were sonicated for 1 h at 37 °C. The tissues were then washed five times with PBS/0.2% Tween-20 with 10 mg/mL heparin for 1 h each at room temperature and protected from light exposure.

Tissue clearing

After the immunolabeling, the tissues were dehydrated with serially concentrated methanol (70% methanol, 95% methanol, and 3 × 100% methanol), incubated with 66% dichloromethane/33% methanol for 3 h, and 100% dichloromethane for 15 min twice, and were finally transferred to dibenzyl ether (DBE) overnight.

Tissue imaging

Immunolabeled tissues were visualized in 3D primarily with a confocal laser scanning microscope (LSM800; Carl Zeiss, Jena, Germany) and when lower power views were needed with a Light Sheet Microscope (Ultramicroscope II; LaVision BioTec, Bielefeld, Germany). The Ultramicroscope II is equipped with a Neo sCMOS camera (Andor Technology, Belfast, UK) and a 4× objective lens that was immersed in DBE in the imaging chamber.

Alexa 488 signals of CK19 expressing epithelial cells (normal ductal and cancer cells) were visualized with a bandpass filter set with an excitation range of 480/40 nm and an emission range of 525/50 nm. DyLight 405 signals of desmin-expressing cells (smooth muscle cells) were visualized with a filter set with an excitation range of 400/40 nm and an emission range of 421/50 nm. Cyanine 3 signals of CD31expressing endothelial cells, of e-cadherin labeled cells, or p53 labeled cancer cells were visualized using a filter set with an excitation range of 550/40 nm and an emission range of 570/50 nm. Although autofluorescence of the tissues was reduced as described in the "Methods" section, the elastic lamina and collagen of blood vessels still had detectable autofluorescence. This autofluorescence, combined with the unique morphology of elastic lamina, was used to identify vessels in addition to desmin labeling. Autofluorescence was observed in an additional filter set of the LaVision Ultramicroscope II (excitation, 405/40 nm; emission, 460/50 nm).

For the LSM800 microscope, the tissue was submerged in DBE in a glass bottom cell culture dish to match the refractive index and to obtain a flat surface at the interface between materials of different refractive indices. We used the 5×, 10×, and 20× objectives. Consecutive 2D images with Z stacks were visualized with Zen (Ver. 2.3, Zeiss) and 3D images were reconstructed with IMARIS software (Ver. 9.4, Bitplane, Zurich Switzerland).

Validation

Seven cases were embedded in paraffin after the tissues had been cleared and visualized. These seven cases were then sectioned, stained with H&E, and the findings in the cleared tissues were compared to the H&E findings.

Briefly, DBE was removed by washing with serially diluted methanol, and the tissues were rehydrated with PBS. Tissues then were FFPE, and sectioned for routine H&E staining. The pathologies observed in the cleared tissues were then compared with those features in the H&E stained slides. In five of the seven cases, the entire tissue block was serially sectioned and one slide taken every 13 µm. These serial slides were stained with H&E and then digitized (NanoZoomer-XR, Hamamatsu, Hamamatsu City, Japan). The scanned slides were then registered in 3D and areas with venous invasion were reconstructed. Serial H&E sections were aligned to each other with rigid image registration using MATLAB 2019a. Registration between adjacent images was achieved by finding the rotational angle and translation which maximized cross correlation between images. This resulted in a continuous digital volume of H&E sections. By manually annotating foci of venous invasion on these serial sections, 3D reconstructions of venous invasion were created and allowed 3D H&E validation of the observations made in the cleared tissues.

RESULTS

Patient and tumor characteristics

Clinicopathologic characteristics of the 34 fresh PDAC cases included in this study are summarized in Supplementary Table 1. Briefly, the mean age (± standard deviation) of the patients was 69.7 ± 11.2 years. Male to female ratio was 1:1. The mean tumor size was 3.3 ± 0.9 cm (range, 1.8–5.7 cm). Twenty-three cases (68%) were located in the pancreatic head, 18 (53%) were moderately differentiated, and 25 (74%) had vascular invasion of any type (lymphatic and or venous) present in the original 2D H&E sections utilized for clinical diagnosis. Seven patients had received neoadjuvant therapy before resection.

Of the 18 FFPE PDACs, the mean age (± standard deviation) of the patients was 58.1 ± 10.9 years. Male to female ratio was 2:1. The mean tumor size was 3.8 ± 0.7 cm (range, 2.5–5.5 cm). Fourteen cases (78%) were located in the pancreatic head. All 18 FFPE cases were selected based on the presence of vascular invasion on the original diagnostic H&E slides and so they were not considered in analyses of the prevalence of venous invasion. None of these 18 had received preoperative neoadjuvant therapy.

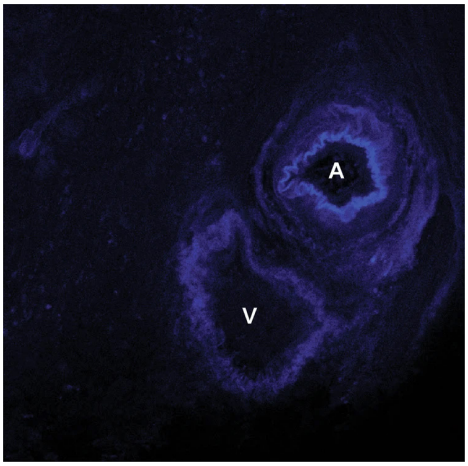

Figure 1. The combination of morphology and patterns of immunolabeling can be used to define key structures in cleared tissues. Desmin immunolabeling of arterial walls (A) is more intense and the media of arteries is thicker than those of muscular veins (V). The concentric wavy autofluorescent lines of the elastic lamina also highlights arterial walls. Blue labeling for desmin highlights the muscular layer in blood vessels

Identifying muscular vessels in cleared tissues

Blood vessels and ducts were identified based on desmin labeling and the distinct morphology of the ducts and of the arterial elastic lamina. Ducts were easily distinguished from vessels. Ducts are in the center of lobular units, while vessels are at the periphery.[9] As a result, normal interlobular ducts are surrounded by acinar cells. In contrast, vessels, because they are in the stroma at the periphery of lobules in the pancreas, are not surrounded by acinar cells.[9] In addition, desmin labeling of the media of blood vessels was distinguished from the weaker desmin labeling of the walls of pancreatic ducts. The media of veins is thicker and label more intensely than do the walls of ducts.

Veins and arteries were distinguished using several features. In general, desmin immunolabeling of arterial walls was more intense than the labeling of both ducts and veins, and the media of arteries was thicker than those of muscular veins. In addition, arterial walls contain elastic lamina, which was visualized as auto-fluorescing regularly concentric wavy lines (Figure 1). The autofluorescence of vessels was easily distinguished from other sources of autofluorescence, including fibroblasts and their associated collagen. First, the nonspecific autofluorescence from fibroblasts provided weaker signals on different excitation wavelengths with different LASERs, including 405 and 488 nm. Second, most muscular veins run parallel to an artery in the pancreas.[9]

Cells of invasive carcinoma were easily distinguished from lobular collections of acinar cells. Unlike acinar cells, the cells of invasive carcinoma vary in size and form irregular haphazard 3D clusters or single cells.

Comparison of detection of venous invasion between 2D and 3D analyses

All 2D diagnostic H&E slides were rereviewed from the 34 fresh cases, and the prevalence of venous invasion identified in the fresh cleared tissue was compared with the prevalence of venous invasion in the original 2D diagnostic H&E slides prepared before clearing. Thus, the venous invasion evaluated in the 2D diagnostic H&E slides was from an adjacent but separate block of tumor. Venous invasion was detected more often in 3D (88%, 30/34 cases) than in conventional 2D H&E slide evaluation (74%, 25/34 case; chi-square test, $P < 0.001$). The 18 FFPE cases were not included in these analyses, as they had been selected specifically because venous invasion was identified on diagnostic H&E slides.

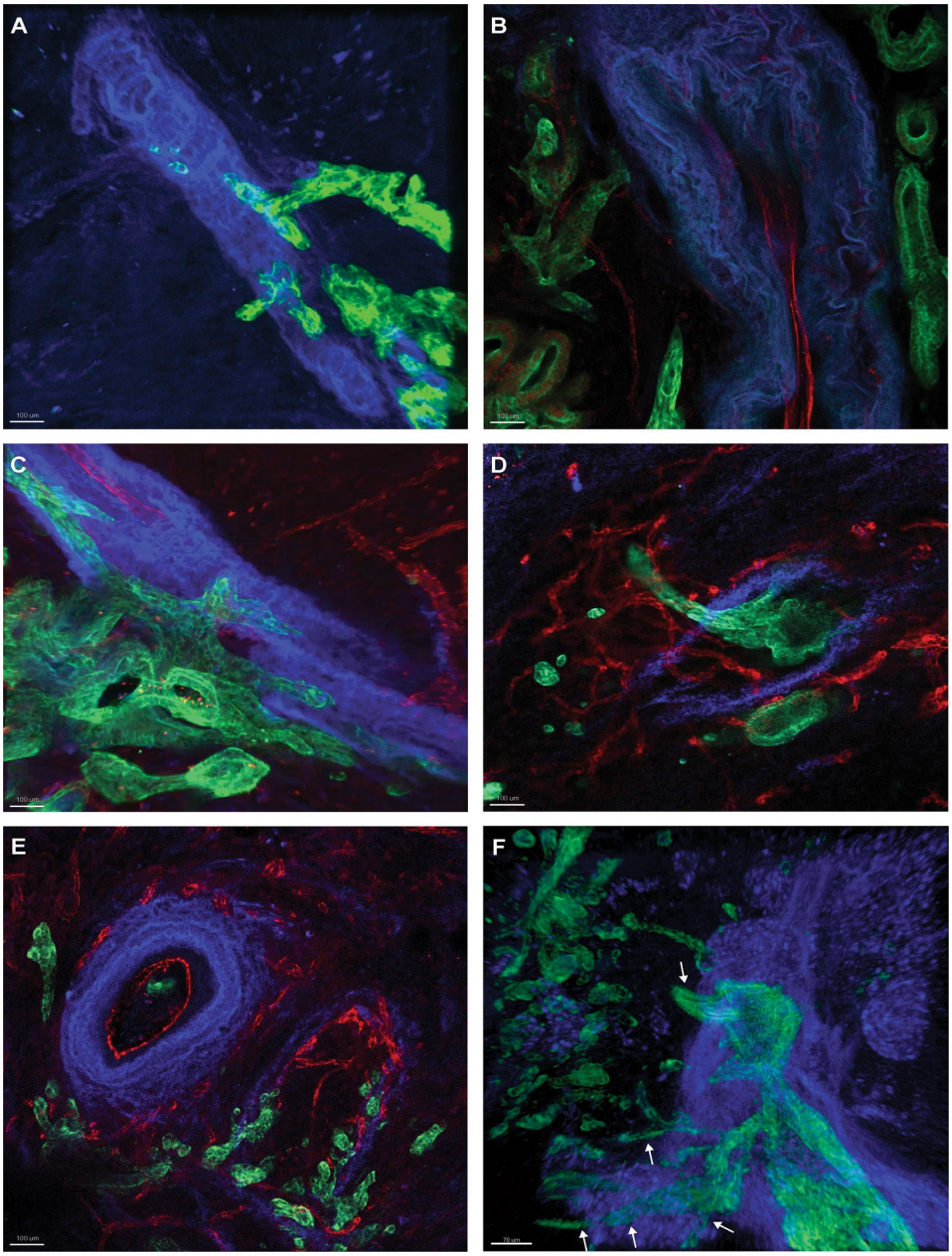

Figure 2. Representative images of multicolor immunofluorescent labeling of pancreatic ductal adenocarcinoma tissues with venous invasion. **a** A cord of cancer cells approaches and then infiltrates a muscular blood vessel. **b** Arterial wall is surrounded by cancer cells. Some cancer cells show nuclear p53 labeling (orange nuclei, lower left). **c** Cohesive cancer cells infiltrate into a muscular vein. **d** Cancer cells from tubular structure inside of a vein and a well-formed tube of neoplastic cells crosses the media of the vein. **e** Small clusters of cancer cells grow into a vein (lower right). Note the adjacent artery (upper left). **f** Cords of cancer cells form well-oriented tube within a vein, and cross the media of the vein at several points (arrows) along the vein. Focal cross reactivity of the antibody to desmin to islets of Langerhans is noted in this case. Green labeling for cytokeratin 19 highlights the neoplastic cells, blue labeling for desmin highlights the muscular layer in blood vessels, red labeling in **b–e** for CD31 marks endothelial cells, and nuclear red labeling for p53 in **b**.

3D pathologic features of PDAC in the stroma adjacent to muscular blood vessels

The neoplastic cells of invasive PDAC typically formed tubes/cords, larger globular masses, or single cells. As previously described using a single antibody, when cords of neoplastic cells approached vessels, they tracked parallel to the vessels (Figure 2a, b, and Supplementary Movies 1 and 2).[8]

3D pathologic features of vascular invasion

Venous invasion was identified in 30 of the 34 fresh cases. In 23 of these 30 cases we observed neoplastic cells crossing the media of the involved veins (Figure 2c–f). Rather than individual cells crossing the media of veins, we most often observed (21 of 23 foci of venous invasion) cords and tube-like growths of cancer cells crossing the media of veins (Figure 2c, d and Supplementary Movies 3 and 4). These cords and tubes often appeared intact, that is the cords were long and relatively uniform without disruption. This pattern was not universal, as in some instances small clusters and individual neoplastic cells were observed spanning the media of veins (Figure 2e). When venous invasion was identified, the neoplastic cells frequently crossed the muscular venous wall at multiple points along the length of the vessel (Figure 2f, Supplementary Movie 5). For example, in Figure 2f and Supplementary Movie 5, at least three separate foci can be identified at which the neoplastic cells cross the media of the involved vessel. Some of the points at which neoplastic cells traversed the media of vessels were associated with the presence of endothelial cells (Figure 2d and Supplementary Movie 4), raising the possibility that the neoplastic cells exploit local weaknesses in the vessel wall created by these preexisting capillary structures. Arterial invasion was much less common (seen in six cases), and when it occurred the pattern was usually that of individual cells or a few clusters of cells within arterial lumina (Figure 2e). We did not observe tumor cells penetrating the media of muscular arteries.

The 3D morphologic features of vascular invasion in the 18 FFPE PDAC cases matched those observed in the 34 fresh PDAC cases.

E-cadherin expression

E-cadherin plays an important role in cell-to-cell adhesion, cell-to-cell recognition, and epithelial polarity, and loss of e-cadherin is considered to be one marker of EMT.[10–14] As expected, e-cadherin labeling was intact in neoplastic cells that formed well-oriented tubes and clusters (Supplementary Figure 2 and Supplementary Movie 8). However, the patterns of e-cadherin expression as neoplastic cells approached, crossed and then populated the intraluminal portions of vessels was unexpected. We observed small tongues of cells projecting out from the leading edges of larger globular masses of neoplastic cells in the stroma (Figure 3a). The neoplastic cells within the globular masses expressed e-cadherin, while these tongues of cells did not label. A similar pattern was observed as the neoplastic cells crossed the media of veins, with intact e-cadherin labeling in the large cohesive cluster of neoplastic cells and loss of e-cadherin only in the tips of small tongues of cells extending out from these clusters (Figure 3b). In contrast, the neoplastic cells entirely within the lumina of veins often had diffuse e-cadherin labeling and formed tubes of well-oriented cells with well-defined lumina (Figure 3c, d, Supplementary Figure 1 and Supplementary Movies 6 and 7).

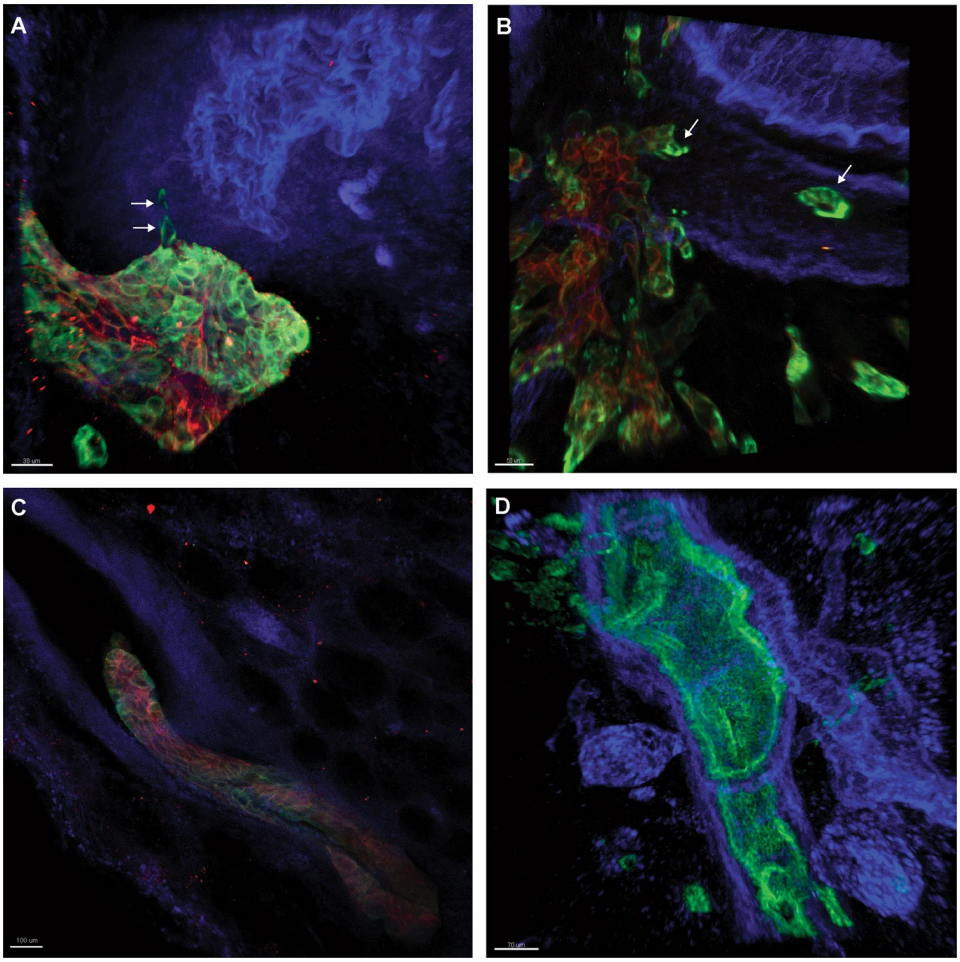

Figure 3. Epithelial-to-mesenchymal transition is not sustained in venous invasion. **a** Loss of e-cadherin expression (arrows) in small tongues of neoplastic cells projecting out from a larger globular mass of neoplastic cells with intact e-cadherin expression. **b** Loss of e-cadherin expression (arrows) in small tongues of neoplastic cells projecting into the lumen of a vein. A detached cluster of neoplastic cells within the vein also show loss of e-cadherin labeling. **c** A well-formed tube of neoplastic cells with intact e-cadherin labeling extending within the lumen of a vein. **d** Well-oriented cancer cells form a long tube growing within a vein. Note the adjacent artery with wavy elastic lamina to the right of the vein. Focal cross reactivity of the antibody to desmin to islets of Langerhans is noted in this case. Green labeling for cytokeratin 19, blue labeling for desmin, and red labeling in **a–c** for e-cadherin.

The combined findings of cell morphology, including cohesive cells forming well-oriented ductal structures, and intact e-cadherin expression suggest that although there may be transient EMT, the neoplastic cells rapidly reexpress markers of epithelial differentiation once inside the veins; thus sustained EMT is not required for venous invasion.

H&E validation

After clearing, seven slabs of tissue with multiple foci of venous invasion in 3D were selected and processed for routine H&E microscopy. These sections revealed definite foci of vascular invasion in

all seven representative cases, and these foci matched the foci of vascular invasion observed in the cleared 3D images. In addition, it was noted that foci of venous invasion were associated with mixed inflammatory cells, intraluminal fibrin thrombi, and disruption of endothelial cells.[15]

Serial 2D H&E slides from these seven cases were digitized and 3D reconstructions of the H&E sections were created. These 3D reconstructions revealed that the neoplastic cells extended within the veins for a distance (Figure 4). The mean length of vascular invasion after reconstruction of 3D H&E images was 565.7 ± 502.3 µm (median, 457.5 µm; range, 65–1800 µm). The neoplastic cells even involved several branches of venous structures as these veins branched (Figure 4). Both of these findings are

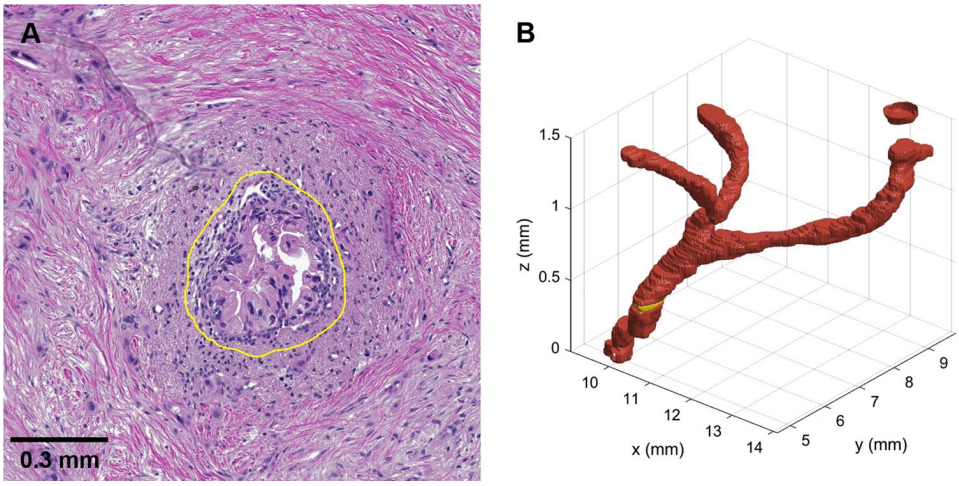

Figure 4. 3D validation of H&E slides reveals branching of vascular invasion over a long distance. **a** Representative 2D H&E slide image of vascular invasion. Cancer cells within the veins replace the endothelial cells and form a well-oriented lumen. Yellow circle indicates outermost contour of cancer cells within vein, **b** 3D reconstruction of venous invasion (red). Yellow color matches location of the representative image shown in **a**.

consistent with observations made in the 3D immunofluorescently labeled cleared tissues.

DISCUSSION

Here we report a detailed 3D study of the patterns of venous invasion in a large series of surgically resected pancreatic cancers using tissue clearing and immunolabeling with multiple antibodies. This 3D analysis revealed that: (1) venous invasion occurs in almost all pancreatic cancers (~90%); (2) pancreatic cancer cells traverse the wall of veins at multiple point; (3) once in veins, the neoplastic cells often form well-oriented cohesive tubes of cells that replace the endothelial cells; (4) the neoplastic cells extend for a distance (at least 1.8 mm) within the veins; (5) sustained EMT is not required during process of vascular invasion.[15]

Venous invasion is more common in PDAC than it is in cancers of other abdominal organs.[2] The previously reported prevalence of venous invasion in PDACs based on the evaluation of conventional H&E slide is 65%[3,4], as compared with ~24% in gastric carcinomas and 21% in colon cancers.[16–19] Here, us-

ing cleared 3D samples we were able to identify venous invasion in close to 90% of pancreatic cancers that were of low enough stage to be surgically resected. This high prevalence in incompletely sampled cancers (a portion of each cancer underwent routine processing for clinical diagnosis) suggests that venous invasion, even in low-stage disease, is an almost universal process in human PDAC. This venous invasion may be one of the reasons for the rapid clinical progression of PDACs from stage I to stage IV disease.[2,20]

One of the advantages of studying tissues in 3D is that one can more accurately calculate the 3D sizes and behavior of lesions. In this study we observed pancreatic cancers growing for a mean of 565.7 µm as they extended intraluminally within veins. This is remarkable as this represents a minimum number, as most of the foci of venous invasion extended to the edges of the tissue blocks. In addition, we observed that as they grew within veins, the neoplastic cells transgressed the walls of the veins at multiple points. Similarly, Nguyen et al., using in vitro models, reported that PDAC cells invade through matrix and into the lumina of vessels, where they ablate the endothelial cells, leaving behind tumor-filled luminal structures.[15] Our observations suggest that intravascular grow may also be responsible for local extension and for intra-pancreatic spreading of cancer cells. We also confirm our previous observation that invasive carcinoma of the pancreas often tracks parallel to veins within the perivascular connective tissue. The presence of a glandular structure next to a muscular blood vessel in the pancreas has been used clinically to aid in the diagnosis of pancreatic cancers in 2D H&E stained slides.[9]

Traditionally, EMT has been believed to play a critical role in dissemination of neoplastic cells from the primary tumor site and intravasation into blood vessels.[21–23] E-cadherin loss has been reported to be a critical part of EMT.[24] For example, Onder et al. observed that loss of e-cadherin induced multiple downstream transcription factors, including Twist, and resulted in metastatic dissemination.[11] We observed intact e-cadherin labeling in cohesive neoplastic cells in the stromal and within the lumina of veins. This finding, coupled with the morphologic findings of cohesive cells forming tubes, indicates that while transient EMT occurs, sustained EMT is not required for venous invasion in human PDAC. Similarly, Brabletz et al. reported heterogeneous EMT at the invasive front of colorectal cancers.[25] They found that mesenchymal genes are expressed at the advancing edges of colorectal cancers, but the central portion of the tumors retain markers of the epithelial phenotype.[25] Our observation of heterogeneous e-cadherin labeling of small clusters of cancer cells at the leading edges of larger groups of cohesive neoplastic cells also parallels observations by Ligorio et al. recently reported in mouse models of pancreatic cancer.[26] They reported heterogeneity of RNA expression at the single cell level within individual cancer glands.[26] This focal loss of e-cadherin protein expression at the projecting ends of cancer cell clusters suggests a transient heterogeneity in the expression of the EMT phenotype which can be quickly reversed once the cells grow within veins.

We should acknowledge some limitations of the present study. For technical reasons, we could apply up to four antibodies at once in our 3D studies. As such, we were limited in the markers we employed to define EMT. While the combination of morphology (loss of cell cohesion and lack of formation of

well-oriented glands) and loss of e-cadherin expression was used to define EMT, the assessment of additional markers of EMT such as TWIST in future studies could help further solidify our conclusions.[11] In addition, assessment of expression of other proteins in 3D may also help elucidate the mechanisms underlying venous invasion in the pancreas. We should also note that we were able to evaluate only the cells that remained in the samples studied. We are not able to comment on the nature of the cells that gained access to the vasculature and then spread beyond the pancreas. Finally, although review by experienced pathologists revealed that neoplastic cells in the stroma, at the point of penetration of muscular veins, and within veins all showed intact e-cadherin labeling, there are currently no approaches to reliably quantify this labeling in cleared 3D pancreatic tissue specimens to make more detailed comparisons. Such comparisons will require development of new approaches for 3D image analysis.

In summary, 3D histopathologic features of venous invasion in human PDACs after tissue clearing demonstrate that venous invasion is present in close to 90% of pancreatic cancers. Pancreatic cancer cells cross the vascular media at multiple points along a single vessel, and sustained EMT is not required during process of vascular invasion. It is our hope that future studies will lead to the identification of novel approaches to block this process and prevent the rapid progression of disease.

REFERENCES

1. Siegel, R. L., Miller, K. D. & Jemal, A. Cancer statistics, 2019. CA Cancer J. Clin. 69, 7–34 (2019).
2. Hruban, R. H. et al. Why is pancreatic cancer so deadly? The pathologist's view. J. Pathol. (2019) doi:10.1002/path.5260.
3. Hong, S.-M. et al. Vascular invasion in infiltrating ductal adenocarcinoma of the pancreas can mimic pancreatic intraepithelial neoplasia: a histopathologic study of 209 cases. Am. J. Surg. Pathol. 36, 235–241 (2012).
4. Yamada, M. et al. Microscopic Venous Invasion in Pancreatic Cancer. Ann. Surg. Oncol. 25, 1043–1051 (2018).
5. Suenaga, M. et al. Pattern of first recurrent lesions in pancreatic cancer: hepatic relapse is associated with dismal prognosis and portal vein invasion. Hepatogastroenterology 61, 1756–1761 (2014).
6. Hamada, Y. & Nakayama, Y. Aggressive venous invasion in the area of carcinoma correlates with liver metastasis as an index of metastasis for invasive ductal carcinoma of the pancreas. Pancreatology 17, 951–955 (2017).
7. Hong, S.-M. et al. A 'Clearer' View of Pancreatic Pathology: A Review of Tissue Clearing and Advanced Microscopy Techniques. Adv. Anat. Pathol. 26, 31–39 (2019).
8. Noë, M. et al. Immunolabeling of Cleared Human Pancreata Provides Insights into Three-dimensional Pancreatic Anatomy and Pathology. Am. J. Pathol. (2018) doi:10.1016/j.ajpath.2018.04.002.
9. Sharma, S. & Green, K. B. The pancreatic duct and its arteriovenous relationship: an underutilized aid in the diagnosis and distinction of pancreatic adenocarcinoma from pancreatic intraepithelial neoplasia. A study of 126 pancreatectomy specimens. Am. J. Surg. Pathol. 28, 613–620 (2004).
10. Jeanes, A., Gottardi, C. J. & Yap, A. S. Cadherins and cancer: how does cadherin dysfunction promote tumor progression? Oncogene 27, 6920–6929 (2008).
11. Onder, T. T. et al. Loss of E-cadherin promotes metastasis via multiple downstream transcriptional pathways. Cancer Res. 68, 3645–3654 (2008).
12. Cao, D. et al. Expression of novel markers of pancreatic ductal adenocarcinoma in pancreatic nonductal neoplasms: additional evidence of different genetic pathways. Mod. Pathol. 18, 752–761 (2005).
13. Winter, J. M. et al. Absence of E-cadherin expression distinguishes noncohesive from cohesive pancreatic cancer. Clin. Cancer Res. 14, 412–418 (2008).
14. Zeisberg, M. & Neilson, E. G. Biomarkers for epithelial-mesenchymal transitions. J. Clin. Invest. 119, 1429–1437 (2009).
15. Nguyen, D.-H. T. et al. A biomimetic pancreatic cancer on-chip reveals endothelial ablation via ALK7 signaling. Sci Adv 5, eaav6789 (2019).
16. Gresta, L. T., Rodrigues-Júnior, I. A., de Castro, L. P. F., Cassali, G. D. & Cabral, M. M. D. Á. Assessment of vascular invasion in gastric cancer: a comparative study. World J. Gastroenterol. 19, 3761–3769 (2013).
17. Inada, K., Shimokawa, K., Ikeda, T. & Ozeki, Y. The clinical significance of venous invasion in cancer of the stomach. Jpn. J. Surg. 20, 545–552 (1990).
18. Hwang, C. et al. Venous Invasion in Colorectal Cancer: Impact of Morphologic Findings on Detection Rate. Cancer Res. Treat. 48, 1222–1228 (2016).
19. Betge, J. et al. Intramural and extramural vascular invasion in colorectal cancer: prognostic significance and quality of pathology reporting. Cancer 118, 628–638 (2012).
20. Yu, J., Blackford, A. L., Dal Molin, M., Wolfgang, C. L. & Goggins, M. Time to progression of pancreatic ductal adenocarcinoma from low-to-high tumour stages. Gut 64, 1783–1789 (2015).
21. Nieto, M. A., Huang, R. Y.-J., Jackson, R. A. & Thiery, J. P. EMT: 2016. Cell 166, 21–45 (2016).
22. Micalizzi, D. S., Haber, D. A. & Maheswaran, S. Cancer metastasis through the prism of epithelial-to-mesenchymal transition in circulating tumor cells. Mol. Oncol. 11, 770–780 (2017).
23. Chen, T., You, Y., Jiang, H. & Wang, Z. Z. Epithelial-mesenchymal transition (EMT): A biological process in the development, stem cell differentiation, and tumorigenesis. J. Cell. Physiol. 232, 3261–3272 (2017).
24. Serrano-Gomez, S. J., Maziveyi, M. & Alahari, S. K. Regulation of epithelial-mesenchymal transition through epigenetic and post-translational modifications. Mol. Cancer 15, 18 (2016).
25. Brabletz, T. et al. Variable beta-catenin expression in colorectal cancers indicates tumor progression driven by the tumor environment. Proc. Natl. Acad. Sci. U. S. A. 98, 10356–10361 (2001).
26. Ligorio, M. et al. Stromal Microenvironment Shapes the Intratumoral Architecture of Pancreatic Cancer. Cell 178, 160–175.e27 (2019).

9

Chapter 10

Why is pancreatic cancer so deadly?

The pathologist's view

Ralph H. Hruban, Matthias M. Gaida, Elizabeth Thompson, Seung-Mo Hong, Michaël Noë, Lodewijk A.A. Brosens, Martine Jongepier, G. Johan A. Offerhaus, Laura D. Wood

The Journal of Pathology, June 2019

ABSTRACT

The remarkable aggressiveness of pancreatic cancer has never been fully explained. Although clearly multifactorial, we postulate that venous invasion, a finding seen in most pancreatic cancers but not in most cancers of other organs, may be a significant, underappreciated contributor to the aggressiveness of this disease.

INTRODUCTION

Pancreatic cancer is one of the deadliest of the solid malignancies.[1] The 5-year survival rate for patients diagnosed with pancreatic cancer is only 9%.[2] The actual survival may be even worse as several studies have shown that a significant fraction of apparent long-term survivors were initially incorrectly diagnosed with less aggressive neoplasms and, in fact, did not have pancreatic cancer.[3] This over-diagnosis may be particularly common for pancreatic cancer as these cancers arise at the anatomic confluence of the distal common bile duct, the ampulla of Vater, and the duodenum, and the histopathology of these less aggressive neoplasms can overlap. A number of hypotheses have been put forward to explain this extremely poor prognosis and these hypotheses formed the basis for a special session at the 2017 Meeting of the American Association for Cancer Research in Washington, DC. This session was chaired by Jordan Berlin, MD; Christine Iacobuzio-Donahue, MD, PhD; and one of the authors of this review (RHH). Possible explanations raised at this thought-provoking session ranged from the late onset of symptoms to the poor chemosensitivity of the neoplastic cells of pancreatic cancer.[4–6] For example, the survival rates for patients diagnosed with pancreatic cancer have increased significantly with the introduction of combination chemotherapy, suggesting that the poor prognosis is, at least in part, due to unmet opportunities in drug development.[7–11]

As pathologists who have collectively reviewed thousands of pancreatic cancers, we postulated that the pathology of pancreatic cancer, by which we restrict ourselves in this review to invasive ductal adenocarcinoma, may provide insight into the aggressiveness of this disease. Here, we systematically evaluate each of the components of the pathology of pancreatic cancer and its precursor lesions to determine if our understanding of the pathology can provide insights into the deadly nature of this malignancy.

PRECANCERS

Almost all epithelial malignancies arise from histologically well-defined precancerous lesions, and in most instances, neoplasms remain in the noninvasive precancerous stage for years, if not decades, providing a large window for early detection and cure.[12–14] Perhaps the one exception to this is precancerous lesions with genomic instability, as can be seen in individuals with Lynch syndrome, which likely progress quickly once initiated.[15]

Is it possible that pancreatic cancer is so deadly because, unlike precancers in most other organs, the precancerous lesions of the pancreas rapidly progress to invasive cancer? To answer this question, we must first define the precancers that give rise to invasive pancreatic cancer. Three well-defined precursors of pancreatic cancer have been defined: intraductal papillary mucinous neoplasms (IPMNs), mucinous cystic neoplasms (MCNs), and pancreatic intraepithelial neoplasia (PanIN).[12,13,16] These lesions do not rapidly progress to invasive cancer. In fact, the vast majority of these precancerous lesions of the pancreas, when clinically recognized, never progress to invasive cancer. IPMNs and MCNs can be

detected using currently available imaging technologies and numerous studies have shown that almost all of these precursor lesions can be safely followed clinically for years because they do not rapidly progress to invasive carcinoma.[17–19] These lesions clinically either tend not to progress or, if they do, develop detectable 'worrisome' features on imaging before they progress to invasive carcinoma.[17–19]

One could, however, argue that the slow progression of the larger IPMNs and MCNs is misleading as PanIN lesions, which are too small to be detected clinically, are the precancers that give rise to most invasive pancreatic cancers, and in contrast to IPMNs and MCNs, PanINs progress rapidly. Somatic genetic mutations can be used as 'molecular clocks' to address this possibility. To define the speed at which nonneoplastic cells in the pancreas progress to invasive carcinoma, Iacobuzio-Donahue and co-workers integrated careful histopathology with genetic sequencing of somatic mutations in pancreatic cancer and its precursors, and have shown that, on average, it takes more than a decade for noninvasive precursor lesions in the pancreas, including PanIN lesions, to progress to invasive carcinoma.[20,21] Similarly, in a 'back of the envelope calculation', Longnecker and co-workers estimated that the probability of a single PanIN lesion ever progressing to invasive carcinoma is less than 1%.[22] Taken together, these clinical and molecular findings suggest that rapid progression of precancerous lesions does not explain the high mortality rate of pancreatic cancer.

STAGE

Is pancreatic cancer so deadly because it is always discovered at an advanced stage? Certainly, this is a significant problem as 80% of patients with pancreatic cancer have distant metastases at the time of diagnosis and advanced stage clearly explains why most pancreatic cancers are so deadly.[2] However, one of the more remarkable things about pancreatic cancer is that even small, low-stage, surgically resected pancreatic cancers metastasize and lead to the death of the patient.[23–27] For example, Egawa et al reported a series of 822 patients with small pancreatic cancers (<2 cm) and found that close to 40% had lymph node metastases and that more than 40% died within 5 years.[23] Similarly, Jung et al followed 74 patients with small (≤2 cm) pancreatic cancers and reported that the 5-year survival rate for patients with stage IA disease was only 23%.[27] These findings contrast dramatically with the outcomes for patients with small cancers of other organs. For example, 5-year survival rates of 88% have been reported for women with small (<2 cm) node-negative and hormone receptor-negative breast cancer.[28] Thus, while advanced stage at diagnosis explains much of the poor prognosis for patients with pancreatic cancer, it does not explain all of it. Furthermore, the advanced stage at diagnosis for most patients with pancreatic cancer raises the more fundamental question that we will try to answer below – why are most pancreatic cancers diagnosed at an advanced stage?

LYMPH NODE METASTASES

Lymph node status is a part of staging, and lymph node metastases are present in the majority of patients with pancreatic cancer at the time of diagnosis. Most studies report lymph node metastases in

70–80% of surgically resected patients with pancreatic cancer, a group that is selected for early-stage disease.[29–33] Lymphatic invasion by the neoplastic cells is also present in most pancreatic cancers, and lymphatic invasion correlates with lymph node metastases and poor survival.[34] However, some very-long-term survivors of pancreatic cancer have lymph node metastases at the time of surgery, indicating that spread to lymph nodes does not universally portend a worse outcome.[35,36]

Although lymph node metastasis is somewhat more common in pancreatic cancer than in other cancers, including breast cancer, lymph node metastases by themselves do not sufficiently account for the large difference in survival.[37] The survival of patients with pancreatic cancer metastatic to lymph nodes is significantly worse than it is for patients with breast cancer metastatic to lymph nodes. In one study, pancreatic cancer patients with lymph node metastases had a 5-year survival of 13%.[30] By contrast, the 5-year survival for breast cancer patients with lymph node metastases is closer to 80%.[38]

Taken together, these data suggest that although there is a significant difference in the prevalence of lymph node metastasis between pancreatic and other cancers, this phenomenon is unlikely to be the entire driver of poor prognosis.[39–41]

COMPONENTS OF METASTATIC SPREAD

The genetics and pathophysiology of the mechanisms by which pancreatic cancer spreads to other organs have been extensively studied, and a number of processes have been identified that contribute to the metastasis of pancreatic cancer.[20,42–46] These include SMAD4 loss, the release of exosomes by the neoplastic cells facilitating liver metastases, the 'seed and soil' hypothesis, and the presence of circulating tumor cells.[20,42–48] These processes clearly may contribute to metastases, but they do not fully account for the aggressiveness of this cancer type. For example, no discernible pattern of somatic mutations was identified when the genetic changes in a large series of pancreatic cancers from long-term survivors were compared with the genetic changes in cancers from short-term survivors.[35]

CELL PROLIFERATION AND DEATH

A high proliferation rate combined with a low cell death rate leads to increased cell numbers which can contribute to cancer progression. Pancreatic cancer and its precursor lesions proliferate faster than normal ductal cells of the pancreas, and the neoplastic cells are relatively resistant to apoptosis.[49–57] Using Ki-67 as an indicator of cell proliferation, the reported percentage of Ki-67-positive cells in invasive pancreatic cancer ranges greatly from around 5% to over 60%, and approximately 90% of pancreatic cancers have a Ki-67 index lower than 50%.[58,59] This range is within the spectrum of rates seen in cancers of other organs. For example, the vast majority of breast cancers also have Ki-67 proliferation rates of less than 50%, and the median proliferation rates for unselected cohorts of invasive breast cancer (between 20% and 40%) are in the range of to those reported in invasive pancreatic cancer.[60–63] Similar proliferation rates, between 20% and 40%, have been reported in carcinomas of the colon and

of the lung.[63] Of note, breast cancer patients with more than 20% Ki-67-positive cells (e.g. luminal B phenotype) or distinct histological subtypes such as medullary breast cancer with high proliferation rates of more than 50% Ki-67-positive cells still have a better overall survival than do patients with pancreatic cancer.[64,65] These data suggest that the proliferation rate itself is not the dominant driver of the aggressiveness of pancreatic cancer.

Perhaps more importantly, if a high proliferation rate combined with a low cell death rate was the explanation of the rapid progression of pancreatic cancer, we would expect pancreatic cancer to have a peculiarly high clinical tumor doubling time. Serial imaging of patients who have not been treated allow us to calculate the doubling time of pancreatic cancer, and the reported mean clinical volume doubling times of pancreatic cancer range from 132 days to 159 days.[66–69] Although the doubling time of pancreatic cancer tends to be shorter than, for example, the tumor volume doubling time reported for the majority of breast cancers (which ranges from 140 days to 185 days), there are some variants of breast cancer with a better prognosis than pancreatic cancer, such as triple-negative breast cancer, that have markedly short tumor volume doubling times of only 100 days.[70–73] Thus, although a high proliferation rate combined with a low cell death rate contributes to the aggressiveness of pancreatic cancer, it does not explain it fully.

GENES

The genetic alterations that drive the progression of pancreatic cancer are now well understood, and they do not appear to explain this cancer's aggressiveness. Germline mutations in *ATM*, *BRCA1*, *BRCA2*, *PALB2*, *PRSS1*, *p16*/*CDKN2A*, *STK11*, and the mismatch repair genes (*MLH1*, etc.) have been shown to predispose to pancreatic cancer.[74–76] These germline changes do not explain the aggressiveness of pancreatic cancer as they are found in only 10% of patients; they also predispose to cancers in other organs that are less aggressive and when present, can be associated with a better, not worse, prognosis.[77–79]

The four genes most commonly somatically mutated in pancreatic cancer are *KRAS*, *p16*/*CDKN2A*, *TP53*, and *SMAD4*.[80,81] Of these, only inactivating mutations in the *SMAD4* gene have been consistently associated with poor prognosis.[44,82,83] The magnitude of the difference in outcome between patients with *SMAD4* mutant and those with *SMAD4* wild-type cancers is, however, small. Furthermore, as noted earlier, the cancers of very-long-term survivors have been studied and there is no specific pattern of somatic mutations in this group.[35] Thus, the germline and somatic genetic drivers of pancreatic cancer, while they explain the better prognosis of some cancers, such as those that arise in patients with germline *BRCA2* mutations, do not appear to explain this cancer's aggressiveness.

CELLULAR DIFFERENTIATION

Is the aggressiveness of pancreatic cancer because pancreatic cancer is a uniformly poorly differ-

entiated neoplasm? There have been several large studies of surgically resected pancreatic cancers and most are surprisingly well differentiated.[29,30] For example, 48% of the 1423 surgically resected pancreatic cancers reported by Winter et al were well or moderately differentiated.[29] Similarly, Warshaw and co-workers reported that 60% of the pancreatic cancers resected at the Massachusetts General Hospital were well or moderately differentiated, as were 52% of the cancers from long-term survivors.[84] These percentages are similar to the percentage of well and moderately differentiated carcinomas reported for clinically less aggressive breast primaries.[85–87] Although the data on differentiation of pancreatic cancer are biased towards surgically resected cases, it is clear that degree of differentiation alone cannot explain the aggressiveness of pancreatic cancer.

EPITHELIAL-MESENCHYMAL TRANSITION

A lot has been written about epithelial–mesenchymal transition (EMT), the process by which neoplastic cells lose cell–cell adhesion and polarity, spindle out into mesenchymal-appearing cells, and gain migratory properties.[88–90] We have reviewed the shortcomings of this concept as applied to pancreatic cancer in detail elsewhere, and therefore will not address them extensively here.[88] Briefly, since the features associated with EMT, such as loss of E-cadherin and upregulated mesenchymal transcription factors, are often very focal in pancreatic cancer, chemoresistance of the bulk tumor in patients is an unlikely consequence of EMT.[91,92] In addition, examples of metastatic pancreatic cancer cells in vessels and in bone with absolutely no evidence for EMT demonstrate that EMT is not a ubiquitous event in the dissemination of pancreatic cancer or that cells that have undergone EMT can revert back to an epithelial phenotype after they have invaded.[93] This observation of widely disseminated pancreatic cancer without any evidence of EMT conceptually deflates EMT as a major driver for a poor prognosis in pancreatic cancer.[88] Furthermore, EMT is not unique to pancreatic cancer. It is observed in many other epithelial cancers, particularly in breast, ovarian, lung, colorectal, and liver cancers.[94–98]

Thus, widely metastatic pancreatic cancer is often gland-forming, and EMT is not unique to pancreatic cancer and therefore EMT does not explain the particular aggressiveness of pancreatic cancer. Of course, despite these objections, one cannot rule out the possibility that focal and transient EMT contributes to the aggressiveness of pancreatic cancer.[93,99]

STROMA

One of the most unique morphological features of pancreatic cancer is its dense desmoplastic stroma.[100–103] As reviewed by Tuveson and co-workers, this stroma is composed of a mixture of extracellular matrix and nonneoplastic cells including fibroblasts, blood vessels, and immune cells.[100] Moreover, it has been suggested that this stroma elevates interstitial pressures within the cancers, preventing chemotherapeutic agents from entering the tumor.[104] While the stroma is clearly quite distinctive in pancreatic cancer, a growing body of evidence suggests that the stroma has both beneficial and deleterious effects.[105] Efforts to alter the stroma therapeutically have met with, at best, mixed results.[101,106–108]

Perhaps most important from the perspective of trying to understand if the stroma can fully explain the aggressiveness of pancreatic cancer is the histological finding of metastases without any stroma that were resistant to therapy.[88] The stroma, although clearly a distinctive feature of pancreatic cancer, by itself does not appear to be the full explanation.

IMMUNE RESPONSE

The immune infiltrate, or tumor immune microenvironment (TiME), is increasingly recognized in multiple tumor types as a potential driver of patient outcome.[109,110] The TiME of pancreatic cancer includes T cells (both CD4+ and CD8+), B cells, macrophages, neutrophils, and even natural killer cells.[109,111,112] Relative to other cancer types, pancreatic cancer seems to have a relative lack of cytotoxic T cells in comparison to immunosuppressive cells and cytokines. Instead, the immune infiltrate of most pancreatic cancers is biased towards an immunosuppressive milieu with high numbers of myeloid-derived suppressive cells (MDSCs), FOXP3+ regulatory T cells, and high levels of IL-10 and transforming growth factor TGF-beta.[112–114] When present, T cells within pancreatic tumors are often found to have low cytotoxic functionality.[115]

It should therefore not be surprising that, relative to other tumor types, pancreatic cancers are not considered highly immunogenic.[116] Melanoma and non-small cell lung cancer induce much more brisk immune responses with more generous T-cell infiltrates. Differences in the mutational load of these tumor types and the subsequent generation of neoantigens for T-cell recognition may partially account for some of these differences.[110] Pancreatic cancers have relatively low mutational burdens, with an average of one mutation per megabase compared with over ten mutations per megabase in melanoma and just under ten mutations per megabase in non-small cell lung cancer (NSCLC).[117] Similarly, there is a low prevalence of microsatellite instability in pancreatic cancer.[118]

While it is tempting to postulate that the TiME may explain the aggressiveness of pancreatic cancer, the reality is very complicated and not yet fully elucidated. For example, breast cancers are also generally considered to have low immunogenicity and have similar high levels of immunosuppression but overall better T-cell function and more promising responses to immunotherapy than pancreatic cancer.[114] On the other hand, subsets of pancreatic tumors do seem to have functional T-cell responses and when present, this evidence of T-cell immunity correlates with better survival.[119–121] On the far extreme, rare, highly inflamed medullary carcinomas of the pancreas, the histologic variant associated with mismatch repair defects, have a surprisingly good prognosis and are predicted to respond to immunotherapy.[79,118,122,123] Conversely, Th17-dominant immune reactions and alternative p38 MAPK activation in tumor-infiltrating T cells have been associated with aggressive disease.[124,125]

Recent evidence also demonstrates that the longest-term survivors of pancreatic cancers are associated with both the highest neoantigen levels (determined by whole-exome sequencing and in silico neoantigen prediction) and the most abundant CD8 T-cell responses, but importantly neither feature

alone was linked to survival.[126] This linkage of neoantigen number and T-cell infiltration implies that the quality of neoantigens is crucial. Importantly, clones demonstrating high quality neoantigens were often lost in metastases, suggesting a means of immune escape in aggressive metastatic spread of disease.

While the TiME may explain some of the aggressiveness of pancreatic cancer, experiences with attempts to boost the immune response to pancreatic tumors again suggest a more complicated reality. Studies have shown that therapeutic targeting of the immunosuppressive milieu can convert the TiME in pancreatic tumors into a more active, inflamed environment. However, the overall responses to immunotherapy and increases in survival remain disappointing, suggesting that even with the generation of a functional immune response, other features of pancreatic cancer drive its highly aggressive behavior.[127]

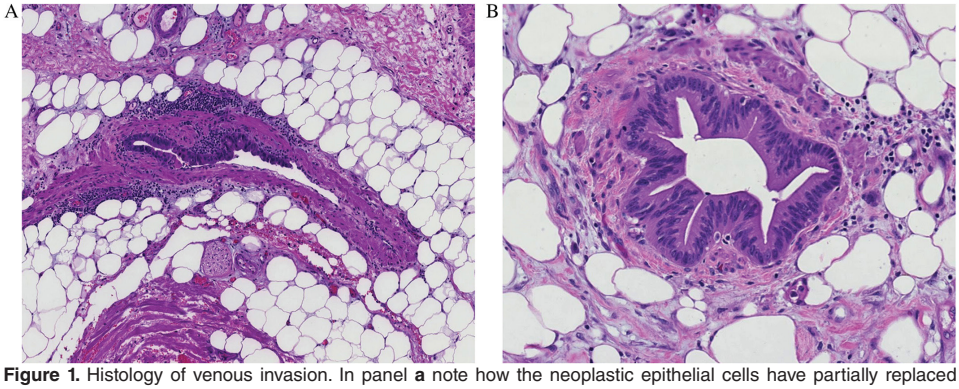

Figure 1. Histology of venous invasion. In panel **a** note how the neoplastic epithelial cells have partially replaced the venous endothelial cells. The cancer cells in panel **b** have relined the full circumference of the vessel and look surprisingly well-differentiated and benign.

PERINEURAL INVASION

The prevalence of perineural invasion is higher in pancreatic cancer than in most other cancer types. Perineural invasion is identified pathologically in the majority (70–98%) of surgically resected pancreatic cancers, and it has been claimed that perineural invasion can be found in 100% of pancreatic cancers if enough sections are examined.[128–133] By contrast, 75–85% of cholangiocarcinomas, 60–75% of gastric cancers, and only 33% of colorectal cancers have perineural invasion.[134–141] Once the neoplastic cells enter the perineural space, they can extend along nerves for several centimeters. This suggests a pathway out of the pancreas and, indeed, perineural invasion in the pancreas has been associated with poorer overall survival and invasion into the retroperitoneum.[133,136,142,143] This involvement of the retroperitoneum would explain local recurrence following surgery, but not distant metastases, and it is the distant metastases that are the biggest cause of death in this disease.[144,145]

CANCERIZATION OF DUCTS

Just as pancreatic cancer frequently grows into and then extends along nerves, so too can invasive

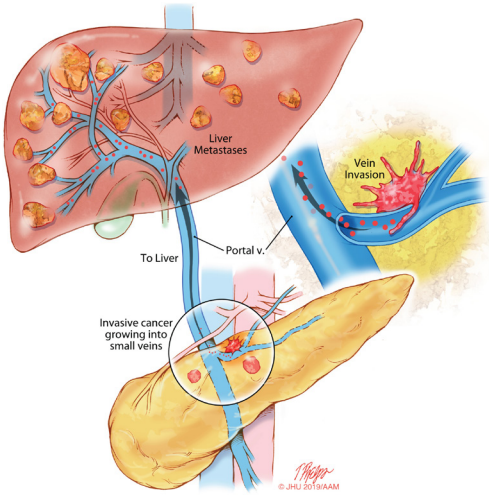

Figure 2. Illustration depicting how venous invasion in the pancreas gives the cancer a direct route to spread to the liver (artwork by Timothy Phelps; copyright Art as Applied to Medicine, Johns Hopkins University School of Medicine. Used with permission).

pancreatic cancer grow back into the normal duct system of the pancreas and then extend along preexisting ducts.[146,147] This process is designated 'cancerization of the ducts'. Cancerization of the ducts has also been reported in indolent cancers such as prostate cancer and is therefore unlikely to explain the aggressiveness of pancreatic cancer.[148,149] Instead, this intraductal spread of neoplastic cells may explain the rare instances of local recurrence in the remnant pancreas following partial pancreatectomy.[146] It does not explain disease outside of the pancreas and therefore is not the cause of pancreatic cancer's aggressiveness.

VENOUS INVASION

The invasion of small veins (vessels with a muscular wall but not a well-defined internal and external elastic lamina) is remarkably common in pancreatic cancer and is a relatively unique feature of this disease compared with cancers of other organs.[147,150] Venous invasion is identifiable in two-thirds (65%) of surgically resected pancreatic cancers, and when pancreatic cancer invades veins, it has a very distinct morphology (Figure 1).[147,150] The neoplastic cells replace the endothelial cells and grow along the inner wall of the vessels.[147,150] It should not be surprising that this venous invasion is associated with liver metastases and a poor prognosis, as the veins in the pancreas drain directly into the liver (Figure 2).[150–153]

Cancer origin	Authors (reference)	No of cases examined	Percent with venous invasion
Gastric cancer	Gresta *et al*[162]	95	40%
	Inada *et al*[163]	235	37%
	Setälä *et al*[164]	255	7%
Colon cancer	Hwang *et al*[161]	93	15%
	Betge *et al*[160]	381	23%
	Messenger *et al*[159]	10435	21%
	(compilation of 13 studies)[159]		(range 8-45%)
Pancreatic cancer	Hong *et al*[150]	209	65%
	Yamada *et al*[151]	352	65%

Table 1. Prevalence of venous invasion in cancers of different organs

Stage for stage, the prognosis for patients with breast cancer is better than it is for patients with pancreatic cancer, and the prevalence of vascular invasion in surgically resected breast cancer is lower (15–46%) than it is in surgically resected pancreatic cancer.[154–158] Similarly, as shown in Table 1, the reported prevalence of venous invasion in gastric cancers (24%) and in colon cancer (21%) is only a third of that reported in pancreatic cancer.[150,151,159–164]

Venous invasion also explains other unique aspects of pancreatic cancer. For example, venous invasion will obstruct venous outflow from the tumor, which will, in turn, reduce in-flow to the tumor. Decreased blood flow may therefore contribute to the poor delivery of chemotherapy to pancreatic cancers as well as to the hypoenhancing nature of these neoplasms on CT scanning.[165–167]

Venous invasion therefore meets two criteria for an explanation of the aggressiveness of pancreatic cancer. First, the finding is much more common in cancers of the pancreas than it is in cancers of other organs. Second, because it gives the cancer uninterrupted access to the liver, it can directly lead to widespread metastatic disease (Figure 2).

Venous invasion, however, does not entirely explain the lethality of pancreatic cancer. Neuroendocrine neoplasms of the small intestine invade veins and metastasize to the liver, but they are not nearly as deadly as pancreatic cancer.[168,169] In addition, venous invasion has not been reported to be prominent in pancreatic cancer metastatic to the liver, and liver metastases are not chemoresponsive. Anatomic location, venous invasion, and drainage into the portal vein to the liver do not entirely account for the aggressiveness of this disease.

SUMMARY AND CONCLUSIONS

There are clearly a number of factors that contribute to the aggressive nature and poor prognosis of pancreatic cancer. By focusing on the pathology, we by no means wish to downplay the importance of any of these other factors. Factors from the relative insensitivity of pancreatic cancer to chemotherapy and radiation therapy, the associated cachexia, and the lack of access to care contribute to the lethality of this disease.[170] Our goal here is not to ignore these other very important contributors, but instead to shine a light on underappreciated aspects of the pathology of pancreatic cancer that have the potential to be significant contributors to the aggressiveness of this disease.

In particular, in reviewing the pathology of pancreatic cancer, we are struck by the prominence of venous invasion in this disease, and by the potential for venous invasion to explain the rapid development of liver metastases and, in so doing, the rapid progression of disease in most patients. An example of rapid progression is shown in the supplementary material, Figure S1 and Video. This patient had no evidence of liver disease on initial imaging but 4 months later, had numerous liver metastases. Extensive access of the cancer to the venous system would explain this clinical finding as this access would give the neoplastic cells a direct portal to the liver, allowing significant numbers of neoplastic cells to spread systemically (Figure 2). We also note that the role of the immune response in driving the poor prognosis of pancreatic cancer needs to be elucidated further.

REFERENCES

1. Leinonen, M. K., Miettinen, J., Heikkinen, S., Pitkäniemi, J. & Malila, N. Quality measures of the population-based Finnish Cancer Registry indicate sound data quality for solid malignant tumours. Eur. J. Cancer 77, 31–39 (2017).
2. Siegel, R. L., Miller, K. D. & Jemal, A. Cancer statistics, 2018. CA Cancer J. Clin. 68, 7–30 (2018).
3. Carpelan-Holmström, M. et al. Does anyone survive pancreatic ductal adenocarcinoma? A nationwide study re-evaluating the data of the Finnish Cancer Registry. Gut 54, 385–387 (2005).
4. Cid-Arregui, A. & Juarez, V. Perspectives in the treatment of pancreatic adenocarcinoma. World J. Gastroenterol. 21, 9297–9316 (2015).
5. Tempero, M. A. Introduction: Pancreatic Adenocarcinoma: The Emperor of All Cancer Maladies. Cancer J. 23, 309 (2017).
6. Kleeff, J. et al. Pancreatic cancer. Nat Rev Dis Primers 2, 16022 (2016).
7. Neoptolemos, J. P. et al. A randomized trial of chemoradiotherapy and chemotherapy after resection of pancreatic cancer. N. Engl. J. Med. 350, 1200–1210 (2004).
8. Neoptolemos, J. P. et al. Adjuvant chemotherapy with fluorouracil plus folinic acid vs gemcitabine following pancreatic cancer resection: a randomized controlled trial. JAMA 304, 1073–1081 (2010).
9. Neoptolemos, J. P. et al. Comparison of adjuvant gemcitabine and capecitabine with gemcitabine monotherapy in patients with resected pancreatic cancer (ESPAC-4): a multicentre, open-label, randomised, phase 3 trial. Lancet 389, 1011–1024 (2017).
10. Conroy, T. et al. FOLFIRINOX or Gemcitabine as Adjuvant Therapy for Pancreatic Cancer. N. Engl. J. Med. 379, 2395–2406 (2018).
11. Tiriac, H. et al. Organoid Profiling Identifies Common Responders to Chemotherapy in Pancreatic Cancer. Cancer Discov. 8, 1112–1129 (2018).
12. Berman, J. J. et al. Precancer: a conceptual working definition -- results of a Consensus Conference. Cancer Detect. Prev. 30, 387–394 (2006).
13. Voltaggio, L. et al. Current concepts in the diagnosis and pathobiology of intraepithelial neoplasia: A review by organ system. CA Cancer J. Clin. 66, 408–436 (2016).
14. Jones, S. et al. Comparative lesion sequencing provides insights into tumor evolution. Proc. Natl. Acad. Sci. U. S. A. 105, 4283–4288 (2008).
15. Seth, S., Ager, A., Arends, M. J. & Frayling, I. M. Lynch syndrome - cancer pathways, heterogeneity and immune escape. J. Pathol. 246, 129–133 (2018).
16. Basturk, O. et al. A Revised Classification System and Recommendations From the Baltimore Consensus Meeting for Neoplastic Precursor Lesions in the Pancreas. Am. J. Surg. Pathol. 39, 1730–1741 (2015).
17. Gausman, V. et al. Predictors of Progression Among Low-Risk Intraductal Papillary Mucinous Neoplasms in a Multicenter Surveillance Cohort. Pancreas 47, 471–476 (2018).
18. Han, Y. et al. Progression of Pancreatic Branch Duct Intraductal Papillary Mucinous Neoplasm Associates With Cyst Size. Gastroenterology 154, 576–584 (2018).
19. Pergolini, I. et al. Long-term Risk of Pancreatic Malignancy in Patients With Branch Duct Intraductal Papillary Mucinous Neoplasm in a Referral Center. Gastroenterology 153, 1284–1294.e1 (2017).
20. Makohon-Moore, A. P. et al. Precancerous neoplastic cells can move through the pancreatic ductal system. Nature 561, 201–205 (2018).
21. Yachida, S. et al. Distant metastasis occurs late during the genetic evolution of pancreatic cancer. Nature 467, 1114–1117 (2010).
22. Terhune, P. G., Phifer, D. M., Tosteson, T. D. & Longnecker, D. S. K-ras mutation in focal proliferative lesions of human pancreas. Cancer Epidemiol. Biomarkers Prev. 7, 515–521 (1998).
23. Egawa, S. et al. Clinicopathological aspects of small pancreatic cancer. Pancreas 28, 235–240 (2004).
24. Ansari, D. et al. Relationship between tumour size and outcome in pancreatic ductal adenocarcinoma. Br. J. Surg. 104, 600–607 (2017).
25. Marchegiani, G. et al. Does Size Matter in Pancreatic Cancer?: Reappraisal of Tumour Dimension as a Predictor of Outcome Beyond the TNM. Ann. Surg. 266, 142–148 (2017).
26. Hur, C. et al. Early Pancreatic Ductal Adenocarcinoma Survival Is Dependent on Size: Positive Implications for Future Targeted Screening. Pancreas 45, 1062–1066 (2016).
27. Jung, K. W. et al. Clinicopathological aspects of 542 cases of pancreatic cancer: a special emphasis on small pancreatic cancer. J. Korean Med. Sci. 22 Suppl, S79–85 (2007).
28. Bhoo-Pathy, N. T. et al. Impact of adjuvant chemotherapy on survival of women with T1N0M0, hormone receptor negative breast cancer. Cancer Epidemiol. 48, 56–61 (2017).
29. Winter, J. M. et al. 1423 pancreaticoduodenectomies for pancreatic cancer: A single-institution experience. J. Gastrointest. Surg. 10, 1199–210; discussion 1210–1 (2006).
30. Riediger, H. et al. The lymph node ratio is the strongest prognostic factor after resection of pancreatic cancer. J. Gastrointest. Surg. 13, 1337–1344 (2009).

31. Massucco, P. et al. Prognostic significance of lymph node metastases in pancreatic head cancer treated with extended lymphadenectomy: not just a matter of numbers. Ann. Surg. Oncol. 16, 3323–3332 (2009).
32. Murakami, Y. et al. Number of metastatic lymph nodes, but not lymph node ratio, is an independent prognostic factor after resection of pancreatic carcinoma. J. Am. Coll. Surg. 211, 196–204 (2010).
33. Pawlik, T. M. et al. Prognostic relevance of lymph node ratio following pancreaticoduodenectomy for pancreatic cancer. Surgery 141, 610–618 (2007).
34. Epstein, J. D. et al. Microscopic lymphovascular invasion is an independent predictor of survival in resected pancreatic ductal adenocarcinoma. J. Surg. Oncol. 116, 658–664 (2017).
35. Dal Molin, M. et al. Very Long-term Survival Following Resection for Pancreatic Cancer Is Not Explained by Commonly Mutated Genes: Results of Whole-Exome Sequencing Analysis. Clin. Cancer Res. 21, 1944–1950 (2015).
36. Riall, T. S. et al. Resected periampullary adenocarcinoma: 5-year survivors and their 6- to 10-year follow-up. Surgery 140, 764–772 (2006).
37. Tseng, H.-S. et al. Tumor characteristics of breast cancer in predicting axillary lymph node metastasis. Med. Sci. Monit. 20, 1155–1161 (2014).
38. Chen, S. L., Hoehne, F. M. & Giuliano, A. E. The prognostic significance of micrometastases in breast cancer: a SEER population-based analysis. Ann. Surg. Oncol. 14, 3378–3384 (2007).
39. Kamarajah, S. K., Burns, W. R., Frankel, T. L., Cho, C. S. & Nathan, H. Validation of the American Joint Commission on Cancer (AJCC) 8th Edition Staging System for Patients with Pancreatic Adenocarcinoma: A Surveillance, Epidemiology and End Results (SEER) Analysis. Ann. Surg. Oncol. 24, 2023–2030 (2017).
40. Jang, N., Choi, J. E., Kang, S. H. & Bae, Y. K. Validation of the pathological prognostic staging system proposed in the revised eighth edition of the AJCC staging manual in different molecular subtypes of breast cancer. Virchows Arch. 474, 193–200 (2019).
41. Plichta, J. K. et al. Implications for Breast Cancer Restaging Based on the 8th Edition AJCC Staging Manual. Ann. Surg. 271, 169–176 (2020).
42. Massoumi, R. L., Hines, O. J., Eibl, G. & King, J. C. Emerging Evidence for the Clinical Relevance of Pancreatic Cancer Exosomes. Pancreas 48, 1–8 (2019).
43. Gemenetzis, G. et al. Circulating Tumor Cells Dynamics in Pancreatic Adenocarcinoma Correlate With Disease Status: Results of the Prospective CLUSTER Study. Ann. Surg. 268, 408–420 (2018).
44. Blackford, A. et al. SMAD4 gene mutations are associated with poor prognosis in pancreatic cancer. Clin. Cancer Res. 15, 4674–4679 (2009).
45. Hanahan, D. & Weinberg, R. A. The hallmarks of cancer. Cell 100, 57–70 (2000).
46. Hanahan, D. & Weinberg, R. A. Hallmarks of cancer: the next generation. Cell 144, 646–674 (2011).
47. Dioufa, N., Clark, A. M., Ma, B., Beckwitt, C. H. & Wells, A. Bi-directional exosome-driven intercommunication between the hepatic niche and cancer cells. Mol. Cancer 16, 172 (2017).
48. Lee, J. W. et al. Hepatocytes direct the formation of a pro-metastatic niche in the liver. Nature 567, 249–252 (2019).
49. Neesse, A., Gress, T. M. & Michl, P. Therapeutic targeting of apoptotic pathways: novel aspects in pancreatic cancer. Curr. Pharm. Biotechnol. 13, 2273–2282 (2012).
50. Röder, C., Trauzold, A. & Kalthoff, H. Impact of death receptor signaling on the malignancy of pancreatic ductal adenocarcinoma. Eur. J. Cell Biol. 90, 450–455 (2011).
51. Fulda, S. Apoptosis pathways and their therapeutic exploitation in pancreatic cancer. J. Cell. Mol. Med. 13, 1221–1227 (2009).
52. Temraz, S. et al. Ki67 and P53 in Relation to Disease Progression in Metastatic Pancreatic Cancer: a Single Institution Analysis. Pathol. Oncol. Res. 25, 1059–1066 (2019).
53. Striefler, J. K. et al. P53 overexpression and Ki67-index are associated with outcome in ductal pancreatic adenocarcinoma with adjuvant gemcitabine treatment. Pathol. Res. Pract. 212, 726–734 (2016).
54. Takeshita, A. et al. Clinicopathologic study of the MIB-1 labeling index (Ki67) and postoperative prognosis for intraductal papillary mucinous neoplasms and ordinary ductal adenocarcinoma. Pancreas 41, 114–120 (2012).
55. Lebe, B. et al. The importance of cyclin D1 and Ki67 expression on the biological behavior of pancreatic adenocarcinomas. Pathol. Res. Pract. 200, 389–396 (2004).
56. Stanton, K. J. et al. Analysis of Ki-67 antigen expression, DNA proliferative fraction, and survival in resected cancer of the pancreas. Am. J. Surg. 186, 486–492 (2003).
57. Klein, W. M., Hruban, R. H., Klein-Szanto, A. J. P. & Wilentz, R. E. Direct correlation between proliferative activity and dysplasia in pancreatic intraepithelial neoplasia (PanIN): additional evidence for a recently proposed model of progression. Mod. Pathol. 15, 441–447 (2002).
58. Kim, H. et al. Ki-67 and p53 expression as a predictive marker for early postoperative recurrence in pancreatic head cancer. Ann Surg Treat Res 88, 200–207 (2015).
59. Buck, A. C. et al. Ki-67 immunostaining in pancreatic cancer and chronic active pancreatitis: does in

vivo FDG uptake correlate with proliferative activity? J. Nucl. Med. 42, 721–725 (2001).
60. Laenkholm, A.-V. et al. An inter-observer Ki67 reproducibility study applying two different assessment methods: on behalf of the Danish Scientific Committee of Pathology, Danish breast cancer cooperative group (DBCG). Acta Oncol. 57, 83–89 (2018).
61. de Azambuja, E. et al. Ki-67 as prognostic marker in early breast cancer: a meta-analysis of published studies involving 12,155 patients. Br. J. Cancer 96, 1504–1513 (2007).
62. Petrelli, F., Viale, G., Cabiddu, M. & Barni, S. Prognostic value of different cut-off levels of Ki-67 in breast cancer: a systematic review and meta-analysis of 64,196 patients. Breast Cancer Res. Treat. 153, 477–491 (2015).
63. Rinehart, J. et al. Multicenter phase II study of the oral MEK inhibitor, CI-1040, in patients with advanced non-small-cell lung, breast, colon, and pancreatic cancer. J. Clin. Oncol. 22, 4456–4462 (2004).
64. Bustreo, S. et al. Optimal Ki67 cut-off for luminal breast cancer prognostic evaluation: a large case series study with a long-term follow-up. Breast Cancer Res. Treat. 157, 363–371 (2016).
65. Chu, Z. et al. Association between axillary lymph node status and Ki67 labeling index in triple-negative medullary breast carcinoma. Jpn. J. Clin. Oncol. 45, 637–641 (2015).
66. Hisa, T. et al. Growth process of small pancreatic carcinoma: a case report with imaging observation for 22 months. World J. Gastroenterol. 14, 1958–1960 (2008).
67. Ahn, S. J., Choi, S. J. & Kim, H. S. Time to Progression of Pancreatic Cancer: Evaluation with Multi-Detector Computed Tomography. J. Gastrointest. Cancer 48, 164–169 (2017).
68. Jang, K. M. et al. Missed pancreatic ductal adenocarcinoma: Assessment of early imaging findings on prediagnostic magnetic resonance imaging. Eur. J. Radiol. 84, 1473–1479 (2015).
69. Furukawa, H., Iwata, R. & Moriyama, N. Growth rate of pancreatic adenocarcinoma: initial clinical experience. Pancreas 22, 366–369 (2001).
70. Nakashima, K. et al. Does breast cancer growth rate really depend on tumor subtype? Measurement of tumor doubling time using serial ultrasonography between diagnosis and surgery. Breast Cancer 26, 206–214 (2019).
71. Zhang, S. et al. Correlation Factors Analysis of Breast Cancer Tumor Volume Doubling Time Measured by 3D-Ultrasound. Med. Sci. Monit. 23, 3147–3153 (2017).
72. Ryu, E. B. et al. Tumour volume doubling time of molecular breast cancer subtypes assessed by serial breast ultrasound. Eur. Radiol. 24, 2227–2235 (2014).
73. Ikeda, D. M., Andersson, I., Wattsgård, C., Janzon, L. & Linell, F. Interval carcinomas in the Malmö Mammographic Screening Trial: radiographic appearance and prognostic considerations. AJR Am. J. Roentgenol. 159, 287–294 (1992).
74. Shindo, K. et al. Deleterious Germline Mutations in Patients With Apparently Sporadic Pancreatic Adenocarcinoma. J. Clin. Oncol. 35, 3382–3390 (2017).
75. Childs, E. J. et al. Association of Common Susceptibility Variants of Pancreatic Cancer in Higher-Risk Patients: A PACGENE Study. Cancer Epidemiol. Biomarkers Prev. 25, 1185–1191 (2016).
76. Roberts, N. J. et al. Whole Genome Sequencing Defines the Genetic Heterogeneity of Familial Pancreatic Cancer. Cancer Discov. 6, 166–175 (2016).
77. Kondo, T. et al. Association between homologous recombination repair gene mutations and response to oxaliplatin in pancreatic cancer. Oncotarget 9, 19817–19825 (2018).
78. O'Reilly, E. M. et al. Phase 1 trial evaluating cisplatin, gemcitabine, and veliparib in 2 patient cohorts: Germline BRCA mutation carriers and wild-type BRCA pancreatic ductal adenocarcinoma. Cancer 124, 1374–1382 (2018).
79. Goggins, M. et al. Pancreatic adenocarcinomas with DNA replication errors (RER+) are associated with wild-type K-ras and characteristic histopathology. Poor differentiation, a syncytial growth pattern, and pushing borders suggest RER+. Am. J. Pathol. 152, 1501–1507 (1998).
80. Cancer Genome Atlas Research Network. Electronic address: andrew_aguirre@dfci.harvard.edu & Cancer Genome Atlas Research Network. Integrated Genomic Characterization of Pancreatic Ductal Adenocarcinoma. Cancer Cell 32, 185–203. e13 (2017).
81. Jones, S. et al. Core signaling pathways in human pancreatic cancers revealed by global genomic analyses. Science 321, 1801–1806 (2008).
82. Iacobuzio-Donahue, C. A. et al. DPC4 gene status of the primary carcinoma correlates with patterns of failure in patients with pancreatic cancer. J. Clin. Oncol. 27, 1806–1813 (2009).
83. Herman, J. M. et al. Smad4 Loss Correlates With Higher Rates of Local and Distant Failure in Pancreatic Adenocarcinoma Patients Receiving Adjuvant Chemoradiation. Pancreas 47, 208–212 (2018).
84. Ferrone, C. R. et al. Pancreatic ductal adenocarcinoma: long-term survival does not equal cure. Surgery 152, S43–9 (2012).
85. Elston, C. W. The assessment of histological differentiation in breast cancer. Aust. N. Z. J. Surg. 54, 11–15 (1984).
86. Hopton, D. S., Thorogood, J., Clayden, A. D. & MacKinnon, D. Histological grading of breast can-

cer; significance of grade on recurrence and mortality. Eur. J. Surg. Oncol. 15, 25–31 (1989).
87. Zhao, X. et al. Increasing negative lymph node count predicts favorable OS and DSS in breast cancer with different lymph node-positive subgroups. PLoS One 13, e0193784 (2018).
88. McDonald, O. G., Maitra, A. & Hruban, R. H. Human correlates of provocative questions in pancreatic pathology. Adv. Anat. Pathol. 19, 351–362 (2012).
89. Gaianigo, N., Melisi, D. & Carbone, C. EMT and Treatment Resistance in Pancreatic Cancer. Cancers 9, (2017).
90. Zhou, P. et al. The epithelial to mesenchymal transition (EMT) and cancer stem cells: implication for treatment resistance in pancreatic cancer. Mol. Cancer 16, 52 (2017).
91. Brabletz, T., Kalluri, R., Nieto, M. A. & Weinberg, R. A. EMT in cancer. Nat. Rev. Cancer 18, 128–134 (2018).
92. Gaida, M. M. et al. Polymorphonuclear neutrophils promote dyshesion of tumor cells and elastase-mediated degradation of E-cadherin in pancreatic tumors. Eur. J. Immunol. 42, 3369–3380 (2012).
93. Rhim, A. D. et al. EMT and dissemination precede pancreatic tumor formation. Cell 148, 349–361 (2012).
94. Taube, J. H. et al. Core epithelial-to-mesenchymal transition interactome gene-expression signature is associated with claudin-low and metaplastic breast cancer subtypes. Proc. Natl. Acad. Sci. U. S. A. 107, 15449–15454 (2010).
95. Mayer, C. et al. Neutrophil Granulocytes in Ovarian Cancer - Induction of Epithelial-To-Mesenchymal-Transition and Tumor Cell Migration. J. Cancer 7, 546–554 (2016).
96. Cui, T. et al. XPC inhibits NSCLC cell proliferation and migration by enhancing E-Cadherin expression. Oncotarget 6, 10060–10072 (2015).
97. Bi, X. et al. Decorin-mediated inhibition of colorectal cancer growth and migration is associated with E-cadherin in vitro and in mice. Carcinogenesis 33, 326–330 (2012).
98. Grosse-Steffen, T. et al. Epithelial-to-mesenchymal transition in pancreatic ductal adenocarcinoma and pancreatic tumor cell lines: the role of neutrophils and neutrophil-derived elastase. Clin. Dev. Immunol. 2012, 720768 (2012).
99. Haeno, H. et al. Computational modeling of pancreatic cancer reveals kinetics of metastasis suggesting optimum treatment strategies. Cell 148, 362–375 (2012).
100. Feig, C. et al. The pancreas cancer microenvironment. Clin. Cancer Res. 18, 4266–4276 (2012).
101. Wang, W.-Q., Liu, L., Xu, J.-Z. & Yu, X.-J. Reflections on depletion of tumor stroma in pancreatic cancer. Biochim. Biophys. Acta Rev. Cancer 1871, 267–272 (2019).
102. Neesse, A. et al. Stromal biology and therapy in pancreatic cancer: ready for clinical translation? Gut 68, 159–171 (2019).
103. Biffi, G. et al. IL1-Induced JAK/STAT Signaling Is Antagonized by TGF-beta to Shape CAF Heterogeneity in Pancreatic Ductal Adenocarcinoma. Cancer Discov. 9, 282–301 (2019).
104. DuFort, C. C. et al. Interstitial Pressure in Pancreatic Ductal Adenocarcinoma Is Dominated by a Gel-Fluid Phase. Biophys. J. 110, 2106–2119 (2016).
105. Whatcott, C. J., Han, H. & Von Hoff, D. D. Orchestrating the Tumor Microenvironment to Improve Survival for Patients With Pancreatic Cancer: Normalization, Not Destruction. Cancer J. 21, 299–306 (2015).
106. Gu, J., Saiyin, H., Fu, D. & Li, J. Stroma - A Double-Edged Sword in Pancreatic Cancer: A Lesson From Targeting Stroma in Pancreatic Cancer With Hedgehog Signaling Inhibitors. Pancreas 47, 382–389 (2018).
107. Neesse, A., Algül, H., Tuveson, D. A. & Gress, T. M. Stromal biology and therapy in pancreatic cancer: a changing paradigm. Gut 64, 1476–1484 (2015).
108. Hingorani, S. R. et al. Phase Ib Study of PEGylated Recombinant Human Hyaluronidase and Gemcitabine in Patients with Advanced Pancreatic Cancer. Clin. Cancer Res. 22, 2848–2854 (2016).
109. Foucher, E. D. et al. Pancreatic Ductal Adenocarcinoma: A Strong Imbalance of Good and Bad Immunological Cops in the Tumor Microenvironment. Front. Immunol. 9, 1044 (2018).
110. Topalian, S. L., Taube, J. M., Anders, R. A. & Pardoll, D. M. Mechanism-driven biomarkers to guide immune checkpoint blockade in cancer therapy. Nat. Rev. Cancer 16, 275–287 (2016).
111. Zheng, L., Xue, J., Jaffee, E. M. & Habtezion, A. Role of immune cells and immune-based therapies in pancreatitis and pancreatic ductal adenocarcinoma. Gastroenterology 144, 1230–1240 (2013).
112. Dougan, S. K. The Pancreatic Cancer Microenvironment. Cancer J. 23, 321–325 (2017).
113. Knudsen, E. S. et al. Stratification of Pancreatic Ductal Adenocarcinoma: Combinatorial Genetic, Stromal, and Immunologic Markers. Clin. Cancer Res. 23, 4429–4440 (2017).
114. Bates, J. P., Derakhshandeh, R., Jones, L. & Webb, T. J. Mechanisms of immune evasion in breast cancer. BMC Cancer 18, 556 (2018).
115. Tsujikawa, T. et al. Quantitative Multiplex Immunohistochemistry Reveals Myeloid-Inflamed Tumor-Immune Complexity Associated with Poor Prognosis. Cell Rep. 19, 203–217 (2017).
116. Luchini, C. et al. Pancreatic undifferentiated carcinoma with osteoclast-like giant cells is genetically

similar to, but clinically distinct from, conventional ductal adenocarcinoma. J. Pathol. 243, 148–154 (2017).
117. Alexandrov, L. B. & Stratton, M. R. Mutational signatures: the patterns of somatic mutations hidden in cancer genomes. Curr. Opin. Genet. Dev. 24, 52–60 (2014).
118. Wilentz, R. E. et al. Genetic, immunohistochemical, and clinical features of medullary carcinoma of the pancreas: A newly described and characterized entity. Am. J. Pathol. 156, 1641–1651 (2000).
119. Carstens, J. L. et al. Spatial computation of intratumoral T cells correlates with survival of patients with pancreatic cancer. Nat. Commun. 8, 15095 (2017).
120. Ino, Y. et al. Immune cell infiltration as an indicator of the immune microenvironment of pancreatic cancer. Br. J. Cancer 108, 914–923 (2013).
121. Hiraoka, N. et al. Intratumoral tertiary lymphoid organ is a favourable prognosticator in patients with pancreatic cancer. Br. J. Cancer 112, 1782–1790 (2015).
122. Bujanda, L. & Herreros-Villanueva, M. Pancreatic Cancer in Lynch Syndrome Patients. J. Cancer 8, 3667–3674 (2017).
123. Le, D. T. et al. PD-1 Blockade in Tumors with Mismatch-Repair Deficiency. N. Engl. J. Med. 372, 2509–2520 (2015).
124. McAllister, F. et al. Oncogenic *Kras* activates a hematopoietic-to-epithelial IL-17 signaling axis in preinvasive pancreatic neoplasia. Cancer Cell 25, 621–637 (2014).
125. Alam, M. S. et al. Selective inhibition of the p38 alternative activation pathway in infiltrating T cells inhibits pancreatic cancer progression. Nat. Med. 21, 1337–1343 (2015).
126. Balachandran, V. P. et al. Identification of unique neoantigen qualities in long-term survivors of pancreatic cancer. Nature 551, 512–516 (2017).
127. Lutz, E. et al. A lethally irradiated allogeneic granulocyte-macrophage colony stimulating factor-secreting tumor vaccine for pancreatic adenocarcinoma. A Phase II trial of safety, efficacy, and immune activation. Ann. Surg. 253, 328–335 (2011).
128. Chatterjee, D. et al. Perineural and intraneural invasion in posttherapy pancreaticoduodenectomy specimens predicts poor prognosis in patients with pancreatic ductal adenocarcinoma. Am. J. Surg. Pathol. 36, 409–417 (2012).
129. Schorn, S. et al. The influence of neural invasion on survival and tumor recurrence in pancreatic ductal adenocarcinoma - A systematic review and meta-analysis. Surg. Oncol. 26, 105–115 (2017).
130. Ozaki, H. et al. The prognostic significance of lymph node metastasis and intrapancreatic perineural invasion in pancreatic cancer after curative resection. Surg. Today 29, 16–22 (1999).
131. Takahashi, T. et al. Perineural invasion by ductal adenocarcinoma of the pancreas. J. Surg. Oncol. 65, 164–170 (1997).
132. Pour, P. M., Bell, R. H. & Batra, S. K. Neural invasion in the staging of pancreatic cancer. Pancreas 26, 322–325 (2003).
133. Hirai, I. et al. Perineural invasion in pancreatic cancer. Pancreas 24, 15–25 (2002).
134. Su, C. H. et al. Factors influencing postoperative morbidity, mortality, and survival after resection for hilar cholangiocarcinoma. Ann. Surg. 223, 384–394 (1996).
135. He, P. et al. Multivariate statistical analysis of clinicopathologic factors influencing survival of patients with bile duct carcinoma. World J. Gastroenterol. 8, 943–946 (2002).
136. Nagakawa, T. et al. Perineural invasion of carcinoma of the pancreas and biliary tract. Br. J. Surg. 80, 619–621 (1993).
137. Horn, A., Dahl, O. & Morild, I. Venous and neural invasion as predictors of recurrence in rectal adenocarcinoma. Dis. Colon Rectum 34, 798–804 (1991).
138. Bellis, D., Marci, V. & Monga, G. Light microscopic and immunohistochemical evaluation of vascular and neural invasion in colorectal cancer. Pathol. Res. Pract. 189, 443–447 (1993).
139. Matsushima, T., Mori, M., Kido, A., Adachi, Y. & Sugimachi, K. Preoperative estimation of neural invasion in rectal carcinoma. Oncol. Rep. 5, 73–76 (1998).
140. Moore, P. A., Dilawari, R. A. & Fidler, W. J. Adenocarcinoma of the colon and rectum in patients less than 40 years of age. Am. Surg. 50, 10–14 (1984).
141. Zhou, Z.-H., Xu, G.-F., Zhang, W.-J., Zhao, H.-B. & Wu, Y.-Y. Reevaluating significance of perineural invasion in gastric cancer based on double immunohistochemical staining. Arch. Pathol. Lab. Med. 138, 229–234 (2014).
142. Takahashi, T., Ishikura, H., Kato, H., Tanabe, T. & Yoshiki, T. Intra-pancreatic, extra-tumoral perineural invasion (nex). An indicator for the presence of retroperitoneal neural plexus invasion by pancreas carcinoma. Acta Pathol. Jpn. 42, 99–103 (1992).
143. Liang, D. et al. New insights into perineural invasion of pancreatic cancer: More than pain. Biochim. Biophys. Acta 1865, 111–122 (2016).
144. Groot, V. P. et al. Implications of the Pattern of Disease Recurrence on Survival Following Pancreatectomy for Pancreatic Ductal Adenocarcinoma. Ann. Surg. Oncol. 25, 2475–2483 (2018).
145. Sahin, I. H., Elias, H., Chou, J. F., Capanu, M. & O'Reilly, E. M. Pancreatic adenocarcinoma: insights into patterns of recurrence and disease behavior. BMC Cancer 18, 769 (2018).
146. Hutchings, D. et al. Cancerization of the Pancreatic Ducts: Demonstration of a Common and Un-

der-recognized Process Using Immunolabeling of Paired Duct Lesions and Invasive Pancreatic Ductal Adenocarcinoma for p53 and Smad4 Expression. Am. J. Surg. Pathol. 42, 1556–1561 (2018).
147. Noë, M. et al. Immunolabeling of Cleared Human Pancreata Provides Insights into Three-dimensional Pancreatic Anatomy and Pathology. Am. J. Pathol. (2018) doi:10.1016/j.ajpath.2018.04.002.
148. Haffner, M. C. et al. Molecular evidence that invasive adenocarcinoma can mimic prostatic intraepithelial neoplasia (PIN) and intraductal carcinoma through retrograde glandular colonization. J. Pathol. 238, 31–41 (2016).
149. De Marzo, A. M., Haffner, M. C., Lotan, T. L., Yegnasubramanian, S. & Nelson, W. G. Premalignancy in Prostate Cancer: Rethinking What we Know. Cancer Prev. Res. 9, 648–656 (2016).
150. Hong, S.-M. et al. Vascular invasion in infiltrating ductal adenocarcinoma of the pancreas can mimic pancreatic intraepithelial neoplasia: a histopathologic study of 209 cases. Am. J. Surg. Pathol. 36, 235–241 (2012).
151. Yamada, M. et al. Microscopic Venous Invasion in Pancreatic Cancer. Ann. Surg. Oncol. 25, 1043–1051 (2018).
152. Suenaga, M. et al. Pattern of first recurrent lesions in pancreatic cancer: hepatic relapse is associated with dismal prognosis and portal vein invasion. Hepatogastroenterology 61, 1756–1761 (2014).
153. Hamada, Y. & Nakayama, Y. Aggressive venous invasion in the area of carcinoma correlates with liver metastasis as an index of metastasis for invasive ductal carcinoma of the pancreas. Pancreatology 17, 951–955 (2017).
154. Munzone, E. et al. Prognostic relevance of peritumoral vascular invasion in immunohistochemically defined subtypes of node-positive breast cancer. Breast Cancer Res. Treat. 146, 573–582 (2014).
155. Hwang, K.-T. et al. The influences of peritumoral lymphatic invasion and vascular invasion on the survival and recurrence according to the molecular subtypes of breast cancer. Breast Cancer Res. Treat. 163, 71–82 (2017).
156. Sabatier, R. et al. Peritumoural vascular invasion: a major determinant of triple-negative breast cancer outcome. Eur. J. Cancer 47, 1537–1545 (2011).
157. Klingen, T. A. et al. Tumour cell invasion into blood vessels is significantly related to breast cancer subtypes and decreased survival. J. Clin. Pathol. 70, 313–319 (2017).
158. Fujii, T. et al. Impact of the prognostic value of vascular invasion, but not lymphatic invasion, of the primary tumor in patients with breast cancer. Anticancer Res. 34, 1255–1259 (2014).
159. Messenger, D. E., Driman, D. K. & Kirsch, R. Developments in the assessment of venous invasion in colorectal cancer: implications for future practice and patient outcome. Hum. Pathol. 43, 965–973 (2012).
160. Betge, J. et al. Intramural and extramural vascular invasion in colorectal cancer: prognostic significance and quality of pathology reporting. Cancer 118, 628–638 (2012).
161. Hwang, C. et al. Venous Invasion in Colorectal Cancer: Impact of Morphologic Findings on Detection Rate. Cancer Res. Treat. 48, 1222–1228 (2016).
162. Gresta, L. T., Rodrigues-Júnior, I. A., de Castro, L. P. F., Cassali, G. D. & Cabral, M. M. D. Á. Assessment of vascular invasion in gastric cancer: a comparative study. World J. Gastroenterol. 19, 3761–3769 (2013).
163. Inada, K., Shimokawa, K., Ikeda, T. & Ozeki, Y. The clinical significance of venous invasion in cancer of the stomach. Jpn. J. Surg. 20, 545–552 (1990).
164. Setälä, L. P. et al. Prognostic factors in gastric cancer: the value of vascular invasion, mitotic rate and lymphoplasmacytic infiltration. Br. J. Cancer 74, 766–772 (1996).
165. Bluemke, D. A. et al. Potentially resectable pancreatic adenocarcinoma: spiral CT assessment with surgical and pathologic correlation. Radiology 197, 381–385 (1995).
166. Lee, E. S. & Lee, J. M. Imaging diagnosis of pancreatic cancer: a state-of-the-art review. World J. Gastroenterol. 20, 7864–7877 (2014).
167. Wang, S.-H., Sun, Y.-F., Liu, Y., Zhou, Y. & Liu, Y. CT contrast enhancement correlates with pathological grade and microvessel density of pancreatic cancer tissues. Int. J. Clin. Exp. Pathol. 8, 5443–5449 (2015).
168. Boudreaux, J. P. et al. The NANETS consensus guideline for the diagnosis and management of neuroendocrine tumors: well-differentiated neuroendocrine tumors of the Jejunum, Ileum, Appendix, and Cecum. Pancreas 39, 753–766 (2010).
169. Niederle, B. et al. ENETS Consensus Guidelines Update for Neuroendocrine Neoplasms of the Jejunum and Ileum. Neuroendocrinology 103, 125–138 (2016).
170. Loehrer, A. P. et al. Health Insurance Expansion and Treatment of Pancreatic Cancer: Does Increased Access Lead to Improved Care? J. Am. Coll. Surg. 221, 1015–1022 (2015).

Part 3

Pancreatic neuroendocrine neoplasms

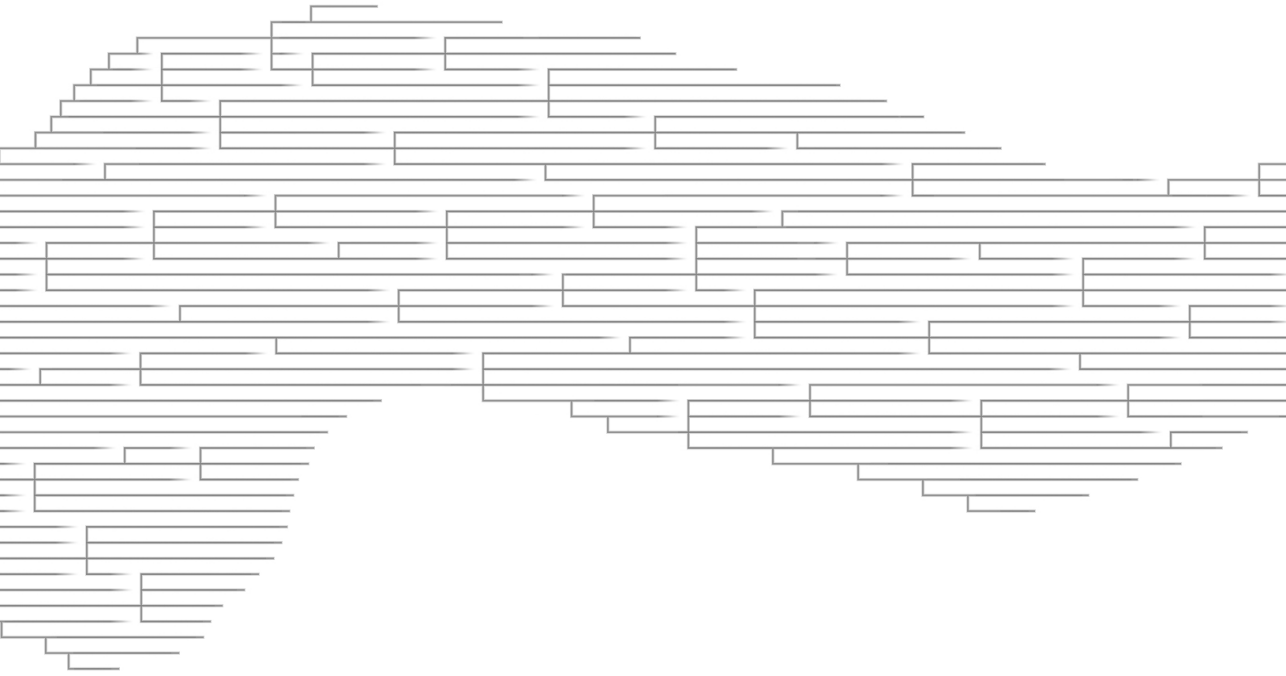

Chapter 11

Genetic analysis of small well-differentiated pancreatic neuroendocrine tumors identifies subgroups with differing risks of liver metastases

Antonio Pea, Jun Yu, Luigi Marchionni, Michaël Noë, Claudio Luchini, Alessandra Pulvirenti, Roeland F. de Wilde, Lodewijk A.A. Brosens, Neda Rezaee, Ammar Javed, Stefano Gobbo, Paolo Regi, Roberto Salvia, Claudio Bassi, Jin He, Matthew J. Weiss, John L. Cameron, G. Johan A. Offerhaus, Ralph H. Hruban, Rita T. Lawlor, Aldo Scarpa, Christopher M. Heaphy, Laura D. Wood, Christopher L. Wolfgang

Annals of Surgery, October 2018

ABSTRACT

Objective: The aim of this study was to investigate the key molecular alterations in small primary pancreatic neuroendocrine tumors (PanNETs) associated with the development of liver metastases.
Background: Well-differentiated PanNETs with small size are typically indolent; however, a limited subset metastasize to the liver.
Methods: A total of 87 small primary PanNETs (<3 cm), including 32 metastatic cases and 55 nonmetastatic cases after a 5-year follow-up, were immunolabeled for DAXX/ATRX and analyzed for alternative lengthening of telomeres (ALT) by Fluorescence In Situ Hybridization. A subset of these cases, 24 that metastasized and 24 that did not metastasize, were assessed by targeted next-generation sequencing and whole-genome copy number variation.
Results: In the entire cohort, high Ki-67 (OR 1.369; 95% CI 1.121–1.673; P = 0.002), N-stage (OR 4.568; 95% CI 1.458–14.312; P = 0.009), and ALT-positivity (OR 3.486; 95% CI 1.093–11.115; P = 0.035) were independently associated with liver metastases. In the subset assessed by next-generation sequencing and copy number variation analysis, 3 molecular subtypes with differing risks of liver metastases were identified. Group 1 (n = 15; 73% metastasized) was characterized by recurrent chromosomal gains, CN-LOH, *DAXX* mutations, and ALT-positivity. Group 2 (n = 19; 42% metastasized, including 5 G1 tumors) was characterized by limited copy number alterations and mutations. Group 3 (n = 14; 35% metastasized) were defined by chromosome 11 loss.
Conclusions: We identified genomic patterns of small PanNETs associated with a different risk for liver metastases. Molecular alterations, such as *DAXX* mutations, chromosomal gains, and ALT, are associated with an increased risk of metastasis in small PanNETs. Therefore, targeted sequencing and/or ALT analysis may help in the clinical decisions for these small PanNETs.

INTRODUCTION

The incidence of pancreatic neuroendocrine tumors (PanNETs) is 1 per 100,000 individuals.[1] However, autopsy studies highlight a prevalence ranging from 1% to 10% in the general population, suggesting that most PanNETs do not progress to clinical diagnosis.[2,3] In recent years, an increasing number of small and asymptomatic PanNETs have been diagnosed incidentally on routine abdominal imaging.[4] As the risk for metastases has been associated with tumor size and high proliferative index, periodic observation without resection has been advocated for small tumors.[5–7] However, such observational approaches have not been universally adopted, due to a small, but existing risk of liver metastases among small tumors, particularly with the absence of biomarkers predictive for progression.[8,9]

Recent whole genome sequencing and expression profiling suggest that an aggressive phenotype is associated with genetic changes in telomere maintenance and/or mTOR signaling.[10–12] Loss of function of DAXX or ATRX genes promotes the activation of the alternative lengthening of telomeres (ALT) pathway.[13,14] ALT is associated with chromosomal instability, larger tumor size, higher Ki67 and, in some studies, metastatic spread.[10,15,16] Alterations in mTOR pathway genes are also associated with a poor prognosis and several therapeutic agents targeting the pathway are available for systemic treatment.[10,17–19]

Thus, there is an urgent need to define early biological mechanisms responsible for tumor progression that may serve as clinically useful biomarkers. Here, we analyzed molecular alterations of small sporadic well-differentiated PanNETs (<3 cm in size) to identify alterations associated with metastasis. In the entire cohort of 87 primary PanNETs, we assessed ATRX and DAXX protein expression, and ALT status. In a subset, 24 primary PanNETs that metastasized and 24 primary PanNETs that did not metastasize, matched for size and proliferation index, were analyzed by targeted next-generation sequencing and for copy number alterations. These genomic analyses identified 3 molecular subtypes with differing risks for liver metastases.

METHODS

Study population

This study was approved by the Institutional Review Board (IRB) of the Johns Hopkins Hospital and tissue samples were retrieved from collaborating institutes with informed consent according to their local Institutional Review Boards. Well-differentiated (G1 and G2) PanNETs < 3 cm in maximum dimension were identified in the pancreatic resection databases of the Johns Hopkins Hospital, University of Verona, Italy; University of Utrecht, The Netherlands; Pederzoli Hospital, Peschiera, Italy. All PanNETs included were sporadic, unifocal, and nonfunctional. The study included patients who developed synchronous or metachronous liver metastases and patients who did not develop distant metastases after a surveillance period of at least 5 years. PanNETs were graded according to the 2017 World Health Organization (WHO) classification based on mitotic rate and Ki-67: < 2 mitoses/10 high-power fields

and Ki-67 < 3% for grade 1 (G1), and 2 to 20 mitoses/10 high-power fields, and Ki-67 of 3% to 20% for grade 2 (G2).[20]

Immunohistochemistry (IHC) and Fluorescence In Situ Hybridization (FISH)

IHC for ATRX and DAXX and telomere-specific FISH were performed on formalin-fixed paraffin-embedded (FFPE) tissues. Nuclear labeling was evaluated for DAXX and ATRX and cases were scored as negative if nuclear expression was completely lost (despite retaining cytoplasmic expression) and adequate internal positive controls were present (eg, nuclear labeling of endothelial cells, lymphocytes, islets of Langerhans).[13,21,22] ALT-positive tumors were identified by cell-to-cell telomere length heterogeneity and the presence of large, ultrabright nuclear foci of FISH signals. As previously defined,[13,14,22] cases were classified as ALT-positive when bright nuclear foci occurred in 1% of tumor cells with at least 500 neoplastic cells evaluated.

DNA extraction

Five micrometer sections from FFPE tissues were manually macrodissected to enrich for neoplastic cellularity, DNA was extracted using QIAamp DNA FFPE Tissue Kit (Qiagen, Germantown) and quantified by Quantifiler Human DNA Quantification kit (Applied Biosystems, Thermo Fisher Scientific, Waltham).

Targeted Next-generation Sequencing

An Ion AmpliSeq Custom Panel (AmpliSeq Designer version 4.4.7; Life Technologies, Thermo Fisher Scientific, Waltham) was used to perform multiplex PCR and sequencing of 18 genes known to be targeted in pancreatic neuroendocrine or ductal neoplasms (*MEN1*, *DAXX*, *ATRX*, *TSC1*, *TSC2*, *PTEN*, *PIK3CA*, *PHLDA3*, *TP53*, *KRAS*, *GNAS*, *SMAD4*, *CDKN2A*, *RNF43*, *TGFBR2*, *ARID1A*, *BRAF*, *MAP2K4*).[10,12,23,24] Briefly, DNA (4 ng) was amplified using Ampliseq reagents for library preparation, which was then loaded and sequenced onto a 318v2 chips using an Ion Torrent Personal Genome Machine (PGM; Life Technologies). Postsequencing data analyses, including alignment to the hg19 human reference genome and variant calling, were performed using NextGENe software (v2.4; SoftGenetics, Chicago, IL). Alignments and putative mutations were visually verified using the Integrative Genomics Viewer (IGV, v2.3; Broad Institute, Cambridge) and the NextGENeViewer (v2.4; SoftGenetics).

SNP Array Analysis

Copy number analysis was performed at the JHU Microarray Core Facility using the Illumina HumanCytoSNP-12 v2.1 BeadChip, according to manufacturer's protocols. Log R ratios (LRRs) and B allele frequencies for each sample were extracted using GenomeStudio software. Prior copy number analysis, LRRs were normalized performing a GC-content correction.[25] We used the Circular Binary Segmentation algorithm to estimate mean LRR for distinct genomic segments, and we applied a mixture model to compute copy number alteration probabilities and to classify each segment accordingly, as implemented in the "CGHcall" and "CGHregion" R-Bioconductor packages.[24,25] Sex chromosomes were not included in this analysis and tumor cellularity was estimated using the "qPure" algorithm.[26] We

used the hg19 human reference genome assembly (GRCh37) to annotate segments of copy number alteration with the associated genes. For regions of normal copy number, we further analyzed the B allele frequency distribution, identifying copy neutral loss of heterozygosis (CN-LOH, loss of 1 allele with duplication of the remaining allele). Chromothripsis was defined as the shattering and reassembly of 1 or more chromosomes and was detected using the CTLP Scanner algorithm.[27]

Statistical Analysis

Continuous variables were reported as median and interquartile range or mean and standard deviation according to the values distribution. Correlation between clinical-pathological characteristics with ALT phenotype and development of liver metastases was assessed by univariate analysis using chi-square test or Fisher exact tests for categorical variables, and Student t test or Mann–Whitney U for continuous variables. A forward stepwise logistic regression model was used to evaluate independent risk factors associated with development of liver metastasis. A 2-tailed P value ≤ 0.05 was considered significant. Data were analyzed using SPSS 24.0 for Windows v24.0.

RESULTS

As illustrated in Figure 1, 87 patients who underwent pancreatectomy for unifocal, well-differentiated primary PanNET < 3 cm in size met the inclusion criteria. These included 32 patients who developed

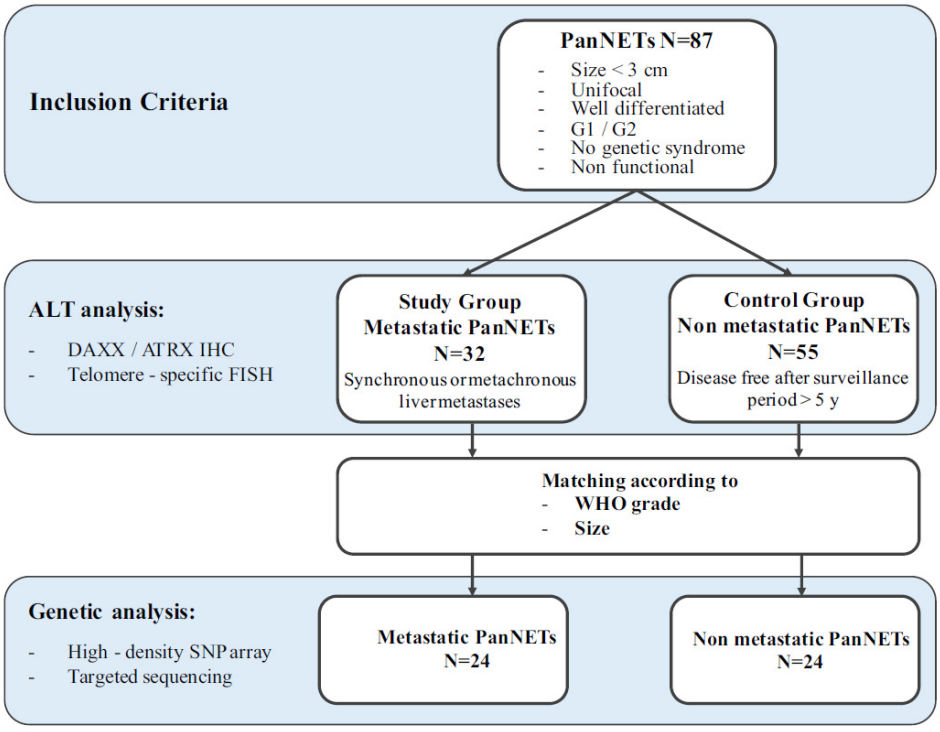

Figure 1. Study workflow

liver metastases (19 synchronous, 13 metachronous), and 55 patients who remained disease-free after at least 5 years of follow-up (mean 117 mo, standard deviation 58 mo).

PanNETs were treated by distal pancreatectomy in 47 patients, pancreatoduodenectomy in 36, and enucleation in 4. There were 54 (62.1%) G1 and 33 (37.9%) G2 tumors (Table 1). Lymphovascular and perineural invasion were present in 19 (21.8%) and 26 (29.9%) tumors, respectively; AJCC stage[28] was T1 for 36 (41.4%), T2 for 31 (35.6%), and T3 for 20 (23.0%) tumors. Regional lymph node metastases were present in 29 (33.3%) tumors.

		ALT n = 85		*P*	Liver Metastases n = 87		
Variables	**All Patients n = 87**	**Negative n = 58**	**Positive n = 27**		**No n = 55**	**Yes n = 32**	***P***
Male, no. (%)	44 (50.6)	32 (55.2)	12 (44.4)	0.485	27 (49.1)	17 (53.1)	0.825
Age, mean (SD), yr	57 (12)	57 (17)	57 (19)	0.884	58 (12)	56 (13)	0.483
Location of tumor				0.643			0.115
Head and uncinate, no. (%)	36 (41.4)	25 (43.1)	10 (37.0)		19 (34.5)	17 (53.1)	
Body and tail, no. (%)	51 (58.6)	33 (56.9)	17 (63)		15 (46.9)	36 (65.5)	
Tumor size, median (IQR), cm	2.2 (1.1)	2.0 (1.1)	2.5 (0.9)	0.070	2.0 (1.1)	2.5 (0.8)	**0.010**
Size				0.098			**0.023**
≤1 cm	6 (6.9)	6 (10.3)	0 (0.0)		6 (10.9)	0 (0)	
1–2 cm	36 (41.4)	25 (43.1)	9 (33.3)		26 (47.3)	10 (31.3)	
>2 cm	45 (51.7)	27 (46.6)	18 (66.7)		23 (41.8)	22 (68.8)	
Ki67 index %, median (IQR)	2.0 (3.3)	1.2 (2.3)	4.0 (4.3)	**0.001**	1.0 (2.1)	4.2 (6.7)	**≤0.001**
WHO grade				**0.004**			**0.001**
G1, no. (%)	54 (62.1)	42 (72.4)	10 (37.0)		42 (76.4)	12 (37.5)	
G2, no. (%)	33 (37.9)	16 (27.6)	17 (63.0)		13 (23.6)	20 (62.5)	
Lymphovascular invasion, no. (%)	19 (21.8)	8 (13.8)	11 (40.7)	**0.010**	8 (14.5)	11 (34.4)	0.057
Perineural invasion, no. (%)	26 (29.9)	10 (17.2)	15 (55.6)	**0.001**	10 (18.2)	16 (50)	**0.003**
T stage, no. (%)				0.210			0.215
T1 stage, no. (%)	36 (41.4)	26 (44.8)	10 (37.0)		26 (47.3)	10 (31.3)	
T2 stage, no. (%)	31 (35.6)	17 (29.3)	13 (48.1)		16 (29.1)	15 (46.9)	
T3 stage, no. (%)	20 (23.0)	15 (25.9)	4 (14.8)		13 (23.6)	7 (21.9)	
N stage, no. (%)				**0.007**			**≤0.001**
Nx-0 stage, no. (%)	58 (66.7)	44 (75.9)	12 (44.4)		45 (81.8)	13 (40.6)	
N1 stage, no. (%)	29 (33.3)	14 (24.1)	15 (55.6)		10 (18.2)	19 (59.4)	
Liver metastases, no. (%)	32 (36.8)	14 (24.1)	18 (66.7)	**≤0.001**			
ALT pos, no. (%)	27/85 (31.8)				9/53 (17)	18/32 (56.3)	**≤0.001**
DAXX neg, no. (%)	20/84 (23.8)	1 (1.8)	19 (70.4)	**≤0.001**	7/52 (13.5)	13/32 (40.6)	**0.008**
ATRX neg, no. (%)	6/85 (7.1)	0 (0)	6 (22.2)	**0.001**	3/53 (5.7)	3/32 (9.4)	0.668

P values in bold represent significant statistical differences.

Table 1. Univariate analysis of clinical, pathological, and biomarker data associated with liver metastases.

DAXX/ATRX immunolabeling and ALT analysis

Immunolabeling for ATRX and DAXX and telomere-specific FISH analysis to detect ALT-positive tumors was performed on 85 of the 87 cases. For 2 cases, the material available for research purposes was limited and only used in the genomic analyses. Loss of DAXX or ATRX was detected respectively in 20/85 (23.5%, 13 metastatic and 7 nonmetastatic) and 6/85 (7.1%, 3 metastatic and 3 nonmeta-

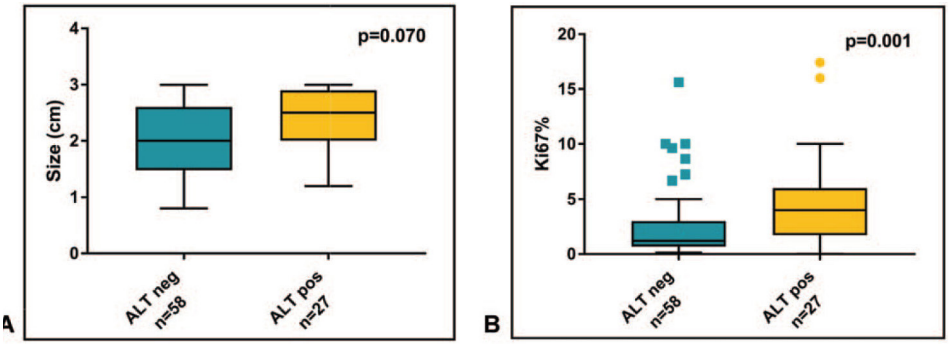

Figure 2. Tumor size (**a**) and Ki67% (**b**) stratified by ALT status. Box and whisker plots depict median and 10 to 90 percentile ranges.

static) tumors; the loss of protein expression in either ATRX or DAXX was mutually exclusive. Twenty-seven of the 85 tumors were ALT-positive (31.8%, 18 metastatic and 9 nonmetastatic). By univariate analysis, ALT was strongly associated with loss of DAXX or ATRX nuclear expression (P < 0.001 and P = 0.001, respectively), Ki-67 index (Figure 2, P = 0.001) and WHO grade (P = 0.004). In all but 3 cases, results from IHC and ALT assessment were concordant. Discordant cases included 2 ALT-positive cases with retention of DAXX and ATRX protein expression, and 1 case with loss of nuclear DAXX expression without concurrent ALT.

Variables	OR	IC 95%	*P*
Ki-67	1.369	1.121 to 1.673	0.002
N stage (N1)	4.568	1.458 to 14.312	0.009
ALT positivity	3.486	1.093 to 11.115	0.035

Table 2. Multivariate analysis of clinical, pathological, and biomarker data associated with liver metastases.

Clinicopathological features associated with the development of liver metastases in univariate analysis were larger tumor size as a continuous (P = 0.010) and as a categorical (P = 0.023) variable, Ki-67 index (P < 0.001), WHO grade (P = 0.001), ALT positivity (P < 0.001), and DAXX loss (P = 0.008). On multivariate analysis, only Ki-67 index (OR 1.369; 95% CI 1.121–1.673; P = 0.002), N stage (OR 4.568; 95% CI 1.458–14.312; P = 0.009), and ALT positivity (OR 3.486; 95% CI 1.093–11.115; P = 0.035) were confirmed to be independent risk factors for liver metastases (Table 2).

Mutational and Copy Number Analysis

Genetic analyses were performed on a subset of these cases, which included 48 primary PanNETs, of which 24 from the metastatic group, from which the extracted DNA passed the quality controls, and 24 from the control group matched for tumor size and WHO grade (Table 1, Supplemental material, http://links.lww.com/SLA/B503).

Targeted next-generation sequencing detected a total of 38 somatic mutations in 7 genes among the 48 tumors, with a range of 0 to 3 mutations per tumor (Figure 3). *MEN1* was mutated in 16 (33%) cases and mTOR pathway genes were mutated in 10 cases, more specifically *TSC2* in 9 cases (19%) and *PTEN* in 1 case (2%). *DAXX* was mutated in 9 cases (19%) and *ATRX* in 1 (2%). *TP53* and *CDKN2A* were mutated in 1 case (2%) each. Comparison of mutations with metastatic status showed that *MEN1* was mutated in 9 metastatic and 7 nonmetastatic cases, *TSC2* in 6 metastatic and 3 nonmetastatic, *ATRX* and *CDKN2A* were mutated in 1 nonmetastatic case each, and *PTEN* and *TP53* were mutated in 1 metastatic case each. Strikingly, *DAXX* was mutated in 8 metastatic cases and 1 nonmetastatic case (P = 0.023). Genome-wide SNP array analysis revealed large chromosomal events including recurrent regions of gain and loss. All chromosomal alterations, along with associated genes and noncoding re-

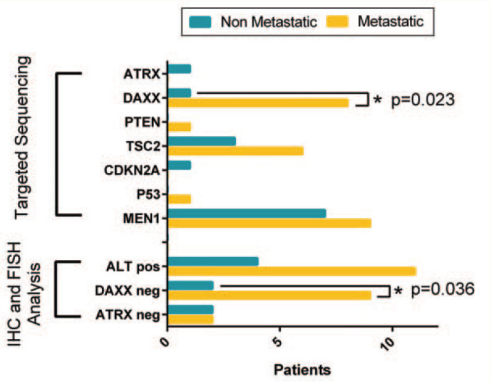

Figure 3. Somatic mutations, ATRX/DAXX protein expression, and ALT status in metastatic and nonmetastatic PanNETs.

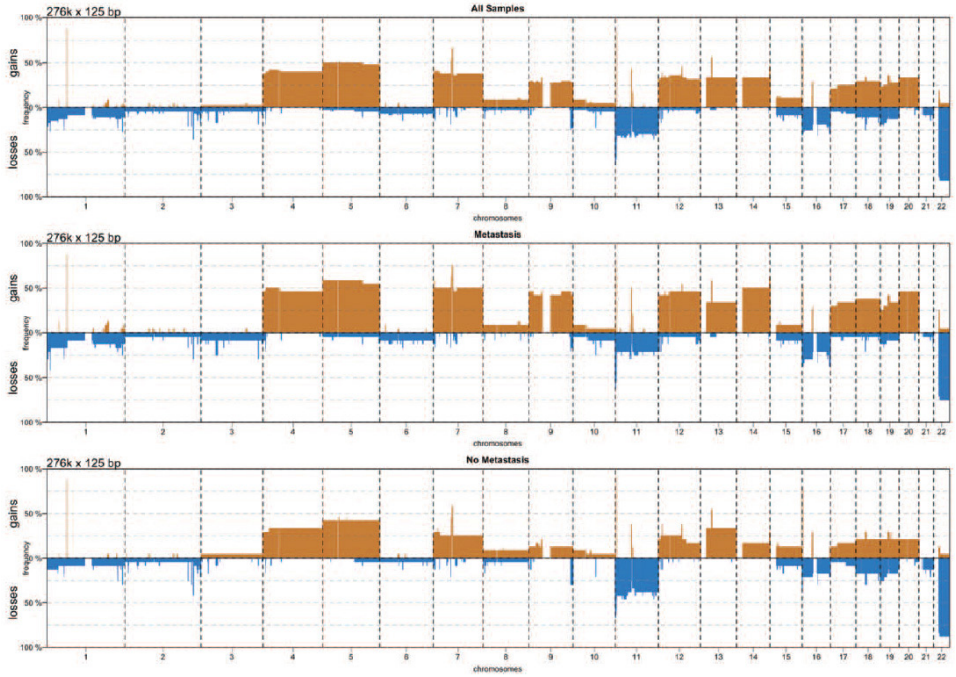

Figure 4. Rate of chromosomal gains (red) and losses (blue) per chromosome in metastatic and nonmetastatic PanNETs.

gions, are listed in Supplementary Dataset S1, http://links.lww.com/SLA/B502. Tumors that metastasized were characterized by a higher prevalence of chromosomal gains (1046 regions of gain vs. 661), while nonmetastatic tumors had more chromosomal losses (756 regions of loss vs. 701). Copy number alterations consisted in broad genomic regions generally spanning entire chromosomes (Figure 4). The most frequent chromosomal gains involved chromosomes 4, 5, 7, 9, 14, 18, and 19 with frequencies ranging from 25% to 50%, while recurrent chromosomal losses were detected in chromosomes 11, 16, and 22 with frequencies ranging from 25% to 75% (Figure 4). PanNETs with frequent chromosomal gains also exhibited recurrent CN-LOH events, involving the other chromosomes (Supplementary Dataset S2, http://links.lww.com/SLA/B502).

Chromosome 11q13.1 containing the *MEN1* locus was lost in 16 cases (33%), while several regions previously described to be gained in PanNETs were also identified in our study: *ERBB2* (chr 17q12) in 12 (25%) cases, *PSPN* (chr 19p13.3) in 10 (21%), and *ULK1* (chr 12q24.33) in 15 (31%). *AKT2* (chr 19q13.2), a serine/threonine-protein kinase that inactivates *TSC2* and therefore upregulates the mTORC1 complex, was amplified in 12 cases (25%), none of which harboring a *TSC2* mutation.

Chromothripsis was detected at chromosome 11 in 4 cases (PanNET2, 11, 27, and 37); at chr 7 in 7 cases (PanNET4, 11, 15, 23, 26, 30, 46); and at chr 9 in PanNET46.

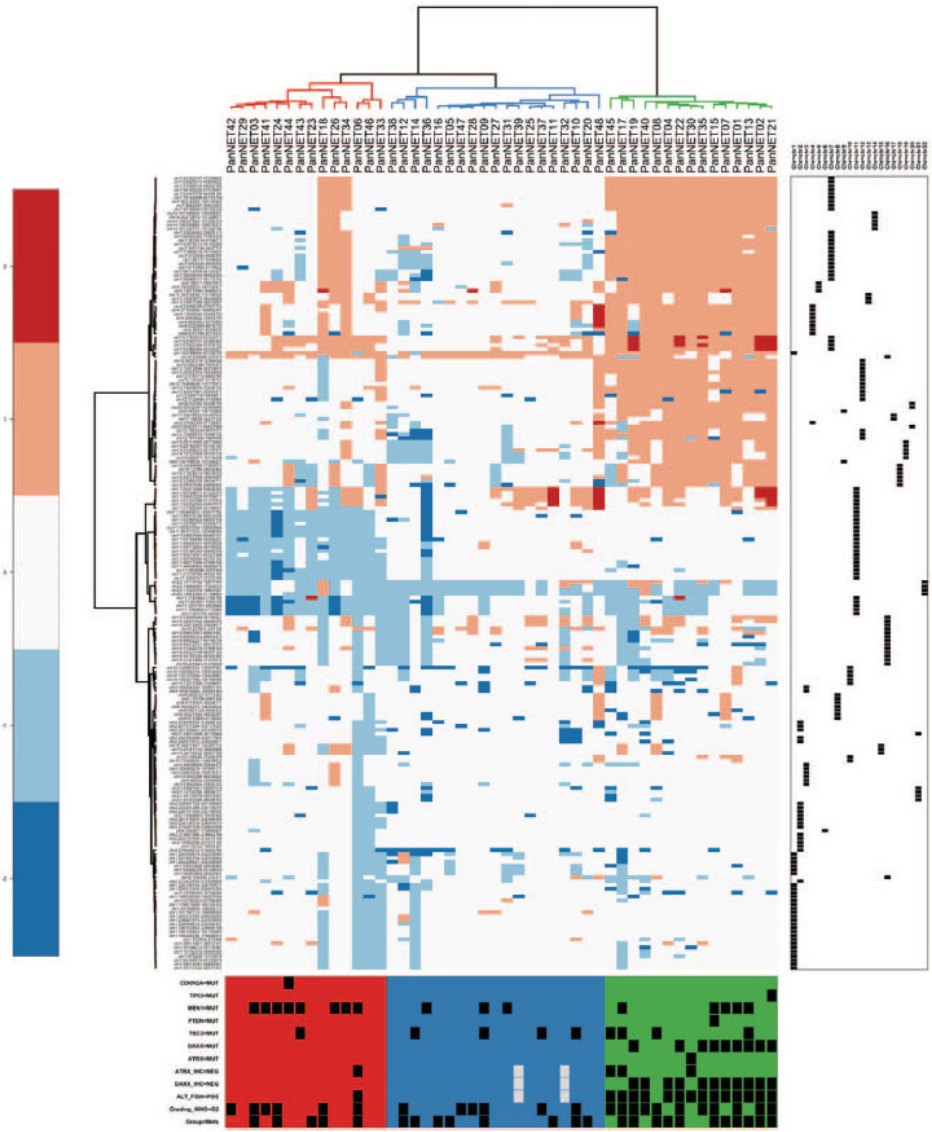

Figure 5. Cluster analysis of the copy number state stratified the tumors into 3 different subtypes characterized by different mutational and clinical patterns (as shown at the bottom). Hierarchical clustering was based on copy number alterations, using the Manhattan distance and the Ward clustering method.

Genomic Subtypes

Cluster analysis of copy number status stratified the tumors into 3 different molecular subtypes on the basis of recurrent chromosomal alterations (Figure 5): Group 1, characterized by chromosomal gains; Group 2, with limited number of chromosomal events; Group 3, presenting a recurrent pattern of chromosome loss, mainly affecting chromosomes 11 and 22. Integrating copy number alterations, single nucleotide variants, and ALT status revealed distinct molecular and clinical patterns for each subtype. Overall, Group 1 was strongly associated with metastases compared with the other groups combined (chi-squared test, $P < 0.03$).

Group 1 included 15 PanNETs that, all except one (PanNET8), were ALT-positive. Strikingly, 14 cases lacked DAXX or ATRX protein expression (respectively in 11 and 3 cases), which was due to mutations in 10 cases (*DAXX* in 9, *ATRX* in 1). As expected, all cases that were wild type at the genetic level for *ATRX* and *DAXX* retained nuclear protein expression. *MEN1* was mutated in 5 cases and mTOR pathway genes in 5 cases (*TSC2* in 4, *PTEN* in 1). The majority of Group 1 tumors were G2 (11/15) and 73% (11/15) were metastatic.

Group 2 included 19 cases characterized by limited copy number and mutational events. *TSC2* and *MEN1* were mutated in 4 (21%) and 3 (16%) cases, respectively. All cases were ALT-negative, wild-type for the *ATRX*/*DAXX* genes, and preserved nuclear ATRX/DAXX protein expression. In this group, 42% (8/19) of tumors developed metastases, including 5 G1 and 3 G2 tumors.

Group 3 included 14 cases, all exhibiting recurrent loss of chromosome 11q *MEN1* locus and associated with *MEN1* somatic mutations in 8 (57%) cases. *TSC2* and *CDKN2A* were mutated in 1 case each. Only 1 G2 case that metastasized (PanNET6) was ALT-positive and displayed loss of nuclear ATRX protein expression. In this group, 35% (5/14) of the tumors were metastatic (4 G2 cases and 1 G1).

DISCUSSION

PanNETs are characterized by a variable spectrum of clinical behavior.[20] Several lines of evidence suggest that most small primary PanNETs are indolent tumors, supporting the idea that surveillance, rather than surgical resection, could be indicated.[4,8,29,30] However, a limited subset of small primary PanNETs are aggressive and will metastasize, predominantly to the liver. The discrimination of small PanNETs with a high risk of metastasis from those with low risk has important prognostic and therapeutic implications. First, we evaluated clinicopathological features and several tissue-based biomarkers in a cohort of 87 primary well-differentiated PanNETs that were all <3 cm in size. We observed that high Ki-67 (OR 1.369), N-stage (OR 4.568), and ALT-positivity (OR 3.486) were independently associated with liver metastases. While our cohort was limited to small PanNETs, these findings are similar to other recent studies assessing cohorts encompassing the entire range of tumor sizes.[15,16,22] Next, vailing of a recent whole genome sequencing study,[10] we investigated a series of small primary PanNETs (<3 cm) using whole genome copy number analysis and targeted deep sequencing of 18 relevant genes to assess the genetic alterations associated with metastatic spread. To this end, we compared the genetic alterations in small primary PanNETs that developed liver metastases with those that were metastases-free after a long post-resection follow-up period. We identified 3 different molecular subtypes of small primary PanNETs on the basis of the copy number status, matching those recently described in Scarpa et al,[10] which were also characterized by different mutational and clinical features.

In Group 1, a large proportion (11/15, 73%) of tumors were metastatic. The defining molecular features of these tumors were recurrent chromosomal gains, CN-LOH, and a high rate of somatic mutations in the driver genes in our targeted panel. In addition, 14 (of 15) cases were also ALT-positive and all

cases displayed loss of either DAXX or ATRX nuclear protein expression and inactivating mutations in either *DAXX* or *ATRX* were observed in 10 of 15 cases, indicating the presence of other possible mechanisms of loss, such as complex karyotype rearrangements in ALT-positive PanNETs.[10] We observed 3 ALT-positive cases, not included in the genetic analysis, which retained DAXX and ATRX nuclear protein expression. These observations may indicate potential additional biological mechanisms, independent of DAXX and ATRX, that promote ALT in a minority of cases, or by genetic alterations conferring a loss-of-function of either *DAXX* and *ATRX* (eg, missense mutations), but not loss of nuclear protein expression.[13,15,16,22,31] In this study, we observed an almost perfect correlation between recurrent patterns of chromosomal gains and ALT, suggesting that chromosomal gains may represent an early stage of genomic instability associated with ALT. Previous studies that investigated ALT prevalence in large cohorts of resected PanNETs described a direct correlation between ALT and larger size or higher grade.[16,21,22] In our series of small primary PanNETs that metastasized, most of the ALT-positive tumors were G2, suggesting that either ALT increases cell proliferation and metastatic potential or that a high proliferative index in PanNETs increases the probability of acquiring the requisite mutations that promote ALT. Interestingly, *TSC2* was mutated in 4 cases (27%), however, all the remnant tumors in Group 1 with wild-type *TSC2* showed copy number gains of chromosome 19q (11/15, 73%), suggesting that potential proto-oncogenes functioning in the mTOR pathway may be located in this region. One possible candidate is *AKT2*, which may upregulate the mTORC1 complex when TSC2 function is retained.[32,33]

In Group 2, a proportion (8/19, 42%) of tumors were metastatic, despite having a low proliferative index in the majority of cases. This group included the majority of G1 metastatic tumors (5 of 9 G1 metastatic PanNETs, 55%). Interestingly, these tumors were characterized by the presence of few mutations and limited chromosomal alterations.

In Group 3, tumors were characterized by frequent biallelic inactivation of *MEN1* and the lowest metastatic potential. In total, PanNETs in our series harbored *MEN1* locus alterations in 69% (33/48) of cases, including chromosomal loss, CN-LOH or chromotripsis, and *MEN1* somatic mutations in 33% (16/48) of cases, which were distributed mainly between Groups 1 and 3. Our data do not provide strong evidence supporting an interaction between *MEN1* and the ALT pathway. However, since menin has a critical role in the biology of telomeres by negatively regulating telomerase,[34,35] it is tempting to speculate that tumors at an early disease stage with partial or complete loss of menin may use upregulated telomerase for telomere maintenance, and thus do not require the ALT pathway.

While ALT and *ATRX*/*DAXX* alterations play pivotal roles in the progression of a subset of PanNETs, metastatic tumors are present also in the other subtypes and the absence of recurrent genetic changes in Groups 2 and 3 suggests that additional biological mechanisms, or genetic alterations not included in our analysis, may contribute to neoplastic progression in these groups. Limitations of our approach were represented by the relatively limited size of the study cohort and by the absence of confirmation of our results in an independent dataset, which are direct consequences of designing our study around

rigorous clinical case selection. Our cohort included patients with either synchronous or metachronous liver metastases; we therefore cannot exclude the possibility that additional genetic alterations occurred after the development of metastatic disease in PanNETs with synchronous metastases. However, in our cohort, no substantial genetic differences were observed between PanNETs with metachronous or synchronous metastases (see Supplementary material, http://links.lww.com/SLA/B503), while we observed a high allele frequency for each mutation indicating that these alterations are present in the majority of neoplastic clones of the primary tumor, regardless of the timing of metastasis. This is also consistent with previous reports evaluating ALT in the primary and metastatic lesions from the same patient indicating that molecular alterations that promote ALT occur prior to the development of metastases.[16]

Recent ENETS consensus guidelines for the management of PanNETs suggest that only asymptomatic G1 tumors <2 cm in size may be suitable for close observation, due to their very low risk of neoplastic progression.[8,36] In our cohort, biased for the development of liver metastases, 9 metastatic cases were <2 cm. While no specific genetic alterations were observed in these tumors (see Supplementary material, http://links.lww.com/SLA/B503), *DAXX* was mutated in 4 cases (3 with Ki67 <5%) highlighting its importance as potential risk-stratification biomarker. We limited our genetic analysis to copy number changes and to targeting driver genes frequently mutated in PanNETs. We did not include analysis of other genes, such as those involved in chromatin remodeling (mutated in approximately 5% of PanNETs), or those containing pathogenic germline variants thought to have a role in the development of up to 17% of sporadic PanNETs.[10] Thus, we cannot exclude that such infrequently altered genes also play some role in metastasis of small PanNETs.

In conclusion, we characterize the biological variability among morphologically similar well-differentiated PanNETs. We identified subtypes of small PanNETs characterized by distinct metastatic potential on the basis of integrated genetic and immunostaining expression data. ALT-positive tumors have the highest prevalence of metastases suggesting that ALT should be considered a potential biomarker of an aggressive phenotype among small tumors and employed for risk stratification. Importantly, NGS with targeted panels can be performed on small samples[37] and ALT can be accurately be detected on endoscopic ultrasound-guided fine needle aspiration.[31] Thus, we propose that, the concomitant integrated evaluation of targeted sequencing, Ki-67, and ALT on endoscopic ultrasound-guided fine needle aspiration specimens could guide the choice of the surgical treatment, as well as the enrollment into surveillance programs for small and asymptomatic tumors.

REFERENCES

1. Yao, J. C. et al. One hundred years after 'carcinoid': epidemiology of and prognostic factors for neuroendocrine tumors in 35,825 cases in the United States. J. Clin. Oncol. 26, 3063–3072 (2008).
2. Grimelius, L., Hultquist, G. T. & Stenkvist, B. Cytological differentiation of asymptomatic pancreatic islet cell tumours in autopsy material. Virchows Arch. A Pathol. Anat. Histol. 365, 275–288 (1975).
3. Kimura, W., Kuroda, A. & Morioka, Y. Clinical pathology of endocrine tumors of the pancreas. Analysis of autopsy cases. Dig. Dis. Sci. 36, 933–942 (1991).
4. Kuo, E. J. & Salem, R. R. Population-level analysis of pancreatic neuroendocrine tumors 2 cm or less in size. Ann. Surg. Oncol. 20, 2815–2821 (2013).
5. Partelli, S. et al. Pattern and clinical predictors of lymph node involvement in nonfunctioning pancreatic neuroendocrine tumors (NF-PanNETs). JAMA Surg. 148, 932–939 (2013).
6. Bettini, R. et al. Tumor size correlates with malignancy in nonfunctioning pancreatic endocrine tumor. Surgery 150, 75–82 (2011).
7. Vagefi, P. A. et al. Evolving patterns in the detection and outcomes of pancreatic neuroendocrine neoplasms: the Massachusetts General Hospital experience from 1977 to 2005. Arch. Surg. 142, 347–354 (2007).
8. Falconi, M. et al. ENETS Consensus Guidelines Update for the Management of Patients with Functional Pancreatic Neuroendocrine Tumors and Non-Functional Pancreatic Neuroendocrine Tumors. Neuroendocrinology 103, 153–171 (2016).
9. Haynes, A. B. et al. Implications of incidentally discovered, nonfunctioning pancreatic endocrine tumors: short-term and long-term patient outcomes. Arch. Surg. 146, 534–538 (2011).
10. Scarpa, A. et al. Whole-genome landscape of pancreatic neuroendocrine tumours. Nature (2017) doi:10.1038/nature21063.
11. Missiaglia, E. et al. Pancreatic endocrine tumors: expression profiling evidences a role for AKT-mTOR pathway. J. Clin. Oncol. 28, 245–255 (2010).
12. Jiao, Y. et al. DAXX/ATRX, MEN1, and mTOR pathway genes are frequently altered in pancreatic neuroendocrine tumors. Science 331, 1199–1203 (2011).
13. Heaphy, C. M. et al. Altered telomeres in tumors with ATRX and DAXX mutations. Science 333, 425 (2011).
14. Heaphy, C. M. et al. Prevalence of the alternative lengthening of telomeres telomere maintenance mechanism in human cancer subtypes. Am. J. Pathol. 179, 1608–1615 (2011).
15. Marinoni, I. et al. Loss of DAXX and ATRX are associated with chromosome instability and reduced survival of patients with pancreatic neuroendocrine tumors. Gastroenterology 146, 453–60.e5 (2014).
16. Singhi, A. D. et al. Alternative Lengthening of Telomeres and Loss of DAXX/ATRX Expression Predicts Metastatic Disease and Poor Survival in Patients with Pancreatic Neuroendocrine Tumors. Clin. Cancer Res. 23, 600–609 (2017).
17. Laplante, M. & Sabatini, D. M. mTOR signaling in growth control and disease. Cell 149, 274–293 (2012).
18. Yao, J. C. et al. Everolimus for advanced pancreatic neuroendocrine tumors. N. Engl. J. Med. 364, 514–523 (2011).
19. Yao, J. C. et al. Everolimus for the Treatment of Advanced Pancreatic Neuroendocrine Tumors: Overall Survival and Circulating Biomarkers From the Randomized, Phase III RADIANT-3 Study. J. Clin. Oncol. 34, 3906–3913 (2016).
20. International Agency for Research on Cancer. WHO Classification of Tumours of Endocrine Organs. (International Agency for Research on Cancer, 2017).
21. de Wilde, R. F. et al. Loss of ATRX or DAXX expression and concomitant acquisition of the alternative lengthening of telomeres phenotype are late events in a small subset of MEN-1 syndrome pancreatic neuroendocrine tumors. Mod. Pathol. 25, 1033–1039 (2012).
22. Kim, J. Y. et al. Alternative Lengthening of Telomeres in Primary Pancreatic Neuroendocrine Tumors Is Associated with Aggressive Clinical Behavior and Poor Survival. Clin. Cancer Res. 23, 1598–1606 (2017).
23. Pea, A. et al. Targeted DNA Sequencing Reveals Patterns of Local Progression in the Pancreatic Remnant Following Resection of Intraductal Papillary Mucinous Neoplasm (IPMN) of the Pancreas. Ann. Surg. (2016) doi:10.1097/SLA.0000000000001817.
24. Luchini, C. et al. Pancreatic undifferentiated carcinoma with osteoclast-like giant cells is genetically similar to, but clinically distinct from, conventional ductal adenocarcinoma. J. Pathol. 243, 148–154 (2017).
25. Diskin, S. J. et al. Adjustment of genomic waves in signal intensities from whole-genome SNP genotyping platforms. Nucleic Acids Res. 36, e126 (2008).
26. Song, S. et al. qpure: A tool to estimate tumor cellularity from genome-wide single-nucleotide polymorphism profiles. PLoS One 7, e45835 (2012).
27. Yang, J. et al. CTLPScanner: a web server for chromothripsis-like pattern detection. Nucleic Acids Res. 44, W252–8 (2016).
28. Amin, M. B. et al. AJCC Cancer Staging Manual.

(Springer International Publishing, 2018).
29. Sadot, E. et al. Observation versus Resection for Small Asymptomatic Pancreatic Neuroendocrine Tumors: A Matched Case-Control Study. Ann. Surg. Oncol. 23, 1361–1370 (2016).
30. Gaujoux, S. et al. Observational study of natural history of small sporadic nonfunctioning pancreatic neuroendocrine tumors. J. Clin. Endocrinol. Metab. 98, 4784–4789 (2013).
31. VandenBussche, C. J. et al. Alternative lengthening of telomeres and ATRX/DAXX loss can be reliably detected in FNAs of pancreatic neuroendocrine tumors. Cancer Cytopathol. 125, 544–551 (2017).
32. Altomare, D. A. & Testa, J. R. Perturbations of the AKT signaling pathway in human cancer. Oncogene 24, 7455–7464 (2005).
33. Cheng, J. Q. et al. Amplification of AKT2 in human pancreatic cells and inhibition of AKT2 expression and tumorigenicity by antisense RNA. Proc. Natl. Acad. Sci. U. S. A. 93, 3636–3641 (1996).
34. Lin, S. Y. & Elledge, S. J. Multiple tumor suppressor pathways negatively regulate telomerase. Cell 113, 881–889 (2003).
35. Mirabello, L. et al. The association of telomere length and genetic variation in telomere biology genes. Hum. Mutat. 31, 1050–1058 (2010).
36. Falconi, M. et al. ENETS Consensus Guidelines for the management of patients with digestive neuroendocrine neoplasms of the digestive system: well-differentiated pancreatic non-functioning tumors. Neuroendocrinology 95, 120–134 (2012).
37. Gleeson, F. C. et al. Assessment of pancreatic neuroendocrine tumor cytologic genotype diversity to guide personalized medicine using a custom gastroenteropancreatic next-generation sequencing panel. Oncotarget 8, 93464–93475 (2017).

11

Chapter 12

Whole-exome sequencing of duodenal neuroendocrine tumors in patients with neurofibromatosis type 1

Michaël Noë, Antonio Pea, Claudio Luchini, Matthäus Felsenstein, Stefano Barbi, Feriyl Bhaijee, Raluca Yonescu, Yi Ning, N. Volkan Adsay, Giuseppe Zamboni, Rita T.. Lawlor, Aldo Scarpa, G. Johan A. Offerhaus, Lodewijk A.A. Brosens, Ralph H. Hruban, Nicholas J. Roberts, Laura D. Wood

Modern Pathology, May 2018

ABSTRACT

Neurofibromatosis type 1 (NF1) is a hereditary cancer predisposition syndrome characterized by frequent cutaneous and nervous system abnormalities. Patients with NF1 also have an increased prevalence of multiple gastrointestinal and peripancreatic neoplasms—neuroendocrine tumors of the ampulla that express somatostatin are particularly characteristic of NF1. In this study, we characterize the genetic alterations of a clinically well-characterized cohort of six NF1-associated duodenal neuroendocrine tumors using whole-exome sequencing. We identified inactivating somatic mutations in the NF1 gene in three of six tumors; the only other gene altered in more than one tumor was *IFNB1*. Copy number analysis revealed deletion/loss of heterozygosity of chromosome 22 in three of six patients. Analysis of germline variants revealed germline deleterious *NF1* variants in four of six patients, as well as deleterious variants in other tumor suppressor genes in two of four patients with deleterious *NF1* variants. Taken together, these data confirm the importance of somatic inactivation of the wild-type *NF1* allele in the formation of NF1-associated duodenal neuroendocrine tumors and suggest that loss of chromosome 22 is important in at least a subset of cases. However, we did not identify any genes altered in the majority of NF1-associated duodenal neuroendocrine tumors that uniquely characterize the genomic landscape of this tumor. Still, the genetic alterations in these tumors are distinct from sporadic neuroendocrine tumors occurring at these sites, highlighting that unique genetic alterations drive syndromic tumors.

INTRODUCTION

Hereditary cancer predisposition syndromes, in which germline alterations lead to an increased risk of neoplasia, represent a unique opportunity to study tumorigenesis, and the results of these studies can have important clinical implications.

Neurofibromatosis type 1 (NF1), also known as von Recklinghausen disease, is an autosomal dominant hereditary cancer predisposition syndrome caused by inactivating germline alterations in the *NF1* gene encoding neurofibromin on chromosome 17q.[1] This syndrome affects ~1 in 3000 individuals and is characterized by a constellation of clinical findings, including café-au-lait spots, axillary freckling, optic gliomas, and neurofibromas, a small proportion of which can transform into malignant peripheral nerve sheath tumors.[1]

Although less common than the cutaneous and nervous system abnormalities, several gastrointestinal and peripancreatic neoplasms also occur at increased prevalence in patients with NF1, including gastrointestinal stromal tumors and neuroendocrine tumors of the duodenum and ampulla.[2] Intriguingly, the majority of these neuroendocrine tumors typically have unique morphological features, including prominent psammomatous calcifications, and express the hormone somatostatin.[2] Previous genomic analysis of NF1-associated malignant peripheral nerve sheath tumors has revealed critical drivers of malignant transformation in the *SUZ12* gene in these tumors.[3] However, little is known about the genetic alterations that drive the formation of gastrointestinal and peripancreatic tumors in NF1 patients. Multiple lines of evidence suggest that functional and syndromic neuroendocrine tumors will harbor genomic alterations distinct from those in sporadic non-functional neuroendocrine tumors that have previously been characterized in depth.[4–6] Whole-exome sequencing of a specific clinicopathological group of pancreatic neuroendocrine tumors, sporadic insulinomas, revealed a unique frequently altered hotpsot mutation, suggesting that specific clinical and pathological categories of neuroendocrine tumors are driven by distinct genetic alterations.[7] In addition, previous studies have demonstrated that gastrointestinal stromal tumors in NF1 patients are genetically distinct from sporadic gastrointestinal stromal tumors.[8] As such, we hypothesize that NF1-associated duodenal neuroendocrine tumors may be a genetically unique category of neuroendocrine tumors. In order to characterize the genomic landscape of these neoplasms in NF1 patients, we performed whole-exome sequencing on a clinically well-characterized cohort of six neoplasms.

MATERIALS AND METHODS

This study (including the analysis of germline DNA) was approved by the Institutional Review Boards of The Johns Hopkins Hospital and Emory University Hospital. The surgical pathology databases of The Johns Hopkins Hospital and Emory University Hospital were searched for surgically resected neuroendocrine tumors of the ampulla with psammomatous calcifications or immunohistochemical reactivity for somatostatin in patients clinically diagnosed NF1. From tumor samples SOM3-6, formalin-fixed

paraffin-embedded tissue blocks of tumor and matched normal were reviewed by a pathologist and macrodissected to enhance neoplastic cellularity. Cores of neoplastic and normal tissue were isolated from formalin-fixed paraffin-embedded blocks using a 0.6 mm needle. For tumor samples SOM7-8, fresh-frozen tumor and normal (harvested at the time of surgery and subsequently banked at –70 °C) were reviewed by a pathologist and macrodissected after frozen section analysis to enhance neoplastic cellularity. DNA was extracted using the QIAamp DNA FFPE tissue kit (Qiagen) or QIAamp DNA mini kit (Qiagen) according to the manufacturer's instructions and quantified using the Qubit 2.0 (Thermo Fisher).

Whole-exome sequencing was performed at Personal Genome Diagnostics with capture using the Agilent SureSelect paired end version 4.0 library preparation followed by sequencing on an Illumina HiSeq, as previously described.[9] Somatic mutations were identified using the VariantDx pipeline as previously described.[9] In order to identify copy number alterations, we utilized the ASCAT software.[10] Specifically, we identified ~40,000 single-nucleotide polymorphisms in the target region with high global minor allele frequency—the normalized number of reads along with the estimated B allele frequency was then used as input for ASCAT. However, owing to high dispersion in local sequencing coverage, most of the samples could not be reliably modeled with ASCAT. Therefore, the plots representing normalized read depth and B allele frequency along the chromosomes were visually inspected to identify large chromosomal alterations based on lower number of reads and absence of the band corresponding to heterozygous single-nucleotide polymorphisms in the B allele frequency plot. In addition, we performed complimentary copy number analysis with CNVkit to utilize both the on-target and off-target reads.[11] Scatterplots were created with CNVkit and visually inspected for each chromosome, and copy number status of tumors were compared to the matched normal sample from the same patient. Deleterious germline variants were identified after alignment of sequence read files to the human genome (hg19) with Burrows-Wheeler Aligner and variant calling with Varscan 2.[12,13] Classification of variants as either benign, of unknown significance, or deleterious was performed as previously described.[14]

Fluorescence in situ hybridization was performed on formalin-fixed paraffin-embedded specimens using a dual color probe (Abbott Molecular). The probe is designed for the detection of chromosomal region 9q34.12 harboring the *ABL1* gene (orange fluorochrome) and the chromosomal region 22q11.23, harboring the *BCR* gene (green fluorochrome). Prior to hybridization, formalin-fixed paraffin-embedded slides were deparaffinized using a VP2000 processor (Abbott Molecular). The slides and the probe were co-denatured at 75 °C for 5 minutes and allowed to anneal over night at 37 °C, in humidified atmosphere. Following incubation the slides were washed in 2 × saline-sodium citrate (SSC)/0.3% NP-40 for 2 minutes at 72 °C, and for 2 minutes at room temperature in 2 × SSC. The slides were counterstained with 4¦6-diamidino-2-phenylindole and a cover slip was applied using Vectashield mounting medium (H-1000, Vector Laboratories, Inc.). A fluorescence microscope was used to evaluate signal patterns generated by each probe. In normal interphase cells, the signal pattern showed two orange signals (two copies of *ABL1* gene) and two green signals (two copies of *BCR* gene). Samples showing > 10% of the 50 analyzed cells with less than or more than two signals are interpreted as loss or gain, respec-

tively, for the targeted chromosome locus.

RESULTS

Clinical and pathological data

We identified six duodenal neuroendocrine tumors occurring in patients who were clinically diagnosed with NF1. Microscopic evaluation of these tumors showed the typical morphological pattern of homogeneous neoplastic cells with abundant clear or granular eosinophilic cytoplasm and round, smooth nuclei with finely stippled chromatic. The neoplastic cells were organized in nests, trabeculae, and acinar structures, often with prominent interspersed psammomatous calcifications (Figure 1). Clinical and pathological features are summarized in Table 1. All the tumors originated in the duodenum or around the major or minor duodenal papilla. The mean age at time of resection was 52 (range 40–61), and 67% of the patients were male. The mean size of the primary tumor was 2.6 cm, and 50% had lymph node metastases at the time of surgery. When performed, Ki67 proliferation rate was < 2% in all cases, consistent with WHO Grade 1 based on current classifications.[15,16] Immunolabeling for somatostatin was positive in four cases, and none had immunolabeling for other commonly expressed pancreatic hormones such as insulin and glucagon. One case was negative for somatostatin labeling, but this case had characteristic glandular psammomatous morphology, as did another tumor in which somatostatin immunohistochemistry was not available. All patients had other histological features suggestive of NF1, including duodenal neurofibromas, duodenal gastrointestinal stromal tumor, and neurofibromatosis-associated vasculopathy.[17]

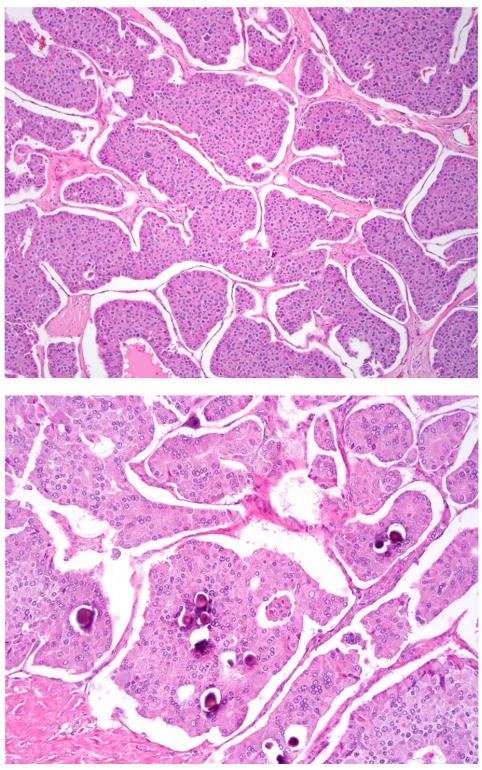

Figure 1. Histopathology of duodenal neuroendocrine tumors in NF1 patients. **a** A low-power view of duodenal neuroendocrine tumor shows characteristic nested architecture. Hematoxylin and eosin, ×10. **b** A high-power view shows characteristic cytologic features, including monotonous round nuclei with finely stippled chromatin, amphophilic granular cytoplasm, and psammomatous calcifications. Hematoxylin and eosin, ×20.

Whole-exome sequencing

Whole-exome sequencing of six NF1-associated duodenal neuroendocrine tumors revealed a range of 2–11 nonsynonymous somatic mutations per tumor (Table 2, Supplementary Table 1, Supplementary Table 2). Only two genes were mutated in more than one tumor: inactivating mutations (two frame-

Case	Age	Sex	Size (cm)	Lymph node metastasis	Somatostatin IHC	Ki67	Psammomatous calcifications	Other pathological features
SOM3	59	M	2.3	No	Positive	<2%	Yes	Neurofibromas in surrounding soft tissue
SOM4	52	F	1.5	Yes	Positive	<2%	Yes	Duodenal GIST
SOM5	61	F	3.4	Yes	Negative	<2%	Yes	Neurofibromatosis-associated vasculopathy
SOM6	46	M	3.4	Yes	Not available	<2%	Yes	Neurofibromatosis-associated vasculopathy
SOM7	40	M	3	No	Positive	Not available	No	Duodenal and cutaneous neurofibromas
SOM8	55	M	2.1	No	Positive	<2%	Yes	Neurofibromatosis-associated vasculopathy

Table 1. Clinical and pathological features of duodenal neuroendocrine tumors in NF1 patients

shift and one nonsense) in *NF1* occurred in three tumors, and missense mutations in *IFNB1* occurred in two tumors. In addition, somatic mutation in the oncogenic hotspot in codon 600 in *BRAF* was identified in a single tumor.

We also utilized the whole-exome sequencing data to identify copy number alterations using two complimentary approaches—ASCAT[10], which analyzed the B allele frequency of germline single-nucleotide polymorphisms in the target region, and CNVkit[11], which analyzed copy number based on read depth in the on-target and off-target reads. Both of these approaches revealed deletion/loss of heterozygosity of chromosome 22 in three tumors (Supplementary Figure 1). Key somatic alterations in each tumor are summarized in Table 3.

Tumor	Gene symbol	Mutation type	Amino-acid change
SOM3	*BRAF*	Nonsynonymous coding	p.V600E
SOM3	*CEACAM20*	Nonsynonymous coding	p.R332W
SOM3	*DCTN1*	Nonsynonymous coding	p.R997L
SOM3	*FAM135B*	Nonsynonymous coding	p.S105N
SOM3	*LRRC39*	Frameshift	p.T240fs
SOM3	*MSN*	In-frame deletion	p.344delE
SOM3	*MTRNR2L2*	Nonsynonymous coding	p.S12L
SOM3	*NEB*	Nonsynonymous coding	p.L560V
SOM3	*NELL2*	Nonsynonymous coding	p.G841V
SOM3	*NF1*	Frameshift	p.F150fs
SOM3	*USP34*	Nonsynonymous coding	p.V609L
SOM4	*PCNT*	Nonsynonymous coding	p.G136S
SOM4	*SMC3*	Splice site acceptor	splice site
SOM5	*CAMKK2*	Nonsynonymous coding	p.R104Q
SOM5	*DACT1*	Nonsynonymous coding	p.S759L
SOM5	*JAKMIP1*	Nonsynonymous coding	p.G108D
SOM5	*PPIP5K1*	Nonsynonymous coding	p.F1144V
SOM5	*RNASE7*	Nonsynonymous coding	p.P48T
SOM5	*SP4*	Nonsynonymous coding	p.K705N
SOM6	*AIM1L*	Nonsynonymous coding	p.R25W
SOM6	*ANO10*	Frameshift	p.D45fs
SOM6	*ATXN10*	Nonsynonymous coding	p.E312K
SOM6	*FETUB*	Frameshift	p.I147fs
SOM6	*FGA*	Splice site acceptor	splice site
SOM6	*IFNB1*	Nonsynonymous coding	p.A76S
SOM6	*RDM1*	Nonsynonymous coding	p.R143K
SOM6	*VWA8*	Nonsynonymous coding	p.I709K
SOM6	*WBSCR17*	Nonsynonymous coding	p.G314R
SOM7	*CDH23*	Nonsynonymous coding	p.G540S
SOM7	*EZH2*	Nonsynonymous coding	p.D185H
SOM7	*IFNB1*	Nonsynonymous coding	p.G135R
SOM7	*MYO1B*	Nonsynonymous coding	p.M493L
SOM7	*NF1*	Frameshift	p.W267fs
SOM8	*AHCYL2*	Nonsynonymous coding	p.R468H
SOM8	*IL5*	Nonsynonymous coding	p.V17M
SOM8	*NF1*	Nonsense	p.Q1822X
SOM8	*PLS3*	Nonsynonymous coding	p.K300N

Table 2. Somatic mutations identified by whole-exome sequencing in NF1-associated duodenal neuroendocrine tumors.

In addition to the identification of somatic genetic events in NF1-associated duodenal neuroendocrine tumors, we also analyzed the germline sequencing data for deleterious variants in human cancer genes (Table 4). We identified three frameshift germline variants and one nonsense germline variant in *NF1*; four patients had deleterious germline variants in *NF1*. In addition, two of these four patients also had deleterious germline variants in other known cancer genes, including a frameshift deletion in *FANCC* and a splice site mutation in *TSC1*, each in one patient.

Fluorescence in situ hybridization

In order to confirm the result of our copy number analysis utilizing whole-exome sequencing data, we performed fluorescence in situ hybridization for chromosomes 9 and 22 on neoplastic formalin-fixed paraffin-embedded tissue from all six tumors. We identified loss of chromosome 22 by fluorescence in situ

hybridization in the three tumors with whole-exome sequencing data suggestive of deletion/loss of heterozygosity, whereas the other three tumors retained two copies of both chromosomes 9 and 22 (Figure 2).

Tumor	Somatic *NF1* mutation	Germline NF1 variant	Chromosome 22 copy number
SOM3	p.F150fs	None identified	Deletion/LOH
SOM4	None identified	p.S436X	Wild-type
SOM5	None identified	p.Q514fs	Deletion/LOH
SOM6	None identified	None identified	Deletion/LOH
SOM7	p.W267fs	p.T1951fs	Wild-type
SOM8	p.Q1822X	p.L1152fs	Wild-type

Table 3. Summary of key genetic alterations in NF1-associatedduodenal neuroendocrine tumors.

Patient	Gene	Genomic DNA alteration	Amino-acid alteration
SOM4	*NF1*	chr17:29533304 C > A	p.S436X
SOM5	*TSC1*	chr9:135773001insA	Splice site
SOM5	*NF1*	chr17:29546036delAG	p.Q514fs
SOM7	*NF1*	chr17:29661957insA	p.T1951fs
SOM8	*FANCC*	chr9:98011507delC	p.D23fs
SOM8	*NF1*	chr17:29559859delACTC	p.L1152fs

Table 4. Deleterious germline variants identified in NF1 patients withduodenal neuroendocrine tumors.

DISCUSSION

We report whole-exome sequencing of a clinically well-characterized cohort of duodenal neuroendocrine tumors arising in patients with NF1. In the literature, these tumors are often described as 'somatostatinomas' owing to their characteristic expression of somatostatin by immunohistochemistry, though clinical symptoms caused by somatostatin expression are exceedingly rare. Other features often seen in neuroendocrine tumors in patients with NF1 are glandular morphology and presence of psammoma bodies. There is substantial overlap between neuroendocrine tumors with somatostatin expression, glandular neuroendocrine tumors with psammoma bodies, and neuroendocrine tumors associated with NF1.[1,18] As such, these lesions have been previously called "ampullary somatostatinoma" and "glandular duodenal neuroendocrine tumor". However, in this study, we use the general term "duodenal neuroendocrine tumor", as not all analyzed lesions expressed somatostatin or showed glandular morphology. The expression of other pancreatic hormones, including gastrin and serotonin, was not analyzed in this study though could be of interest for future studies describing these lesions at the protein level. Of note, sporadic somatostatinomas can show focal expression for gastrin or serotonin.[19]

The most common intragenic somatic alteration in this tumor type was inactivating mutation in *NF1* (either by frameshift or nonsense mutation), which occurred in three tumors. In addition to these small somatic mutations, we also identified somatic deletion/loss of heterozygosity of chromosome 22 in three tumors in our whole-exome sequencing data and confirmed these deletions by fluorescence in situ hybridization. Because the deletion includes the entire chromosome, it is not possible to identify the targeted driver gene. However, multiple well-characterized tumor suppressor genes are located on chromosome 22, including *NF2* and *SMARCB1*, which lead to neurofibromatosis type 2 and schwannomatosis, respectively.[20–22] Still, the lack of somatic mutations in these tumor suppressor genes raises the alternative possibility that other types of alterations, such as epigenetic modifications or alterations in non-coding regions, may complement the deletion/loss of heterozygosity of chromosome 22.

Overall, the somatic mutations identified in duodenal neuroendocrine tumors in NF1 patients are unique from those identified in sporadic pancreatic neuroendocrine tumors well as sporadic small intestinal neuroendocrine tumors[4–6]—mutations in *NF1* and *IFNB1* do not occur commonly in these other

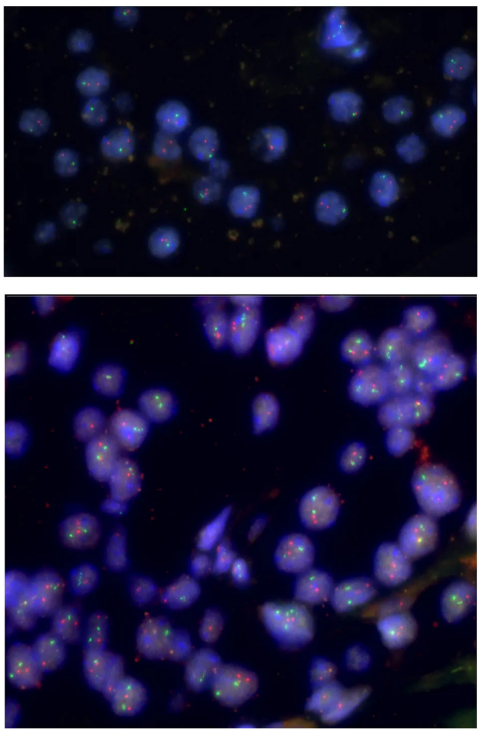

Figure 2. Fluorescence in situ hybridization of chromosomes 9 and 22 in NF1-associated duodenal neuroendocrine tumors. **a** Fluorescencein situ hybridization demonstrates loss of chromosome 22 in neoplastic cells, as they contain two red signals (chromosome 9) but only one green signal (chromosome 22). **b** Fluorescence in situ hybridization ona tumor without chromosome 22 deletion shows two signals in both the red and green probes.

tumor types, nor does loss of chromosome 22. In addition, somatic mutations in genes frequently altered in pancreatic neuroendocrine tumors (*MEN1*, *ATRX*, *DAXX*) and small intestinal neuroendocrine tumors (*CDKN1B*) were absent in our cohort. However, to our knowledge, no study has specifically analyzed sporadic duodenal neuroendocrine tumors, which would be the most appropriate comparison for our lesions. Analysis of these sporadic lesions, with subsequent comparison with the genetic alterations in syndromic lesions, remains a future direction.

The genomic landscapes of NF1-associated neoplasms reported in the literature to date is variable. The mutations in the duodenal neuroendocrine tumors in our cohort are distinct from those previously reported in malignant peripheral nerve sheath tumors, which is one of most comprehensively characterized NF1-associated neoplasms. Although the somatic "second hit" in *NF1* has been reported in NF1-associated malignant peripheral nerve sheath tumors, our tumors lacked mutations in *SUZ12*, *EED*, and *CDKN2A* that frequently occur in this tumor type.[3,23] However, deletions of IFNB1 (the only gene other than *NF1* with somatic mutations in more than one tumor in our cohort) have been reported in 20% of malignant peripheral nerve sheath tumors, suggesting perhaps a common genetic driver among NF1-associated neoplasms.[24] Overall, the alterations in NF1-associated duodenal neuroendocrine tumors are more similar to those reported in plexiform neurofibromas in NF1 patients—whole-exome sequencing has previously revealed only a small number of somatic mutations in these benign NF1-associated neoplasms, with somatic mutations in *NF1* as the most common alteration.[25] Similarly, whole-genome sequencing analysis of a small number of NF1-associated pilocytic astrocytomas revealed that somatic inactivation of *NF1* was the only recurrent genetic alteration.[26] Of note, loss of chromosome 22 has not been previously reported in NF1-associated neoplasms.

In three of the six tumors, we did not identify somatic *NF1* mutations. In these cases, deletion/loss of heterozygosity of the wild-type *NF1* allele may not have been accurately identified by our approach. Although our copy number analysis could robustly identify arm-level chromosomal alterations (such as deletion/loss of heterozygosity of chromosome 22), it is possible that our analysis missed focal

deletions of the wild-type copy of the gene in these cases due to sequencing approach and coverage depth. Such focal deletions have been previously reported as a mechanism for somatic *NF1* inactivation.[3] Alternatively, methylation has been reported as an alternative mechanism for inactivation of the second *NF1* allele, which would not have been identified by our whole-exome sequencing approach.[26] Although immunohistochemical detection of the neurofibromin protein encoded by *NF1* is another possible assay to interrogate this gene, immunohistochemistry has not been shown to be a reliable predictor of genetic and epigenetic alterations in *NF1*.[27,28] Thus, we did not use neurofibromin protein expression as a surrogate for *NF1* gene status in our study.

Germline deleterious *NF1* variants were identified in four of the six patients. In two of the four patients with a germline *NF1* mutation we were able to demonstrate bi-allelic inactivation of this critical tumor suppressor gene with a second somatic hit to the gene. Of interest, we identified deleterious germline variants in other known familial cancer genes, including a frameshift deletion in *FANCC* and a splice site mutation in *TSC1*—both of these occurred in patients who also had germline deleterious variants in *NF1*. Although this could be chance, it could be that the combination of two germline changes increases the penetrance of the phenotype. This phenomenon has been demonstrated on other hereditary diseases: for example, previous data have demonstrated that patients with the clinical finding of familial pancreatitis often have two distinct germline events that together contribute to the phenotype.[29,30] In two of the six cases, we did not identify a disease-causing germline *NF1* variant, as the remainder of the germline variants identified in the coding region of this gene were synonymous. However, the clinical history of NF1 in each patient in our cohort is well documented, and previous studies have highlighted the difficulties in identifying germline *NF1* mutations, as numerous molecular approaches are necessary for comprehensive variant identification.[31] Thus, our whole-exome sequencing approach was likely not sensitive enough to detect all the disease-causing germline alterations in our cohort.

Taken together, our data reveal the importance of somatic *NF1* mutation and chromosome 22 loss in duodenal neuroendocrine tumors in patients with NF1, highlighting the unique genomic landscape of this syndromic neoplasm.

REFERENCES

1. Gutmann, D. H. et al. Neurofibromatosis type 1. Nat Rev Dis Primers 3, 17004 (2017).
2. Relles, D., Baek, J., Witkiewicz, A. & Yeo, C. J. Periampullary and duodenal neoplasms in neurofibromatosis type 1: two cases and an updated 20-year review of the literature yielding 76 cases. J. Gastrointest. Surg. 14, 1052–1061 (2010).
3. Zhang, M. et al. Somatic mutations of SUZ12 in malignant peripheral nerve sheath tumors. Nat. Genet. 46, 1170–1172 (2014).
4. Jiao, Y. et al. DAXX/ATRX, MEN1, and mTOR pathway genes are frequently altered in pancreatic neuroendocrine tumors. Science 331, 1199–1203 (2011).
5. Francis, J. M. et al. Somatic mutation of CDKN1B in small intestine neuroendocrine tumors. Nat. Genet. 45, 1483–1486 (2013).
6. Banck, M. S. et al. The genomic landscape of small intestine neuroendocrine tumors. J. Clin. Invest. 123, 2502–2508 (2013).
7. Cao, Y. et al. Whole exome sequencing of insulinoma reveals recurrent T372R mutations in YY1. Nat. Commun. 4, 2810 (2013).
8. Maertens, O. et al. Molecular pathogenesis of multiple gastrointestinal stromal tumors in NF1 patients. Hum. Mol. Genet. 15, 1015–1023 (2006).
9. Hosoda, W. et al. Genetic analyses of isolated high-grade pancreatic intraepithelial neoplasia (HG-PanIN) reveal paucity of alterations in TP53 and SMAD4. J. Pathol. 242, 16–23 (2017).
10. Van Loo, P. et al. Allele-specific copy number analysis of tumors. Proc. Natl. Acad. Sci. U. S. A. 107, 16910–16915 (2010).
11. Talevich, E., Shain, A. H., Botton, T. & Bastian, B. C. CNVkit: Genome-Wide Copy Number Detection and Visualization from Targeted DNA Sequencing. PLoS Comput. Biol. 12, e1004873 (2016).
12. Li, H. & Durbin, R. Fast and accurate short read alignment with Burrows–Wheeler transform. Bioinformatics 25, 1754–1760 (2009).
13. Koboldt, D. C., Steinberg, K. M., Larson, D. E., Wilson, R. K. & Mardis, E. R. The next-generation sequencing revolution and its impact on genomics. Cell 155, 27–38 (2013).
14. 14. Roberts, N. J. et al. Whole Genome Sequencing Defines the Genetic Heterogeneity of Familial Pancreatic Cancer. Cancer Discov. 6, 166–175 (2016).
15. Klimstra, D. S. et al. Neuroendocrine neoplasms of the pancreas. in WHO Classification of Tumours of the Digestive System (eds. Bosman, F. T., Carneiro, F., Hruban, R. H. & Theise, N. D.) 322–326 (International Agency for Research on Cancer, 2010).
16. Klöppel, G. et al. Pancreatic Neuroendocrine Tumors: Update on the New World Health Organization Classification. AJSP: Reviews & Reports 22, 233 (2017).
17. Lie, J. T. Vasculopathies of Neurofibromatosis Type 1 (von Recklinghausen Disease). Cardiovasc. Pathol. 7, 97–108 (1998).
18. Usui, M. et al. Somatostatinoma of the papilla of Vater with multiple gastrointestinal stromal tumors in a patient with von Recklinghausen's disease. J. Gastroenterol. 37, 947–953 (2002).
19. Garbrecht, N. et al. Somatostatin-producing neuroendocrine tumors of the duodenum and pancreas: incidence, types, biological behavior, association with inherited syndromes, and functional activity. Endocr. Relat. Cancer 15, 229–241 (2008).
20. Trofatter, J. A. et al. A novel moesin-, ezrin-, radixin-like gene is a candidate for the neurofibromatosis 2 tumor suppressor. Cell 72, 791–800 (1993).
21. Rouleau, G. A. et al. Alteration in a new gene encoding a putative membrane-organizing protein causes neuro-fibromatosis type 2. Nature 363, 515–521 (1993).
22. Hulsebos, T. J. M. et al. Germline mutation of INI1/SMARCB1 in familial schwannomatosis. Am. J. Hum. Genet. 80, 805–810 (2007).
23. Sohier, P. et al. Confirmation of mutation landscape of NF1-associated malignant peripheral nerve sheath tumors. Genes Chromosomes Cancer 56, 421–426 (2017).
24. Lee, W. et al. PRC2 is recurrently inactivated through EED or SUZ12 loss in malignant peripheral nerve sheath tumors. Nat. Genet. 46, 1227–1232 (2014).
25. Pemov, A. et al. The primacy of NF1 loss as the driver of tumorigenesis in neurofibromatosis type 1-associated plexiform neurofibromas. Oncogene 36, 3168–3177 (2017).
26. Gutmann, D. H. et al. Somatic neurofibromatosis type 1 (NF1) inactivation characterizes NF1-associated pilocytic astrocytoma. Genome Res. 23, 431–439 (2013).
27. Stenman, A. et al. Immunohistochemical NF1 analysis does not predict NF1 gene mutation status in pheochromocytoma. Endocr. Pathol. 26, 9–14 (2015).
28. Burnichon, N. et al. Somatic NF1 inactivation is a frequent event in sporadic pheochromocytoma. Hum. Mol. Genet. 21, 5397–5405 (2012).
29. LaRusch, J., Barmada, M. M., Solomon, S. & Whitcomb, D. C. Whole exome sequencing identifies multiple, complex etiologies in an idiopathic hereditary pancreatitis kindred. JOP 13, 258–262 (2012).
30. Pfützer, R. H. et al. SPINK1/PSTI polymorphisms act as disease modifiers in familial and idiopathic chronic pancreatitis. Gastroenterology 119, 615–623 (2000).
31. Jett, K. & Friedman, J. M. Clinical and genetic aspects of neurofibromatosis 1. Genet. Med. 12, 1–11 (2010).

12

Chapter 13

Well-differentiated pancreatic neuroendocrine tumor in a patient with familial atypical multiple mole melanoma syndrome (FAMMM)

Michaël Noë, Wenzel Hackeng, Wendy de Leng, Menno Vergeer, Frank P. Vleggaar, Folkert H.M. Morsink, Laura D. Wood, Ralph H. Rhuban, G. Johan A. Offerhaus, Lodewijk A.A. Brosens

The American Journal of Surgical Pathology, September 2019

ABSTRACT

Germline mutations in *CDKN2A* result in Familial Atypical Multiple Mole Melanoma Syndrome (FAMMM), which is associated with an increased risk for pancreatic ductal adenocarcinoma and melanoma. *CDKN2A* is somatically inactivated in multiple neoplasms, raising the possibility that, although the data are not conclusive, germline *CDKN2A* mutation may also impose an increased risk for other neoplasms. We present a patient with a *CDKN2A* germline mutation (p16-Leiden mutation) and mosaicism for neurofibromatosis type 2, who presented with a small asymptomatic pancreatic lesion, detected during endoscopic ultrasound screening of the pancreas. After resection, the lesion was found to be a well-differentiated pancreatic neuroendocrine tumor (PanNET). Molecular analysis of the tumor showed somatic loss of the second allele, supporting a causal relation of the PanNET to the underlying FAMMM syndrome. Recent data, showing the association between certain single-nucleotide polymorphisms in the *CDKN2A* gene and an increased incidence for PanNET, further support a role for germline *CDKN2A* alterations in PanNET risk. We conclude that PanNETs can be a phenotypic expression of FAMMM syndrome. This can have implications for screening and for the diagnosis of pancreatic neoplasms in carriers of germline *CDKN2A* mutations.

INTRODUCTION

p16, the protein encoded by the tumor suppressor gene, *CDKN2A*, is expressed in most senescent cells and plays a causal role in their growth arrest.[1] Germline mutations in senescence genes, including *CDKN2A*, can significantly predispose to cancer. This is illustrated by studies, wherein mice with even subtle perturbations of the senescence machinery are dramatically more susceptible to cancer.[2,3]

The *CDKN2A* gene can be somatically inactivated through homozygous deletions, intragenic mutations in one allele combined with loss of the second allele, or through promoter methylation.[4–6] Large deletions on chromosome 9p that inactivate *CDKN2A* can also affect neighboring genes such as *MTAP*. This gene is located approximately 100 kb telomeric from *CDKN2A* and is contained in the *CDKN2A* homozygous deletions in 90% of malignant mesotheliomas, in 75% to 100% of T-cell acute lymphoblastic leukemias, and in 50% to 100% of pancreatic cancers.[7–11]

Deleterious germline mutations in *CDKN2A* produce the Familial Atypical Multiple Mole Melanoma Syndrome (FAMMM), and have been shown to predispose to cancer, particularly pancreatic cancer and melanoma.[12] A subset of FAMMM patients harbor a specific Dutch founder mutation: a 19bp-deletion in exon 2 (p16-Leiden mutation).[13,14] These patients have a 15% to 20% lifetime risk of developing pancreatic cancer.[15,16] Melanoma presents at an earlier age in FAMMM patients, as compared with patients with sporadic melanoma; earlier occurrence of pancreatic cancer has not been observed.[17–19] Because of the increased risk to develop pancreatic cancer, some patients with a germline p16-Leiden mutation are being screened, as recommended by the "International Cancer of the Pancreas Screening Consortium."[20,21] The goal of this screening is to detect precursor lesions and early pancreatic cancer. Precursor lesions are curable because they have not yet invaded the tissues, and a growing body of evidence suggests that some small asymptomatic pancreatic cancers are curable, due to limited invasion in the surrounding structures.[22–25]

Although it is known that patients with FAMMM (including those with a p16-Leiden mutation) have an increased risk for pancreatic adenocarcinoma and melanoma, the association of germline *CDKN2A* mutations with other neoplasms is less clear.[26–29] Somatic inactivation of *CDKN2A* has been observed as a late event in the progression of some pancreatic neuroendocrine tumors (PanNETs) and is associated with the development of metastases. However, an increased incidence of PanNETs in patients with germline *CDKN2A* mutations has not yet been shown.[30] Neuroendocrine tumors in the pancreas can pose diagnostic problems for clinicians screening individuals with a germline *CDKN2A* mutation, as the treatment for PanNETs can be very different from the treatment of pancreatic adenocarcinomas. The case reported here, in which we show a germline *CDKN2A* mutation coupled with an additional loss of heterozygosity (LOH) of *CDKN2A* in the tumor, provides compelling evidence for a causal relationship between the patient's underlying FAMMM syndrome and the development of their PanNET.

The patient was a 51-year-old man with a known germline mutation in *CDKN2A* (p16-Leiden mutation). The hereditary nature of this mutation was illustrated by the patient's strong family cancer history, which included first, second, and third-degree relatives affected by melanoma or pancreatic cancer. At age 47, the patient himself was diagnosed with a small melanoma (Breslow thickness, 0.5 mm). This was treated with local resection. In addition, the patient was mosaic for neurofibromatosis type 2, and he developed multiple schwannomas, all containing the same deletion of the whole *NF2* gene. Germline analysis on lymphocytic DNA of the patient could not retrieve this deletion, suggesting mosaicism, which is often seen in patients with neurofibromatosis type 2.[31,32] The schwannomas were surgically removed, sometimes in combination with local radiotherapy.

Because of the patient's increased risk for developing pancreatic cancer, he was included at age 50 in a screening program for early detection of pancreatic cancer. The first endoscopic ultrasound (EUS) of the pancreas revealed a small, hypoechogenic lesion (6.2×4.4 mm) in the uncinate process of the pancreas. Because of the very small dimensions of this lesion, the decision was made to follow-up on this lesion, and a second EUS, 8 months later, showed that the lesion had slightly increased in size (7.5×5.2 mm). A fine-needle aspiration of the lesion produced atypical cells, with both ductal and neuroendocrine features, suggestive for adenocarcinoma (Figure 1A). Additional computed tomography and magnetic resonance imaging were not able to visualize the lesion.

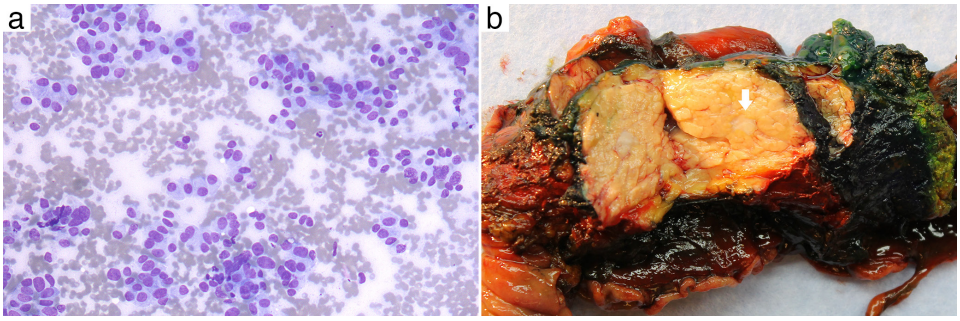

Figure 1. a Fine-needle aspiration cytology showed plasmacytoid cells with nuclear atypia. **b** Gross appearance of the Whipple specimen shows a well-demarcated 5 mm lesion (arrow) in the uncinate process of the pancreas.

On the basis of the results of the EUS and the fine-needle aspiration, the decision was made to resect the lesion during a Whipple procedure. Macroscopic examination of the specimen showed a 5 mm, slightly pale, and indurated lesion in the uncinate process of the pancreas (Figure 1B). Microscopic examination of this lesion showed a proliferation of nested cells with a varying amount of cytoplasm and enlarged, slightly irregular round to oval nuclei with coarse chromatin, surrounded by a stromal reaction (Figure 2A). Focal solid growth with some interspersed blood vessels resembled an islet of Langerhans. No clear ductal differentiation was found; however, some normal ducts were entrapped in the proliferation. There was perineural growth (Figure 2A). Nearby acini were being infiltrated by the tumor cells and showed some signs of atrophy. Labeling for chromogranin, synaptophysin (Figure 2B),

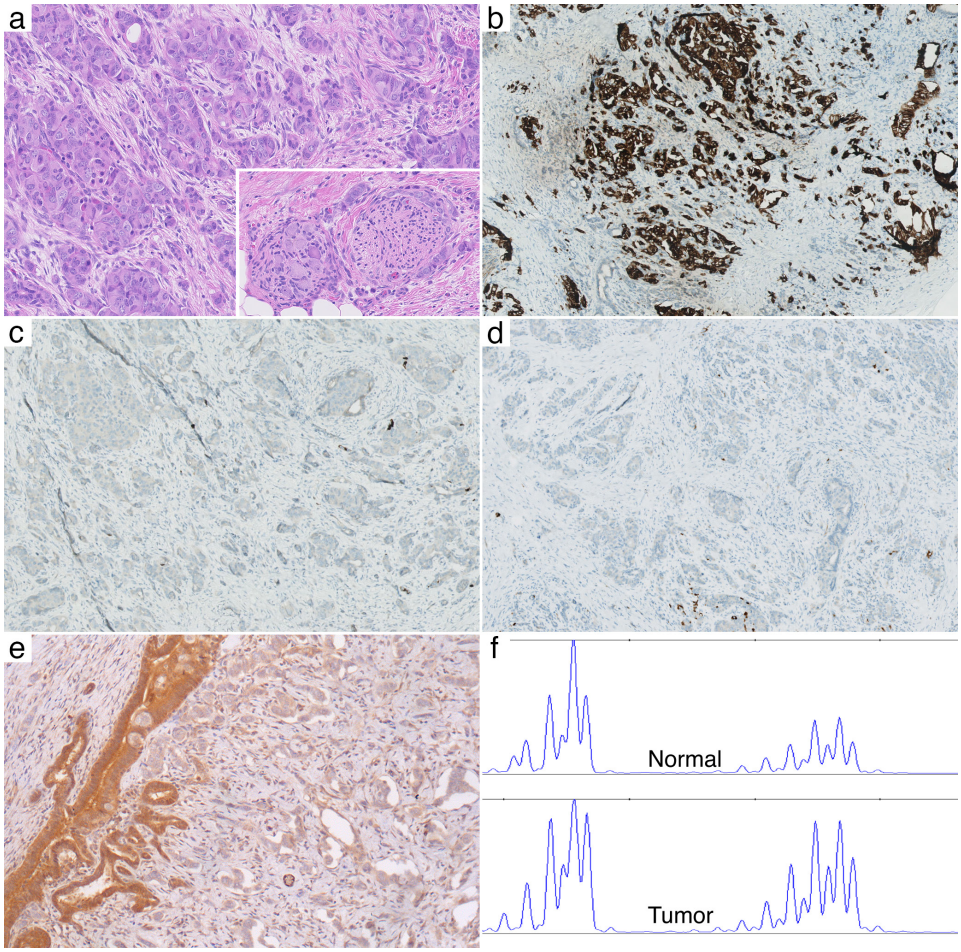

Figure 2. a Hematoxylin and eosin staining of the neoplasm in the pancreas shows cellular atypia. The smaller inset shows perineural growth. **b** Immunohistochemistry for synaptophysin shows strong labeling of the neoplastic cells. **c** Immunohistochemistry for BCL10 shows absence of labeling in the neoplastic cells. **d** Absence of immunolabeling for P16 in the neoplasm. Some non-neoplastic cells, caught in between the neoplastic cells, show labeling for P16. **e** Immunohistochemistry for the MTAP protein, showing less labeling in the neoplastic cells, while a pancreatic duct, caught in the tumor, shows preserved labeling. **f** LOH analysis for the D9S1749 probe shows allelic imbalance, resulting from disproportional signals in the tumor, in comparison with the signals from the normal tissue. These disproportional signals meet the criteria for LOH.

and somatostatin receptor 2A was positive, while BCL10 was negative (Figure 2C). The tumor showed expression of both pancreatic endocrine transcription factors ARX and PDX1. Ki-67 showed a labeling index of 11%, consistent with a well-differentiated neuroendocrine tumor, grade 2. The tumor was negative for P16 labeling (Figure 2D) and showed loss of MTAP (Figure 2E), while ATRX, DAXX, SMAD4 and p53 showed normal (wild type) expression. LOH analysis of the *MTAP-CDKN2A/B* region showed LOH for 2 (D9S162 and D9S1749) of the 4 tested markers (Figure 2F). The other markers did not show LOH, but it should be mentioned that the tumor had low tumor cellularity, due to its infiltrative growth in the surrounding normal tissue. A fluorescence in situ hybridization with a probe against *CDKN2A* showed also loss of one of the 2 copies of the gene. There was not enough DNA to carry out an LOH

analysis for *NF2* on the tumor, but MLPA showed that the mosaic *NF2* deletion was not present in the patients with normal pancreatic tissue.

MATERIALS AND METHODS

Formalin-fixed paraffin-embedded (FFPE) tissue of the resected tumor was macrodissected to enhance neoplastic cellularity. DNA was extracted using the Qiagen QIAamp DNA FFPE tissue kit (Qiagen, Hilden, Germany) according to the manufacturer's instructions. Allelic status (LOH) was assessed by comparing constitutionally heterozygous (informative) alleles with the corresponding alleles in the tumor. Four fluorescent end-labelled microsatellite markers that map to the *MTAP-CDKN2A/B* region were used: D9S162, D9S1749, D9S916, and D9S932. D9S162 is located telomeric to *MTAP*, D9S1749 and D9S916 are located in the *MTAP* gene, and D9S932 is located centromeric of *CDKN2A/B*. After PCR amplification, the products were separated using an ABI Prism 310 genetic analyzer (Applied Biosystems, Waltham, MA). One microliter of the PCR product was mixed with 23 µL of formamide and 0.5 µL of GeneScanTM ROX-500 (Invitrogen Corporation, Waltham, MA) as a size marker. Markers with 2 distinctly sized alleles in the normal were termed informative. For the informative marker, the allelic imbalance factor was calculated, as described by Cawkwell et al.[33] LOH was assumed if the allelic imbalance factor was <0.7 or >1.3. A similar approach was used to do the LOH analysis for NF2. There was not enough DNA left to carry out the analysis on the tumor, but neighboring normal pancreatic tissue was used to detect the germline *NF2*-gene deletion, previously found in the schwannomas of the patient. To investigate the role of the mosaic *NF2* deletion previously found in the schwannomas of this patient in the development of his PanNET, *NF2* MLPA was performed using MLPA P044 *NF2* probe mix according to the manufacturer's instructions (MRC Holland, Amsterdam, the Netherlands).

Immunohistochemistry with antibodies against chromogranin, synaptophysin, somatostatin receptor 2A, BCL10, Ki-67, p16, ATRX, SMAD4, and p53 was performed using the Leica Bond III fully automated immunohistochemistry stainer on FFPE tissue. MTAP, DAXX, ARX, and PDX1 immunohistochemistry was performed by hand using a monoclonal antibody against MTAP (clone EPR6893, 1:1000; Abcam, Cambridge, UK), DAXX (clone HPA008736, 1:100; Sigma-Aldrich, St. Louis, MO), ARX (clone 11F6.2, 1:2000; Millipore Burlington, MA), and PDX1 (clone EPR3358(2), 1:2000; Abcam), respectively.

Fluorescence in situ hybridization for *CDKN2A* was performed with the ZytoLight SPEC CDKN2A/CEN 9 Dual Color Probe (ZytoVision, Bremerhaven, Germany). At least 100 normal cells and 100 tumor cells were counted for the *CKDN2A*-probe signal. Cells showed 0, 1, or 2 signals, and a 2×3 contingency table was made. The Fisher exact test showed statistical significance, with a P-value smaller than 0.05 ($P=1.78e{-}26$).

DISCUSSION

We present a patient with a germline mutation in *CDKN2A* and mosaicism for neurofibromatosis type 2, who developed a small, PanNET, detected during screening for pancreatic ductal adenocarcinoma (PDAC). Labeling for p16 (the product of *CDKN2A*) was negative, although normal tissue does not express this protein either, as is considered normal for nonsenescent cells. The PanNET also showed loss of expression for the MTAP protein, encoded by its gene neighboring *CDKN2A*. In addition, the somatic LOH on chromosome 9p was shown for heterozygous SNPs around the *CDKN2A* and *MTAP* genes. This provides compelling evidence that the PanNET in this patient was causally related to the patient's underlying germline *CDKN2A* mutation and was not a coincidence.

Patients with germline *CDKN2A* mutations have an increased risk for certain cancers, including PDAC. However, it is not known whether these patients also have an increased risk to develop PanNETs. The background of common genetic susceptibility to PanNETs is largely unknown. Targeted association studies in patients with PanNETs have found associations between variants of genes coding for inflammatory proteins such as the *TNF-alpha*, *IL-2*, and *IL12A* genes; however, a variant of a gene that modulates apoptosis, *DAD1*, has also been reported to be associated with an increased risk for gastroenteropancreatic NETs.[34–36] A recent, larger study studied the association of 13 SNPs in the *CDKN2A*/*B* genes and PanNETs in 320 patients and 4436 controls, and found an association between homozygotes for the minor A allele of the rs2518719 SNP in *CDKN2A* and an increased risk for developing a PanNET.[37] It is worth mentioning that this SNP was in linkage disequilibrium with another variant in the gene (rs3731217) that is a well-known pleiotropic susceptibility polymorphism, and it has been associated with an increased risk for developing childhood acute lymphoblastic leukemia, thyroid carcinoma, and salivary gland carcinoma.[38–41]

The somatic genetic alterations in PanNETs have been well characterized with whole-exome and whole-genome sequencing approaches.[30,42,43] These studies have shown that the most frequently somatically mutated genes in PanNETs are the *MEN1*, *DAXX*, and *ATRX* genes. *CDKN2A* is also often deleted or its promoter is methylated in PanNETs, but it is considered a late event in the tumorigenesis, associated with the development of metastases.[30,42,44] In many familial cancer syndromes, germline mutations can be found in genes that are completely inactivated early in the neoplastic transformation. However, germline inactivation of genes, normally inactivated later in the tumorigenesis of a neoplasm, can still result in an increased risk for the neoplasm, due to the increased likelihood to acquire only one inactivating mutation instead of acquiring 2 inactivating mutations in the same gene. Thus, patients with germline mutations in *CDKN2A*, might have a higher risk to develop PanNETs with *CDKN2A* inactivation, through the accrual of a second hit, despite being a late event in the sporadic tumorigenesis of PanNETs.[45] It has been shown that these PanNETs with *CDKN2A* inactivation are associated with metastatic disease and thus more aggressive disease.[30]

In other tumor types, the deletion of *CDKN2A* is often associated with a codeletion of the nearby *MTAP* gene. In the present case, we showed somatic loss of this gene in the neoplastic cells by immunohistochemistry and LOH analysis. The *MTAP* gene codes for methylthioadenosine phosphorylase (MTAP), and loss results in increased concentrations of methylthioadenosine (MTA) in the cell. MTA inhibits the enzymatic activity of the protein arginine methyltransferase 5 (PRMT5). Further inhibition of PRMT5 by a small molecule inhibitor, or by the administration of more MTA, results in modest impairment of cell viability in MTAP-null cancer cell lines.[46] This is a possible therapeutic target for tumors with an *MTAP* deletion.

The patient showed mosaicism for *NF2* and had been treated for multiple schwannomas. *NF2* is located on chromosome 22, which is often deleted in ampullary somatostatinomas, a specific type of PanNET, often occurring in patients with neurofibromatosis type 1.[47] There is one case report of a pancreatic gastrinoma in a patient with neurofibromatosis type 2, although no clear molecular relationship was found.[48] Analysis of the neighboring normal pancreatic tissue in our patient, did not show the specific *NF2* gene deletion that was found in the schwannomas, showing that the mosaicism was absent in the pancreas.

In conclusion, we presented a patient with a germline mutation for *CDKN2A*, at risk to develop PDAC. A small asymptomatic well-differentiated PanNET was found on screening. Molecular analysis supported the contention that the PanNET in this patient was causally related to the underlying germline *CDKN2A* mutation and was not a coincidence. This is the first report to molecularly link the development of a PanNET with the FAMMM syndrome. This finding can have implications for the screening, diagnosis, and treatment of pancreatic lesions in carriers of germline *CDKN2A* mutations.

REFERENCES

1. He, S. & Sharpless, N. E. Senescence in Health and Disease. Cell 169, 1000–1011 (2017).
2. Sharpless, N. E. et al. Loss of p16Ink4a with retention of p19Arf predisposes mice to tumorigenesis. Nature 413, 86–91 (2001).
3. Lindsten, T. et al. The combined functions of proapoptotic Bcl-2 family members bak and bax are essential for normal development of multiple tissues. Mol. Cell 6, 1389–1399 (2000).
4. Schutte, M. et al. Abrogation of the Rb/p16 tumor-suppressive pathway in virtually all pancreatic carcinomas. Cancer Res. 57, 3126–3130 (1997).
5. Wilentz, R. E. et al. Inactivation of the p16 (INK4A) tumor-suppressor gene in pancreatic duct lesions: loss of intranuclear expression. Cancer Res. 58, 4740–4744 (1998).
6. Bailey, P. et al. Genomic analyses identify molecular subtypes of pancreatic cancer. Nature 531, 47–52 (2016).
7. Chen, Z. H., Zhang, H. & Savarese, T. M. Gene deletion chemoselectivity: codeletion of the genes for p16(INK4), methylthioadenosine phosphorylase, and the alpha- and beta-interferons in human pancreatic cell carcinoma lines and its implications for chemotherapy. Cancer Res. 56, 1083–1090 (1996).
8. Harasawa, H. et al. Chemotherapy targeting methylthioadenosine phosphorylase (MTAP) deficiency in adult T cell leukemia (ATL). Leukemia 16, 1799–1807 (2002).
9. Efferth, T., Miyachi, H., Drexler, H. G. & Gebhart, E. Methylthioadenosine phosphorylase as target for chemoselective treatment of T-cell acute lymphoblastic leukemic cells. Blood Cells Mol. Dis. 28, 47–56 (2002).
10. Illei, P. B., Rusch, V. W., Zakowski, M. F. & Ladanyi, M. Homozygous deletion of CDKN2A and codeletion of the methylthioadenosine phosphorylase gene in the majority of pleural mesotheliomas. Clin. Cancer Res. 9, 2108–2113 (2003).
11. Hustinx, S. R. et al. Concordant loss of MTAP and p16/CDKN2A expression in pancreatic intraepithelial neoplasia: evidence of homozygous deletion in a noninvasive precursor lesion. Mod. Pathol. 18, 959–963 (2005).
12. Goldstein, A. M. et al. Increased risk of pancreatic cancer in melanoma-prone kindreds with p16INK4 mutations. N. Engl. J. Med. 333, 970–974 (1995).
13. Cannon-Albright, L. A. et al. Assignment of a locus for familial melanoma, MLM, to chromosome 9p13-p22. Science 258, 1148–1152 (1992).
14. Kamb, A. et al. A cell cycle regulator potentially involved in genesis of many tumor types. Science 264, 436–440 (1994).
15. Gruis, N. A. et al. Homozygotes for CDKN2 (p16) germline mutation in Dutch familial melanoma kindreds. Nat. Genet. 10, 351–353 (1995).
16. Vasen, H. F. et al. Risk of developing pancreatic cancer in families with familial atypical multiple mole melanoma associated with a specific 19 deletion of p16 (p16-Leiden). Int. J. Cancer 87, 809–811 (2000).
17. Lynch, H. T. et al. Phenotypic variation in eight extended CDKN2A germline mutation familial atypical multiple mole melanoma-pancreatic carcinoma-prone families: the familial atypical mole melanoma-pancreatic carcinoma syndrome. Cancer 94, 84–96 (2002).
18. Goldstein, A. M., Struewing, J. P., Chidambaram, A., Fraser, M. C. & Tucker, M. A. Genotype-phenotype relationships in U.S. melanoma-prone families with CDKN2A and CDK4 mutations. J. Natl. Cancer Inst. 92, 1006–1010 (2000).
19. Hruban, R. H. et al. Familial pancreatic cancer. Ann. Oncol. 10 Suppl 4, 69–73 (1999).
20. Vasen, H. F. A. et al. Magnetic Resonance Imaging Surveillance Detects Early-Stage Pancreatic Cancer in Carriers of a p16-Leiden Mutation. Gastroenterology 140, 850–856 (2011).
21. Canto, M. I. et al. International Cancer of the Pancreas Screening (CAPS) Consortium summit on the management of patients with increased risk for familial pancreatic cancer. Gut 62, 339–347 (2013).
22. Winter, J. M. et al. Periampullary and pancreatic incidentaloma: a single institution's experience with an increasingly common diagnosis. Ann. Surg. 243, 673–80; discussion 680–3 (2006).
23. Lahat, G. et al. Pancreatic incidentalomas: high rate of potentially malignant tumors. J. Am. Coll. Surg. 209, 313–319 (2009).
24. Takeda, Y. et al. Asymptomatic Pancreatic Cancer: Does Incidental Detection Impact Long-Term Outcomes? J. Gastrointest. Surg. (2017) doi:10.1007/s11605-017-3421-2.
25. Canto, M. I. et al. Risk of Neoplastic Progression in Individuals at High Risk for Pancreatic Cancer Undergoing Long-term Surveillance. Gastroenterology 155, 740–751.e2 (2018).
26. Zhao, R., Choi, B. Y., Lee, M.-H., Bode, A. M. & Dong, Z. Implications of Genetic and Epigenetic Alterations of CDKN2A (p16(INK4a)) in Cancer. EBioMedicine 8, 30–39 (2016).
27. Eckerle Mize, D., Bishop, M., Resse, E. & Sluzevich, J. Familial Atypical Multiple Mole Melanoma Syndrome. in Cancer Syndromes (eds. Riegert-Johnson, D. L., Boardman, L. A., Hefferon, T. & Roberts, M.) (National Center for Biotechnology Information (US), 2011).
28. de Snoo, F. A. et al. Increased risk of cancer other than melanoma in CDKN2A founder mutation (p16-Leiden)-positive melanoma families. Clin.

Cancer Res. 14, 7151–7157 (2008).
29. Potjer, T. P. et al. Prospective risk of cancer and the influence of tobacco use in carriers of the p16-Leiden germline variant. Eur. J. Hum. Genet. 23, 711–714 (2015).
30. Roy, S. et al. Loss of Chromatin Remodeling Proteins and/or CDKN2A Associates With Metastasis of Pancreatic Neuroendocrine Tumors and Reduced Patient Survival Times. Gastroenterology (2018) doi:10.1053/j.gastro.2018.02.026.
31. Evans, D. G. et al. Somatic mosaicism: a common cause of classic disease in tumor-prone syndromes? Lessons from type 2 neurofibromatosis. Am. J. Hum. Genet. 63, 727–736 (1998).
32. Kluwe, L. et al. Molecular study of frequency of mosaicism in neurofibromatosis 2 patients with bilateral vestibular schwannomas. J. Med. Genet. 40, 109–114 (2003).
33. Cawkwell, L. et al. Rapid detection of allele loss in colorectal tumours using microsatellites and fluorescent DNA technology. Br. J. Cancer 67, 1262–1267 (1993).
34. Berkovic, M. C. et al. IL-2 -330 T/G SNP and serum values-potential new tumor markers in neuroendocrine tumors of the gastrointestinal tract and pancreas (GEP-NETs). J. Mol. Med. 88, 423–429 (2010).
35. Berkovic, M., Cacev, T., Zjacic-Rotkvic, V. & Kapitanovic, S. TNF-alpha promoter single nucleotide polymorphisms in gastroenteropancreatic neuroendocrine tumors. Neuroendocrinology 84, 346–352 (2006).
36. Ter-Minassian, M. et al. Genetic associations with sporadic neuroendocrine tumor risk. Carcinogenesis 32, 1216–1222 (2011).
37. Campa, D. et al. Common germline variants within the CDKN2A/2B region affect risk of pancreatic neuroendocrine tumors. Sci. Rep. 6, 39565 (2016).
38. Migliorini, G. et al. Variation at 10p12.2 and 10p14 influences risk of childhood B-cell acute lymphoblastic leukemia and phenotype. Blood 122, 3298–3307 (2013).
39. Sherborne, A. L. et al. Variation in CDKN2A at 9p21.3 influences childhood acute lymphoblastic leukemia risk. Nat. Genet. 42, 492–494 (2010).
40. Zhang, F. et al. Significance of MDM2 and P14 ARF polymorphisms in susceptibility to differentiated thyroid carcinoma. Surgery 153, 711–717 (2013).
41. Jin, L. et al. Genetic variation in MDM2 and p14ARF and susceptibility to salivary gland carcinoma. PLoS One 7, e49361 (2012).
42. Scarpa, A. et al. Whole-genome landscape of pancreatic neuroendocrine tumours. Nature (2017) doi:10.1038/nature21063.
43. Jiao, Y. et al. DAXX/ATRX, MEN1, and mTOR pathway genes are frequently altered in pancreatic neuroendocrine tumors. Science 331, 1199–1203 (2011).
44. Muscarella, P. et al. Genetic alterations in gastrinomas and nonfunctioning pancreatic neuroendocrine tumors: an analysis of p16/MTS1 tumor suppressor gene inactivation. Cancer Res. 58, 237–240 (1998).
45. Langeveld, D. et al. SMAD4 immunohistochemistry reflects genetic status in juvenile polyposis syndrome. Clin. Cancer Res. 16, 4126–4134 (2010).
46. Kryukov, G. V. et al. MTAP deletion confers enhanced dependency on the PRMT5 arginine methyltransferase in cancer cells. Science 351, 1214–1218 (2016).
47. Noë, M. et al. Whole-exome sequencing of duodenal neuroendocrine tumors in patients with neurofibromatosis type 1. Mod. Pathol. (2018) doi:10.1038/s41379-018-0082-y.
48. Massironi, S. et al. Gastrinoma and neurofibromatosis type 2: the first case report and review of the literature. BMC Gastroenterol. 14, 110 (2014).

13

Part 4
Conclusion

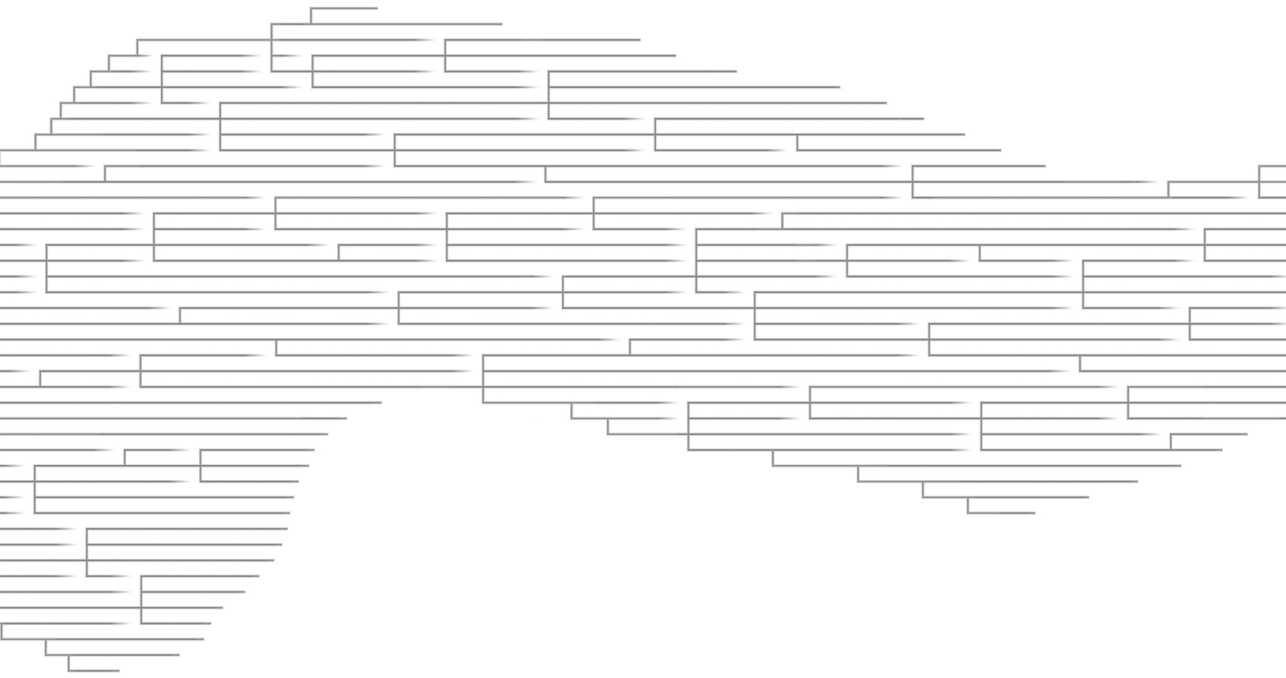

Chapter 14

Summarizing discussion

The pathogenesis of cancer starts with a non-invasive, clonal outgrowth.[1] Human evolution has selected mechanisms that suppress the fixation and further emergence of clonal outgrowths through the optimal organization of our cells.[2,3] Despite these mechanisms, precursor lesions to cancer develop in all people, especially in organs with a high cellular turnover. It has been modeled that cancer risk is related to the amount of stem cell divisions in an organ.[4,5] In this thesis, we studied the molecular and morphologic features of pancreatic cancer and its precursor lesions. We focused specifically on the precursors of pancreatic ductal adenocarcinoma (PDAC): a tumor that is often detected in an advanced stage.[6] Early detection strategies offer the best chance for curative treatment and have proven to reduce the disease-specific mortality in other cancer-types like breast cancer, colon cancer and cervical cancer.[7] Some precursor lesions that can evolve into pancreatic cancer, can easily be detected by medical imaging. These precursors are macroscopic cysts like intraductal papillary mucinous neoplasms (IPMNs) and mucinous cystic neoplasms (MCNs).[8] Because these cysts are abundant in the population, risk stratification and identification of patients at high risk to develop pancreatic cancer is necessary to focus screening and prophylactic treatment efforts. [9–11]

Part 1: Molecular evolution of intraductal neoplasms

In the first part of this thesis, we studied the moment of invasion by comparing both the genetic alterations found in high-grade precursor lesions and PDACs. In chapter 3, we compared exome sequencing data from IPMNs and MCNs with their associated invasive components. Although we did not discover a molecular event that could explain invasive behaviour in every case, we did see *SMAD4* and *TGFBR2* mutations in the invasive components of 4 of the 18 studied cases. *SMAD4* is an essential downstream regulator of the TGF-beta pathway and the bone morphogenic protein (BMP) pathway. In colonic organoid models, mutations in these pathways made the organoids grow without the inhibitor of the BMP pathway, Noggin.[12] In organoids from normal colonic epithelium, it is necessary to inhibit the pathway in order to expand the organoids outside their normal tissue context.[13] From the perspective of these organoid studies, the inactivation of the TGF-beta pathway and the BMP pathway results in an acquired independence of the cells to grow without the presence of certain factors. Similar acquired independence from growth factors has been observed when other driver-mutations were induced.[12] More evidence for the acquired independence from certain factors can be found in the histology of both cancerized ducts in patients with PDACs and in the colonic polyps of patients with juvenile polyposis, an autosomal-dominant, gastroinestinal polyposis syndrome in which germline *SMAD4* mutations have been found. In the cancerized ducts, cancer cells can be observed to grow on top of each other.[14,15] Normally, each cell delineating the pancreatic duct is attached to the basement membrane. The growth of cells that don't attach to the basement membrane can be seen as a form of acquired independence from trophic factors that are present in the basement membrane. In patients with juvenile polyposis, colonic hamartomatous polyps can develop. These polyps are characterized by ectopic crypts: the proliferative compartment of the crypt is not confined to the bottom of the crypt, but can also be found higher up in the crypt.[16] This can also be interpreted as the acquired independence of the proliferative compartment to grow outside the intended area at the bottom of the crypt.

In chapter 4, we describe that in a cohort of patients with high-grade PanIN lesions, without a concomitant cancer, *SMAD4* or *P53* mutations could not be detected in these high-grade precursors. This gives extra evidence for the role and timing of *SMAD4* mutations in pancreatic carcinogenesis and for their importance during invasion. In the previous chapter (chapter 3), we sometimes observed *SMAD4* mutations in both the cancer and the intra-ductal growth of the neoplasm. This observation seems to be in conflict with the previous indications that cells with inactivated TGF-beta and BMP pathways, have acquired invasive behaviour. However, cells with invasive properties can still be observed in the duct system of the pancreas. There are two possible explanations for this observation:

- When a PDAC grows and spreads through the tissue of the pancreas, it might encounter normal pancreatic ducts. The invasive properties of the cancer cells might result in the cancer invading a pancreatic duct. In this case, the cells have already obtained invasive behaviours, but can still be found in a pancreatic duct. The cancer cells in the duct can further evolve neutrally and acquire more passenger mutations than the cancer cells that are out of the duct, due to its spatial separation. This description explains our observations in case MTP19, as described in chapter 3 and is called 'cancerization of ducts'.
- When, by the stochastic process of mutagenesis, an inactivating mutation in *SMAD4* or *TGFBR2* occurs in a cell that does not neighbour the surrounding connective tissue of an IPMN (for example, a cell on the tip of papillae in an IPMN, far away from the surrounding pancreatic tissue), the cell won't be able to immediately exert it's invasive behaviour. The clone must expand in order to reach the surrounding tissue or the cyst wall. This can explain the detection of *SMAD4*/*TGFBR2*-mutated cells in the duct, which in theory could already be observed before invasion.

Some pathologists might assume that the intraductal growth of a neoplasm is an indication that the neoplastic cells have not yet obtained the capacities to invade in the surrounding tissue. This might not be the case and this assumption might have resulted in conflicting results while studying the molecular events that lead to cancer invasion. Because of this, the observations of missing *SMAD4* mutations in high-grade precursor lesions like PanIN, gives extra evidence for the invasion-promoting effects of *SMAD4* or *TGFBR2* inactivation.

If invasion is the result of the complete independence of neoplastic cells from all local trophic factors, one might wonder if there is still a biological hurdle to jump before a cell can metastasize out of its organ of origin. Although researchers have looked for molecular evidence of such a hurdle in cells of metastases, this evidence has been difficult to find.[17–19] Based on our results and the concepts discussed in this thesis, such a hurdle might not even exist. It should be said that absence of evidence for a molecular event that gives a cell its metastatic potential should not be interpreted as evidence of its absence.

Our exome-sequencing study has also confirmed the sequence of mutations in driver genes observed by other researchers. *KRAS* and *GNAS*-activating mutations and *CDKN2A*-inactivating mutations are considered early driver-mutations, followed by *RNF43*-inactivating mutations. *SMAD4* and *P53*-inactivating mutations are considered late in the carcinogenesis of pancreatic ductal adenocarcinoma. The

importance of this sequence is also reflected in by the frequent detection of mutations in the same gene in lesions of the same grade. In early lesions, we observed multiple *KRAS* mutations, while different locations in the high-grade IPMNs often contained different *RNF43* mutations. It shows that mutations in a specific gene give the cell an evolutionary advantage and that driver mutations can only be accumulated in a specific order. It is by chance that a mutation hits a cell in a specific gene. Patients with McCune-Albright syndrome, caused by mosaicism of activating mutations in *GNAS*, have a higher chance to develop lesions that are caused by these mutations, like IPMNs and other lesions (chapter 6), because the causative mutation occurred during embryogenesis.

Similar dynamics are seen in other cancer syndromes. In chapter 13 we discussed a patient with a germline mutation in *CDKN2A*, which causes familial atypical multiple mole melanoma (FAMMM) syndrome. These patients are also at risk to develop PDAC, where *CDKN2A*-inactivating mutations are considered early driver mutations. *CDKN2A* is a tumor suppressor gene and both alleles must be inactivated to impair the function of the gene.[20] In general, it will take more time to inactivate two functional alleles of this tumor suppressor in the same cell through random mutagenesis than only one functional allele. This mechanism is considered the reason why patients with a germline mutation in a tumor suppressor gene have a higher risk to develop cancer. In chapter 12, we studied pancreatic neuroendocrine tumors in patients with neurofibromatosis type 1 (NF1). These patients have a germline mutation in the *NF1* gene. As predicted by the principles described above, the most common somatic mutation in the tumors were mutations in *NF1* as a second hit to completely inactivate the gene.

Theoretically, the risk to develop precursor lesions is higher when a germline mutation is present in an early driver-gene in comparison with a germline mutation in a late driver-gene. We can explain this statement by considering the timing of the evolution of precursor lesions. In chapter 3, we have used the principle of the 'molecular clock' to calculate the time it takes to develop a PDAC from a high-grade IPMN: 3 years. Because patients often present with PDAC when they are in their 7th decade, the initial evolution of early and late precursor lesions must take much longer.[21–25] Activating *KRAS* or *GNAS* mutations are considered a requirement for the development of early precursor lesions and obtaining these mutations through random mutagenesis, followed by the outgrowth of the mutated cell can take a long time. Because of that, patients who are born with this early mutation (McCune-Albright Syndrome, chapter 6) will develop these precursor lesions much faster. In contrast, when the average time to evolve from high-grade IPMN into a PDAC through the inactivation of a late driver gene is only 3 years, the effect of a germline mutation in that late driver-gene has probably less impact on the lifetime risk to develop these cancers. This difference in time needed to evolve can be explained by the observation that over time and over decreasing differentiation, the clone will increase its division rate and possibly its mutation rate.[26] Normal cells have a mutation rate that is considered a function of the cell division rate. It is difficult to study the changes in mutation rate per cell division during the evolution of precursor lesions, but based on observations in mismatch-repair deficient tumors, it has been shown that at least in some cancers, there is an increase in the mutation rate. The increase in cell division rate and mutation rate can contribute to explaining why the evolution of high-grade IPMNs to PDACs only takes 3 years.

In chapter 5, we have used targeted sequencing of the pancreatic driver genes to investigate the relatedness of synchronous IPMNs and PDACs. Both IPMN and PanIN lesions are considered precursors to pancreatic cancer, however their relative contribution is not equal: IPMNs are observed in 8% of the cancers, and the rest is thought to originate from PanINs. Because of the high a priori probability that a PDAC originates from a PanIN, the simultaneous presence of a PDAC and IPMN does not automatically mean that they are related. The study of driver mutations confirms this and showed that 18% of the synchronous PDACs and IPMNs are not related.

Part 2: Three-dimensional histopathology through tissue clearing

We developed a tissue-clearing technique, based on methods used for tissue clearing of murine brain tissue. The optimization of the technique was complicated by the abundance of a dense extracellular matrix, which obstructed penetrating antibodies.[27] Chapter 7 is an in-depth review of the literature on the different tissue clearing techniques and three-dimensional imaging techniques to investigate which techniques might yield the best results for human pancreatic tissues.

The development of tissue clearing techniques that enable the study of histopathology in three dimensions has resulted in some remarkable observations. In pancreatic ductal adenocarcinomas, we observed frequent invasion of the veins, as described in chapter 8 and 9. Since veins are the highways out of the pancreas, invasion in veins is probably an important step in the development of metastasis. This could explain why patients with PDAC often present in an advanced stage with multiple metastases in the liver (chapter 10). Other studies have also observed that venous invasion is prevalent in pancreatic cancers and have described how the cancer cells often replace the endothelial cells in the vein.[28,29] Because of this, structures can be formed that look very similar to ducts. Our three-dimensional studies have confirmed these observations of venous invasion (chapter 9). The growth of cancer cells in veins, which are often located next to arteries, can result in a histologic hallmark sign of pancreatic cancer: cancer ducts next to muscularized blood vessels, like arterial vessels.[30]

Emerging tissue clearing techniques allow for the first time, to investigate histology in three dimensions. Regular, two-dimensional histopathology is an inaccessible branch of science, as it requires extensive training. Tissue clearing techniques can help pathologists to explain certain histologic concepts to other professionals. One such concept is ‘tumor-budding’: single tumor cells or a small groups of tumor cells, that are often located at the invasive front of the tumor. Although this feature is an independent prognostic factor for adverse clinical outcomes, it is difficult to explain what these single cells represent and how this feature in two-dimensional microscopy is organized in three-dimensions.[31] Studies are underway to visualize tumor budding in 3D through tissue clearing techniques, in order to better understand this phenomenon.

Part 3: Pancreatic neuroendocrine neoplasms

In chapter 11, we characterized the molecular features associated with metastasizing potential in small

neuroendocrine tumors of the pancreas. Clustering of these neuroendocrine tumors based on copy number status identified 3 different groups. The group with the highest ratio (group 1) of metastasizing tumors was associated with copy-number gains, alternative lengthening of telomeres (ALT), and loss of DAXX and ATRX. The other two groups had lower ratios of metastasizing tumors. Group 2 was associated with minimal chromosomal alterations, no ALT, and no loss of DAXX or ATRX. Tumors in group 3 had deletions or mutations of *MEN1*, located on chromosome 11q and a negative regulator of telomerase.[32,33] Deletions of chromosome 22, absence of ALT, and normal expression of DAXX and ATRX were also common in this group. Overall, multivariate analysis showed that the Ki-67 index and the ALT-status is statistically significant associated with liver metastasis.

A recent, larger study investigated the molecular features associated with metastases over all the solid tumors.[19] Genome duplication events were found in 56% of the metastases. Another study restricted to PDACs found genome duplication in 48% of the tumors.[34] This last study modeled that most copy number losses and gains occurred after polyploidization. Although some copy number changes occured before polyploidization, chromosomal deletions and gains occuring after genome doubling were more structurally damaging. In other organisms like yeast and plants, polyploidization has been associated with rapid adaptation to new environments.[35,36] Because most mutations are deleterious, polyploidization buffers the effects of partially recessive, deleterious mutations which can then accumulate, providing a reservoir of mutations that might be adaptive in a new environment.[37,38] In these organisms, polyploidization is also often followed by larger structural changes in the genome.[35,36] Although these comparisons with other organisms have limitations, they can provide new ideas on how polyploidization can promote cancer invasion. In the plants, polyploidization has even been shown to promote the invasion of plants in new environments.[36]

In chapter 12, we describe the genetic alterations of a clinically well-characterized cohort of six NF1-associated duodenal neuroendocrine tumors using whole-exome sequencing. NF1 is a hereditary cancer predisposition syndrome characterized by frequent cutaneous and nervous system abnormalities. Patients with NF1 also have an increased prevalence of multiple gastrointestinal and peripancreatic neoplasms, including neuroendocrine tumors of the ampulla that express somatostatin. These tumors often had somatic mutations in *NF1* which, together with germline mutations in the other allele, caused the complete inactivation of the *NF1* gene. We also found frequent deletions of chromosome 22 in these tumors.

In chapter 13, we described a patient with a germline *CDKN2A* mutations (FAMMM syndrome), at high risk to develop a PDAC. During screening, a pancreatic lesion was detected which was resected and diagnosed as a small neuroendocrine neoplasm. We found that the tumor had loss of heterozygosity for *CDKN2A* (the second hit), and we raised the possibility that neuroendocrine pancreatic neoplasms, which often have late driver-mutations in *CDKN2A*, might be part of this cancer predisposition syndrome. This case was discussed under part 1 of the summarizing discussion.

REFERENCES

1. Fearon, E. R. & Vogelstein, B. A genetic model for colorectal tumorigenesis. Cell 61, 759–767 (1990).
2. Hanahan, D. & Weinberg, R. A. Hallmarks of cancer: the next generation. Cell 144, 646–674 (2011).
3. Lieberman, E., Hauert, C. & Nowak, M. A. Evolutionary dynamics on graphs. Nature 433, 312–316 (2005).
4. Tomasetti, C. & Vogelstein, B. Cancer etiology. Variation in cancer risk among tissues can be explained by the number of stem cell divisions. Science 347, 78–81 (2015).
5. Tomasetti, C., Li, L. & Vogelstein, B. Stem cell divisions, somatic mutations, cancer etiology, and cancer prevention. Science 355, 1330–1334 (2017).
6. Siegel, R. L., Miller, K. D. & Jemal, A. Cancer statistics, 2019. CA Cancer J. Clin. 69, 7–34 (2019).
7. Prasad, V., Lenzer, J. & Newman, D. H. Why cancer screening has never been shown to 'save lives'--and what we can do about it. BMJ 352, h6080 (2016).
8. Winter, J. M. et al. Periampullary and pancreatic incidentaloma: a single institution's experience with an increasingly common diagnosis. Ann. Surg. 243, 673–80; discussion 680–3 (2006).
9. Tanaka, M. et al. International consensus guidelines 2012 for the management of IPMN and MCN of the pancreas. Pancreatology 12, 183–197 (2012).
10. Tanaka, M. et al. International consensus guidelines for management of intraductal papillary mucinous neoplasms and mucinous cystic neoplasms of the pancreas. Pancreatology 6, 17–32 (2006).
11. Vege, S. S. et al. American gastroenterological association institute guideline on the diagnosis and management of asymptomatic neoplastic pancreatic cysts. Gastroenterology 148, 819–22; quize12–3 (2015).
12. Drost, J. et al. Sequential cancer mutations in cultured human intestinal stem cells. Nature 521, 43–47 (2015).
13. Sato, T. et al. Long-term expansion of epithelial organoids from human colon, adenoma, adenocarcinoma, and Barrett's epithelium. Gastroenterology 141, 1762–1772 (2011).
14. Hutchings, D. et al. Cancerization of the Pancreatic Ducts: Demonstration of a Common and Under-recognized Process Using Immunolabeling of Paired Duct Lesions and Invasive Pancreatic Ductal Adenocarcinoma for p53 and Smad4 Expression. Am. J. Surg. Pathol. 42, 1556–1561 (2018).
15. Ban, S., Shimizu, Y., Ogawa, F. & Shimizu, M. Reevaluation of 'Cancerization of the Duct' by Pancreatic Cancers. (2007).
16. Haramis, A.-P. G. et al. De novo crypt formation and juvenile polyposis on BMP inhibition in mouse intestine. Science 303, 1684–1686 (2004).
17. Yachida, S. et al. Distant metastasis occurs late during the genetic evolution of pancreatic cancer. Nature 467, 1114–1117 (2010).
18. Makohon-Moore, A. P. et al. Limited heterogeneity of known driver gene mutations among the metastases of individual patients with pancreatic cancer. Nat. Genet. (2017) doi:10.1038/ng.3764.
19. Priestley, P. et al. Pan-cancer whole-genome analyses of metastatic solid tumours. Nature 575, 210–216 (2019).
20. Knudson, A. G., Jr. Mutation and cancer: statistical study of retinoblastoma. Proc. Natl. Acad. Sci. U. S. A. 68, 820–823 (1971).
21. Salvia, R. et al. Main-duct intraductal papillary mucinous neoplasms of the pancreas: clinical predictors of malignancy and long-term survival following resection. Ann. Surg. 239, 678–85; discussion 685–7 (2004).
22. Chari, S. T. et al. Study of recurrence after surgical resection of intraductal papillary mucinous neoplasm of the pancreas. Gastroenterology 123, 1500–1507 (2002).
23. Ingkakul, T. et al. Predictors of the presence of concomitant invasive ductal carcinoma in intraductal papillary mucinous neoplasm of the pancreas. Ann. Surg. 251, 70–75 (2010).
24. Sohn, T. A. et al. Intraductal papillary mucinous neoplasms of the pancreas: an updated experience. Ann. Surg. 239, 788–97; discussion 797–9 (2004).
25. Crippa, S. et al. Mucin-producing neoplasms of the pancreas: an analysis of distinguishing clinical and epidemiologic characteristics. Clin. Gastroenterol. Hepatol. 8, 213–219 (2010).
26. Takeshita, A. et al. Clinicopathologic study of the MIB-1 labeling index (Ki67) and postoperative prognosis for intraductal papillary mucinous neoplasms and ordinary ductal adenocarcinoma. Pancreas 41, 114–120 (2012).
27. Tian, C. et al. Proteomic analyses of ECM during pancreatic ductal adenocarcinoma progression reveal different contributions by tumor and stromal cells. Proc. Natl. Acad. Sci. U. S. A. 116, 19609–19618 (2019).
28. Hong, S.-M. et al. Vascular invasion in infiltrating ductal adenocarcinoma of the pancreas can mimic pancreatic intraepithelial neoplasia: a histopathologic study of 209 cases. Am. J. Surg. Pathol. 36, 235–241 (2012).
29. Yamada, M. et al. Microscopic Venous Invasion in Pancreatic Cancer. Ann. Surg. Oncol. 25, 1043–1051 (2018).
30. Sharma, S. & Green, K. B. The pancreatic duct and

its arteriovenous relationship: an underutilized aid in the diagnosis and distinction of pancreatic adenocarcinoma from pancreatic intraepithelial neoplasia. A study of 126 pancreatectomy specimens. Am. J. Surg. Pathol. 28, 613–620 (2004).
31. Lino-Silva, L. S., Salcedo-Hernández, R. A. & Gamboa-Domínguez, A. Tumour budding in rectal cancer. A comprehensive review. Contemp. Oncol. 22, 61–74 (2018).
32. Lin, S. Y. & Elledge, S. J. Multiple tumor suppressor pathways negatively regulate telomerase. Cell 113, 881–889 (2003).
33. Mirabello, L. et al. The association of telomere length and genetic variation in telomere biology genes. Hum. Mutat. 31, 1050–1058 (2010).
34. Notta, F. et al. A renewed model of pancreatic cancer evolution based on genomic rearrangement patterns. Nature 538, 378–382 (2016).
35. Selmecki, A. M. et al. Polyploidy can drive rapid adaptation in yeast. Nature 519, 349–352 (2015).
36. te Beest, M. et al. The more the better? The role of polyploidy in facilitating plant invasions. Ann. Bot. 109, 19–45 (2012).
37. Storchová, Z. et al. Genome-wide genetic analysis of polyploidy in yeast. Nature 443, 541–547 (2006).
38. Dewhurst, S. M. et al. Tolerance of whole-genome doubling propagates chromosomal instability and accelerates cancer genome evolution. Cancer Discov. 4, 175–185 (2014).

14

Chapter 15

Nederlandse samenvatting

Hoofdstuk 1 is een algemene introductie tot deze thesis. In delen 1 en 2 bestuderen we voornamelijk intraductale papillaire mucineuze neoplasie (intraductal papillary mucinous neoplasm; IPMN) en ductaal adenocarcinoom van de pancreas (pancreatic ductal adenocarcinoma; PDAC). IPMNs zijn cysteuze voorlopers van PDAC. Deze voorlopers zijn klinisch detecteerbaar en komen voor bij een aanzienlijk deel van de bevolking. Bij slechts een klein deel van deze patiënten evolueert de IPMN tot een PDAC. Vanaf het ontstaan van een PDAC uit een IPMN (vanaf het moment dat invasie van het omliggend weefsel begint), wordt de prognose slechter. Kankers zoals PDAC hebben een slechte prognose wanneer ze metastaseren. Om dit te voorkomen probeert men deze tumoren vroeg te detecteren en te behandelen. Daarom is 'het moment van invasie' klinisch relevant en kan de studie ervan mogelijks impact hebben op behandelingsstrategieën. Reeds veel onderzoekers hebben invasie onderzocht, maar de technieken waren niet altijd toereikend om te bepalen wat de oorzaak van invasie is. Wij gebruiken 2 recent ontwikkelde technieken: 'next-generation' DNA sequencen en driedimensionale histologie door middel van transparant weefsel.

'Next-generation' sequencen laat ons toe door middel van het parallelliser, een enorme hoeveel informatie te verzamelen over de tumoren en hun voorlopers. Hierdoor kunnen we het deel van het genoom onderzoeken dat codeert voor proteïnen.

Om de histologie van PDAC in drie dimensies te bestuderen hebben we het weefsel doorzichtig gemaakt. Door zowel de tumorcellen als de bloedvaten aan te kleuren met verschillende fluoroforen kunnen we hun onderlinge relatie in drie dimensies bestuderen.

In het derde deel van deze thesis onderzoeken we neuroendocriene tumoren van de pancreas. Zo karakteriseren we de moleculaire eigenschappen van neuroendocriene tumoren die metastaseren naar de lever. We sequencen een neuroendocriene tumoren die voornamelijk voorkomen in de pancreas van patiënten met neurofibromatosis type 1 (NF1). Tot slot bespreken we een patiënt met familiaal atypisch meervoudig moedervlek melanoomsyndroom (FAMMM syndroom) en een neuroendocriene tumor in de pancreas.

DEEL 1: DE MOLECULAIRE EVOLUTIE VAN INTRADUCTALE NEOPLASIEËN

Hoofdstuk 2 is een overzicht van de verschillende voorloper laesies in de pancreas die aanleiding kunnen geven tot een PDAC. Pancreatische, intraepitheliale neoplasie (PanIN), is een kleine laesie waarbij het epitheel van de afvoerbuisjes morfologische veranderingen vertoont. Er is gebleken dat deze laesies clonaal zijn uitgegroeid uit één cel en verder kunnen evolueren tot ze ontaarden in een PDAC. De andere voorloper laesies zijn cysteus en kunnen dus opgespoord worden met beeldvormingstechnieken wanneer zij groot genoeg worden. Er worden 3 cystische voorlopers onderscheiden: IPMN, mucineuze cystische neoplasie (mucinous cystic neoplasm; MCN), en intraductale tubulopapillaire neoplasie (intraductal tubullopapillary neoplasm; ITPN). Van alle voorlopers bespreken we enkele klinische gegevens, specifieke histologische kenmerken en de somatische moleculaire veranderingen in het genetische materiaal van deze laesies.

Hoofdstuk 3 beschrijft een studie waarin we het DNA analyseren van zowel IPMNs als PDACs in 18 patiënten. De PDAC is verder geëvolueerd uit de IPMN en beschikt zowel over de mutaties van de IPMN als een aantal extra mutaties, die mogelijks aanleiding gaven tot invasie van het omgevend weefsel. Door de mutaties in beide laesies te vergelijken met elkaar hopen we een kleine groep van mutaties te isoleren die uniek zijn voor PDAC. Mogelijks zit in deze groep de mutatie die invasie veroorzaakt. We vonden 2 genen met PDAC-unieke mutaties in meerdere patienten: *SMAD4* en *TGFBR2*. Vermoedelijk is het inactiveren van één van deze twee genen verantwoordelijk voor invasieve groei.
Met de enorme hoeveelheid data konden we nog andere conclusies trekken. Mutaties ontstaan bij elke celdeling vermits het mechanisme dat ons DNA kopieert soms een fout maakt. De frequentie van deze fouten is vrij constant en daardoor is het aantal mutaties een soort 'moleculaire klok' die bijhoudt hoeveel celdelingen er geweest zijn. Het verschil in het aantal mutaties in een IPMN en een PDAC is een parameter voor de tijd waarop een hooggradige IPMN evolueert tot een PDAC. Ons model wees op een tijdspanne van 3 jaar. Deze periode biedt de kans om via vroegdetectie en behandeling ziekte te voorkomen.
De data gaf ook inzicht in de dynamiek van invasie. Als het basaal membraan rondom een duct doorbroken wordt en de PDAC het weefsel rondom de duct invadeert, kan deze tumor soms andere ducten tegenkomen. Wanneer deze gezonde ducten geïnvadeerd worden door de PDAC, vervangen kankercellen het normale epitheel van deze duct en lijkt het voor een patholoog alsof een voorloper laesie aanwezig is in de duct. Deze cellen verschillen echter fundamenteel in hun biologisch gedrag van echte voorloper laesies. Wij vonden moleculaire aanwijzingen voor dit fenomeen in één van de onderzochte tumoren.

Hoofdstuk 4 beschrijft de moleculaire veranderingen in hooggradige PanIN laesies van patiënten die geen PDAC hebben. We hebben ons beperkt tot het sequencen van de belangrijkste genen die gemuteerd zijn in PDACs. Ook deze studie onderzoekt welke mutaties noodzakelijk zijn voor invasieve groei, maar de aanpak is verschillend van de studie in hoofdstuk 3. *SMAD4* mutaties worden niet aangetroffen in deze hooggradige voorloper laesies. Dit levert indirect bewijs op voor de rol die *SMAD4* speelt bij de transitie van voorloper naar kanker.

Hoofdstuk 5 is een studie naar het verwantschap tussen IPMNs en PDACs. Bij ongeveer 8% van de PDACs wordt ook een IPMN waargenomen. Men vermoedt dus dat de meeste PDACs ontstaan uit PanINs, de microscopische voorlopers van PDAC. Door deze hoge a priori probabiliteit is het mogelijk dat wanneer een PDAC voorkomt in combinatie met een IPMN, een deel van de PDACs toch is ontstaan uit een PanIN laesie. Bij deze patiënten veronderstellen we misschien te snel verwantschap tussen de IPMN en de PDAC. Sequencen van de genen die de meeste driver-mutaties in PDACs bevatten, leverde inderdaad een genuanceerd beeld op. 18% van de concomitante IPMNs en PDACs bleek niet verwant te zijn.

Hoofdstuk 6 beschrijft de laesies die kunnen worden aangetroffen in de gastro-intestinale tractus van patiënten met McCune-Albright syndroom. Dit syndroom wordt veroorzaakt door een postzygotische,

activerende mutatie in GNAS tijdens de embryogenese waardoor zij mosaïcisme vertonen voor deze mutatie. Sommige cellen bevatten de mutatie, terwijl andere cellen de mutatie niet bevatten. Vermits *GNAS* ook een vroege mutatie is in de ontwikkeling van IPMN, valt het niet te verbazen dat deze patiënten een grotere kans hebben op IPMN. Daarnaast werden ook gastrische heterotopie/metaplasie, gastrische hyperplastische poliepen, fundus poliepen, en een hamartomateuze poliep aangetroffen in de hoge tractus digestivus van deze patiënten.

DEEL 2: DRIEDIMENSIONALE HISTPATHOLOGY DOOR TRANSPARANTE WEEFSEL

Hoofdstuk 7 geeft een overzicht van de technieken die gebruikt worden om weefsel transparant te maken. Dit is mogelijk doordat de variatie in refractieve index wordt geminimaliseerd. Vetten, zoals in de membranen van de cel., hebben een hoge refractieve index. Water heeft een lage refractieve index. Wanneer licht doorheen materialen schijnt met verschillende refractieve indices, buigt het en weerkaatst het. Dit kan geminimaliseerd worden door ofwel het water van het cytoplasma te vervangen door een stof met een hoge refractieve index, zoals olie, of door de celmembranen te verwijderen uit het weefsel. Alle verschillende technieken die weefsel doorzichtig maken zijn gebaseerd op dit principe. Aankleuren van de verschillende cellen gebeurt met antilichamen, waaraan een fluorofoor is gebonden. De visualisatie van het weefsel gebeurt met een microscoop waarmee driedimensionale reconstructies kunnen gemaakt worden zoals een 'light-sheet' microscoop, een confocale microscoop, en een 'two-photon' microscoop.

Hoofdstukken 8 en 9 beschrijven twee studies waarin we de histologie van PDACs in drie dimensies bestuderen. In hoofdstuk 8 wordt slechts één antilichaam gebruikt, gericht tegen CK19 dat tot expressie komt in de ductale cellen van de pancreas en in de kankercellen van een PDAC. In hoofdstuk 9 worden meerdere antilichamen gebruikt gericht tegen CK19, desmine, CD31, p53, en e-cadherine. Beide studies beschrijven invasie van tumorcellen in venes in de meeste tumoren (88%). Vaak vervangen de tumorcellen het endotheel van de venes en groeit de tumor op het basaal membraan van de vene. Hierdoor worden structuren gevormd worden die goed lijken op de afvoerbuisjes van de pancreas. Als de cytologische atypie in deze kankercellen beperkt is, zijn deze buisjes soms een diagnostische uitdaging voor een patholoog. Echter, doordat venes vaak naast arteries liggen, kunnen deze wel herkend worden als kanker, vermits normale afvoerbuisjes nooit naast arteries liggen. Een kleuring voor e-cadherine laat zien dat de expressie van dit proteïne soms verminderd is in de kankercellen, wat kan wijzen op een fenomeen dat gelinkt wordt aan invasie: epitheel-naar-mesenchym transitie (EMT). Hierbij krijgen de epitheliale cellen een meer mesenchymaal expressiepatroon, wat gelinkt wordt aan invasie van deze cellen in het omgevend weefsel.

Hoofdstuk 10 beschrijft de verschillende histologische eigenschappen van PDAC. Op basis van een literatuurstudie wordt nagegaan welke eigenschappen geassocieerd zijn met agressiviteit en slechte prognose over de verschillende kankertypes heen. Tot slot wordt geprobeerd te verklaren waarom PDAC zo een slechte prognose heeft: komen bepaalde kenmerken die een sterke associatie hebben

met agressiviteit meer voor in PDAC? Invasie van de kanker in de venes, is geassocieerd met metastasen op afstand en met een slechte prognose. Dit werd in de meeste PDACs aangetroffen, terwijl de frequentie van veneuze invasie in andere tumoren lager is. De venes in de pancreas draineren naar de lever, alwaar vaak ook de eerste metastasen van een PDAC worden aangetroffen. We opperen dat de frequente veneuze invasie mogelijks een reden is waarom PDAC zo snel metastaseert en moeilijk te behandelen is.

Deel 3: NEUROENDOCRIENE TUMOREN VAN DE PANCREAS

Hoofdstuk 11 beschrijft de moleculaire karakteristieken van neuroendocriene tumoren van pancreas (PanNETs) die metastaseren door deze te vergelijken met PanNETs die niet metastaseren. Er werden enkel kleine tumoren geïncludeerd, zodanig dat er geen bias ontstond op basis van tumorgrootte. De studie vond een statistisch significante associatie tussen alternatieve verlenging van de telomeren (alternative lengthening of telomeres; ALT) en een verhoogde Ki-67 index (een indicator van de proliferatieve activiteit) enerzijds en het ontwikkelen van levermetastasen anderzijds.

Hoofdstuk 12 is een beschrijving van de genetische veranderingen in de neuroendcriene tumoren in de pancreas van patienten die lijden aan neurofibromatosis type 1 (NF1). Deze patienten hebben een mutatie in een van de allelen van het *NF1* gen. In de tumoren zagen we dan ook vaak de inactivatie van het tweede allel van dit gen, zodanig dat het gen volledig wordt geïnactiveerd. Een tweede bevinding was het frequent verlies van een kopie van chromosoom 22. Dit werd bevestigd met fluorescente in-situ hybridisatie (FISH) waarbij één probe gericht was tegen chromosoom 22 (het *BCR* gen) en een andere probe tegen chromosoom 9 (het *ABL* gen). Deze FISH test is normaal een test voor het Philadelphia chromosoom, waarbij beide chromosomen een fuseren. In tumoren met verlies van chromosoom 22 wordt slecht 1 signaal voor dit chromosoom per cel gezien, terwijl er nog steeds twee signalen zijn van chromosoom 9 ter controle.

Hoofdstuk 13 is een beschrijving van een patient met het FAMMM syndroom. Deze patiënten hebben een kiembaanmutatie in het *CDKN2A* gen en hebben een verhoogd risico op melanoom en PDAC. Daarom worden de patiënten frequent onderzocht voor PDAC met echografie. Toen een kleine laesie werd gezien in de pancreas heeft men dit laagdrempelig gereseceerd. De tumor bleek echter geen PDAC te zijn, maar een PanNET. Zowel PDAC als PanNET bevatten vaak mutaties in *CDKN2A*. In PDAC is de inactivatie van *CDKN2A* een vroege driver-mutatie, terwijl in PanNET dit eerder een late driver-mutatie is. We bespreken de rol van de kiembaanmutaties in de pathogenese van de tumor en de impact op het risico om een tumor te ontwikkelen.

Part 5
Appendix

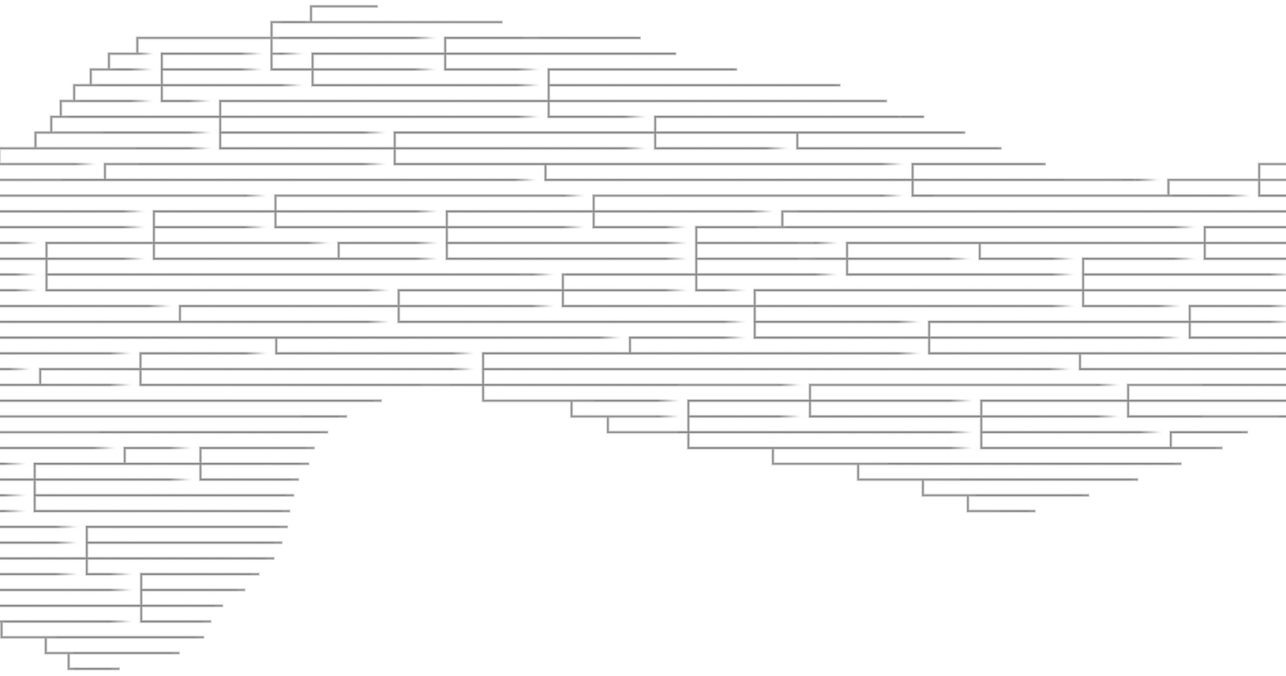

CURRICULUM VITAE

Michaël Noë was born on April 21st, 1987 in Oudenaarde, Belgium. After graduating from the Sint-Bernardus College in Oudenaarde in 2005, he started medical school at the University of Ghent. During his studies, Michaël got interested in research and he contributed to different research-projects at the department of radiology and at the department of clinical pathology, where he also did extra-curricular internships. After graduating in 2012, he joined the pathology residency program at the University Hospital of Ghent. After one and a half years, he left the program. While transitioning to join the pathology residency program at the University of Utrecht in the Netherlands, Michaël worked for 3 months as a fellow under Dr. Marc Haspeslagh in a private dermatopathology laboratory in Roeselare and in the department of dermatology at the University Hospital in Ghent,

In Utrecht, Michaël got interested by the research of the gastro-intestinal pathology group, headed by Prof. Dr. G. Johan. A. Offerhaus. Prof. Offerhaus introduced Michaël to Dr. Lodewijk A.A. Brosens, who was looking for a PhD candidate to continue a project at the Johns Hopkins University in Baltimore, USA. Supported by a couple of travel grants from the Living With Hope Foundation and the Nijbakker-Morra Foundation, Michaël moved in 2015 to Baltimore as a PhD-candidate, where he worked in the group of Dr. Laura D. Wood. The 3 years of experience as a resident in pathology that Michaël had, came in handy while working on histopathology-focused projects. During his stay, he also worked on projects with Prof. Dr. Ralph H. Hruban, the head of the department of pathology at the Johns Hopkins University. The projects often required a lot of technical optimization, sparking his interest in the technical aspects of research. An opportunity arose to continue doing research under Prof. Dr. Victor E. Velculescu, an oncologist, known for his contributions to the development of DNA-sequencing techniques, the sequencing of cancer genomes and the development of liquid biopsies. Michaël is currently still appointed as a post-doctoral fellow in the lab of Prof. Velculescu, where he finished the project that was initiated by Dr. Brosens and works on other projects, focused on the analysis of circulating tumor DNA.

PhD PORTFOLIO

PhD Candidate:	Michaël Patrick Marthe Noë
PhD Period:	2015-2020
Affiliation:	The department of pathology, UMC Utrecht, Utrecht, the Netherlands & The department of pathology, Johns Hopkins University, School of Medicine, Baltimore, USA
Promotors:	Prof. dr. G.J.A. Offerhaus
	Prof. dr. R. Hruban
Co-promotors:	Dr. L.A.A. Brosens
	Dr. L.D. Wood

Courses

E-course: Basic human subjects Research (2015, JHSOM)

E-course: Bloodborne pathogens (2015, JHSOM)

E-course: Conflict of interest and commitment (2015, JHSOM)

E-course: EPIC - IP - Patient privacy and confidentiality (2015, JHSOM)

E-course: HIPAA for research (2015, JHSOM)

E-course: Preparing for an active shooter in the clinical and non-clinical environment (2015, JHSOM)

E-course: Privacy course for healthy care providers (2015, JHSOM)

Course: 15th Annual current topics in gastrointestinal and liver pathology (2015, JHSOM)

Course: The pathology of neoplastic diseases (2016, MSKCC)

Course: 6th Annual practical genomics workshop: from biology to biostatistics (2016, JHSOM)

Course: 16th Annual current topics in gastrointestinal and liver pathology (2016, JHSOM)

Course: 38th Annual current concepts in surgical pathology (2016, Harvard Medical School)

Course: Great experiments in biology by Dr. Jeremy Nathans (2017, JHSOM)

Seminars, workshops and master classes

Weekly:	Wood-lab labmeeting (2015 - 2017, JHSOM)
Weekly:	Pathology grand rounds (2015 - 2018, JHSOM)
Weekly:	GI-Pathology interesting case conference (2015-2018, JHSOM)
Weekly:	Sidney Kimmel Comprehensive Cancer Center translational research conference (2015-2020, JHSOM)
Weekly:	GI-Core center seminar (2016-2018, JHSOM)
Twice a month:	GI-Pathology journal club (2015-2017, JHSOM)

Grants

Nijbakker-Morra Foundation Stipend

Living with Hope Foundation Travel Grant

Presentations

- Poster: Noë M, Wood LD, Hackeng WM, Brosens LAA, Bhaijee F, Debeljak M, Yu J, Singhi AD, Boyce A, Robinson C, Eshleman JR, Goggins MG, Hruban RH, Collins MT, Lennon AM, Montgomery EA. Patients with McCune-Albright syndrome have a broad spectrum of abnormalities in the gastrointestinal tract and pancreas. USCAP Annual Meeting, 2017, San Antonio
- Platform-presentation: Noë M, Rezaee N, Asrani K, Skaro M, Groot VP, Wu P-H, Olson MT, Hong S-M, Kim SJ, Weiss MJ, Wolfgang CL, Makary MA, He J, Cameron JL, Wirtz D, Roberts NJ, Offerhaus GJA, Brosens LAA, Wood LD, Hruban RH. Immunolabeling of cleared human pancreata provides insights into three-dimensional pancreatic anatomy and pathology. USCAP Annual Meeting, 2018, Vancouver

LIST OF PUBLICATIONS

Publications in this thesis

1. **Noë M**, Brosens LAA. Pathology of pancreatic cancer precursor lesions. Surg Pathol Clin. 2016 Dec 1
2. **Noë M**, Niknafs N, Fischer CG, Hackeng WM, Guthrie VB, Hosoda W, Debeljak M, Papp E, Adleff V, White JR, Luchini C, Pea A, Scarpa A, Butturini G, Zamboni G, Castelli P, Hong S-M, Yachida S, Hiraoka N, Gill AJ, Samra JS, Offerhaus GJA, Hoorens A, Verheij J, Jansen C, Adsay NV, Jiang W, Winter J, Albores-Saavedra J, Terris B, Thompson ED, Roberts NJ, Hruban RH, Karchin R, Scharpf RB, Brosens LAA, Velculescu VE, Wood LD. Genomic characterization of malignant progression in neoplastic pancreatic cysts. Under review at Nat Commun (under embargo)
3. Hosoda W, Chianchiano P, Griffin JF, Pittman ME, Brosens LAA, **Noë M**, Yu J, Shindo K, Suenaga M, Rezaee N, Yonescu R, Ning Y, Albores-Saavedra J, Yoshizawa N, Harada K, Yoshizawa A, Hanada K, Yonehara S, Shimizu M, Uehara T, Samra JS, Gill AJ, Wolfang CL, Goggins MG, Hruban RH, Wood LD. Genetic analyses of isolated high-grade pancreatic intraepithelial neoplasia (HG-PanIN) reveal paucity of alterations in TP53 and SMAD4. J Pathol. 2017 May 1
4. Felsenstein M, **Noë M**, Masica DL, Hosoda W, Chianchiano P, Fischer CG, Lionheart G, Brosens LAA, Pea A, Yu J, Gemenetzis G, Groot VP, Makary MA, He J, Weiss MJ, Cameron JL, Wolfgang CL, Hruban RH, Roberts NJ, Karchin R, Goggins MG, Wood LD. IPMNs with co-occurring invasive cancers: neighbours but not always relatives. Gut. 2018 Sep 1
5. Wood LD, **Noë M**, Hackeng W, Brosens LAA, Bhaijee F, Debeljak M, Yu J, Suenaga M, Singhi AD, Zaheer A, Boyce A, Robinson C, Eshleman JR, Goggins MG, Hruban RH, Collins MT, Lennon AM, Montgomery EA. Patients with McCune-Albright syndrome have a broad spectrum of abnormalities in the gastrointestinal tract and pancreas. Virchows Arch. 2017 Apr 1
6. Hong S-M, **Noë M**, Hruban CA, Thompson ED, Wood LD, Hruban RH. A “Clearer” View of Pancreatic Pathology: A Review of Tissue Clearing and Advanced Microscopy Techniques. Adv Anat Pathol. 2019 Jan 1
7. **Noë M**, Rezaee N, Asrani K, Skaro M, Groot VP, Wu P-H, Olson MT, Hong S-M, Kim SJ, Weiss MJ, Wolfgang CL, Makary MA, He J, Cameron JL, Wirtz D, Roberts NJ, Offerhaus GJA, Brosens LAA, Wood LD, Hruban RH. Immunolabeling of cleared human pancreata provides insights into three-dimensional pancreatic anatomy and pathology. Am J Pathol. 2018 Jul 1
8. Hong S-M, Jung D, Kiemen A, Gaida MM, Yoshizawa T, Braxton AM, **Noë M**, Lionheart G, Oshima K, Thompson ED, Burkhart R, Wu P-H, WIrtz D, Hruban RH, Wood LD. Three-dimensional visualization of cleared human pancreas cancer reveals that sustained epithelial-to-mesenchymal transition is not required for venous invasion. Mod Pathol. 2019 Nov 7
9. Hruban RH, Gaida MM, Thompson E, Hong S-M, **Noë M**, Brosens LAA, Jongepier M, Offerhaus GJA, Wood LD. Why is pancreatic cancer so deadly? The pathologist’s view. J Pathol. 2019 Jun
10. Pea A, Yu J, Marchionni L, **Noë M**, Luchini C, Pulvirenti A, de Wilde RF, Brosens LAA, Rezaee N, Javed A, Gobbo S, Regi P, Salvia R, Bassi C, He J, Weiss MJ, Cameron JL, Offerhaus GJA, Hruban RH, Lawlor RT, Scarpa A, Heaphy CM, Wood LD, Wolfgang CL. Genetic analysis of small well-differentiated pancreatic neuroendocrine tumors identifies subgroups with differing risks of

liver metastases. Ann Surg. 2018 Oct 17

11. **Noë M***, Pea A*, Luchini C, Felsenstein M, Barbi S, Bhaijee F, Yonescu R, Ning Y, Adsay NV, Zamboni G, Lawlor RT, Scarpa A, Offerhaus GJA, Brosens LAA, Hruban RH, Roberts NJ, Wood LD. Whole-exome sequencing of duodenal neuroendocrine tumors in patients with neurofibromatosis type 1. Mod Pathol. 2018 May 30 (*both authors contributed equally)
12. **Noë M**, Hackeng WM, de Leng WWJ, Vergeer M, Vleggaar FP, Morsink FHM, Wood LD, Hruban RH, Offerhaus GJA, Brosens LAA. Well-differentiated pancreatic neuroendocrine tumor in a patient with familial atypical multiple mole melanoma syndrome (FAMMM). Am J Surg Pathol. 2019 Sep

Other publications

1. Carlier M, **Noë M**, De Waele JJ, Stove V, Verstraete AG, Lipman J, Roberts JA. Population pharmacokinetics and dosing simulations of amoxicillin/clavulanic acid in critically ill patients. J Antimicrob Chemother. 2013 Nov
2. Carlier M, **Noë M**, Roberts JA, Stove V, Verstraete AG, Lipman J, De Waele JJ. Population pharmacokinetics and dosing simulations of cefuroxime in critically ill patients: non-standard dosing approaches are required to achieve therapeutic exposures. J Antimicrob Chemother. 2014 Oct
3. Haspeslagh M, **Noë M**, De Wispelaere I, Degryse N, Vossaert K, Lanssens S, Facchetti F, Van Den Bossche K, Brochez L. Rosettes and other white shiny structures in polarized dermoscopy: histological correlate and optical explanation. J Eur Acad Dermatol Venereol. 2016 Feb
4. Haspeslagh M, Vossaert K, Lanssens S, **Noë M**, Hoorens I, Chevolet I, De Wispelaere I, Degryse N, Facchetti F, Brochez L. Comparison of ex vivo and in vivo dermoscopy in dermatopathologic evaluation of skin tumors. JAMA Dermatol. 2016 Mar
5. Hackeng WM, Brosens LA, Poruk KE, **Noë M**, Hosoda W, Poling JS, Rizzo A, Campbell-Thompson M, Atkinson MA, Konukiewitz B, Klöppel G, Heaphy CM, Meeker AK, Wood LD. Aberrant Menin expression is an early event in pancreatic neuroendocrine tumorigenesis. Hum Pathol. 2016 Oct
6. Debeljak M, Mocci E, Morrison MC, Pallavajjalla A, Beierl K, Amiel M, **Noë M**, Wood LD, Lin MT, Gocke CD, Klein AP, Fuchs EJ, Jones RJ, Eshleman JR. Haplotype counting for sensitive chimerism testing: potential for early leukemia relapse detection. J Mol Diagn. 2017 May
7. Anglesio MS, Papadopoulos N, Ayhan A, Nazeran TM, **Noë M**, Horlings HM, Lum A, Jones S, Senz J, Seckin T, Ho J, Wu RC, Lac V, Ogawa H, Tessier-Cloutier B, Alhassan R, Wang A, Wang Y, Cohen JD, Wong F, Hasanovic A, Orr N, Zhang M, Popoli M, McMahon W, Wood LD, Mattox A, Allaire C, Segars J, Williams C, Tomasetti C, Boyd N, Kinzler KW, Gilks CB, Diaz L, Wang TL, Vogelstein B, Yong PJ, Huntsman DG, Shih IM. Cancer-associated mutations in endometriosis without cancer. N Engl J Med. 2017 May 11
8. Labidi-Galy SI, Papp E, Hallberg D, Niknafs N, Adleff V, **Noë M**, Bhattacharya R, Novak M, Jones S, Phallen J, Hruban CA, Hirsch MS, Lin DI, Schwartz L, Maire CL, Tille JC, Bowden M, Ayhan A, Wood LD, Scharpf RB, Kurman R, Wang TL, Shih IM, Karchin R, Drapkin R, Velculescu VE. High grade serous ovarian carcinomas originate in the fallopian tube. Nat Commun. 2017 Oct 23
9. Luchini C, Pea A, Lionheart G, Mafficini A, Nottegar A, Veronese N, Chianchiano P, Brosens LA,

Noë M, Offerhaus GJA, Yonescu R, Ning Y, Malleo G, Riva G, Piccoli P, Cataldo I, Capelli P, Zamboni G, Scarpa A, Wood LD. Pancreatic undifferentiated carcinoma with osteoclast-like giant cells is genetically similar to, but clinically distinct from, conventional ductal adenocarcinoma. J Pathol. 2017 Oct

10. Liu L, Zhu Y, **Noë M**, Li Q, Pasricha PJ. Neuronal Transforming Growth Factor beta signaling via SMAD3 contributes to pain in animal models of chronic pancreatitis. Gastroenterology. 2018 Jun
11. Groot VP, Thakker SS, Gemenetzis G, **Noë M**, Javed AA, Burkhart RA, Noveiry BB, Cameron JL, Weiss MJ, VandenBussche CJ, Fishman EK, Hruban RH, Wolfgang CL, Lennon AM, He J. Lessons learned from 29 lymphoepithelial cysts of the pancreas: institutional experience and review of the literature. HPB (Oxford). 2018 Jul
12. **Noë M**, Ayhan A, Wang TL, Shih IM. Independent development of endometrial epithelium and stroma within the same endometriosis. J Pathol. 2018 Jul
13. Debeljak M, **Noë M**, Riel SL, Haley LM, Norris AL, Anderson DA, Adams EM, Suenaga M, Beierl KF, Lin MT, Goggins MG, Gocke CD, Eshleman JR. Validation strategy for ultrasensitive mutation detection. Mol Diagn Ther. 2018 Oct
14. Robinson C, Estrada A, Zaheer A, Singh VK, Wolfgang CL, Goggins MG, Hruban RH, Wood LD, **Noë M**, Montgomery EA, Guthrie LC, Lennon AM, Boyce AM, Collins MT. Clinical and radiographic gastrointestinal abnormalities in McCune-Albright Syndrome. J Clin Endocrinol Metab. 2018 Nov 1
15. Luchini C, Cros J, Pea A, Pilati C, Veronese N, Rusev B, Capelli P, Mafficini A, Nottegar A, Brosens LAA, **Noë M**, Offerhaus GJA, Chianchiano P, Riva G, Piccoli P, Parolini C, Malleo G, Lawlor RT, Corbo V, Sperandio N, Barbareschi M, Fassan M, Cheng L, Wood LD, Scarpa A. PD-1, PD-L1, and CD163 in pancreatic undifferentiated carcinoma with osteoclast-like giant cells: expression patterns and clinical implications. Hum Pathol. 2018 Nov
16. Papp E, Hallberg D, Konecny GE, Bruhm DC, Adleff V, **Noë M**, Kagiampakis I, Palsgrove D, Conklin D, Kinose Y, White JR, Press MF, Drapkin R, Easwaran H, Baylin SB, Slamon D, Velculescu VE, Scharpf RB. Integrated genomic, epigenomic, and expression analyses of ovarian cancer cell lines. Cell Rep. 2018 Nov 27
17. Faghih M, Boortalary T, Jalaly NY, Brewer Gutierrez OI, Chen YI, Azadi JR, Parsa N, **Noë M**, Fan C, Kumbhari V, Kalloo AN, Zaheer A, Khashab MA, Singh VK. Low serum trypsin levels predict deep pancreatic cannulation failure during endoscopic retrograde cholangiopancreatography in patients with symptomatic obstructive chronic pancreatitis. Pancreas. 2019 Jul
18. Rodriguez FJ, Graham MK, Brosnan-Cashman JA, Barber JR, Davis C, Vizcaino MA, Palsgrove DN, Giannini C, Pekmezci M, Dahiya S, Gokden M, **Noë M**, Wood LD, Pratilas CA, Morris CD, Belzberg A, Blakeley J, Heaphy CM. Telomere alterations in neurofibromatosis type 1-associated solid tumors. Acta Neuropathol Commun. 2019 Aug 28
19. Asrani K, Murali S, Lam B, Na CH, Phatak P, Sood A, Kaur H, Khan Z, **Noë M**, Anchoori RK, Talbot CC Jr, Smith B, Skaro M, Lotan TL. mTORC1 feedback to AKT modulates lysosomal biogenesis through MiT/TFE regulation. J Clin Invest. 2019 Dec 2

ACKNOWLEDGEMENTS

I would like to thank everybody who contributed to this work and has contributed to my development as a researcher. I want to specifically thank the following people:

- I would like to thank all the **patients** who contributed to this research. I truly hope your contribution will help others as a result of the scientific knowledge gained from the studies.

- **Prof. Dr. Offerhaus, Johan** en **Dr. Brosens, Lodewijk**, ik kan jullie niet genoeg bedanken voor de mogelijkheden die ik van jullie gekregen heb. Als AIOS vond ik het al bijzonder interessant om de discussies te aanhoren rond interessante gevallen en bepaalde concepten in de pathologie. Als ik iets probeerde in te brengen, werd ik ook altijd serieus genomen ondanks mijn onervarenheid. Het type onderzoek dat jullie doen vond ik heel interessant, creatief en origineel: het onderzoek overstijgt de pathologie. Mijn normen en waarden voor 'goed onderzoek' zijn sterk beïnvloed door jullie. Het was een fantastisch avontuur waarin ik de kans kreeg om mezelf verder te ontwikkelen. Ik dank jullie van harte voor jullie vertrouwen, steun, betrokkenheid, tijd en optimisme waarmee jullie me door het promotietraject hebben geleid.

- **Dr. Wood, Laura**, thank you very much for your hospitality and giving me the opportunity to do research in your group. You were always available and prepared to discuss the projects. As you mentioned, it was sometimes difficult to work in a brand new lab, but it was also a wonderful experience to meet researchers from different backgrounds and countries, all thinking about the problems we encountered. Thank you for giving me the freedom to explore my own ideas.

- **Prof. Dr. Hruban**, thank you for your hospitality, your support and your guidance. Your enthusiasm for science is very inspiring. You are not only a great researcher with bold ideas, but you also enable other researchers to develop themselves. I have learned a lot from our meetings and from your interventions in the pathology grand rounds, interesting case conferences and journal clubs. I did not really like the picture of me that you used in your presentations on tissue clearing, as it was taken on a bad hair day, but you taught me to put aside my vanity.

- **Prof. Dr. Velculescu**, thank you for letting me finish my PhD project in your lab and under your guidance. I truly appreciate the time, support and advice you gave me.

- Dear **members of the thesis committee**, Prof. Dr. Bernards, Prof. Dr. Kranenburg, Prof. Dr. Meijer, Prof. Dr. van Diest and Prof. Dr. Wolfgang. Thank you very much for reading and critically assessing my thesis.

Further I would like to mention the following people for their support and friendship:

- The members of the Wood lab: Ale, Antonio, Cathy, DongJun, Gemma, Matthäus, Michael, Peter, Seung-Mo, Tadashi, Waki, Wenji, Yea Ji, Yuko

- The members of the Velculscu lab: Adith, Alessandro, Ashok, Carlie, Daniel, Dimitrios, Dorothy, Elsa, Gavin, Jacob, James, Jamie, Jennifer, Jillian, Joe, Leo, Mara, Melody, Noushin, Rachel, Rhymee, Rob, Stephen, Vilmos, Zineb

- The friends from the surrounding labs: Anne, Asli, Charlie, Kaushal, Marija, Marco, Michael, Qingfeng, Sam

- The members of GI-pathology at UMC Utrecht: Folkert, Huiying, Marjon, Miangela, Wendy, Wenzel

- The members of GI-pathology at Johns Hopkins: Dr. Eshleman, Dr. Goggings, Dr. Roberts

- The people from the Oncology Tissue Core: Andre, Bonnie, Helen, Wanda

- The 'Dutchies' in Baltimore: Arlene, Emma, Egbert, Floortje, Joost, Maite, Marise, Martine, Niek, Toby, Vincent

- The residents in pathology from UMC Utrecht: Amelie, Annelotte, Annemiek, Clothaire, Gwen, Jan Willem, Jonathan, Joy, Laura, Loudy, Magda, Marc, Mariëtte, Mihaela, Myrtle, Nadège, Niek, Rachel, Ruben, Sebastiaan, Sander, Sanneke, Shahrzad, Shoko, Sjors, Steffie

- The pathologists from UMC Utrecht: Aryan, Celien, Lotte, Marijke, Marijn, Miangela, Mirthe, Paul, Peter, Pieter, Roel, Ronald, Roos, Stefan, Tri, Trudy, Uta, Willeke, Wim

- The Flemish pathologists: Anne-Sophie, Erik

- My wife, Nicole

- My parents, Jo and Frans

- My family